Università degli Studi di Ferrara

DOCTORATE IN
ENGINEERING SCIENCE

CYCLE XXIX

COORDINATOR Prof. Stefano Trillo

Force-Based Seismic Design of Dual System RC Structures

Academic Discipline ICAR/09

Ph.D. student

Matteo Zerbin

Supervisor

Prof. Alessandra Aprile, UNIFE

Co-Supervisor

Prof. Enrico Spacone, UNICH

Years 2014/2016

Università degli Studi di Ferrara

DOCTORATE IN
ENGINEERING SCIENCE

CYCLE XXIX

COORDINATOR Prof. Stefano Trillo

Force-Based Seismic Design of Dual System RC Structures

Academic Discipline ICAR/09

Ph.D. student

Matteo Zerbin

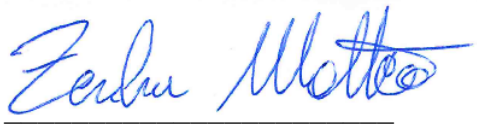

Supervisor

Prof. Alessandra Aprile, UNIFE

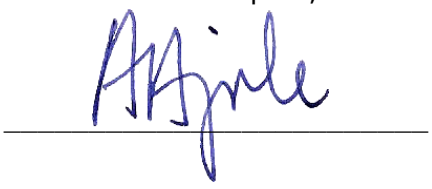

Co-Supervisor

Prof. Enrico Spacone, UNICH

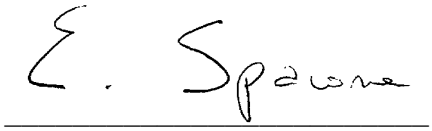

Years 2014/2016

Abstract

Seismic design of standard structures is typically based on a force-based design approach. Over the years, this approach has proven to be robust and easy to apply by design engineers and – in combination with capacity design principles – it provided a good protection against premature structural failures. However, it is also known that the force-based design approach as it is implemented in the current generation of seismic design codes suffers from some shortcomings. One of these relates to the fact that the base shear is computed using a pre-defined force reduction factor, which is constant for a certain type of structural system. As a result of this, for the same design input, structures of the same type but different geometry are subjected to different ductility demands and show therefore a different performance during an earthquake. The objective of this research is to present an approach for computing force reduction factors using simple analytical models. These analytical models describe the deformed shape at yield and ultimate displacement of the structure and only require input data that are available when starting the design process, such as geometry and general material properties. The displacement profiles are obtained from section dimensions and section ductility capacities that can be estimated at the beginning of the design process. The so computed displacement ductility is taken as proxy of the force reduction factor. Such analytical models allow to link global to local ductility demands and therefore to compute an estimate of the force ductility reduction factors for wall and frame structures. Finally, this research develops an approach for frame-wall structures as combination of results obtained for wall and frame systems. The proposed method is applied to a set of frame-wall structures and validated by means of nonlinear time history analyses. Obtained results show that the proposed method yields a more accurate seismic performance than the current code design approach. The presented work therefore contributes to the development of revised force-based design guidelines for the next generation of seismic design codes.

Keywords: frame-wall structures, ductility reduction factor, force-based seismic design, performance-based design, nonlinear analyses.

Sommario

La progettazione sismica di strutture è tipicamente basato su un approccio progettuale basato sulle forze. Nel corso degli anni, questo approccio ha dimostrato di essere robusto e facile da applicare dai progettisti e, in combinazione con il principio di gerarchia delle resistenze, fornisce una buona protezione contro i meccanismi di collasso fragili. Tuttavia, è anche noto che l'approccio di progettazione in forze così come attuato nell'odierna generazione di normative soffre di alcune carenze. Uno di questi riguarda il fatto che il tagliante alla base è calcolato utilizzando un fattore di struttura predefinito, cioè costante per tipo di sistema strutturale. Di conseguenza, per lo stesso input di progettazione, strutture dello stesso tipo ma diversa geometria sono sottoposti ad una diversa domanda di duttilità e mostrano quindi una diversa prestazione durante un evento sismico. L'obiettivo di questo studio è quello di presentare un approccio per il calcolo fattori di struttura utilizzando modelli analitici semplici. Questi modelli analitici descrivono la deformata a snervamento e spostamento ultimo della struttura e richiedono solo dati di input disponibili all'inizio del processo di progettazione, quali dati geometrici e proprietà dei materiali. La deformata della struttura ottenuta dalle dimensioni delle sezioni e la capacità in termini di duttilità sezionale possono essere stimati all'inizio della progettazione. La duttilità è alla base della formulazione del fattore di struttura come proposto dai modelli analitici presentati. Tali modelli analitici permettono di collegare le duttilità sezionali alla duttilità strutturale e quindi calcolare una stima del fattore di struttura per struttura a pareti e a telaio. Infine, si sviluppa un approccio per strutture duali di tipo telaio-parete come combinazione di risultati ottenuti per i sistemi singoli. Il metodo proposto è applicato ad un insieme di strutture duali e validato con analisi dinamiche non lineari. Si dimostra che il metodo proposto produce una più accurata prestazione sismica rispetto all'approccio progettuale delle normative odierne. Il lavoro presentato contribuisce pertanto allo sviluppo di nuove linee guida per la progettazione sismica nella prossima generazione di normative.

Parole chiave: strutture telaio-parete, fattore di struttura, progettazione sismica basata sulle forze, progettazione basata sulla prestazione, analisi non lineari.

Acknowledgements

This research has been carried out at the Engineering Department (ENDIF) at the Università degli Studi di Ferrara (UNIFE) under the supervision of Prof. Alessandra Aprile. It is first to her that I want to express my gratitude. Thank you for the commitment to this research, the guidance and the help during these years.

I sincerely thank my Co-Supervisor Prof. Enrico Spacone of the Department of Engineering and Geology (INGEO) at the Università degli Studi "G. d'Annunzio" di Chieti-Pescara (UNICH) and my Host Tutor Prof. Katrin Beyer of the Earthquake Engineering and Structural Dynamics Laboratory (EESD) at the Ecole Polytechnique Fédérale de Lausanne (EPFL) for the precious suggestions and ideas.

I would like to thank the appraisers, Prof. Theodore L. Karavasilis, University of Southampton (SOTON, UK), and Prof. Dimitrios Vamvatsikos, National Technical University of Athens (NTUA, Greece) for judging this thesis.

I wish to thank my office mates at UNIFE, Alberto and Giulia, and all friends I met at EPFL. In particular my office mates, Filippo and Dario, and all the others, Alessandro, Raffaele, Francesco V., Angelica, Danilo, Francesco C., Fabio, Marco, Ioannis.

I would like to thank Claudia and all my friends from Taglio di Po, my hometown, and Ferrara. In particular, Stefano V., Andrea, Luca, Loris, Sara, Silvia, Stefano S. Thanks for the friendship and the beautiful moments we spent together.

Finally I want to thank my parents, Serenella and Patrizio, my brother, Enrico, and my grandparents, Elena and Giuseppe. Thanks for the support and the strength you gave me. Grazie, vi voglio bene!

Table of Contents

Symbols list

A	maximum ground acceleration
A_c	section area of the column
A_w	section area of the wall
a	regression coefficient
a_1	regression coefficient
a_f	regression coefficient of the frame
a_w	regression coefficient of the wall
b	regression coefficient
b_1	regression coefficient
b_c	width of the column
b_Δ	hardening ratio of the shear-displacement hinge
b_f	regression coefficient of the frame
b_θ	hardening ratio of the moment-rotation hinge
b'_θ	equivalent hardening ratio of the moment-rotation hinge
b_w	regression coefficient of the wall
b_w	width of the wall
C	elastic design spectrum
C	factor depending on the fundamental period
C_d	design response spectrum
C_s	seismic response coefficient
c	regression coefficient
c_1	regression coefficient
c_f	regression coefficient of the frame
c_w	regression coefficient of the wall
$d_{bl,f}$	maximum diameter of rebars in the base column of the frame
$d_{bl,w}$	maximum diameter of rebars in the base section of the wall
d_c	control displacement for the MDOF system
d_c^*	control displacement for the SDOF system
$d_{c,f,i}$	ultimate displacement capacity at the *i-th* storey of the frame
$d_{c,w}$	ultimate displacement capacity of the wall system
d_d^*	inelastic displacement demand
$d_{d,f,i}$	ultimate displacement demand at the *i-th* storey of the frame
$d_{d,w}$	ultimate displacement demand of the wall system

$d_{p,f}^*$	plastic displacement of the SDOF frame system
$d_{p,w}^*$	plastic displacement of the SDOF wall system
$d_{p1,f}^*$	plastic displacement of the first-storey SDOF frame system
d_u	ultimate displacement
$d_{u,i}$	ultimate displacement at *i-th* storey
$d_{u,f}^*$	ultimate displacement of the SDOF frame system
$d_{u,f,i}$	ultimate displacement at *i-th* storey of the frame
$d_{u,f,i,max}$	maximum displacement at *i-th* storey of the frame
$d_{u,w}^*$	ultimate displacement of the SDOF wall system
d_y	yield displacement
d_y^*	yield displacement of the SDOF system
$d_{y,f}^*$	yield displacement of the SDOF frame system
$d_{y,w}^*$	yield displacement of the SDOF wall system
$d_{y,f,i}$	yield displacement at *i-th* storey of the frame
$d_{y1,f}^*$	yield displacement of the first-storey SDOF frame system
$d_{y,i}$	yield displacement at *i-th* storey
E_c	Young modulus of concrete
$E_{c,f}$	equivalent Young modulus is defined at the yield moment of the column
$E_{c,f}I_{w,f}$	flexural stiffness of the column
$E_{c,w}$	equivalent Young modulus is defined at the yield moment of the wall
$E_{c,w}I_{w,y}$	flexural stiffness of the wall
$E_{k,MDOF}$	elastic energy of the MDOF system
$E_{k,SDOF}$	elastic energy of the SDOF system
EI	flexural stiffness
$EI_{f,y}$	yield flexural stiffness of the frame
$EI_{w,y}$	yield flexural stiffness of the wall
F	lateral force
F_i	applied force at *i-th* storey
f_c	concrete mean compressive strength
f_u	steel mean tensile strength
f_y	steel mean yield strength
$GA_{f,y}$	yield shear stiffness of the frame
g	gravitational acceleration, 9.806 m/s^2
H	building height
H_f	frame height
H_w	wall height
h^*	height of the SDOF system
h_1^*	height of the first mode SDOF system
h_e	effective height
h_f^*	height of the first mode SDOF frame system
h_G	height of application of the lateral force
h_i	*i-th* storey height
h_s	storey height

$h_w{}^*$	height of the first mode SDOF wall system
IDR_{max}	maximum interstorey drift ratio
IDR_u	ultimate interstorey drift ratio
IDR_y	yield interstorey drift ratio
I_c	moment of inertia of the column
I_e	importance factor
I_w	moment of inertia of the wall
$I_w{}^*$	moment of inertia of the SDOF wall system
K	factor depending on building type
K_e	effective stiffness
k	parameter of the ground motion
k	plastic hinge coefficient
k	section shape factor
k^*	stiffness of the SDOF system
$k_1{}^*$	stiffness of the first mode SDOF system
k_Δ	initial elastic tangent stiffness of the shear-displacement hinge
$k_f{}^*$	stiffness of the first mode SDOF frame system
k_θ	initial elastic tangent stiffness of moment-rotation hinge
k'_θ	equivalent initial elastic tangent stiffness of moment-rotation hinge
k_u	reduction factor
k_w	factor reflecting the prevailing failure mode in structural systems with walls
$k_w{}^*$	stiffness of the first mode SDOF wall system
$L_{p,f}$	plastic hinge length of the base column of the frame
$L_{p,w}$	plastic hinge length of the wall
$L_{sp,f}$	strain penetration length of the base column of the frame
$L_{sp,w}$	strain penetration length of the wall
$L_{s,w}$	shear span length of the wall
l_w	length of the wall
$M_{b,MDOF}$	elastic base moment of the MDOF system
$M_{b,SDOF}$	elastic base moment of the SDOF system
$M_{u,f}$	ultimate moment of the base column of the frame
$M_{u,w}$	ultimate moment of the base section of the wall
$M_{y,f}$	yield moment of the base column of the frame
$M_{y,w}$	yield moment of the base section of the wall
m^*	mass of the SDOF system
$m_1{}^*$	mass of the first mode SDOF system
$m_d{}^*$	mass of the SDOF dual system
m_e	effective mass
$m_f{}^*$	mass of the SDOF frame system
m_i	floor mass at *i-th* storey
$m_{l,f}$	mass per unit height of the frame
$m_{l,w}$	mass per unit height of the wall
m_{MDOF}	mass of the MDOF system
m_{SDOF}	mass of the SDOF system

$m_w{}^*$	mass of the SDOF wall system
n	total number of analyses
n_{big}	a big number, 1000
n_{big2}	a big number, $1e07$
n_c	number of columns of the frame
n_s	number of storeys
q	behavior factor
q_0	basic value of the behavior factor
R	force reduction factor
R^*	ductility reduction factor for periods higher than the characteristic period
R_ζ	damping force reduction factor
R_μ	ductility force reduction factor
R_M	modification factor
$R_{M,f}$	modification factor of the frame
$R_{M,w}$	modification factor of the wall
$R_{\mu,MDOF}$	ductility reduction factor for a MDOF system
$R_{\mu,MDOF,d,1}$	first expression of ductility reduction factor for a MDOF dual system
$R_{\mu,MDOF,d,2}$	second expression of ductility reduction factor for a MDOF dual system
$R_{\mu,MDOF,f}$	ductility reduction factor for a MDOF frame system
$R_{\mu,MDOF,f,d}$	ductility reduction factor for the frame-equivalent MDOF system
$R_{\mu,MDOF,w}$	ductility reduction factor for a MDOF wall system
$R_{\mu,MDOF,w,d}$	ductility reduction factor for the wall-equivalent MDOF system
$R_{\mu,SDOF}$	ductility reduction factor for a SDOF system
$R_{\mu,SDOF,f}$	ductility reduction factor for a SDOF frame system
$R_{\mu,SDOF,w}$	ductility reduction factor for a SDOF wall system
R_r	structural redundancy force reduction factor
RSS	sum of the squares of residuals
R_s	overstrength force reduction factor
S_a	spectral inelastic acceleration
S_{ae}	spectral elastic acceleration
S_d	spectral inelastic displacement
S_{D1}	design spectral response acceleration parameter at 1-second period
S_{de}	spectral elastic displacement
S_{DS}	design spectral response acceleration parameter at short periods
S_p	structural performance factor
T	fundamental period
T^*	characteristic period
T^*	elastic period of the SDOF system
T_0	characteristic period of the ground motion
T_1	fundamental period
$T_1{}^*$	period of the first mode SDOF system
$T_{1,d}$	fundamental period of the dual system
$T_{1,f}$	fundamental period of the frame
$T_{1,w}$	fundamental period of the wall

T_g	predominant period of the ground motion
T_L	long-period transition period
u_f	use rate for the frame-equivalent system
$u_{rmax(d)}$	design target roof displacement
$u_{rmax(IDR)}$	roof displacement due to maximum interstorey drift ratio
$u_{rmax(\mu)}$	roof displacement due to local ductility
u_{ry}	yield roof displacement
u_w	use rate for the wall-equivalent system
V	maximum ground velocity
V_b	base shear force
V_b	base shear force for the MDOF system
$V_b{}^*$	base shear force for the SDOF system
$V_{b,1}$	base shear at first flexural resistance
$V_{b,MDOF}$	base shear force for a MDOF system
$V_{b,MDOF,d}$	base shear force for a MDOF dual system
$V_{b,MDOF,f}$	base shear force for a MDOF frame system
$V_{b,MDOF,f,d}$	base shear force of the frame for a MDOF dual system
$V_{b,MDOF,tot}$	sum of base shears of MDOF wall and frame as single systems
$V_{b,MDOF,w}$	base shear force for a MDOF wall system
$V_{b,MDOF,w,d}$	base shear force of the wall for a MDOF dual system
$V_{b,SDOF}$	base shear force for a SDOF system
$V_{b,SDOF,f}$	base shear force for a SDOF frame system
$V_{b,SDOF,f,d}$	base shear force for a frame-equivalent SDOF system
$V_{b,SDOF,w}$	base shear force for a SDOF wall system
$V_{b,SDOF,w,d}$	base shear force for a wall-equivalent SDOF system
$V_{b,u}$	ultimate base shear
V_c	total concrete volume of the resisting structures
$V_{u,f}$	ultimate base shear of the frame
$V_{u,f}{}^*$	ultimate base shear of the first mode SDOF frame system
$V_{u,w}$	ultimate base shear of the wall
$V_{u,w}{}^*$	ultimate base shear of the first mode SDOF wall system
$V_{y,f}$	yield base shear of the frame
$V_{y,f}{}^*$	yield base shear of the first mode SDOF frame system
$V_{y,w}$	yield base shear of the wall
$V_{y,w}{}^*$	yield base shear of the first mode SDOF wall system
$v_{b,MDOF,d}$	normalised base shear for dual systems
v_f	base shear ratio for the frame-equivalent system
v_w	base shear ratio for the wall-equivalent system
W	building weight
α	beam-to-column stiffness ratio
α	ratio of the post-yield stiffness and the initial stiffness
α	regression coefficient

α_1	value of base shear by which the first flexural resistance is reached
α_f	regression coefficient of the frame
α_w	regression coefficient of the wall
α_u	value of base shear by which structural instability is developed
β	coefficient depending on building properties
β	regression coefficient
Γ	modal participation factor
Γ_1	modal participation factor of the first mode
γ_d	performance assessment provided by N2 method
Δ_d	design displacement
Δ_i	displacement at *i-th* storey
Δ_u	ultimate interstorey drift ratio
Δ_y	yield interstorey drift ratio
ζ_1	viscous damping ratio of the first mode
${\zeta_1}^*$	viscous damping ratio of the first mode SDOF system
ζ_e	equivalent viscous damping ratio
η_ζ	damping reduction factor
$\theta_{c,w}$	rotational capacity of the wall base hinge
$\theta_{d,w}$	rotational demand of the wall base hinge
$\theta_{p,w}$	plastic rotation of the moment-rotation hinge
$\theta_{u,w}$	ultimate rotation of the moment-rotation hinge
$\theta_{u,w,i}$	ultimate rotation at the *i-th* storey of the moment-rotation hinge
$\theta_{u,w,i,max}$	maximum rotation at the *i-th* storey of the moment-rotation hinge
$\theta_{y,w}$	yield rotation of the moment-rotation hinge
${\theta'}_{y,w}$	equivalent yield rotation of the moment-rotation hinge
μ	displacement ductility
μ	roof displacement ductility
μ	structural ductility
μ^*	target displacement ductility
μ_d	design roof displacement ductility
μ_Δ	displacement ductility
μ_Δ	storey displacement ductility
μ_θ	the maximum local ductility
μ_{IDR}	interstorey drift ductility
$\mu_{\varphi,f}$	curvature ductility of the base column of the frame
$\mu_{\varphi,w}$	curvature ductility of the base section of the wall
${\mu_f}^*$	target displacement ductility of the frame
${\mu_{f,d}}^*$	target displacement ductility of the frame in the dual system
${\mu_w}^*$	target displacement ductility of the wall
${\mu_{w,d}}^*$	target displacement ductility of the wall in the dual system
ρ	column-to-beam stiffness ratio
Φ	parameter depending on ground properties
ϕ^0	overstrength factor relating to flexural strength to design strength
φ_{ea}	amplification factor for ground motion acceleration

φ_{ev}	amplification factor for ground motion velocity
ϕ_i	first mode deflected shape ordinate for the *i-th* storey
$\phi_{i,f}$	first mode deflected shape ordinate for the *i-th* storey of the frame
$\phi_{i,w}$	first mode deflected shape ordinate for the *i-th* storey of the wall
$\varphi_{u,f}$	ultimate curvature of the base column of the frame
$\varphi_{u,f}{}^*$	ultimate curvature of the SDOF frame system
$\varphi_{u,w}$	ultimate curvature of the base section of the wall
$\varphi_{u,w}{}^*$	ultimate curvature of the SDOF wall system
$\varphi_{y,f}$	yield curvature of the base column of the frame
$\varphi_{y,f}{}^*$	yield curvature of the SDOF frame system
$\varphi_{y,w}$	yield curvature of the base section of the wall
$\varphi_{y,w}{}^*$	yield curvature of the SDOF wall system
ω_1	fundamental frequency
$\omega_1{}^*$	frequency of the first mode SDOF system
$\omega_{v,\mu}$	shear dynamic amplification factor for frame
$\omega_{v,Ti}$	shear dynamic amplification factor for wall
$-OS$	subscript of symbols which refers to numerical analyses

1. Introduction

1.1. Motivations

Dual system structures, such as reinforced concrete (RC) frame-wall structures, are largely used as structural resisting systems to horizontal loads.

Coupling two resisting systems allows overcoming structural deficiencies of single resisting systems and takes advantages by synergy. It is evidenced that frame structures are versatile and allow architectural flexibility, but they are deformable especially at low stories. On the other hand, wall system structures are very stiff at low stories but they impose rigid architectural constrains to openings and windows.

Static behavior of frame-wall systems subjected to horizontal actions is well known thanks to early studies performed in 60's and 70's (Goodsir, 1985), for instance, the "shear-flexural cantilever model" (Rosman, 1974; Pozzati, 1977) shows accurate results regarding the distribution of horizontal load between two coupled systems, but this method presents the shortcoming to be valid for elastic analysis only.

Nowadays, the Force-Based Design (FBD) approach is the standard method to design structures to seismic loads. Over the years, this approach has proven to be robust and easy to apply by design engineers and – in combination with capacity design principles – it provided a good protection against premature structural failures. This approach requires static analyses, which are easy to apply and fast to perform. Inelasticity behavior is based on the *force reduction factor* or *behavior factor*, which allows converting nonlinear behavior in a reduction of static forces to be applied in static analyses.

Usually building codes define force reduction factors for various type of resisting system but they do not provide accurate force reduction factor for dual systems, with the exception of some particular cases. Furthermore, force reduction factors are constant for a certain type of structural system. As a result of this, for the same design input, structures of the same type but different geometry are subjected to different ductility demands and show therefore a different performance during an earthquake.

Thanks to its simplicity and large diffusion among designers, Force-Based Design still remains the standard method to design structures under seismic actions. The advantage of defining a new refined method to provide accurate force reduction factors can update the method to become more effective and attain a more uniform performance.

1.2. Objectives

The objective of this thesis is to present an approach for computing force reduction factors using simple analytical models.

These analytical models describe the deflected shape at yield and ultimate displacement of the structure and only require input data that are available when starting the design process, such as geometry and general material properties. The so computed displacement ductility is taken as proxy of the force reduction factor. Such analytical models allow linking global to local ductility demands and therefore to compute an estimate of the force ductility reduction factors.

The presented work therefore contributes to the development of revised Force-Based Design guidelines for the next generation of seismic design codes.

1.3. Methodology

An analytical method to estimate the ductility force reduction factor is proposed for wall and frame when considered single systems and then for frame-wall systems.

Three levels of sectional ductility are investigated for both wall and frame structures and three combinations of the precedent sectional ductilities are investigated for frame-wall structures.

Structures with a number of storeys ranged from 3 to 12 are considered in the present work. Therefore, low-rise and mid-rise buildings are investigated, but high-rise buildings are not studied in the present work.

To validate the applicability of the proposed method, a database of 34 natural ground motions is selected and a total of 1020 nonlinear time history analyses (NLTHA) are computed for wall and frame systems and 5100 analyses for dual systems, respectively.

1.4. Outline of the thesis

This Thesis is composed of 6 Sections.

The Section 2 introduces topics relevant for the study of force reduction factor. Section 2.1 outlines main design methods, that are Force-Based Design (FBD), Direct Displacement-Based Design (DDBD) and Hybrid Force/Displacement-based seismic Design (HFD) methods. The methods are briefly compared; advantages and shortcomings are evidenced. Section 2.2, 2.3 and 2.4 resume the definition of force reduction factor, the ductility reduction factor for single-degree of freedom (SDOF) system and the ductility reduction factor multi-degree of freedom (MDOF) system, respectively. A literature review of main contributions to the presented topic is reported. Section 2.5 introduces dual system structures. Section 2.6 briefly reports design standards of main international codes. Section 2.7 introduces the “N2 method” to assess nonlinear structural performance.

The section 3 reports the proposed analytical models. Section 3.1 introduces the definition equivalent SDOF system. Section 3.2, 3.3 and 3.4 describe the analytical models for wall, frame and dual systems, respectively.

The Section 4 reports the implemented numerical models. Section 4.1 introduces numerical models for wall, frame and dual systems; Section 4.2 describes the investigated structural systems and the numerical procedures to compute the ductility force reduction factor. An iterative procedure is implemented and applied to all analyses in order to find the ultimate capacity of the structures at each ground motions.

The Section 5 shows the obtained results. In particular results of wall, frame and dual systems are reported in Section 5.1, 5.2 and 5.3, respectively. Numerical results are interpreted in detail and compared with analytical results provided by the proposed models.

The section 6 develops two design cases to show the application of the proposed analytical design method for dual system step-by-step. Two RC frame-wall structures are designed following the proposed analytical method and compared with the same structures designed following Eurocode 8 (UNI EN 1998-1, 2013).

The Section 7 reports main conclusions of the present work and future research outlook in Section 7.1 and 7.2, respectively.

2. State of the art

This Section 2 introduces topics relevant for the study of force reduction factor. Section 2.1 outlines main design methods, that are Force-Based Design (FBD), Direct Displacement-Based Design (DDBD) and Hybrid Force/Displacement-based seismic Design (HFD) methods. Section 2.2, 2.3 and 2.4 resumes the definition of force reduction factor, the ductility reduction factor for single-degree of freedom (SDOF) system and the ductility reduction factor multi-degree of freedom (MDOF) system, respectively. Section 2.5 introduces dual system structures. Section 2.6 briefly reports design standards of main international codes. Section 2.7 introduces the "N2 method" to assess nonlinear structural performance.

2.1. Design methods

The definition of force reduction factor, the ductility reduction factor for single-degree of freedom (SDOF) system and the ductility reduction factor multi-degree of freedom (MDOF) system are reported in Section 2.2, 2.3 and 2.4, respectively.

2.1.1. Force-Based Design (FBD) method

Pioneers of earthquake engineering were: Biot (1932), who introduced the formulation of what would later become known as the Response Spectrum Method (RSM); Housner (1959), who attempted to combine the response spectrum and the dissipation of seismic energy through plastic deformations, and Veletsos and Newmark (1960), who started to study the inelastic spectrum for the elastic-perfectly plastic structures.

The first to be developed and conventional procedure for seismic design of buildings is the force-based design (FBD) method. The performance of structures is checked in two levels, one ultimate limit state (ULS) and one serviceability limit state (SLS), subjected to two seismic intensities, respectively. Furthermore, the capacity design principle avoids local mechanism of collapse and brittle failure of structural elements.

The ULS is the performance level that guarantees the life safety of occupants and avoids complete collapse, but it allows the structure to damage. This limit state is associated with global collapse of the structure during a very strong earthquake. The resistance and energy-

dissipation capacity to be assigned to the structure are related to the extent to which its non-linear response is to be exploited. In other words, the elastic forces given by the response spectrum are divided by a force reduction factor or behavior factor representing the ductility capacity and the overstrength of the structure. Subsequently, the reduced forces are properly distributed along the height of the structure and elastic analyses are performed to determine the seismic response. Differently, the SLS corresponds to requirements governing normal use and durability state, so the structure has to be lightly damaged and inexpensively reparable after a low-intensity earthquake. This limit state is associated with frequent earthquakes and the structure responds elastically. The serviceability limit state is checked after the detailing of the structures.

Current design practice implies that the structure is first designed at the ULS and then checked at SLS following national or international standards, for instance UNI EN 1998-1 (2013) and DM 14/1/2008 (2008). The design spectrum at ULS is obtained by reducing the elastic spectrum with the reduction or behavior factor, given by design codes. A linear static analysis or an elastic dynamic analysis is then performed. Inelastic displacements are obtained from elastic displacements applying the "equal displacement rule". At the SLS, maximum interstorey drift ratios are checked in order to the limit the damage.

FBD is a robust method and easy to apply, furthermore it can be applied to any type of MDOF structure without the need of conversion of the multi-degree of freedom (MDOF) system into an equivalent single-degree of freedom (SDOF) system. It is noted that the FBD method is SDOF-free only concerning the application of the method but the force reduction factor on which it is based requires the definition of an equivalent SDOF system, as explained in Section 2.2. However, some shortcomings still remain in the method: (i) the force reduction factors are defined for different typologies of structural systems, but irrespectively of their geometry and ductility demand; (ii) the assumption of stiffness independent of strength is not valid (Priestley, 2003); (iii) the equal displacement rule is not always appropriate.

2.1.2. Direct Displacement-Based Design (DDBD) method

An alternative design method is the Direct Displacement-Based Design (DDBD) method, which is based on the concept of equivalent linearization (Priestley and Kowalsky, 2000; Priestley *et al*., 2007). A comprehensive description and comparison of various displacement-based seismic design methods may be found in Sullivan *et al*. (2003). This procedure uses the maximum interstorey drift ratio (IDR) for describing performance levels. Furthermore, the DDBD method replaces the MDOF structure by the equivalent linearized SDOF structure associated with the equivalent secant stiffness at the maximum displacement response. Inelastic displacement response spectrum is employed to determine the effective period of the SDOF system for the selected value of the target displacement and to compute the value of the effective damping.

The fundamentals of DDBD are briefly summarized in the following. Given m_i and Δ_i the floor masses and storey displacements and h_i the storey height, the design displacement Δ_d, effective mass m_e and effective height h_e are calculated as:

$$\Delta_d = \frac{\sum_{i=1}^{n_s} m_i \Delta_i{}^2}{\sum_{i=1}^{n_s} m_i \Delta_i} \quad (1)$$

$$m_e = \frac{\sum_{i=1}^{n_s} m_i \Delta_i}{\sum_{i=1}^{n_s} \Delta_d} \quad (2)$$

$$h_e = \frac{\sum_{i=1}^{n_s} m_i \Delta_i h_i}{\sum_{i=1}^{n_s} \Delta_d} \quad (3)$$

In addition to Δ_d, the bilinear envelope of the SDOF system is characterized by defining the yield displacement from which the displacement ductility demand, μ_Δ, is found. The μ_Δ is then used to determine the equivalent viscous damping ratio, ζ_e, representing the elastic damping and the hysteretic energy absorbed by the structure during inelastic deformations. Once the equivalent viscous damping ratio ζ_e is known, from the damping reduction factor, η_ζ given by Equation (4), the over-damped displacement spectrum is calculated and used to find the effective period of the structure, T_e, which corresponds to the period associated with the design displacement, Δ_d.

$$\eta_\zeta = \left(\frac{0.07}{0.02 + \zeta_e}\right)^{0.5} \quad (4)$$

From T_e and m_e the effective stiffness, K_e, of the structure and the design base shear force, V_b, are derived:

$$K_e = \frac{4\pi^2 m_e}{T_e{}^2} \quad (5)$$

$$V_b = K_e \Delta_d \quad (6)$$

As presented in Priestley *et al*. (2007), equations for calculating the equivalent viscous damping ratio, ζ_e, for different structural types and materials are proposed. For instance, the ζ_e for reinforced concrete wall and frame are given respectively by Equations (7) and (8):

$$\zeta_e = 0.05 + 0.444\left(\frac{\mu_\Delta - 1}{\mu_\Delta \pi}\right) \quad (7)$$

$$\zeta_e = 0.05 + 0.565\left(\frac{\mu_\Delta - 1}{\mu_\Delta \pi}\right) \quad (8)$$

The method is graphically explained in the following Figure 1.

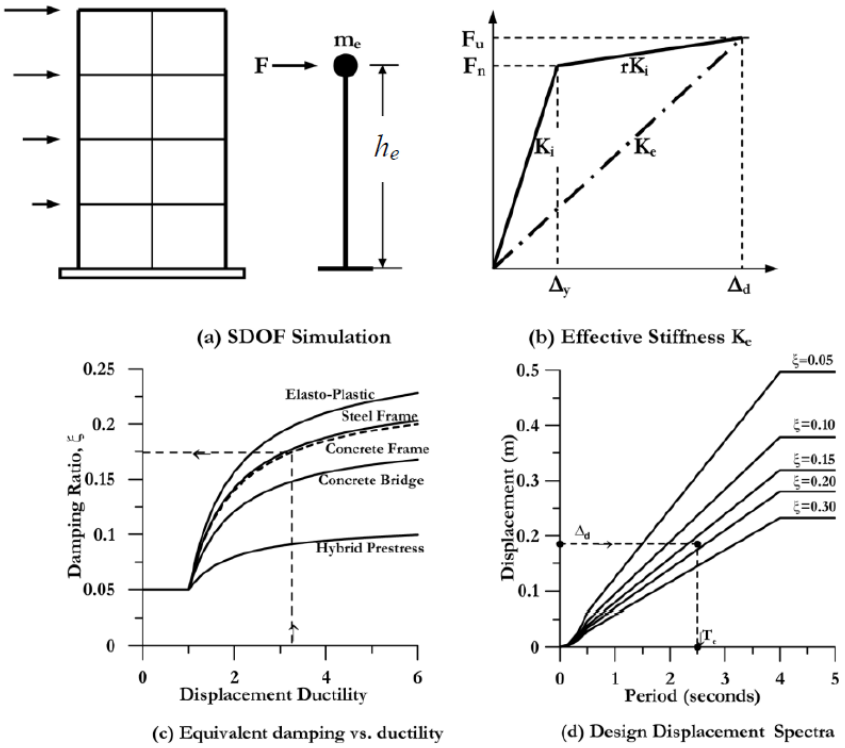

Figure 1: Fundamentals of DDBD, from Priestley *et al*. (2007).

Paulay (2002) and Sullivan *et al*. (2005, 2006) improved the DDBD in order to be applied to frame-wall structures. Furthermore, an innovative set of capacity design recommendations are developed to protect against undesirable plastic mechanisms by making allowance for the large higher mode forces that can develop in frame-wall structures.

More recently, Paparo and Beyer (2015) proposed a DDBD method for mixed reinforced concrete wall and unreinforced masonry wall (RC-URM) structures. Authors' objective is to develop two simple tools able to check the displacement profile of mixed RC-URM wall structures and to estimate the contribution of RC slabs to the overturning moment capacity of the dual system. Authors observed that the presence of RC walls provides a linear displacement profile over the height. The displacement shape of these mixed structures is estimated with the so-called "shear-flexure cantilever model", which treats flexural walls and frames as flexural and shear cantilevers respectively (Rosman, 1974; Pozzati, 1977). This is one of the simplified models to describe the interaction between shear and flexure dominated systems which has been studied over the last 50 years and it is still used by many authors in recent studies (Miranda and Akkar, 2006; Miranda and Taghavi, 2005; Taghavi and Miranda, 2005). Another approach to distribute lateral load between interconnected shear walls and frames is the "component stiffness method" (MacLeod, 1972), based on the conversion of a multi-bay frame to a single bay frame (MacLeod, 1971).

The DDBD method has some advantages: (i) displacement is the main parameter from the beginning of the design process, which allows the control of the damage; (ii) maximum interstorey drift ratio, used to describe performance levels, leads to a more uniform performance for structures; (iii) elastic design spectra are reduced through effective damping which depends on the displacement ductility demand. However, the introduction of an

equivalent SDOF systems occurs, which introduces a loss of modeling accuracy. Furthermore, the definition of the displacement design spectrum is required, which is not as familiar as the acceleration design spectrum.

2.1.3. Hybrid Force/Displacement-based seismic Design (HFD) method

A further seismic design method is explained in detail by Tzimas *et al.* (2013). It is called the Hybrid Force/Displacement-based seismic Design (HFD) method and it was developed for steel building frames. The HFD method adopts the performance-based seismic design philosophy. The starting point in the HFD method is the maximum allowable roof displacement of the MDOF structure computed through a new simple expression proposed by Karavasilis *et al*. (2008a,b,c), which takes into account structure properties and seismic excitation characteristics. Then, a new relation for the calculation of the behavior factor is proposed.

In the following, fundamental steps of the HFD are described and for the sake of brevity, expressions for regular moment resisting frame (MRF) are presented only. At the beginning of the process local ductilities and geometrical and mechanical attributes are defined. Because the method is developed for steel buildings, authors suggest to obtain initial estimate of input variables by designing the steel frame only for strength requirements under a frequent occurred earthquake (SLS) by assuming elastic behavior, i.e., with elastic spectra, combined to capacity design rules. Through the use of some expressions, these initial inputs are transformed in roof displacement. The design target roof displacement, $u_{rmax(d)}$, is defined as the minimum value of the roof displacement due to maximum interstorey drift ratio, $u_{rmax(IDR)}$, and the roof displacement due to local ductility, $u_{rmax(\mu)}$.

$$u_{rmax(d)} = \min\{u_{rmax(IDR)}, u_{rmax(\mu)}\} \tag{9}$$

where:

$$u_{rmax(IDR)} = \beta \cdot IDR_{max} \cdot H \tag{10}$$

$$u_{rmax(\mu)} = \mu \cdot u_{ry} \tag{11}$$

$$\beta = 1 - 0.19(n_s - 1)^{0.54}\rho^{0.14}\alpha^{-0.019} \tag{12}$$

$$\mu = 1 + 1.35(\mu_\theta - 1)^{0.86}\alpha^{-0.019}{n_s}^{-0.31} \tag{13}$$

where H is the building height; n_s the number of storeys; ρ the column-to-beam stiffness ratio; α the beam-to-column stiffness ratio; u_{ry} the yield roof displacement; μ_θ the maximum local ductility, i.e., rotation ductility for beams/columns. The calculation of the design value of the roof displacement ductility and the corresponding behavior factor is given by:

$$\mu_d = \frac{u_{rmax(d)}}{u_{ry}} \tag{14}$$

$$for\ \mu_d \leq 5.8 \qquad q = 1 + 1.39(\mu_d - 1) \tag{15}$$

$$for\ \mu_d > 5.8 \qquad q = 1 + 8.84({\mu_d}^{0.32} - 1) \tag{16}$$

Equations (15) and (16) are empirical and obtained by analyses regression. The method is finally completed by an elastic modal analysis procedure with ULS spectrum reduced with the behavior factor q.

This method tries to overcome the limit of both FBD and DDBD methods: (i) it avoids the use of an equivalent SDOF system as in DDBD method; (ii) displacements are input parameters; (iii) force reduction factor are more rational and adaptable than the ones in FBD method. The HFD has the disadvantage to need empirical expressions to provide the drift profile of the structure and the force reduction factor. These expressions may be available by Karavasilis *et al*. (2008a,b,c) for steel building frames, but similar expressions are needed for other kinds of system in order to apply HFD.

2.2. Force reduction factor

The value of the force reduction factor mainly depends on the ductility of the structure, on the strength reserves that normally exist in a structure, which is based mainly on its structural redundancy and on the overstrength of individual members, and on the damping of the structure; all these factors directly affect the energy dissipation capacity of a structure. An appropriate and general definition of the force reduction factor is suggested in the following form by ATC-19 (1995):

$$R = R_\mu R_s R_\zeta \approx R_\mu R_s \tag{17}$$

where R_μ is the ductility-dependent component, R_s the overstrength-dependent component, and R_ζ the damping-dependent component of the force reduction factor, which usually is neglected by codes; the latter is of interest mainly in the case of structures with supplemental damping device. A separate factor relating to the structural redundancy only, R_r, is also introduced, but usually it is included in R_s.

The ductility reduction factor for a SDOF system, $R_{\mu,SDOF}$, is defined as the ratio of the lateral yielding strength required to maintain the system elastic, $V_{b,SDOF}(\mu = 1)$, to the lateral yielding strength required to maintain the displacement ductility demand less or equal to a target displacement ductility, $V_{b,SDOF}(\mu = \mu^*)$.

$$R_{\mu,SDOF} = \frac{V_{b,SDOF}(\mu = 1)}{V_{b,SDOF}(\mu = \mu^*)} \tag{18}$$

The ductility is defined as the ratio of an ultimate or failure quantity and a yield quantity.

For a SDOF system, the top displacement ductility, μ, is equal to interstorey drift ductility, μ_{IDR}, and storey displacement ductility, μ_{Δ}. Let us recall that the story displacement is defined as the displacement difference between the storey i and the bottom storey $i-1$; the interstorey drift is the storey displacement divided by the storey height, h_s.

$$\mu_{IDR} = \frac{IDR_u}{IDR_y} = \frac{\frac{\Delta_u}{h_s}}{\frac{\Delta_y}{h_s}} = \frac{\Delta_u}{\Delta_y} = \frac{d_{u,i} - d_{u,i-1}}{d_{y,i} - d_{y,i-1}} = \mu_{\Delta} \xrightarrow{SDOF\ system} \mu_{IDR} = \mu_{\Delta} = \mu = \frac{d_u}{d_y} \tag{19}$$

Generally, structures have a much more complex behavior than SDOF systems, and the force reduction factors have to be adapted in order to be valid for MDOF systems. Thus, the, $R_{\mu,SDOF}$, needs to be modified for the design of MDOF structures, $R_{\mu,MDOF}$, multiplying it by the modification factor, R_M, that takes into account the amplification of the base shear due to higher mode effects:

$$R_{\mu,MDOF} = R_M R_{\mu,SDOF} \tag{20}$$

$$R_{\mu,MDOF} = \frac{V_{b,SDOF}(\mu = 1)}{V_{b,MDOF}(\mu = \mu^*)} \tag{21}$$

$$R_M = \frac{V_{b,SDOF}(\mu = \mu^*)}{V_{b,MDOF}(\mu = \mu^*)} \tag{22}$$

The overstrength-dependent component, R_s, of the force reduction factor is not object of the present work and for the purpose of this study R_s is evaluated by means of nonlinear analyses in design examples of Section 6. Detailed information about the overstrength can be found in Mwafy and Elnashai (2002), Elnashai and Mwafy (2002) and Aydemir M.E. and Aydemir C. (2016).

2.3. Ductility reduction factor for SDOF systems

A lot of research have been done in the past about the ductility reduction factor for SDOF systems and several expressions have been proposed. These studies concluded that the two parameters mainly governing the ductility reduction factor are the displacement ductility and the fundamental period of the system. A review and comparison of these works is presented in detail by Miranda and Bertero (1994). In this section, main studies that investigated force reduction factor for SDOF systems are reviewed.

Newmark and Hall (1973) developed expressions for $R_{\mu,SDOF}$ based on elastic and inelastic response of El Centro ground motion. The parameters that control the reduction factor are

the fundamental period, the ductility and the properties of the ground motion spectra. The authors observed that: (i) in the long-period and medium-period spectral regions, an elastic and inelastic system have approximately the same maximum displacement, i.e. $R_{\mu,SDOF} \propto \mu$; (ii) in the extremely short-period region, an elastic and inelastic system have approximately the same force $R_{\mu,SDOF} \cong 1$; (iii) in the moderately low period region, the principles of conservation of energy can be valid, and $R_{\mu,SDOF} \propto \sqrt{2\mu - 1}$.

Riddel and Newmark (1979) proposed force reduction factors for SDOF systems based on elastic and inelastic response of 10 ground motions recorded on rock and alluvium sites. Authors improved expressions of Newmark and Hall (1973) including more parameters such as the damping ratio, but expression became more complex.

Lai and Biggs (1980) proposed more simplified expression for $R_{\mu,SDOF}$ based on elastic and inelastic response of 20 artificial ground motions whose elastic response spectra were compatible with the elastic design spectra of Newmark and Hall (1973). In this study, the parameters that control the reduction factor are the fundamental period, T, and the ductility, μ, only. Their proposed expression, given by Equation (23), is applicable to whole period range, but regression coefficients, α and β, were defined in three period ranges and listed in Table 1.

$$R_{\mu,SDOF} = \alpha + \beta \log T \tag{23}$$

Table 1: Parameters α and β in Lai and Biggs (1980).

Period range	Coefficient	$\mu = 2$	$\mu = 3$	$\mu = 4$	$\mu = 5$
$0.1 \leq T < 0.5\ s$	α	1.6791	2.2296	2.6587	3.1107
	β	0.3291	0.7296	1.0587	1.4307
$0.5 \leq T < 0.7\ s$	α	2.0332	2.7722	3.3700	3.8336
	β	1.5055	2.5320	3.4217	3.8323
$0.7 \leq T < 4.0\ s$	α	1.8409	2.4823	2.9853	3.4180
	β	0.2642	0.6605	0.9380	1.1493

Expressions proposed by Newmark and Hall (1973), Riddel and Newmark (1979) and Lai and Biggs (1980) are compared in Figure 2.

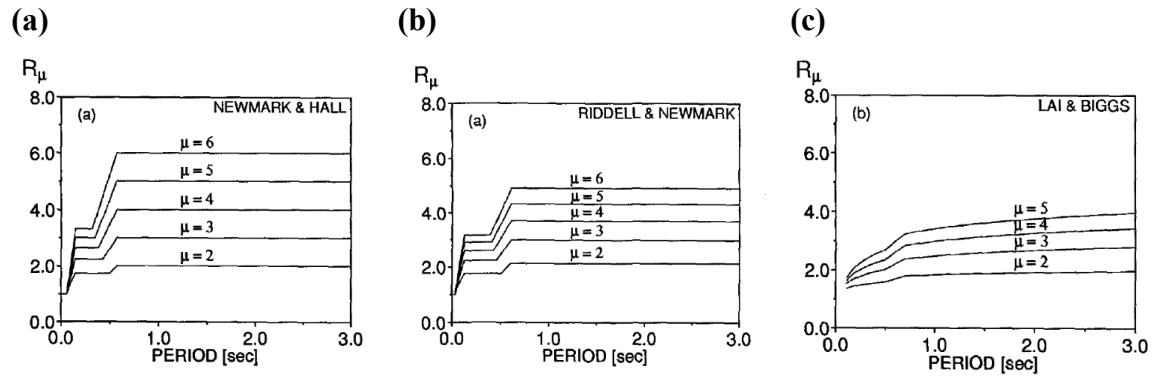

Figure 2: (a): Newmark and Hall (1973), (b): Riddel and Newmark (1979), (c): Lai and Biggs (1980); figures from Miranda and Bertero (1994).

Riddel et al. (1989) introduced other simplifications to obtain two expressions to cover the period range of interest and regression coefficients, R^* and T^*, listed in Table 2, referred to ductility only. R^* is the ductility reduction factor for periods higher than the characteristic period T^*. The study is based on four sets of earthquake records computed for SDOF systems with an elasto-plastic hysteretic behavior.

$$for\ 0 \leq T \leq T^* \qquad R_{\mu,SDOF} = 1 + \frac{R^* - 1}{T^*} T \tag{24}$$

$$for\ T > T^* \qquad R_{\mu,SDOF} = R^* \tag{25}$$

Table 2: Parameters R^* and T^* in Riddel et al. (1989).

Parameter	$\mu = 2$	$\mu = 3$	$\mu = 4$	$\mu = 5$	$\mu = 6$	$\mu = 7$	$\mu = 8$
R^*	2.0	3.0	4.0	5.0	5.6	6.2	6.8
T^*	0.1	0.2	0.3	0.4	0.4	0.4	0.4

Hidalgo and Aria (1990) refined the previous work in order to obtain one nonlinear expression applicable in the whole period range. Parameters k and T_0 were reported to vary for different groups of ground motions.

$$R_{\mu,SDOF} = 1 + \frac{T}{kT_0 + \frac{T}{\mu - 1}} \tag{26}$$

Expressions proposed by Riddel et al. (1989) and Hidalgo and Aria (1990) are reported in Figure 3.

(a) **(b)**

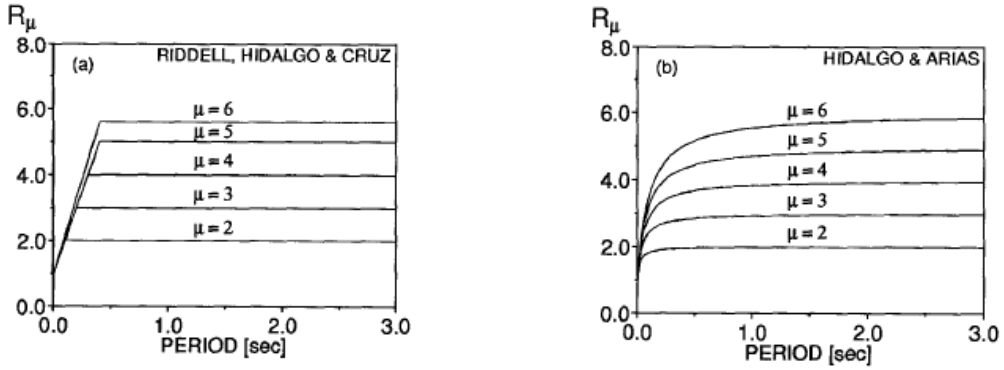

Figure 3: (a): Riddel et al. (1989), (b): Hidalgo and Aria (1990); figures from Miranda and Bertero (1994).

Nassar and Krawinkler (1991) proposed a regression expression based on the response of SDOF nonlinear systems subjected to 15 ground motions with 5% critical damping. The sensitivity to different natural periods, yield level, strain hardening ratio and inelastic material behavior was examined. Based on mean strength reduction factors, the following expression was proposed:

$$R_{\mu,SDOF} = (c(\mu - 1) + 1)^{\frac{1}{c}} \tag{27}$$

where:

$$c = \frac{{T_1}^a}{1 + {T_1}^a} + \frac{b}{T_1} \tag{28}$$

where: T_1 is the fundamental period and parameters a and b are defined as a function of the rate α, i.e. the ratio of the post-yield stiffness and the initial stiffness of the system expressed in per cent. Parameters a and b are given by the following expressions:

$$a = 1 + 0.5\alpha \quad (29)$$

$for\ 0.00 \leq \alpha \leq 0.02$

$$b = 0.42 - 2.5\alpha \quad (30)$$

$$a = 1.0625 - 2.625\alpha \quad (31)$$

$for\ 0.02 \leq \alpha \leq 0.10$

$$b = 0.39 - \alpha \quad (32)$$

$$a = 0.80 \quad (33)$$

$for\ \alpha > 0.10$

$$a = 0.29 \quad (34)$$

Which are derived by interpolation of the values reported in Table 3.

Table 3: Parameters a and b in Nassar and Krawinker (1991).

$\boldsymbol{\alpha}$	$\boldsymbol{a}$	$\boldsymbol{b}$
0.00	1.00	0.42
0.02	1.01	0.37
0.10	0.80	0.29

Vidic *et al*. (1994) studied the reduction factors for bilinear and stiffness degrading SDOF systems based on elastic and inelastic response of 20 recorded ground motion sets with 5% damping ratio. The parameters that control the reduction factor are the fundamental period, T, the ductility, μ, and the properties of the ground motion spectra. The simplified expressions consist in two linear segments inspired by the work of Riddel et al. (1989):

$for\ T \leq T_0$ $$R_{\mu,SDOF} = 1 + (\mu - 1)\frac{T}{T_0} \quad (35)$$

$for\ T > T_0$ $$R_{\mu,SDOF} = \mu \quad (36)$$

where T_0 is defined as a function of the properties of the ground motion spectra:

$$T_0 = 0.65\mu^{0.3}T_1 \quad (37)$$

$$T_1 = 2\pi\frac{\varphi_{ev}V}{\varphi_{ea}A} \quad (38)$$

where φ_{ev} and φ_{ea} are amplification factors; A and V are the maximum ground acceleration and maximum ground velocity, respectively.

Expressions proposed by Nassar and Krawinker (1991) and Vidic *et al*. (1994) are plotted in Figure 4.

(a) **(b)**

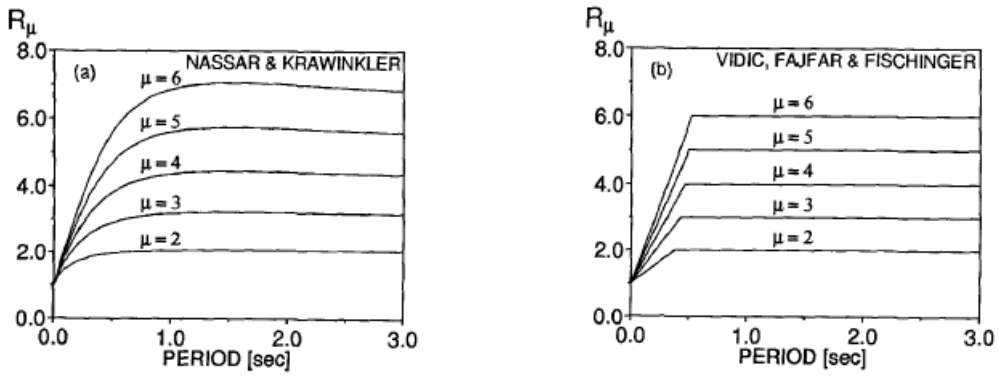

Figure 4: (a): Nassar and Krawinker (1991), (b): Vidic *et al*. (1994); figures from Miranda and Bertero (1994).

To the best of author's knowledge, Elghadamsi and Mohraz (1987) firstly studied the effect of soil conditions on the force reduction factor for SDOF system, but the work of Miranda (1993) made an effort to consider 124 recorded ground motions on a wide range of soil conditions. Authors proposed three expressions for force reduction factor on rock, alluvium and soft soils sites respectively:

$$R_{\mu,SDOF} = 1 + \frac{\mu - 1}{\Phi} \geq 1 \tag{39}$$

where:

$$for\ rock\ sites \qquad \Phi = 1 + \frac{1}{10T - \mu T} - \frac{1}{2T}\exp\left[-\frac{3}{2}\left(\ln T - \frac{3}{5}\right)^2\right] \tag{40}$$

$$for\ allluvium\ sites \qquad \Phi = 1 + \frac{1}{12T - \mu T} - \frac{2}{5T}\exp\left[-2\left(\ln T - \frac{1}{5}\right)^2\right] \tag{41}$$

$$for\ soft\ soil\ sites \qquad \Phi = 1 + \frac{T_g}{3T} - \frac{3T_g}{4T}\exp\left[-3\left(\ln\frac{T}{T_g} - \frac{1}{4}\right)^2\right] \tag{42}$$

where: T_g is the predominant period of the ground motion.

Expressions proposed Miranda (1993) are plotted in Figure 5.

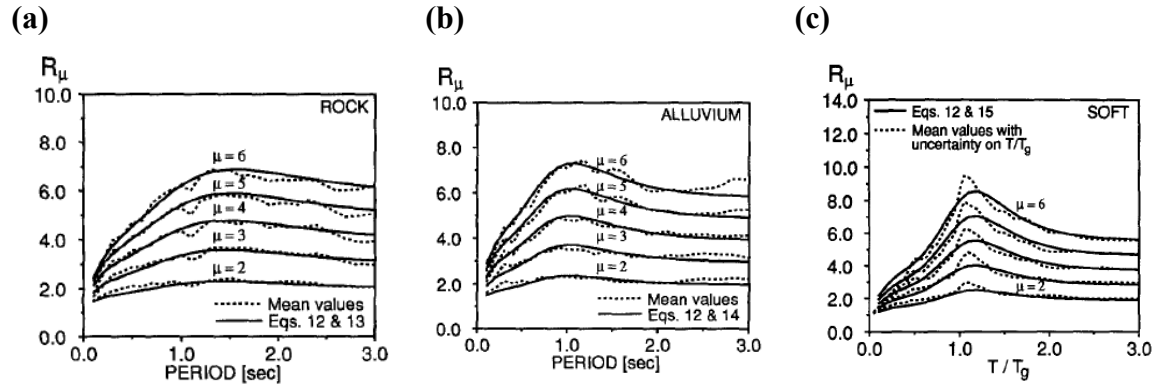

Figure 5: Miranda (1993): (a): rock sites, (b): alluvium sites; (c): soft soil sites; figures from Miranda (1993)

The influence of soil condition is assessed also by Watanabe and Kawashima (2002). Authors developed reduction factors for bilinear SDOF systems based on elastic and inelastic response of 70 recorded ground motion with 5% damping. Stiff, moderate and soft soils were evaluated. This study focuses on the effect of damping ratios. and provides quite close results than the ones proposed by Nassar and Krawinkler (1991) and Miranda and Bertero (1994), if damping ratios are assumed equal to 5%.

Borzi and Elnashai (2000) proposed trilinear expressions of reduction factor for elastic perfectly-plastic and hysteretic hardening-softening models of SDOF systems based on elastic and inelastic response of 364 recorded ground motions. Authors concluded that hysteretic models examined only mildly influenced the inelastic acceleration spectra. Therefore the force reduction factor is not heavily influenced by the system global hysteretic behavior.

An alternative method, based on the observed similarity between elastic displacement spectra and spectra of strength-reduction factors, is developed by Ordaz and Perez-Rocha (1998). Authors proposed a rule to estimate the ductility reduction factor which depends only on elastic displacement spectra and two empirically determined parameters, but a physical interpretation of the proposed rule is unknown to the authors.

Vamvatsikos and Cornell (2006) introduced SPO2IDA, a software tool that is capable of recreating the seismic behaviour of SDOF systems with bilinear up to quadrilinear backbones. It provides a direct connection between the static pushover curve and the results of incremental dynamic analysis, a computer-intensive procedure that offers thorough demand and capacity prediction capability by using a series of nonlinear dynamic analyses under a suitably scaled suite of ground motion records. SPO2IDA, is a tool for performance-based earthquake engineering that can estimate demands and limit-state capacities, strength reduction R-factors and inelastic displacement ratios for SDOF systems.

2.4. Ductility reduction factor for MDOF systems

As shown in Section 2.3, several authors studied the force reduction factor for SDOF systems. In this section, main literature about the force reduction factor for MDOF systems is presented.

To the author's knowledge, the relationship between MDOF and SDOF system response was first studied by Veletsos and Vann (1971). The objective of their study was to identify the parameters which have a dominant influence on the response of MDOF elastoplastic systems. The systems considered were shear-building structures. This study concluded that for systems having two and three degrees of freedom, the relationship between the required yield deformation and the absolute maximum deformation of the associated linear system could be considered the same as that for a SDOF system with the same period. Instead, for systems having more than three degrees of freedom, the proposed design rules for SDOF systems were not sufficiently accurate and could lead to unconservative estimates of the required lateral yield resistance, and that errors tended to increase as the number of degrees of freedom increased.

Nassar and Krawinkler (1991) studied three types of simplified MDOF models to estimate the modifications required to the inelastic strength demands obtained from bilinear SDOF systems in order to limit the story ductility demand in the first story of the MDOF systems to a prescribed value. The three types of MDOF models were "beam-hinge" frame in which plastic hinges could be formed in beams only; "column hinge" frame in which plastic hinges could be formed in columns only; "weak story" frame in which plastic hinges could be formed in columns of the first story only. The ductility demands in the MDOF models were compared to those of the SDOF systems when subjected to the same ground motions as those used for the SDOF systems. The study concluded that MDOF story ductility demands differ significantly from those of the corresponding SDOF systems and the failure mechanism strongly affect the force reduction factor.

The amplification of base shear in MDOF systems respect to SDOF systems was explained by Chopra (1995). Buildings with 2, 5, 10, 20, 30 and 40 number of storeys, idealised as elastoplastic shear frames, were analysed. Base shear of these MDOF systems were compared with the base shear of their corresponding SDOF systems. In the linearly elastic range, natural period and damping ratio of the SDOF system were the same as the fundamental mode properties of the MDOF system. The mass of the corresponding SDOF system was the same as the total mass of the MDOF system. Both systems were elastoplastic with identical values for the yield base shear. Systems were subjected to El Centro ground motion. Author calculated the inverse of the modification factor, R_M, which is given by Equation (22):

$$\frac{1}{R_M} = \frac{V_{b,MDOF}(\mu = \mu^*)}{V_{b,SDOF}(\mu = \mu^*)} \tag{43}$$

Results for the inverse of the modification factor given by (43) is shown in Figure 6. The author observed that: (i) MDOF system has larger base shear than the corresponding SDOF system; (ii) the modification factor decreases with the increasing of period and hence the number of storeys; (iii) the modification factor decreases with the allowable ductility.

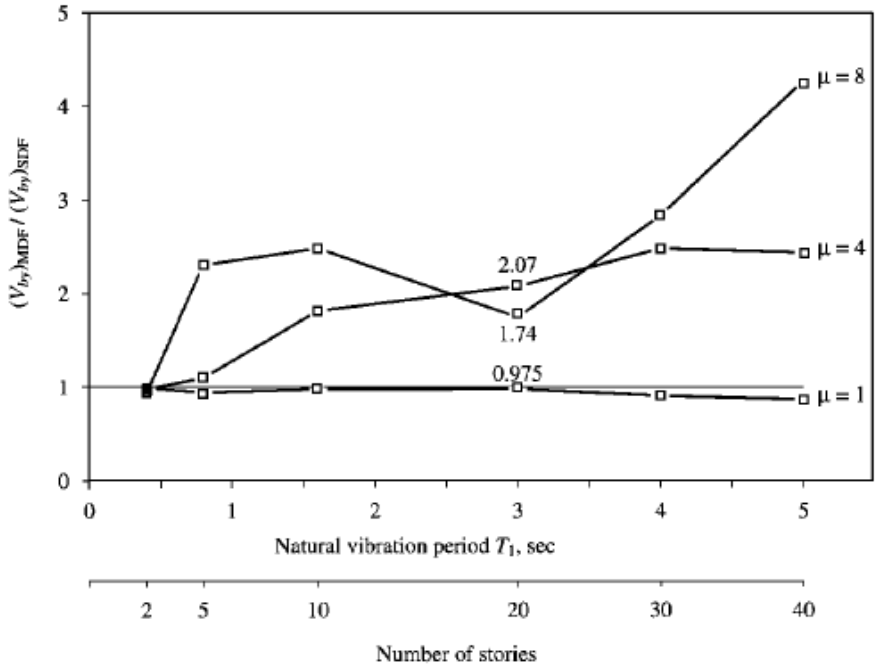

Figure 6: Inverse of modification factor; figure from Chopra (1995).

Moghaddam and Mohammadi (2001) studied the inelastic seismic response of MDOF shear-building structures; in this study, 5, 10, 15 storey buildings were subjected to 21 recorded ground motion with 5% damping and the following correlation between the modification factor, R_M, and the number of storeys, n_s, was proposed.

$$R_M = {n_s}^{-0.26} \tag{44}$$

Santa-Ana and Miranda (2000) and Santa-Ana (2004) proposed a method to evaluate force reduction factors which permits to estimate the strength demand of MDOF systems from strength demand of SDOF systems. The equivalent SDOF system has the same mass and fundamental period of the respective MDOF system. The study is based on the computation of modification factors for ten steel moment-resisting frame buildings undergoing different levels of inelastic deformation when subjected to 92 earthquake ground motions corresponding to firm and soft sites. The R_M was evaluated by following this methodology: (i) MDOF system base shear, $V_{b,MDOF}$, was computed by scaling the intensity of the ground motion until the maximum storey displacement ductility ratio in the MDOF structure was equal to the maximum allowable ductility, μ^*, within a 1% tolerance. The scaling factor was obtained by an iterative procedure; (ii) SDOF system base shear, $V_{b,SDOF}$, was computed by iteration on the lateral strength of the SDOF system when subjected to the same ground motion and same scale factor of the step (i) until the displacement ductility ratio in the MDOF structure was, within a 1% tolerance, equal to the maximum allowable ductility, μ^*. Authors concluded that: (i) lateral strengths required to control maximum story ductilities in multi-storey buildings are typically larger than those of SDOF systems having periods of vibration equal to the fundamental period of the MDOF structures; (ii) mean ratios of MDOF to SDOF lateral strength demands increase with the number of stories; (iii) from a limited number of results it appears that ratios of MDOF to SDOF lateral strength demands are more affected by the number of stories than by the fundamental period of vibration; (iv) for the

site classes considered in this study, soil conditions have only a small effect on mean ratios of MDOF to SDOF lateral strength demands.

Wang *et al.* (2013) studied the inelastic seismic response of 100 MDOF shear-building structures, on four ground type. In this study, lumped-mass shear-type MDOF systems were employed to investigate on the modification factor, R_M. Equivalent SDOF system was modelled corresponding to each MDOF system, with same total mass and same fundamental period. Systems were subjected to five recorded ground motion with 5% damping. Authors drew the following conclusions: (i) the modification factor is mainly affected by the ductility ratio, μ, and fundamental period, T, and it usually decreases with the increment of ductility ratio and fundamental period; (ii) the site conditions have small effects on the modification factor. The regression expression proposed by authors is given by:

$$R_M = (0.01\mu^2 - 0.10\mu + 0.47)(0.75T^2 - 2.40T + 4.26) \tag{45}$$

Wang *et al*. (2014) continued the previous work to compare flexural-type building structures and shear-type building structures. Multi-mass column cantilever systems were employed to simulate flexure-type shear wall structures, while multi-mass series spring connection systems were used to simulate shear-type frame structures. Four earthquake records in hard soil site were selected to perform nonlinear dynamic time history analysis. Results are illustrated in Figure 7. Main conclusions drawn from this study were: (i) the seismic response in terms of structural displacement ductility, base shear and top displacement in flexural-type structures are different from those in shear-type systems, due to different deformation mechanism; (ii) storey ductility and number of storeys have significant influence on ductility reduction factors; (iii) the ductility reduction factors of flexural-type structure are generally about 40% larger than those for shear-type structures.

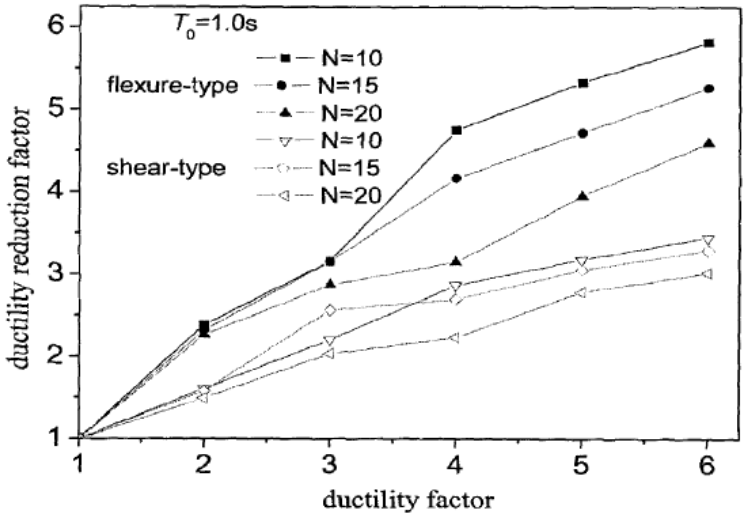

Figure 7: Ductility reduction factors for flexural-type and shear-type structures; figures from Wang *et al*. (2014).

Gerami *et al*. (2015) studied the influence of higher mode effects on MDOF systems. They proposed modification factors performing 1764 nonlinear dynamic analysis of two-dimensional steel frames with moment-resisting system. Systems were subjected to 14

recorded ground motion with 5% damping. Results showed that the $R_{\mu,MDOF}$ decreases with the period and contribution of higher modes. Therefore, neglecting these effects would lead to non-conservative design results, especially for high-rise buildings. In other words, if the structure is designed on the basis of code proposed reduction factor, R, for the flexible models with long period, the expected behavior is not realistic since during the earthquake, the demand base shear is greater than the code base shear due to higher mode effects.

FEMA P695 (2009) describes a recommended methodology for a reliable quantification of structural system performance and response parameters for seismic design applications. This methodology consists of a framework for establishing seismic performance factors that involves the development of detailed system design information and probabilistic assessment of collapse risk. It utilizes nonlinear analysis techniques, and explicitly considers uncertainties in ground motion, modeling, design, and test data. The technical approach is a combination of traditional code concepts, advanced nonlinear dynamic analyses, and risk-based assessment techniques. The procedure completely bypasses the SDOF approach and offers force reduction factors that are directly but quite expensively computed on the basis of MDOF structures.

This FEMA P695 methodology provides a rational basis for establishing global seismic performance factors, including the force reduction factor and the overstrength factor of seismic resisting systems. Collapse assessment is performed using both nonlinear static and nonlinear dynamic analysis procedures. Nonlinear static analyses are used to help validate the behavior of nonlinear models and to provide statistical data on system overstrength and ductility capacity. Nonlinear dynamic analyses are used to assess median collapse capacities and collapse margin ratios. The trial value of the force reduction factor is evaluated in terms of the acceptability of a calculated collapse margin ratio, which is the ratio of the ground motion intensity that causes median collapse, to the Maximum Considered Earthquake (MCE) ground motion intensity defined by the building code. For collapse evaluation, ground motions are systematically scaled to increasing earthquake intensities until median collapse is established. If the collapse margin ratio is large enough to result in an acceptably small probability of collapse at the MCE, then the trial value of force reduction factor is acceptable.

2.5. Dual system RC structures

Dual system structures represent all structural system composed of two different resisting systems which collaborate to support gravity loads and seismic loads. The two coupled systems can be also different in materials, such as reinforced concrete and masonry systems or reinforced concrete and steel systems. In the present work, the considered dual system systems are RC frame-wall structures, but the proposed method is general and can be applied to other dual structures. A typical portrayal of wall system building, frame system building and frame-wall dual system building are shown in Figure 8 respectively.

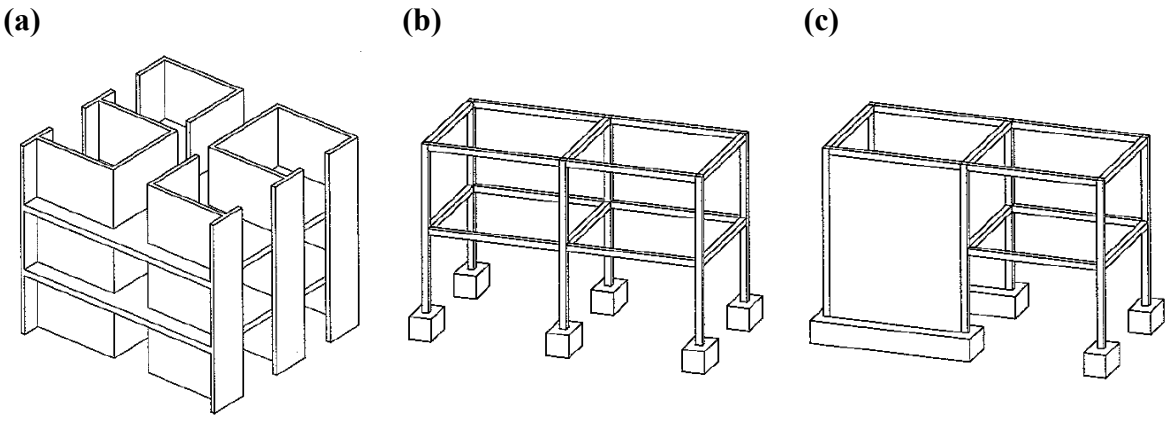

Figure 8: (a): Wall system building, (b): Frame system building, (c): Frame-wall dual system building; figures from Arie, G. (2003).

RC frame-wall structures, provide a good structural solution able to combine the stiffness and resistance of the walls and the versatility of the frame. Furthermore, coupling two resisting systems allows overcoming structural deficiencies of single resisting systems and takes advantages by synergy. It is evidenced that frame structures are versatile and allow architectural flexibility, but they are deformable especially at low stories. On the other hand, wall system structures are very stiff at low stories but they impose rigid architectural constrains to openings and windows.

Static behavior of frame-wall systems subjected to horizontal actions is well known thanks to early studies performed in 60's and 70's (Goodsir, 1985). Among them, the "shear-flexural cantilever model" (Rosman, 1974; Pozzati, 1977; Miranda and Akkar, 2006; Miranda and Taghavi, 2005; Taghavi and Miranda, 2005) shows accurate results regarding the distribution of horizontal loads between two coupled systems. However, this method presents the shortcoming to be valid for elastic analysis only, while the response of dual systems in the nonlinear field is necessary to perform an efficient and reliable seismic design. To the author's knowledge, advanced studies on simplified and effective models to represent the dynamic behaviour of dual systems are not available.

Usually building codes define force reduction factors for various type of resisting systems but they do not provide accurate force reduction factor for dual systems, with the exception of some particular cases. Furthermore, force reduction factors are constant for a certain type of structural system. As a result of this, for the same design input, structures of the same type but different geometry are subjected to different ductility demands and show therefore a different performance during an earthquake.

2.6. Design codes

The force-based design method as it is implemented in the current generation of seismic design codes suffers from some shortcomings. One of these relates to the fact that the base shear is computed using a pre-defined force reduction factor. Furthermore, the Force-Based Design approach is difficult to apply to dual structural systems for which only few codes

provide force reduction factors. In this section, design codes focused on reinforced concrete (RC) structures only are reported.

To the author's knowledge, the force reduction factor firstly appears in the SEAOC Blue Book (1959) in an attempt to unify the design approach providing minimum standards to structures. Before the Blue Book, the Uniform Building Code, UBC (ICBO, 1958), regulations calculated lateral force without considering structural system effects and the lateral force, F, was a constant percentage of total building weight, W, as shown in Equation (46).

$$F = 0.075\mathrm{W} \tag{46}$$

The 1959 edition of the Blue Book introduced a force reduction factor called "K factor" to address different building type as well as redefining the "C factor", which is a horizontal force factor depending on the fundamental period, T. Lateral base shear, V, was given by:

$$V = \mathrm{KCW} \tag{47}$$

$$C = \frac{0.05}{\sqrt[3]{T}} \tag{48}$$

The numerical coefficient based on basic structural system, K, was intended to modify the base shear using a number representing bonus characteristics of the structure in question and prescribed values are shown in Table 4.

Table 4: Basic value of the "K factor", SEAOC Blue Book (1959).

Basic structural system	***K***
Bearing wall	1.33
Building frame	1.00
Dual	0.80
Moment resisting frame	0.67

After few decades of evolution of seismic codes, a briefly overview of main current design codes is presented. Eurocode 8 (UNI EN 1998-1, 2013) defines force reduction factor – called behavior factor – for reinforced concrete buildings to account for energy dissipation capacity as follows:

$$q = q_0 k_w \geq 1.5 \tag{49}$$

Where q_0 is the basic value of the behavior factor, depending on the type of the structural system and on its regularity in elevation; k_w is the factor reflecting the prevailing failure mode in structural systems with walls (equal to 1 for frame and frame-equivalent dual systems). The design spectrum is obtained dividing the elastic spectrum ordinates by q. Basic value of the behavior factor for systems regular in elevation are given in the following Table

5; structures are distinguished for medium ductility class (DCM) and high ductility class (DCH) structures, respectively.

Table 5: Basic value of the behavior factor, q_0, for systems regular in elevation, UNI EN 1998-1 (2013).

Structural type	**DCM**	**DCH**
Frame system, dual system, coupled wall system	$3.0\alpha_u/\alpha_1$	$4.5\alpha_u/\alpha_1$
Uncoupled wall system	3.0	$4.0\alpha_u/\alpha_1$
Torsionally flexible system	2.0	3.0
Inverted pendulum system	1.5	2.0

The ratio α_u/α_1 represents the overall structural overstrength: α_1 is the value by which the horizontal seismic design action is multiplied in order to reach the first flexural resistance in any member of the structure, while all other design actions remain constant; α_u is the value by which the horizontal seismic design action is multiplied, in order to form plastic hinges in a number of sections sufficient for the development of the overall structural instability, while all other design actions remain constant. When the multiplication factor α_u/α_1 has not been evaluated through an explicit calculation, for buildings which are regular in plan the approximate values of α_u/α_1 reported in Table 6 may be used.

Table 6: Basic value of α_u/α_1 for systems regular in plan, UNI EN 1998-1 (2013).

Frames or frame-equivalent dual systems	$\boldsymbol{\alpha_u/\alpha_1}$
One-storey buildings	1.1
Multistorey, one-bay frames	1.2
Multistorey, multi-bay frames or frame-equivalent dual structures	1.3
Walls or wall-equivalent dual systems	$\boldsymbol{\alpha_u/\alpha_1}$
Wall systems with only two uncoupled walls per horizontal direction	1.0
Other uncoupled wall systems	1.1
Wall-equivalent dual, or coupled wall systems	1.2

Building irregularities are taken into account in the following ways: for buildings which are not regular in elevation, the value of q_0 should be reduced by 20%; for buildings which are not regular in plan, the approximate value of α_u/α_1 that may be used is equal to the average of 1.0 and of the value given in the previous Table 6.

The Italian Building Code (DM 14/1/2008, 2008) assumes the same definition and the same values of Eurocode 8 for the force reduction factor concerning RC structures.

The American Society of Civil Engineers (ASCE) in the Minimum Design Loads for Buildings and Other Structures (ASCE/SEI 7-10, 2010) prescribes force reduction factors for several structural systems. Concerning dual system structures, reinforced concrete (RC) moment resisting frames (MRF) and steel frames coupled with shear walls systems are identified. In particular, the force reduction factors for frame-wall systems are shown in the following Table 7; ordinary, intermediate and special elements are expected to withstand

minimal, moderate and significant inelastic behaviour, therefore the stringency of the detailing requirements is related to the expected behaviour.

Table 7: Basic value of the reduction factor for frame-wall systems, ASCE/SEI 7-10 (2010).

Seismic force-resisting system	**R**
Special RC shear walls and special RC-MRF	7.0
Special RC shear walls and intermediate RC-MRF	6.5
Ordinary RC shear walls and special RC-MRF	6.0
Ordinary RC shear walls and intermediate RC-MRF	5.5
Ordinary RC shear walls and ordinary RC-MRF	4.5

The seismic base shear, V, in a given direction shall be determined in accordance with the following equation:

$$V = C_s W \tag{50}$$

where W is the effective seismic weight and $C_s(T)$ is the seismic response coefficient at the period T that is given by:

$$for\ T \le T_L \qquad C_s(T) = \frac{S_{DS}(T)}{\left(\frac{R}{I_e}\right)} \le \frac{S_{D1}(T)}{T\left(\frac{R}{I_e}\right)} \tag{51}$$

$$for\ T > T_L \qquad C_s(T) = \frac{S_{DS}(T)}{\left(\frac{R}{I_e}\right)} \le \frac{S_{D1}(T)T_L}{T^2\left(\frac{R}{I_e}\right)} \tag{52}$$

where S_{DS} is the design spectral response acceleration parameter at short periods; S_{D1} is the design spectral response acceleration parameter at 1-second period; T_L is the long-period transition period; I_e is the importance factor.

In Earthquake Actions Standard (NZS 1170.5, 2004) of New Zealand, the design response spectrum $C_d(T)$ at the period T is obtained from the elastic design spectrum $C(T)$ by:

$$C_d(T) = \frac{C(T)S_p}{k_u} \tag{53}$$

where S_p is the structural performance factor, equal to 1.0 for a structural ductility factor of 1 and equal to 0.7 for a structural ductility factor of 2 or more; k_u is the reduction factor given by:

$$for\ T < 0.7 \qquad k_u = 1 + \frac{(\mu - 1)T}{0.7} \tag{54}$$

$$for\ T \geq 0.7 \qquad k_u = \mu \tag{55}$$

where μ is the structural ductility.

Japan Building Standard Law (BCJ, 2013) defines structural characteristic coefficients D_s, which are the reciprocal of force reduction factors, because D_s multiply elastic forces in Japanese base shear expression.

Canadian Build Code (NRCC, 2015) defines reduction factor as product of R_d, ductility-related force modification factor reflecting the seismic energy dissipation capacity of structure, and R_0, overstrength related force modification factor accounting for the dependable portion of reserve strength.

It can be observed that the main international building codes approaching the seismic design with FBD method present similar definition of the reduction factor.

2.7. N2 method

In this Section, the "N2 method" (Fajfar, 2000) is briefly reported; it will be used to assess the performance of example structures designed in Section 6.

The N2 method is a nonlinear method for the seismic analysis of structures which combines the pushover analysis of a MDOF system with the response spectrum analysis of an equivalent SDOF system. The method is formulated in the acceleration-displacement format, the so called acceleration-displacement response spectrum (ADRS), which enables the visual interpretation of the procedure and of the relations between the basic quantities controlling the seismic response. Generally, the results of the N2 method are reasonably accurate, provided that the structure oscillates predominantly in the first mode.

Basically, starting from the acceleration spectrum in the conventional acceleration-period format, S_{ae}-T, the ADRS spectrum is obtained by replacing the period, T, in x-axis with the displacement spectrum, S_{de}, that, for an elastic SDOF system, is given by:

$$S_{de} = \frac{T^2}{4\pi^2} S_{ae} \tag{56}$$

The inelastic ADRS response spectrum is obtained using Expression (35) and (36) proposed by Vidic *et al*. (1994), already introduced in Section 2.3; then the inelastic acceleration, S_d, and the inelastic displacement, S_d, become:

$$S_a = \frac{S_{ae}}{R_\mu} \tag{57}$$

$$S_d = \frac{\mu}{R_\mu} S_{de} = \frac{\mu}{R_\mu} \frac{T^2}{4\pi^2} S_{ae} = \mu \frac{T^2}{4\pi^2} S_a \tag{58}$$

The elastic ADRS spectrum ($\mu = 1$) and the inelastic ADRS spectrum for ductility μ equal to 2, 3 and 5 are obtained from the acceleration spectrum of Figure 59 in Section 6 and illustrated in Figure 9. In the N2 method the ADRS spectrum represent the seismic demand.

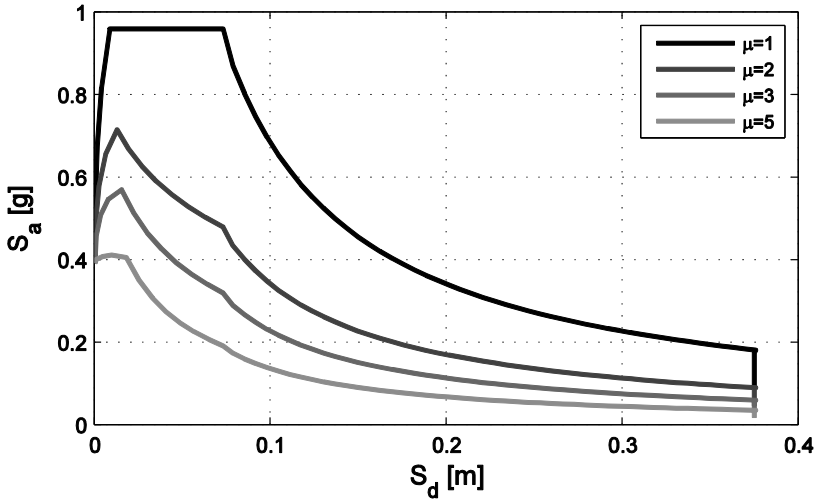

Figure 9: Elastic and inelastic ADRS spectra.

The second step of the method is to define the capacity curve of the structure which represents the seismic capacity. Performing a pushover analysis subjected to a load distribution proportional to the first mode deflection shape, the MDOF capacity curve in V_b-d_c format is obtained, where V_b is the base shear and d_c the displacement of the control point, conventionally taken at the rooftop of the structure.

To transform the MDOF curve to a SDOF curve, base shear, V_b, and control displacement, d_c, are divided by the modal participation factor, Γ, given by:

$$\Gamma = \frac{\sum_{i=1}^{n_s} m_i \phi_i}{\sum_{i=1}^{n_s} m_i {\phi_i}^2} \tag{59}$$

$$V_b{}^* = \frac{V_b}{\Gamma} \tag{60}$$

$$d_c{}^* = \frac{d_c}{\Gamma} \tag{61}$$

where m_i and ϕ_i are the mass and the first mode deflected shape ordinate for the *i-th* storey; $V_b{}^*$ and $d_c{}^*$ the base shear and the control displacement of the equivalent SDOF system, respectively.

The elastic period of the idealised bilinear system, T^*, is expressed by:

$$T^* = 2\pi \sqrt{\frac{m^* {d_y}^*}{{V_b}^*}} \tag{62}$$

where m^* and ${d_y}^*$ are the equivalent mass and the yield displacement of the SDOF system, respectively.

Moreover, the SDOF curve is bilinearised to be compared with the ADRS spectrum. The MDOF curve, the SDOF curve and the bilinearised SDOF curve of the Example 1 designed in Section 6.1.2 are shown in Figure 10, for instance.

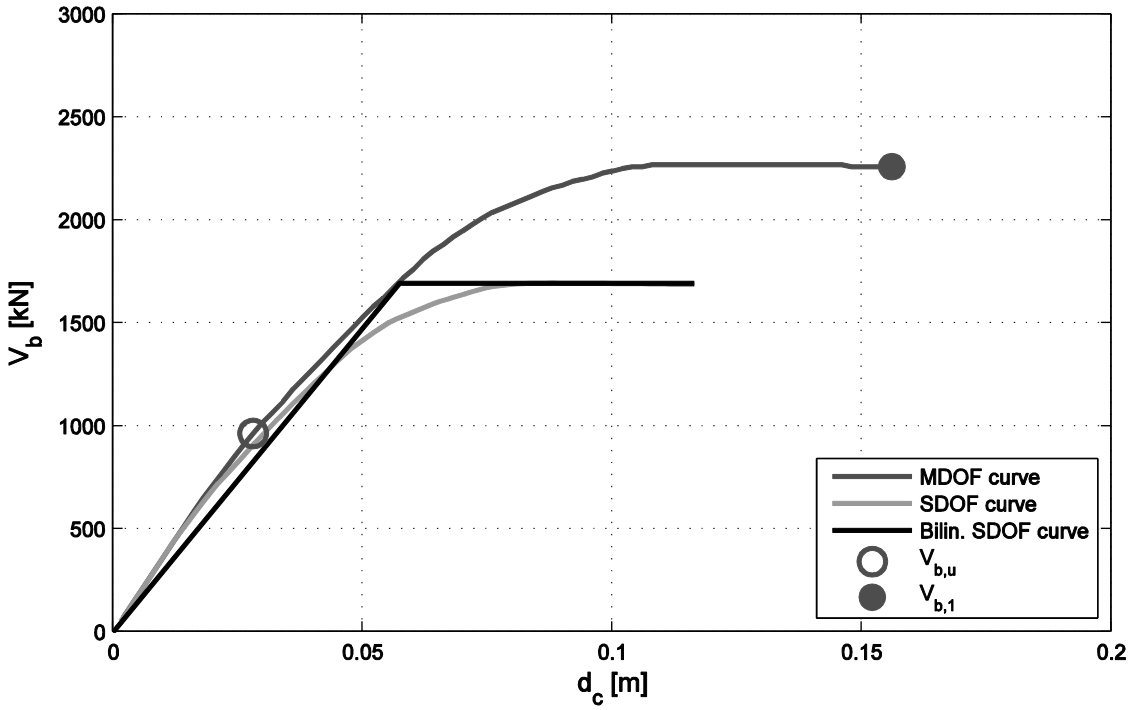

Figure 10: Bilinearization of SDOF curve of Example 1 designed applying the proposed method.

Furthermore the values of the ultimate base shear, $V_{b,u}$, and the base shear at first flexural resistance, $V_{b,1}$, are plotted in Figure 10. It is noted that the ratio α_u/α_1 is equal to the ratio $V_{b,u}/V_{b,1}$:

$$R_s = \frac{\alpha_u}{\alpha_1} = \frac{V_{b,u}}{V_{b,1}} \tag{63}$$

Finally, global performance evaluation is assessed comparing seismic demand and seismic capacity in terms of displacements. The performance assessment of the structure is given by the ratio γ_d:

$$\gamma_d = \frac{{d_c}^*}{{d_d}^*} \tag{64}$$

where ${d_c}^*$ is the ultimate displacement of the bilinearised SDOF curve, which is the displacement capacity of the system, and ${d_d}^*$ is the inelastic displacement demand required by the ADRS spectrum.

If the ratio γ_d is equal or larger than 1 then the structures is adequate to support the assigned seismic actions. The performance evaluation is graphically illustrated in Figure 11.

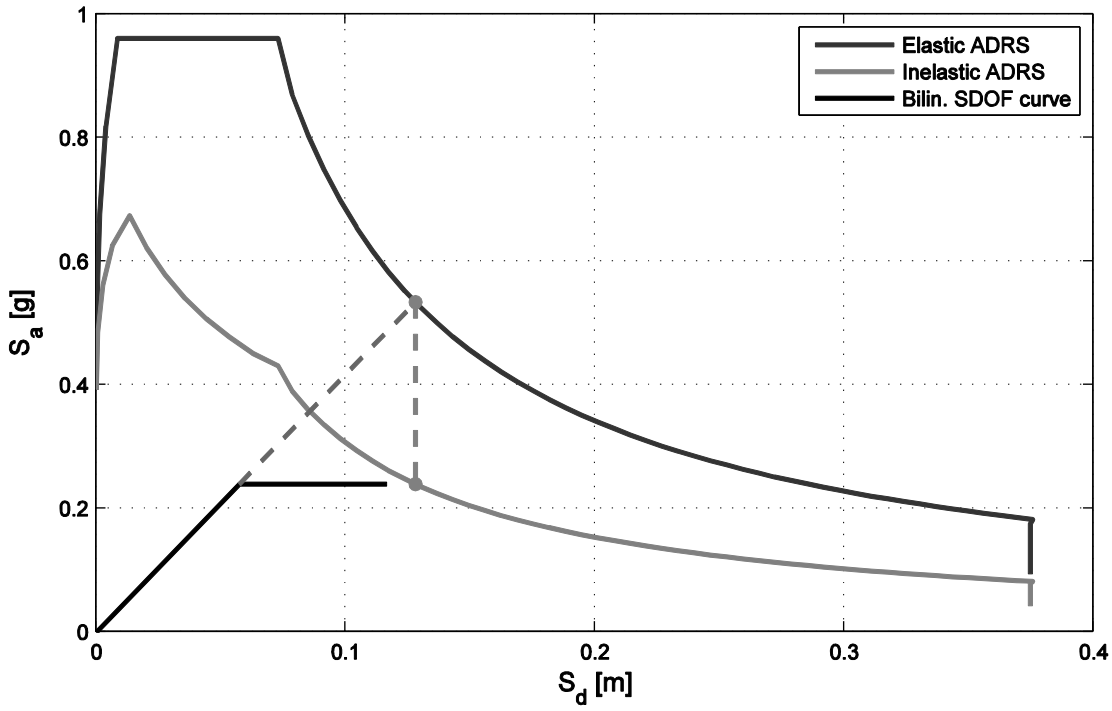

Figure 11: Structural performance of Example 1 designed to the proposed method.

Limitations and further considerations about N2 method are explained in detail in Fajfar (2000).

3. Analytical models

This section 3 reports the proposed analytical models. Section 3.1 introduces the definition equivalent SDOF system. Section 3.2, 3.3 and 3.4 describe the analytical models for wall, frame and dual systems respectively.

3.1. Equivalent SDOF system

The proposed analytical method is based on the transformation of the structure from a multi-degree of freedom (MDOF) system to an equivalent single-degree of freedom (SDOF) system. Floors are considered rigid diaphragm in this study, so the number of degrees of freedom is equal to the number of storeys, n_s.

Current practice to obtain the properties of the equivalent SDOF system are explained in Chopra (2006) and they are implicitly based on the following assumptions:

1. Equal elastic base shear between SDOF system, $V_{b,SDOF}$, and MDOF system, $V_{b,MDOF}$.

$$V_{b,SDOF} = S_a(T_1){m_1}^* \equiv V_{b,MDOF} = S_a(T_1)\Gamma_1 \sum_{i=1}^{n_s} m_i\phi_i \tag{65}$$

2. Equal elastic base moment between SDOF system, $M_{b,SDOF}$, and MDOF system, $M_{b,MDOF}$.

$$M_{b,SDOF} = S_a(T_1){m_1}^*{h_1}^* \equiv M_{b,MDOF} = S_a(T_1)\Gamma_1 \sum_{i=1}^{n_s} m_i\phi_i\, h_i \tag{66}$$

3. Equal energy between SDOF system, $E_{k,SDOF}$, and MDOF system, $E_{k,MDOF}$.

$$E_{k,SDOF} = \frac{1}{2}{m_1}^*\left(\frac{S_a(T_1)}{{\omega_1}^*}\right)^2 \equiv E_{k,MDOF} = \frac{1}{2}\left(\frac{S_a(T_1)\Gamma_1}{\omega_1}\right)^2 \sum_{i=1}^{n_s} m_i{\phi_i}^2 \tag{67}$$

4. Equal fundamental period between SDOF system, ${T_1}^*$, and MDOF system, T_1.

$$\frac{2\pi}{T_1{}^*} = \omega_1{}^* = \sqrt{\frac{m_1{}^*}{k_1{}^*}} \equiv \omega_1 = \frac{2\pi}{T_1} \tag{68}$$

5. Equal damping ratio between SDOF system, $\zeta_1{}^*$, and MDOF system, ζ_1.

$$\zeta_1{}^* \equiv \zeta_1 = 0.05 \tag{69}$$

where $S_a(T_1)$ is the pseudo-acceleration spectral ordinate evaluated at fundamental period T_1; m_i and ϕ_i the mass and the first mode deflected shape ordinate for the *i-th* storey; h_i the distance between the *i-th* storey and the ground level; n_s the number of storeys; $m_1{}^*$ and $h_1{}^*$ mass and height of the first mode SDOF system.

In the present work, only the equivalent SDOF system corresponding to the first mode is considered. To supply the fact that only one mode is taken into account, the equivalent mass of the SDOF system is defined equal to the total mass of the MDOF system. This assumption is adopted also by Chopra (2006) and Santa-Ana (2004) for the calculation of the modification factor, R_M. In this way, the SDOF system can approximate better the total base shear of MDOF system when regular building are considered. This assertion means that the equivalent mass of the first mode is dominant compared to the equivalent mass of other modes and it is sufficient to represent the response of the system accurately. Then, to supply the fact that the base shear related to the first mode is an underestimation of the total base shear (Chopra, 2006), the equivalent mass of the first mode is replaced by the total mass of the structure. Furthermore, the use of the total mass is consistent with building codes, which usually compute the base shear starting from the total weight of the structures (i.e., simplified linear static analysis).

To derive the properties of a SDOF system defined in such way, previous assumption 3 need to be modified by replacing the hypothesis of equal energy with the hypothesis of equal mass, that means that Equation (67) is replaced by Eq. (70).

$$m_{SDOF} = m^* = m_1{}^* \equiv m_{MDOF} = \sum_{i=1}^{n_s} m_i \tag{70}$$

For the sake of simplicity, $m_1{}^*$ and $h_1{}^*$ are named m^* and h^* in the following, because the equivalent SDOF system is always referring to the first mode SDOF system. From expression (65) and (66), the effective height of the equivalent SDOF system, h^*, can be written as:

$$h^* = h_1{}^* = \frac{\sum_{i=1}^{n_s} m_i \phi_i h_i}{\sum_{i=1}^{n_s} m_i \phi_i} \tag{71}$$

Consequently, given the stiffness of the SDOF system, k^*:

$$k^* = \frac{4\pi^2 m^*}{{T_1}^2} \tag{72}$$

the flexural stiffness, EI, of the elastic cantilever beam can be derived as follows:

$$EI = \frac{k^* {h_s}^3}{3} = \frac{4\pi^2}{3}\frac{m^* {h_s}^3}{{T_1}^2} \tag{73}$$

A representation of the SDOF system is drawn in Figure 12.

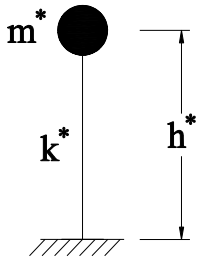

Figure 12: SDOF system.

3.2. Analytical model for wall systems

For the sake of simplicity, structures with uniform storey mass, $m_{s,w}$, and uniform storey height, h_s, are assumed for all storeys, n_s, but the method is still applicable for structures with different storey weights and different storey heights. It is noted that the model consists in one wall, which is representative of the wall system, so $m_{s,w}$ is the storey mass supported by the considered wall in the wall structure.

The building total height, H, is then equal to:

$$H = H_w = n_s h_s \tag{74}$$

An analytical estimation of the fundamental period of a pure-flexural cantilever wall, $T_{1,w}$, can be found in Goel and Chopra (1998):

$$T_{1,w} = \frac{2\pi}{3.516}\sqrt{\frac{m_{l,w}}{EI_{w,y}}}H^2 \tag{75}$$

where $m_{l,w}$ and $EI_{w,y}$ are the mass per unit height and the yield flexural stiffness of the wall, respectively, given as:

$$m_{l,w} = \frac{m_{s,w}}{h_s} \tag{76}$$

$$EI_{w,y} = \frac{M_{y,w}}{\varphi_{y,w}} \tag{77}$$

where $M_{y,w}$ and $\varphi_{y,w}$ are the yield moment and the yield curvature of the base section of the wall, respectively. The plastic hinge length, $L_{p,w}$, is defined as suggested in Priestley *et al*. (2007):

$$L_{p,w} = \max\{kL_{s,w} + 0.2l_w + L_{sp,w}; 2L_{sp,w}\} \tag{78}$$

where:

$$L_{s,w} = h_G = \frac{\sum_{i=1}^{n_s} F_i h_i}{\sum_{i=1}^{n_s} F_i} \overset{serie}{\Longrightarrow} \frac{2n_s + 1}{3n_s} H \tag{79}$$

$$L_{sp,w} = 0.022 f_y d_{bl,w} \tag{80}$$

$$k = 0.2\left(\frac{f_u}{f_y} - 1\right) \tag{81}$$

where: $L_{s,w}$ and $L_{sp,w}$ are the shear span length and the strain penetration length; f_y and f_u are the mean steel yield strength and the mean steel tensile strength; $d_{bl,w}$ is the maximum diameter of rebars in the base section of the wall; l_w is the section height, respectively. Plastic hinge is graphically shown in Figure 13(a). The shear span length is assumed in the case of an inverse triangular load of horizontal forces, F_i, applied at storey heights, h_i, as shown in Figure 13(b).

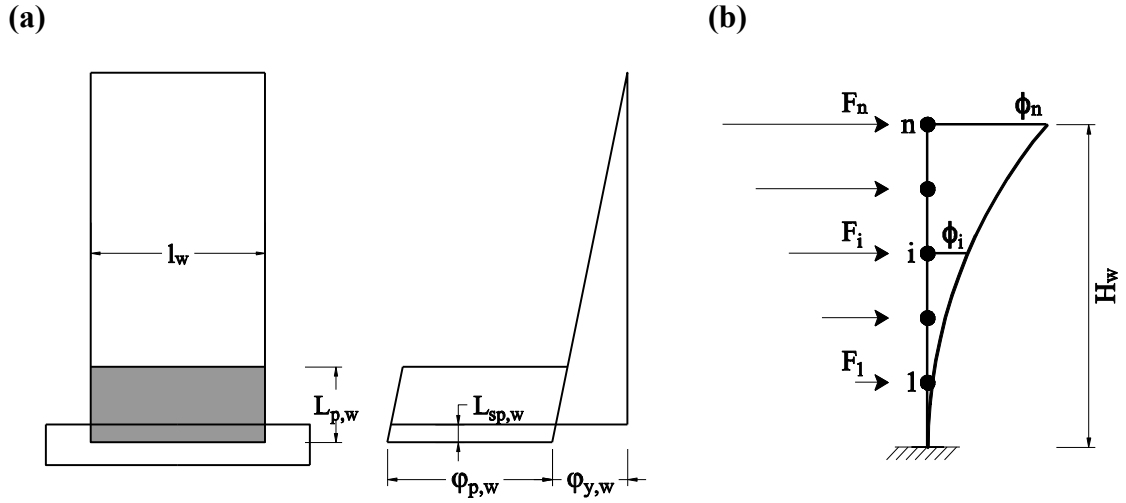

Figure 13: (a): Plastic hinge for walls, (b): Inverse triangular load of horizontal forces and wall displacement shape.

The analytical model for wall system is based on equivalent SDOF system able to predict the ductility reduction factor of the MDOF system, $R_{\mu,MDOF,w}$, through a modification factor,

$R_{M,w}$, which approximates higher mode effects. The first step is to define the first-mode displacement shape, which is necessary to define the equivalent SDOF system. The elastic displacement shape for wall structure is estimated through the expression proposed by Priestley *et al.* (2007), by assuming an inverse triangular load of horizontal forces as shown in Figure 13(b):

$$\phi_{i,w} = \frac{3}{2}\frac{{h_i}^2}{H^2}\left(1 - \frac{h_i}{3H}\right) \tag{82}$$

Where $\phi_{i,w}$ is the first mode deflected shape ordinate for the *i-th* storey of the wall structure.

Properties of the equivalent SDOF system for wall structure (${m_w}^*$, ${h_w}^*$, ${k_w}^*$) can be calculated from Equations (70), (71) and (72).

The yield base shear, ${V_{y,w}}^*$, the failure base shear, ${V_{u,w}}^*$, the yield displacement, ${d_{y,w}}^*$, of the equivalent SDOF system are respectively:

$${V_{y,w}}^* = \frac{M_{y,w}}{{h_w}^*} \tag{83}$$

$${V_{u,w}}^* = \frac{M_{u,w}}{{h_w}^*} \tag{84}$$

$${d_{y,w}}^* = \frac{{V_{y,w}}^*}{{k_w}^*} \tag{85}$$

where $M_{y,w}$ and $M_{u,w}$ is the yield and ultimate moment of the base section of the wall, respectively. The equivalent yield curvature, ${\varphi_{y,w}}^*$, for the equivalent SDOF system can be derived from Equation (73) and (77):

$${\varphi_{y,w}}^* = \frac{3M_{y,w}}{{k_w}^*{{h_w}^*}^3} \tag{86}$$

In order to obtain the same sectional ductility, $\mu_{\varphi,w}$, of the wall section in the plastic hinge of the equivalent SDOF system, the ultimate curvature of the equivalent SDOF system, ${\varphi_{u,w}}^*$, is written as:

$${\varphi_{u,w}}^* = \mu_{\varphi,w}{\varphi_{y,w}}^* = \frac{\varphi_{u,w}}{\varphi_{y,w}}{\varphi_{y,w}}^* \tag{87}$$

where $\varphi_{y,w}$ and $\varphi_{u,w}$ are the yield and ultimate curvature of the base section of the wall, respectively. The plastic displacement, ${d_{p,w}}^*$, ultimate displacement, ${d_{u.w}}^*$, and displacement ductility, ${\mu_w}^*$, for the equivalent SDOF system are then given by, respectively:

$$d_{p,w}{}^{*} = \left(\varphi_{u,w}{}^{*} - \varphi_{y,w}{}^{*}\right) L_{p,w} h_{w}{}^{*} \tag{88}$$

$$d_{u.w}{}^{*} = d_{y,w}{}^{*} \frac{V_{u,w}{}^{*}}{V_{y,w}{}^{*}} = d_{y,w}{}^{*} \frac{M_{u,w}}{M_{y,w}} + d_{p,w}{}^{*} \tag{89}$$

$$\mu_{w}{}^{*} = \frac{d_{u,w}{}^{*}}{d_{y,w}{}^{*}} \tag{90}$$

Once the structural ductility, $\mu_{w}{}^{*}$, is known, the force reduction factor for the equivalent SDOF system can be estimated with one of the method reviewed in Section 2. Among the others, the expression of Nassar and Krawinkler (1991) is chosen and the ductility reduction factor for the equivalent SDOF system for wall structure, $R_{\mu,SDOF,w}$, is given by:

$$R_{\mu,SDOF,w} = \left(c_w(\mu_{w}{}^{*} - 1) + 1\right)^{\frac{1}{c_w}} \tag{91}$$

$$c_w = \frac{T_{1,w}{}^{a_w}}{1 + T_{1,w}{}^{a_w}} + \frac{b_w}{T_{1,w}} \tag{92}$$

where parameters, a_w and b_w, are calculated with Equations (29)-(34). The post-yield stiffness, α_w, is also required in Equations (29)-(34), (91) and (92); for equivalent SDOF wall system α_w is defined as:

$$\alpha_w = \frac{V_{u,w}{}^{*} - V_{y,w}{}^{*}}{d_{u,w}{}^{*} - d_{y,w}{}^{*}} \frac{d_{y,w}{}^{*}}{V_{y,w}{}^{*}} \tag{93}$$

Finally, the ductility reduction factor for MDOF system of wall structures, $R_{\mu,MDOF,w}$, is given by the following expression:

$$R_{\mu,MDOF,w} = R_{M,w} R_{\mu,SDOF,w} \tag{94}$$

where the modification factor $R_{M,w}$ is introduced to take into account higher mode effects for wall structures.

A method to assess higher mode effects for wall structures is proposed by Priestley *et al*. (2007), which defines the amplified base shear for walls:

$$V_{b,MDOF,w} = \phi^{0} \omega_{v,Ti} V_{b,SDOF,w} \tag{95}$$

$$\omega_{v,Ti} = 1 + \frac{\mu_{w}{}^{*}}{\phi^{0}} c_{2,Tw} \tag{96}$$

$$c_{2,Tw} = 0.067 + 0.4\left(T_{1,w} - 0.5\right) \quad \begin{cases} \leq 1.150 \\ \geq 0.067 \end{cases} \tag{97}$$

where ϕ^0 is the overstrength factor relating the maximum feasible flexural strength to design strength; in this work ϕ^0 is equal to 1 because mean values of material properties are assumed instead of design ones. This method is validated for the following displacement ductility and fundamental period ranges, respectively: $1 \leq {\mu_w}^* \leq 7$; $0.5\ s \leq T_{1,w} \leq 3.9\ s$. From Equation (22) and Equation (95), the modification factor for wall structures, $R_{M,w}$, is assumed equal to:

$$R_{M,w} = \frac{V_{b,SDOF,w}}{V_{b,MDOF,w}} = \frac{1}{\phi^0 \omega_{v,Ti}} \tag{98}$$

The modification factor for wall structures, $R_{M,w}$, as a function of the displacement ductility demand, ${\mu_w}^*$, is plotted in Figure 14.

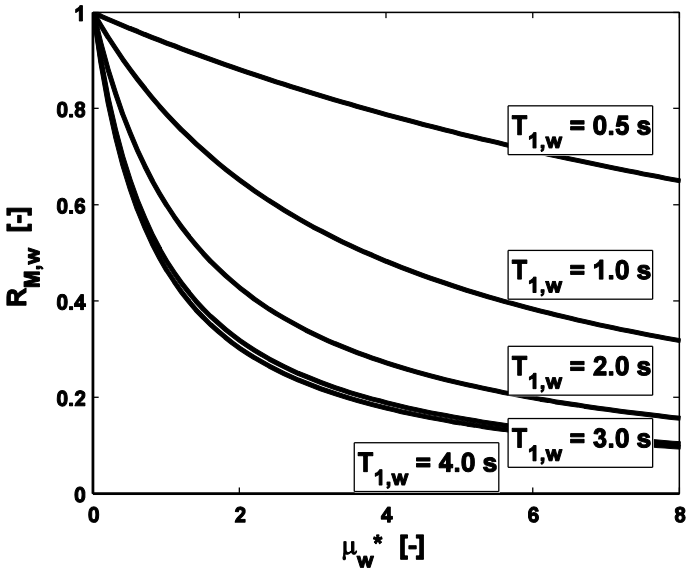

Figure 14: Modification factor for wall structures, $R_{M,w}$.

3.3. Analytical model for frame systems

As for wall systems, structures with uniform storey mass, $m_{s,f}$, and uniform storey height, h_s, are assumed for all storeys, n_s, but the method is still valid for structures with different storey weights and different storey heights. It is noted that the model consists in one column, which is representative of the frame system, so $m_{s,f}$ is the storey mass supported by the considered column in the frame structure.

An analytical estimation of the fundamental period of a pure-shear cantilever, $T_{1,f}$, can be found in Goel and Chopra (1998):

$$T_{1,f} = 4\sqrt{\frac{m_{l,f}}{kGA_{f,y}}}H \tag{99}$$

where k is the shape factor to account for non-uniform distribution of shear stresses, equal to $5/6$ for rectangular sections and $m_{l,f}$, $GA_{f,y}$ and $EI_{f,y}$ are the mass per unit height, the base column yield shear stiffness and the base column yield flexural stiffness of the shear cantilever, respectively, that are given by the following expressions:

$$m_{l,f} = \frac{m_{s,f}}{h_s} \tag{100}$$

$$GA_{f,y} = \frac{12EI_{f,y}}{{h_s}^2} \tag{101}$$

$$EI_{f,y} = \frac{M_{y,f}}{\varphi_{y,f}} \tag{102}$$

where $M_{y,f}$ and $\varphi_{y,f}$ are the yield moment and the yield curvature of the base column of the frame, respectively. The plastic hinge length, $L_{p,f}$, is defined as suggested by Priestley *et al*. (2007):

$$L_{p,f} = 0.08h_s + L_{sp,f} \tag{103}$$

$$L_{sp,f} = 0.022f_y d_{bl,f} \tag{104}$$

where $L_{sp,f}$ is the strain penetration length; h_s is the storey height; $d_{bl,f}$ is the maximum diameter of rebars in the base columns of the frame, respectively. Plastic hinges are graphically shown in Figure 15(a). The case of inverse triangular load of horizontal forces, F_i, applied at storey heights, h_i, is shown in Figure 15(b).

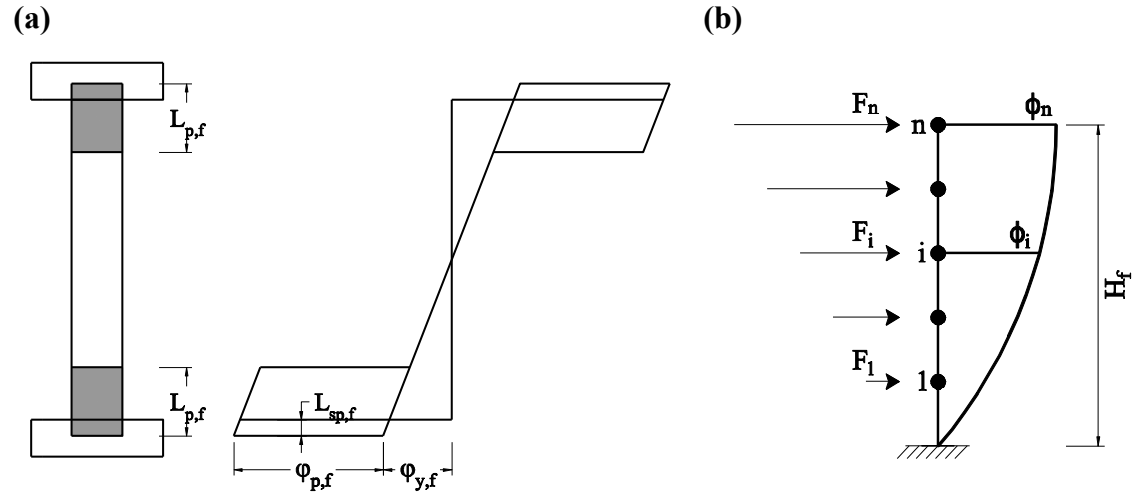

Figure 15: (a): Plastic hinge for frame, (b): Inverse triangular load of horizontal forces and frame displacement shape.

Similarly to wall system, the analytical model for frame system is based on equivalent SDOF system able to predict the ductility reduction factor of the MDOF system, $R_{\mu,MDOF,f}$, through a modification factor, $R_{M,f}$, which approximates higher mode effects. In the case of frames, the elastic displacement shape for frame structures is estimated making use of the expression proposed by Priestley *et al.* (2007), by assuming an inverse triangular load of horizontal forces as in Figure 15(b):

$$\phi_{i,f} = \frac{4}{3}\frac{h_i}{H}\left(1 - \frac{h_i}{4H}\right) \tag{105}$$

Where $\phi_{i,f}$ is the first mode deflected shape ordinate for the *i-th* storey of the frame structure.

Properties of the equivalent SDOF system for wall structure, ${m_f}^*$, ${h_f}^*$, ${k_f}^*$, can be calculated from Equations (70), (71) and (72). The effective height of the equivalent SDOF, ${h_f}^*$, is not a necessary parameter for the analytical procedure in the case of frames, because ${h_f}^*$ is defined as the storey height, h_s. In other words, frame structures are idealised as a two fixed-end beam, which is the case of shear-frame systems, as illustrated in Figure 15(a), and it represents the first storey of the frame.

The yield base shear, ${V_{y,f}}^*$, the failure base shear, ${V_{u,f}}^*$, the yield displacement, ${d_{y,f}}^*$, of the equivalent SDOF system are respectively:

$${V_{y,f}}^* = \frac{M_{y,f}}{h_s/2} \tag{106}$$

$${V_{u,f}}^* = \frac{M_{u,f}}{h_s/2} \tag{107}$$

$$d_{y,f}{}^{*} = \frac{F_{y,f}{}^{*}}{k_f{}^{*}} \tag{108}$$

where $M_{y,f}$ and $M_{u,f}$ is the yield and ultimate moment of the base column of the frame, respectively.

The yield displacement, $d_{y1,f}{}^{*}$, and the plastic displacement, $d_{p1,f}{}^{*}$, for the first-storey equivalent SDOF system are given by:

$$d_{y1,f}{}^{*} = \frac{V_{y,f}{}^{*}}{12EI_f/{h_s}^3} \tag{109}$$

$$d_{p1,f}{}^{*} = (\varphi_{u,f} - \varphi_{y,f})L_{p,f}h_s \tag{110}$$

where $\varphi_{y,f}$ and $\varphi_{u,f}$ are the yield and ultimate curvature of the base column of the frame, respectively.

In order to obtain the same plastic displacement for the equivalent SDOF system, $d_{p,f}{}^{*}$, the plastic displacement for the first-storey equivalent SDOF, $d_{p1,f}{}^{*}$, is written as:

$$d_{p,f}{}^{*} = \frac{d_{p1,f}{}^{*}}{d_{y1,f}{}^{*}} d_{y,f}{}^{*} \tag{111}$$

The ultimate displacement, $d_{u.f}{}^{*}$, and displacement ductility, $\mu_f{}^{*}$, for the equivalent SDOF system are then given by, respectively:

$$d_{u,f}{}^{*} = d_{y,f}{}^{*}\frac{V_{u,f}{}^{*}}{V_{y,f}{}^{*}} + d_{p,f}{}^{*} = d_{y,f}{}^{*}\frac{M_{u,f}}{M_{y,f}} + d_{p,f}{}^{*} \tag{112}$$

$$\mu_f{}^{*} = \frac{d_{u,f}{}^{*}}{d_{y,f}{}^{*}} \tag{113}$$

Once the structural ductility, $\mu_f{}^{*}$, is known, the force reduction factor for the equivalent SDOF system can be estimated using the expression of Nassar and Krawinkler (1991). The ductility reduction factor for the equivalent SDOF system for frame structures, $R_{\mu,SDOF,f}$, is given by:

$$R_{\mu,SDOF,f} = \left(c_f(\mu_f{}^{*} - 1) + 1\right)^{\frac{1}{c_f}} \tag{114}$$

$$c_f = \frac{{T_{1,f}}^{a_f}}{1 + {T_{1,f}}^{a_f}} + \frac{b_f}{T_{1,f}} \tag{115}$$

where parameters, a_f and b_f, are calculated with Equations (29)-(34). The post-yield stiffness, α_f, is also required in Equations (29)-(34), (91) and (92); for equivalent SDOF frame system α_f is defined as:

$$\alpha_f = \frac{{V_{u,f}}^* - {V_{y,f}}^*}{{d_{u,f}}^* - {d_{y,f}}^*} \frac{{d_{y,f}}^*}{{V_{y,f}}^*} \tag{116}$$

Finally, the ductility reduction factor for MDOF system of wall structures, $R_{\mu,MDOF,f}$, is given by the following expression:

$$R_{\mu,MDOF,f} = R_{M,f} R_{\mu,SDOF,f} \tag{117}$$

Where the modification factor, $R_{M,f}$, is introduced to take into account higher mode effects for frame structures.

A method to assess higher mode effects for wall structures is proposed by Priestley *et al*. (2007), which defines the amplified base shear for frames:

$$V_{b,MDOF,f} = \omega_{v,\mu} V_{b,SDOF,f} \tag{118}$$

$$\omega_{v,\mu} = \phi^0 + 0.1{\mu_f}^* \tag{119}$$

where ϕ^0 is the overstrength factor relating the maximum feasible flexural strength to design strength; in this work ϕ^0 is equal to 1 because mean values of material properties are assumed instead of design ones.

Equation (119) is obtained from nonlinear time history analyses of RC frame structures designed according to the DDBD but it can be considered valid also for shear frames. The shear frame is still representative of a frame system even though it is designed according to capacity design rules because it shows anyway a dominant shear deformation shape, also due to the presence of a rigid floor. In other words, the floor is rigid and not necessarily the beams.

From Equation (43) and Equation (95), the modification factor for wall structures, $R_{M,f}$, is defined equal to:

$$R_{M,f} = \frac{V_{b,SDOF,f}}{V_{b,MDOF,f}} = \frac{1}{\omega_{v,\mu}} \tag{120}$$

The modification factor for wall structures, $R_{M,f}$, is plotted as a function of the displacement ductility demand, ${\mu_f}^*$, in Figure 14.

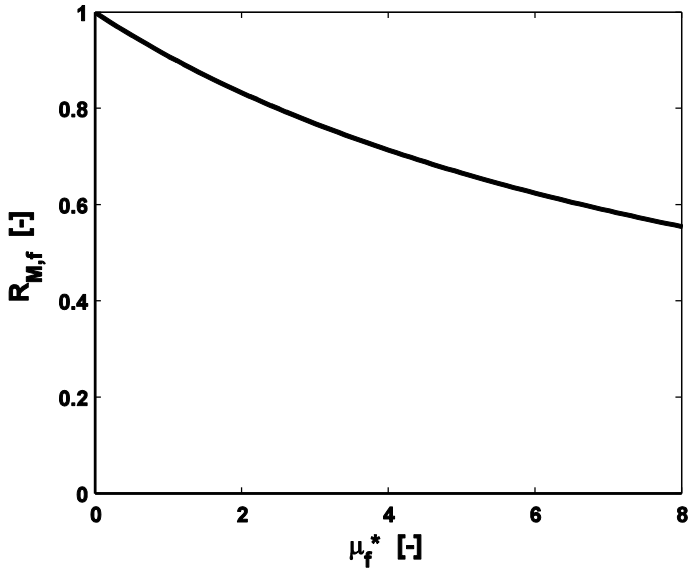

Figure 16: Modification factor for frame structures, $R_{M,f}$.

3.4. Analytical model for dual systems

The formulation wants to be a pioneering approach to calculate the ductility reduction factor for dual systems, $R_{\mu,MDOF,d}$. Basically, the idea is that $R_{\mu,MDOF,d}$ depends on the ductility reduction factor of the single system which it is composed of, i.e. the wall system, $R_{\mu,MDOF,w}$, and the frame system, $R_{\mu,MDOF,f}$, and on their ductility demands, ${\mu_w}^*$ and ${\mu_f}^*$. This choice is decided because the analytical model for dual systems wants to be related to quantities already known from the analytical models of single systems.

The ductility reduction factor for the dual system is defined empirically and two expressions, $R_{\mu,MDOF,d,1}$ and $R_{\mu,MDOF,d,2}$, are proposed.

The first expression, $R_{\mu,MDOF,d,1}$, is a polynomial regression of results. This expression has no evidenced mechanical meaning, but it has been determined as the best fit to results and it is given by:

$$R_{\mu,MDOF,d,1} = a_1 \frac{{R_{\mu,MDOF,w}}^{c_1}}{{\mu_w}^{*b_1}} + a_2 \frac{{R_{\mu,MDOF,f}}^{c2}}{{\mu_f}^{*b_2}} \tag{121}$$

The second expression, $R_{\mu,MDOF,d,2}$, is a simpler expression than Equation (121) and it is equal to:

$$R_{\mu,MDOF,d,2} = a_1 R_{\mu,MDOF,w} + a_2 \frac{R_{\mu,MDOF,f}}{\sqrt{{\mu_f}^*}} \tag{122}$$

More details about these expressions are given in Section 5.3.

4. Numerical analyses

This Section 4 reports the implemented numerical models. Section 4.1 introduces numerical models and Section 4.2 the numerical procedures to compute the ductility force reduction factor.

4.1. Numerical models

The software used to perform numerical analyses of considered structural systems is the Open System for Earthquake Engineering Simulation (OpenSees, 2015). It is a open-source framework software for simulating the seismic response of structural and geotechnical systems. OpenSees has been developed as the computational platform for research in performance-based earthquake engineering at the Pacific Earthquake Engineering Research Center (PEER), that is a multi-institutional research and education center with headquarters at the University of California, Berkeley, USA (Mazzoni *et al.*, 2007). Pre-processing and post-processing of data were conducted with the software Matlab (2013).

4.1.1. Model for wall system

The wall system is modelled as a flexural beam. As introduced in Section 3.2, the analytical model consists of one wall, which is representative of the wall system. Particularly, it consists of Euler-Bernoulli elastic beams with a bilinear moment-rotation hinge (or rotational spring) at each storey level, as shown in Figure 17. The rotational springs are placed only at storey level because it is ascertained that hinges usually develop at the base or due to the constrains imposed by rigid floors. The moment-rotation relationship is assumed bilinear for the sake of simplicity and to limit the time of computation. Masses are assigned to each floor level.

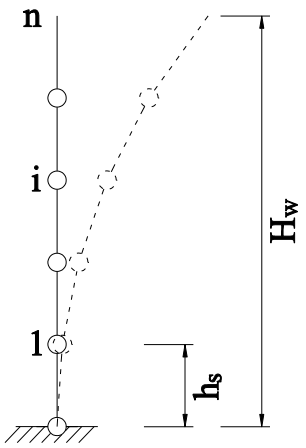

Figure 17: MDOF model of wall system.

Properties of the Euler-Bernoulli elastic beams are the following:

(i) Area, A_w, equal to the base section of the wall:

$$A_w = b_w h_w \tag{123}$$

where b_w is wall width and h_w is wall length;

(ii) Moment of inertia of the wall, I_w:

$$I_w = \frac{b_w {h_w}^3}{12} \tag{124}$$

(iii) Equivalent Young modulus is defined at the yield moment of the wall, in order to assign the proper reduction of stiffness due to cracking:

$$E_{c,w} = E_c \frac{E_{c,w} I_{w,y}}{E_c I_w} = E_c \frac{M_{y,w}/\varphi_{y,w}}{E_c I_w} = \frac{M_{y,w}}{\varphi_{y,w} I_w} \tag{125}$$

where the flexural stiffness of the wall, $E_{c,w} I_{w,y}$, is equal to the ratio of the yield moment, $M_{y,w}$, and the yield curvature, $\varphi_{y,w}$ (Priestley *et al.*, 2007); the Young modulus of concrete in *GPa*, E_c, is given by (UNI EN 1992-1-1, 2004):

$$E_c = 22 \left(\frac{f_c}{10}\right)^{0.3} \tag{126}$$

where f_c is the concrete mean compressive strength in MPa.

The moment-rotation spring is modelled as a zero-length element in OpenSees, based on the uniaxial bilinear material called “Steel01”. The plastic hinge needs to be modelled with an expedient because OpenSees does not provide rigid-elastic material. The assumed properties of the bilinear moment-rotation hinge are described in the following and illustrated in Figure 18.

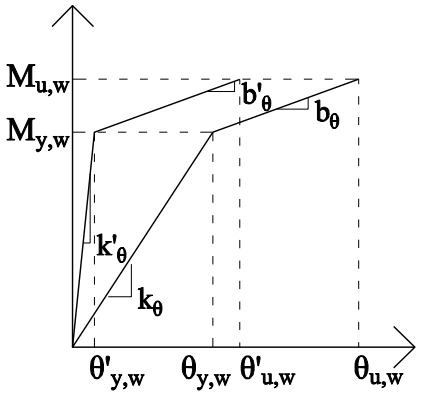

Figure 18: Bilinear moment-rotation hinge.

The initial elastic tangent stiffness, k_θ, is multiplied by big number, $n_{big} = 1000$, to obtain an equivalent initial elastic tangent stiffness, k'_θ, which is necessary to model a plastic hinge with a bilinear material as reported in Equation (127). In other words, the yield rotation, $\theta_{y,w}$, divided by n_{big} becomes negligible, $\theta'_{y,w} \ll 1$, as shown in Equation (128). Consequently, the ultimate rotation, $\theta_{u,w}$, is assumed coincident to the plastic rotation, $\theta_{p,w}$, given by Equation (129).

$$k'_\theta = \frac{M_{y,w}}{\theta'_{y,w}} = \frac{n_{big} M_{y,w}}{\theta_{y,w}} = n_{big} k_\theta \gg 1 \tag{127}$$

$$\theta'_{y,w} = \frac{\theta_{y,w}}{n_{big}} \ll 1 \tag{128}$$

$$\theta_{u,w} = \theta_{p,w} + \theta'_{y,w} \frac{M_{u,w}}{M_{y,w}} \approx \theta_{p,w} = \left(\varphi_{u,w} - \varphi_{y,w}\right) L_{p,w} \tag{129}$$

where $M_{u,w}$, $\varphi_{u,w}$ and $L_{p,w}$ are the yield moment, the yield curvature and the plastic hinge length of the wall, as introduced in Section 3.2 for the equivalent SDOF system for wall.

The hardening ratio, b'_θ, which is defined as the ratio between post-yield tangent and initial elastic tangent, is then given by:

$$b'_\theta = b_\theta = \frac{M_{u,w} - M_{y,w}}{\theta_{u,w} - \theta'_{y,w}} \cdot \frac{1}{k'_\theta} \approx \frac{M_{u,w} - M_{y,w}}{\theta_{p,w}} \cdot \frac{1}{k'_\theta} \tag{130}$$

The mechanical properties of the equivalent SDOF system for wall structures (Figure 19) defined in Section 3.1 are derived following the previous procedure as well. The SDOF model consists in a beam of height, $h_w{}^*$, area, A_w, and mass, $m_w{}^*$, placed on top. The moment of inertia, $I_w{}^*$, is derived from the following expression:

$$I_w{}^* = \frac{k_w{}^* h_w{}^{*3}}{3E_{c,w}} \tag{131}$$

Where the $k_w{}^*$ is the stiffness of the equivalent SDOF system as given by Equation (72).

It is noted that the properties of the SDOF system, in particular the fundamental period and the first mode deflected shape, are calculated through a modal analysis – i.e., linear dynamic analysis – also performed in OpenSees.

Properties of the bilinear moment-rotation hinge are calculate with Equations (127)-(130) by replacing $\varphi_{y,w}$ and $\varphi_{u,w}$ with $\varphi_{y,w}{}^*$ and $\varphi_{u,w}{}^*$, which are given by Equations (86) and (87). Properties of the equivalent SDOF system are already explained in detail in Section 3.1. It is noted that the hinge of equivalent SDOF system has the same ductility than the wall section, as introduced by Equation (87).

The elastic equivalent SDOF system for wall structures corresponds to the equivalent SDOF system model with an elastic rotational hinge at the base.

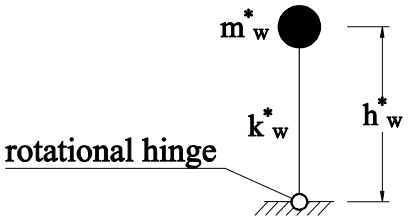

Figure 19: SDOF model of wall system.

4.1.2. Model for frame system

The frame structure is modelled as a shear beam. As introduced in Section 3.3, the analytical model consists of one column, which is representative of the frame system. Particularly, it consists of Euler-Bernoulli elastic beams with a bilinear shear-displacement hinge or translational spring at each storey level, as shown in Figure 20. The translational springs are placed only at storey level because it is ascertained that hinges usually develop at the ends of columns due to the constrains imposed by rigid floors. The shear-displacement relationship is assumed bilinear for the sake of simplicity and to limit the time of computation. Masses are assigned to each floor level.

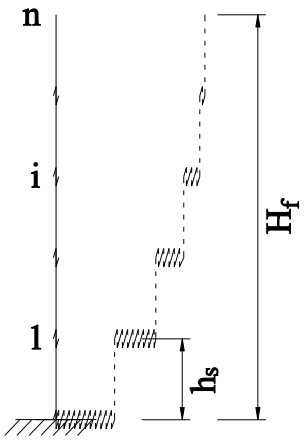

Figure 20: MDOF model of frame system.

Beams are defined rigid by multiplying the Young modulus by $n_{big2} = 1e07$, in order to simulate a shear-type system.

Properties of the Euler-Bernoulli elastic beam are the following:

(i) Area, A_f, is equal to the base section of the frame:

$$A_f = n_c b_c h_c \tag{132}$$

where n_c is the number of storeys; b_c and h_c are section width the section depth of the base column, respectively;

(ii) Moment of inertia of the frame, I_f:

$$I_f = \frac{n_c b_c {h_c}^3}{12} \tag{133}$$

(iii) Equivalent Young modulus is defined at the yield moment of the column, in order to assign the proper reduction of stiffness due to cracking:

$$\begin{aligned} E'_{c,f} = n_{big2} E_{c,f} = n_{big2} E_c \frac{E_{c,f} I_{f,y}}{E_c I_f} = n_{big2} E_c \frac{n_c M_{y,f}/\varphi_{y,f}}{E_c I_f} \\ = n_{big2} \frac{n_c M_{y,f}}{I_f \varphi_{y,f}} \end{aligned} \tag{134}$$

where the flexural stiffness of the column, $E_{c,f} I_{f,y}$, is equal to the ratio of the yield moment, $M_{y,f}$, and the yield curvature, $\varphi_{y,f}$ (Priestley *et al*., 2007).

The shear-displacement spring is modelled as a zero-length element in OpenSees, based on the uniaxial bilinear material "Steel01". The assumed properties of the bilinear shear-displacement hinge are the following and illustrated in Figure 21.

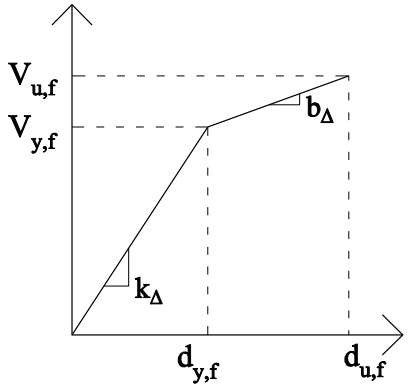

Figure 21: Bilinear shear-displacement hinge.

The initial elastic tangent stiffness, k_Δ, the yield displacement, $d_{y,f}$, and the ultimate displacement, $d_{u,f}$, are respectively defined as:

$$k_\Delta = \frac{12EI_{f,y}}{{h_s}^3} = \frac{12n_c M_{y,f}/\varphi_{y,f}}{{h_s}^3} = \frac{12n_c M_{y,f}}{\varphi_{y,f}{h_s}^3} \tag{135}$$

$$d_{y,f} = \frac{V_{y,f}}{k_\Delta} = \frac{\frac{n_c M_{y,f}}{h_s/2}}{\frac{12EI_{f,y}}{{h_s}^3}} = \frac{\frac{n_c M_{y,f}}{h_s/2}}{\frac{12n_c M_{y,f}/\varphi_{y,f}}{{h_s}^3}} = \frac{\varphi_{y,f}{h_s}^2}{6} \tag{136}$$

$$\begin{aligned} d_{u,f} &= d_{p,f} + d_{y,f}\frac{V_{u,f}}{V_{y,f}} = d_{p,f} + d_{y,f}\frac{M_{u,f}}{M_{y,f}} \\ &= 2\left(\varphi_{u,f} - \varphi_{y,f}\right)L_{p,f}\frac{h_s}{2} + d_{y,f}\frac{M_{u,f}}{M_{y,f}} \end{aligned} \tag{137}$$

Where $V_{y,f}$, $V_{u,f}$, $M_{u,f}$, $\varphi_{u,f}$ and $L_{p,f}$ are the yield shear, the ultimate shear, the yield moment, the yield curvature and the plastic hinge length of the frame, respectively, as introduced in Section 3.3 for the equivalent SDOF system for wall.

The hardening ratio, b_Δ, which is the ratio between post-yield tangent and initial elastic tangent, is then given by:

$$b_\Delta = \frac{V_{u,f} - V_{y,f}}{d_u - d_y} \cdot \frac{1}{k_\Delta} \tag{138}$$

The mechanical properties of the equivalent SDOF system for frame structures (Figure 22) defined in Section 3.3 are derived following the same procedure of wall structures. The SDOF model consists in a rigid beam of, length, ${h_f}^*$, area, A_f, and mass, ${m_f}^*$ placed on top. The initial elastic tangent, ${k_f}^*$, the yield displacement, ${d_{y,f}}^*$, and the yield displacement, ${d_{u,f}}^*$, are defined by Equations (72), (108)-(112). Properties of the equivalent SDOF system

are already explained in detail in Section 3.1. It is noted that the hinge of equivalent SDOF system has the same ductility than the column section, as introduced in Equation (111).

The elastic equivalent SDOF system for frame structures corresponds to the equivalent SDOF system model with a linear elastic shear-displacement hinge at the base, which has initial elastic tangent stiffness, $k_f{}^*$.

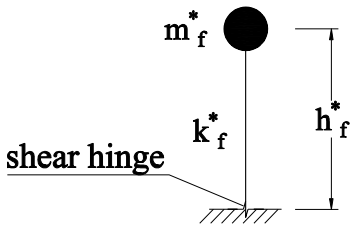

Figure 22: SDOF model of frame system.

4.1.3. Model for dual system

The dual system is modelled with coupling a flexural beam and a shear beam (Figure 23). The two systems are linked together by axial rigid trusses at each storey level. Truss length, l_b, is conventional and taken equal to 1 meter. Stiffness and capacity of hinges are the sum of stiffness and capacity of elements of the structure to idealise. In other words, if the lateral resisting system of the considered structure is composed of n_w walls and n_c columns, the stiffness and capacity of hinges of flexural and shear beams are the sum of stiffness and capacity of hinges of the n_w wall and n_c columns, respectively.

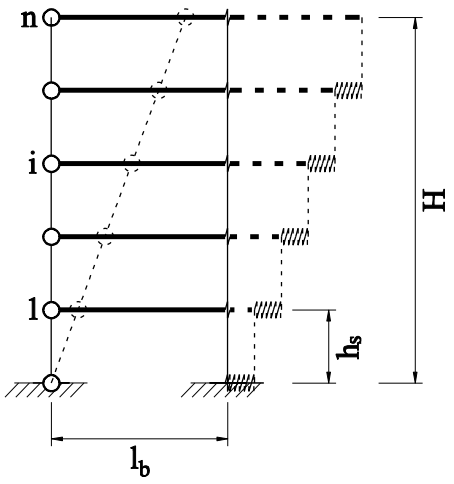

Figure 23: MDOF model of dual system.

As will be explained in next Section 4.2, the dual system structure requires the definition of two equivalent SDOF systems, one equivalent to wall structure and one equivalent to frame structure, defined following the procedure reported in Section 4.1.1 and 4.1.2 and illustrated in Figure 24(a) and Figure 24(b), respectively. The equivalent mass of the two SDOF systems, $m_d{}^*$, is equal to the sum of the masses of the flexural system, $m_w{}^*$, and shear

system, $m_f{}^*$, because the equivalent SDOF system wants to be representative of the dual structure, as given by (139).

$$m_d{}^* = m_w{}^* + m_f{}^* \tag{139}$$

The two equivalent SDOF systems, which are representative of the dual system, have the inelastic properties of the two single systems, in particular the rotational hinge for wall-equivalent SDOF system and the shear hinge for frame-equivalent SDOF system.

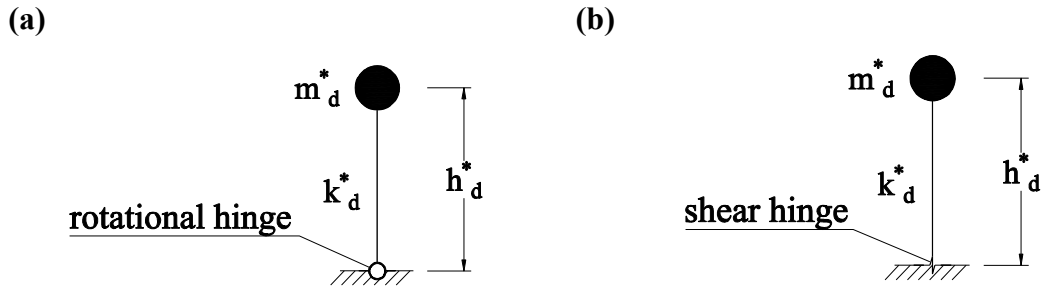

Figure 24: SDOF models of dual system, (a): wall-equivalent SDOF, (b): frame-equivalent SDOF.

4.2. Numerical procedure for ductility reduction factor computation

In this section, considered structural systems, nonlinear dynamic analyses and ductility reduction factor for wall, frame and dual systems are reported.

4.2.1. Considered structural systems

A total of 21 series of analyses are computed in this work, in particular 3 series for wall systems, 3 for frame systems and 15 for dual systems, i.e., frame-wall systems.

Each analysis consists in the evaluation of the ductility reduction factor for SDOF and MDOF system and the corresponding modification factor. Structures with a number of storeys, n_s, ranging from 3 to 12 is investigated for each group of sectional properties (Figure 25); storey height, h_s, is assumed equal to $3.00\ m$.

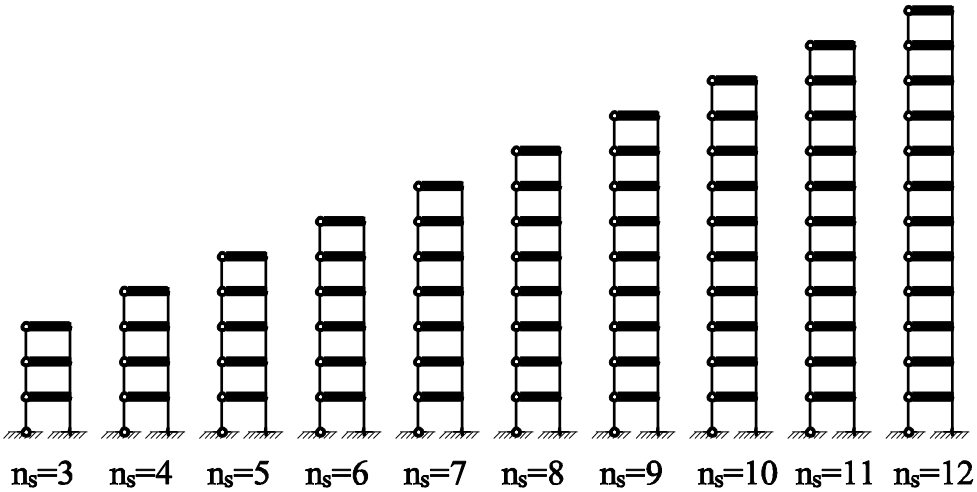

Figure 25: Numbers of storeys, n_s, investigated for each group of analyses.

Material properties which are used in analyses, are: mean concrete compressive strength $f_c = 38.0\ MPa$; mean steel yield strength $f_{y,s} = 550.0\ MPa$; mean steel tensile strength $f_{u,s} = 632.5\ MPa$; steel Young modulus $E_s = 200\ GPa$; maximum diameter of rebars $d_{bl} = 20\ mm$. Structural RC member weight is assumed equal to $25.0\ kN/m^3$.

Storey gravity loads in seismic combination, q_E, is equal to $7.8\ kN/m^2$ on a influence area of $25.0\ m^2$, which means a bay length, l_b, of $5.0\ m$ and a storey span, i_b, of $5.0\ m$; these loads are applied to all considered structures. All structures have the same beam section dimensions $b_b = 0.40\ m$ and $h_b = 0.40\ m$.

Concerning wall systems, three series of wall structures are considered and they are called "W1", "W2" and "W3", respectively. Each series is composed of 10 systems, with a number of storeys, n_s, ranging from 3 to 12 with a storey height $h_s = 3.00\ m$. They have the same section dimensions of the wall: section width $b_w = 0.30\ m$ and section length $l_w = 2.10\ m$. The main mechanical parameters of walls are reported in Table 8, in particular the difference between series is the sectional ductility, equal to 9.3, 11.7 and 14.0 for the three group, respectively.

Table 8: Mechanical properties for wall systems.

Properties	**W1**	**W2**	**W3**
Yield moment, $M_{y,w}\ [KNm]$	3498.0	3498.0	3498.0
Ultimate moment, $M_{u,w}\ [KNm]$	4065.0	4065.0	4065.0
Yield curvature, $\varphi_{y,w}\ [m^{-1}]$	0.0024	0.0024	0.0024
Ultimate curvature, $\varphi_{u,w}\ [m^{-1}]$	0.0224	0.0280	0.0336
Curvature ductility, $\mu_{\varphi,w}\ [-]$	9.3	11.7	14.0

Concerning frame systems, three series of frame structures are considered and they are called "F1", "F2" and "F3", respectively. Each series is composed of 10 systems, with a number of storeys, n_s, ranging from 3 to 12 with a storey height $h_s = 3.00\ m$. They have the same section dimensions of the base columns: section width $b_c = 0.40\ m$ and section depth $h_c =$

$0.40\ m$. The main mechanical parameters of frames are reported in Table 9, in particular the difference between series is the sectional ductility. It is noted that the values are assigned starting with the properties labelled "storey 12" as the top storey; i.e., if the considered structure is a 5 storey-height, the fifth storey has the properties labelled "storey 12" and the first storey has the properties labelled "storey 8". This procedure is because sectional properties are calculated with the proper axial forced applied.

Table 9: Mechanical properties for frame systems.

Properties	**F1**	**F2**	**F3**
Yield moment, $M_{y,f}$ $[KNm]$, storey 1	523.0	523.0	523.0
Yield moment, $M_{y,f}$ $[KNm]$, storey 2	514.0	514.0	514.0
Yield moment, $M_{y,f}$ $[KNm]$, storey 3	503.7	503.7	503.7
Yield moment, $M_{y,f}$ $[KNm]$, storey 4	494.3	494.3	494.3
Yield moment, $M_{y,f}$ $[KNm]$, storey 5	484.7	484.7	484.7
Yield moment, $M_{y,f}$ $[KNm]$, storey 6	471.5	471.5	471.5
Yield moment, $M_{y,f}$ $[KNm]$, storey 7	473.9	473.9	473.9
Yield moment, $M_{y,f}$ $[KNm]$, storey 8	465.5	465.5	465.5
Yield moment, $M_{y,f}$ $[KNm]$, storey 9	452.6	452.6	452.6
Yield moment, $M_{y,f}$ $[KNm]$, storey 10	440.0	440.0	440.0
Yield moment, $M_{y,f}$ $[KNm]$, storey 11	426.7	426.7	426.7
Yield moment, $M_{y,f}$ $[KNm]$, storey 12	405.4	405.4	405.4
Ultimate moment, $M_{u,f}$ $[KNm]$, storey 1	550.0	550.0	550.0
Ultimate moment, $M_{u,f}$ $[KNm]$, storey 2	549.9	549.9	549.9
Ultimate moment, $M_{u,f}$ $[KNm]$, storey 3	551.9	551.9	551.9
Ultimate moment, $M_{u,f}$ $[KNm]$, storey 4	551.4	551.4	551.4
Ultimate moment, $M_{u,f}$ $[KNm]$, storey 5	548.1	548.1	548.1
Ultimate moment, $M_{u,f}$ $[KNm]$, storey 6	541.3	541.3	541.3
Ultimate moment, $M_{u,f}$ $[KNm]$, storey 7	533.7	533.7	533.7
Ultimate moment, $M_{u,f}$ $[KNm]$, storey 8	526.3	526.3	526.3
Ultimate moment, $M_{u,f}$ $[KNm]$, storey 9	517.2	517.2	517.2
Ultimate moment, $M_{u,f}$ $[KNm]$, storey 10	504.9	504.9	504.9
Ultimate moment, $M_{u,f}$ $[KNm]$, storey 11	490.9	490.9	490.9
Ultimate moment, $M_{u,f}$ $[KNm]$, storey 12	475.0	475.0	475.0
Yield curvature, $\varphi_{y,f}$ $[m^{-1}]$, storey 1	0.0254	0.0254	0.0254
Yield curvature, $\varphi_{y,f}$ $[m^{-1}]$, storey 2	0.0246	0.0246	0.0246
Yield curvature, $\varphi_{y,f}$ $[m^{-1}]$, storey 3	0.0236	0.0236	0.0236
Yield curvature, $\varphi_{y,f}$ $[m^{-1}]$, storey 4	0.0226	0.0226	0.0226
Yield curvature, $\varphi_{y,f}$ $[m^{-1}]$, storey 5	0.0214	0.0214	0.0214
Yield curvature, $\varphi_{y,f}$ $[m^{-1}]$, storey 6	0.0198	0.0198	0.0198
Yield curvature, $\varphi_{y,f}$ $[m^{-1}]$, storey 7	0.0186	0.0186	0.0186
Yield curvature, $\varphi_{y,f}$ $[m^{-1}]$, storey 8	0.0176	0.0176	0.0176
Yield curvature, $\varphi_{y,f}$ $[m^{-1}]$, storey 9	0.0168	0.0168	0.0168
Yield curvature, $\varphi_{y,f}$ $[m^{-1}]$, storey 10	0.0164	0.0164	0.0164

Yield curvature, $\varphi_{y,f}$ $[m^{-1}]$, storey 11	0.0162	0.0162	0.0162
Yield curvature, $\varphi_{y,f}$ $[m^{-1}]$, storey 12	0.0158	0.0158	0.0158
Ultimate curvature, $\varphi_{u,f}$ $[m^{-1}]$, storey 1	0.0720	0.0540	0.0360
Ultimate curvature, $\varphi_{u,f}$ $[m^{-1}]$, storey 2	0.0742	0.0557	0.0371
Ultimate curvature, $\varphi_{u,f}$ $[m^{-1}]$, storey 3	0.0798	0.0599	0.0399
Ultimate curvature, $\varphi_{u,f}$ $[m^{-1}]$, storey 4	0.0860	0.0645	0.0430
Ultimate curvature, $\varphi_{u,f}$ $[m^{-1}]$, storey 5	0.0900	0.0675	0.0450
Ultimate curvature, $\varphi_{u,f}$ $[m^{-1}]$, storey 6	0.0946	0.0709	0.0473
Ultimate curvature, $\varphi_{u,f}$ $[m^{-1}]$, storey 7	0.0988	0.0741	0.0494
Ultimate curvature, $\varphi_{u,f}$ $[m^{-1}]$, storey 8	0.1130	0.0848	0.0565
Ultimate curvature, $\varphi_{u,f}$ $[m^{-1}]$, storey 9	0.1260	0.0945	0.0630
Ultimate curvature, $\varphi_{u,f}$ $[m^{-1}]$, storey 10	0.1346	0.1010	0.0673
Ultimate curvature, $\varphi_{u,f}$ $[m^{-1}]$, storey 11	0.1408	0.1056	0.0704
Ultimate curvature, $\varphi_{u,f}$ $[m^{-1}]$, storey 13	0.1460	0.1095	0.0730
Curvature ductility, $\mu_{\varphi,f}$ $[-]$, storey 1	2.8	2.1	1.4
Curvature ductility, $\mu_{\varphi,f}$ $[-]$, storey 2	3.0	2.2	1.5
Curvature ductility, $\mu_{\varphi,f}$ $[-]$, storey 3	3.4	2.6	1.7
Curvature ductility, $\mu_{\varphi,f}$ $[-]$, storey 4	3.8	2.9	1.9
Curvature ductility, $\mu_{\varphi,f}$ $[-]$, storey 5	4.2	3.2	2.1
Curvature ductility, $\mu_{\varphi,f}$ $[-]$, storey 6	4.8	3.6	2.4
Curvature ductility, $\mu_{\varphi,f}$ $[-]$, storey 7	5.3	4.0	2.7
Curvature ductility, $\mu_{\varphi,f}$ $[-]$, storey 8	6.4	4.8	3.2
Curvature ductility, $\mu_{\varphi,f}$ $[-]$, storey 9	7.5	5.6	3.8
Curvature ductility, $\mu_{\varphi,f}$ $[-]$, storey 10	8.2	6.2	4.1
Curvature ductility, $\mu_{\varphi,f}$ $[-]$, storey 11	8.7	6.5	4.4
Curvature ductility, $\mu_{\varphi,f}$ $[-]$, storey 12	9.2	6.9	4.6

Concerning dual systems, frame-wall structures are obtained with three combination of wall and frame systems, in particular the coupled systems labelled: “W1F1”, “W2F2” and “W3F3”, respectively, are obtained by combining the *i-th* wall with the *i-th* frame. Furthermore, for each of these three groups, 5 frame with different stiffness are considered: a single wall is coupled with a shear system which models a frame composed of 2, 5, 10, 15 and 20 columns, respectively (in other words, a 1, 4, 9, 14 and 19 bays frame, respectively). Consequently, previous group labels are completed with the number of columns, n_c, for instance, “W1F1C2” means system W1F1 with a 2 columns shear frame (Table 10). Number of wall is $n_w = 1$ for all groups. The portrayal of a dual system with $n_s = 4$ and $n_c = 5$, i.e., W1F1C5 or W2F2C5 or W3F3C5, is shown in Figure 26.

Table 10: Nomenclature of dual systems.

Wall	Frame	Dual systems				
		$n_c = 2$	$n_c = 5$	$n_c = 10$	$n_c = 15$	$n_c = 20$
W1	F1	W1F1C2	W1F1C5	W1F1C10	W1F1C15	W1F1C20
W2	F2	W2F2C2	W2F2C5	W2F2C10	W2F2C15	W2F2C20
W3	F3	W3F3C2	W3F3C5	W3F3C10	W3F3C15	W3F3C20

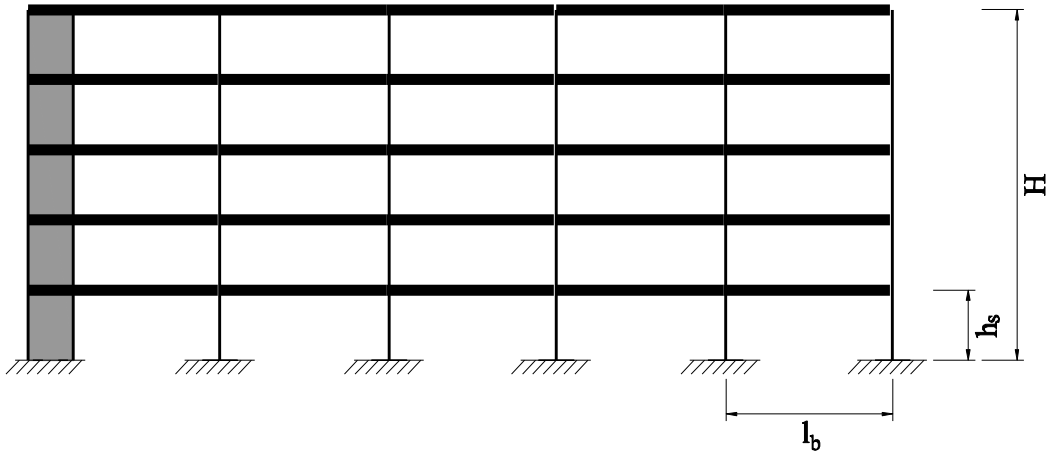

Figure 26: Portrayal of dual system with $n_s = 4$ and $n_c = 5$, i.e., W1F1C5 or W2F2C5 or W3F3C5.

4.2.2. Nonlinear dynamic analyses

Nonlinear Time History Analyses (NLTHA) are performed to calculate the ductility reduction factor. For each structure, a set of 34 natural ground motions. A total of 1020 nonlinear time history analyses (NLTHA) were computed for wall and frame systems and 5100 analyses for dual systems, respectively.

Natural ground motions are taken from Karavasilis *et al*. (2007), which were selected from the PEER (2005) ground motion database, and reported in Table 11. The magnitude, M_w, the soil type (UNI EN 1998-1, 2013), and peak ground acceleration, PGA, of the Far-Fault ground motions considered are presented in Table 11, while their elastic acceleration spectra are portrayed in Figure 27.

Concerning MDOF systems, Rayleigh damping matrix is assigned by considering a damping coefficient $\zeta = 5\%$ to the first two structural periods. The mass contribute is assigned to nodes with masses and the stiffness contribute is assigned to beams through the tangent stiffness matrix (Chopra, 2006). Concerning SDOF systems, a damping coefficient $\zeta = 5\%$ is assigned through the initial stiffness matrix. The analysis time step is defined as the minimum value between $T_1/20$, the time step of the ground motion and 0.02 seconds. The Newmark method with constant average acceleration is used ($\gamma = 0.5$ and $\beta = 0.25$), which is unconditionally stable (Bathe, 1996). Further details about the solver of OpenSees are available in Mazzoni *et al*. (2007).

Table 11: Characteristics of ground motions, Karavasilis *et al*. (2007).

ID	Event	Station	M_w	D $[Km]$	Soil	PGA [g]
FF1	Landers 1992/06/28	Yermo Fire Station	7.2	24.9	C	0.25
FF2	Loma Prieta 1989/10/18	Hollister City Hall	6.9	28.2	C	0.25
FF3	Superstition Hills(B) 1987/11/02	Wildlife Liquef. Array	6.4	24.4	D	0.21
FF4	Imperial Valley 1979/10/15	Delta	6.5	43.6	C	0.35
FF5	Loma Prieta 1989/10/18	Hollister - South & Pine	6.9	28.8	D	0.37
FF6	Northridge 1994/01/17	Canoga Park - Topanga Can	6.7	15.8	C	0.42
FF7	Loma Prieta 1989/10/22	Hollister Diff. Array	6.9	25.8	D	0.28
FF8	Irpinia, Italy 1980/11/23	Sturno	6.5	32.0	C	0.36
FF9	Loma Prieta 1989/10/18	Golden Gate Bridge	6.9	85.1	B	0.23
FF10	Northridge 1994/01/10	LA - Century City CC North	6.7	25.7	B	0.26
FF11	Kobe 1995/01/16	Kakogawa	6.9	26.4	D	0.35
FF12	Northridge 1994/01/17	Santa Monica City Hall	6.7	27.6	B	0.88
FF13	Loma Prieta 1989/10/18	Gilroy Array #4	6.9	16.1	C	0.42
FF14	Loma Prieta 1989/10/21	Coyote Lake Dam (SW Abut)	6.9	21.8	A	0.48
FF15	Loma Prieta 1989/10/24	Sunnyvale - Colton Ave.	6.9	28.8	C	0.21
FF16	Northridge 1994/01/17	Beverly Hills - 14145 Mulhol	6.7	19.6	B	0.52
FF17	Northridge 1994/01/22	Castaic - Old Ridge Route	6.7	22.6	B	0.57
FF18	Northridge 1994/01/17	Hollywood - Willoughby Ave	6.7	25.7	B	0.25
FF19	Northridge 1994/01/17	LA - Wonderland Ave	6.7	22.7	A	0.17
FF20	Landers 1992/06/28	Desert Hot Springs	7.2	23.2	A	0.17
FF21	Northridge 1994/01/17	LA - N Faring Rd	6.7	23.9	C	0.27
FF22	Northridge 1994/01/17	LA - Hollywood Stor FF	6.7	25.5	C	0.36

FF23	Loma Prieta 1989/10/18	APEEL 2 - Redwood City	6.9	47.9	D	0.27
FF24	Coalinga 1983/07/22	Pleasant Valley P.P. - yard	5.8	17.4	D	0.60
FF25	Northridge 1994/01/17	Stone Canyon	6.7	22.2	B	0.39
FF26	Loma Prieta 1989/10/18	SF Intern. Airport	6.9	64.4	C	0.33
FF27	Whittier Narrows 1987/10/01	Compton - Castlegate St	5.9	16.9	C	0.33
FF28	Northridge 1994/01/21	Santa Susana Ground	6.7	19.3	B	0.29
FF29	Northridge 1994/01/24	LA - Chalon Rd	6.7	23.7	B	0.23
FF30	Whittier Narrows 1987/10/04	Inglewood-Union Oil	5.9	18.3	C	0.16
FF31	Cape Mendocino 1992/04/25	Rio Dell Overpass – FF	7.1	18.5	B	0.55
FF32	Coalinga 1983/05/02	Cantua Creek School	6.4	25.5	D	0.28
FF33	Northridge 1994/01/18	Moorpark - Fire Station	6.7	28.0	D	0.29
FF34	Northridge 1994/01/22	LA - S Grand Avenue	6.7	36.9	C	0.29

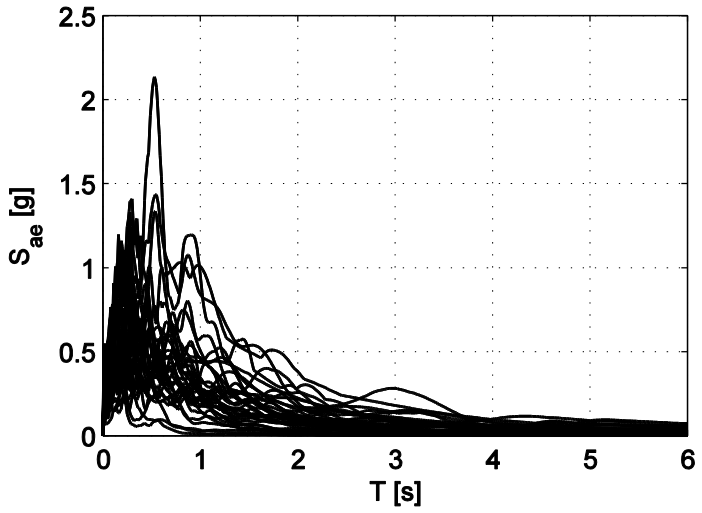

Figure 27: Elastic acceleration spectra of natural ground motions.

4.2.3. Ductility reduction factor computation for wall system

The procedure to calculate the reduction factor for wall systems is defined by the following steps and graphically shown in the flowchart of Figure 28; it is based on the works carried out by Santa-Ana (2004) and Wang *et al*. (2013).

1. The properties of the equivalent SDOF system are defined in Section 4.1.1.
2. The base shear of the MDOF system at the maximum target ductility capacity, $V_{b,MDOF,w}(\mu = \mu_w \equiv {\mu_w}^*)$, is computed by scaling the intensity of the ground motion until the maximum rotation, $\theta_{u,w,i} = \theta_{u,w,i,max}$, in one of the n_s hinges, is attained within a 5% tolerance. For this reason, the scaling factor is obtained using an iterative procedure. The target ductility for the MDOF system, ${\mu_w}^*$, is defined as the displacement ductility evaluated at the effective modal height ${h_w}^*$; at each iteration ${\mu_w}^*$ is calculated as the ratio of the ultimate displacement, $d_u({h_1}^*)$, and the yield displacement, $d_y({h_1}^*)$:

$$ {\mu_w}^* = \frac{d_u({h_1}^*)}{d_y({h_1}^*)} \tag{140} $$

   The yield displacement, $d_y({h_1}^*)$, is obtained from a pushover analysis of the MDOF system subjected to an inverse triangular load distribution, which is representative of the first mode deflected shape. If the effective modal height is not a multiple of the story height, displacements are evaluated through linear interpolation between the displacement at the story above and the story below ${h_w}^*$.
3. The base shear of the SDOF system at the maximum target ductility capacity, $V_{b,SDOF,w}(\mu = {\mu_w}^*)$, is computed by iteration on the yield moment of the base hinge of the SDOF system, when subjected to the same ground motion and same scale factor of step 2, until the displacement ductility, μ, of the SDOF structure is equal to the target ductility ${\mu_w}^*$ within a 5% tolerance error. The yield displacement is identified as the top displacement corresponding to the yield moment at the base hinge.
4. The base shear of the elastic SDOF system, $V_{b,SDOF,w}(\mu = 1)$, is computed for the elastic SDOF system when subjected to the same ground motion and same scale factor of step 2.
5. The ductility reduction factor for the SDOF wall system, $R_{\mu,SDOF,w}$, the ductility reduction factor for the MDOF wall system, $R_{\mu,MDOF,w}$, and the modification factor for wall system, $R_{M,w}$, are straightforward calculated making use of Equations (18), (21) and (22), respectively.

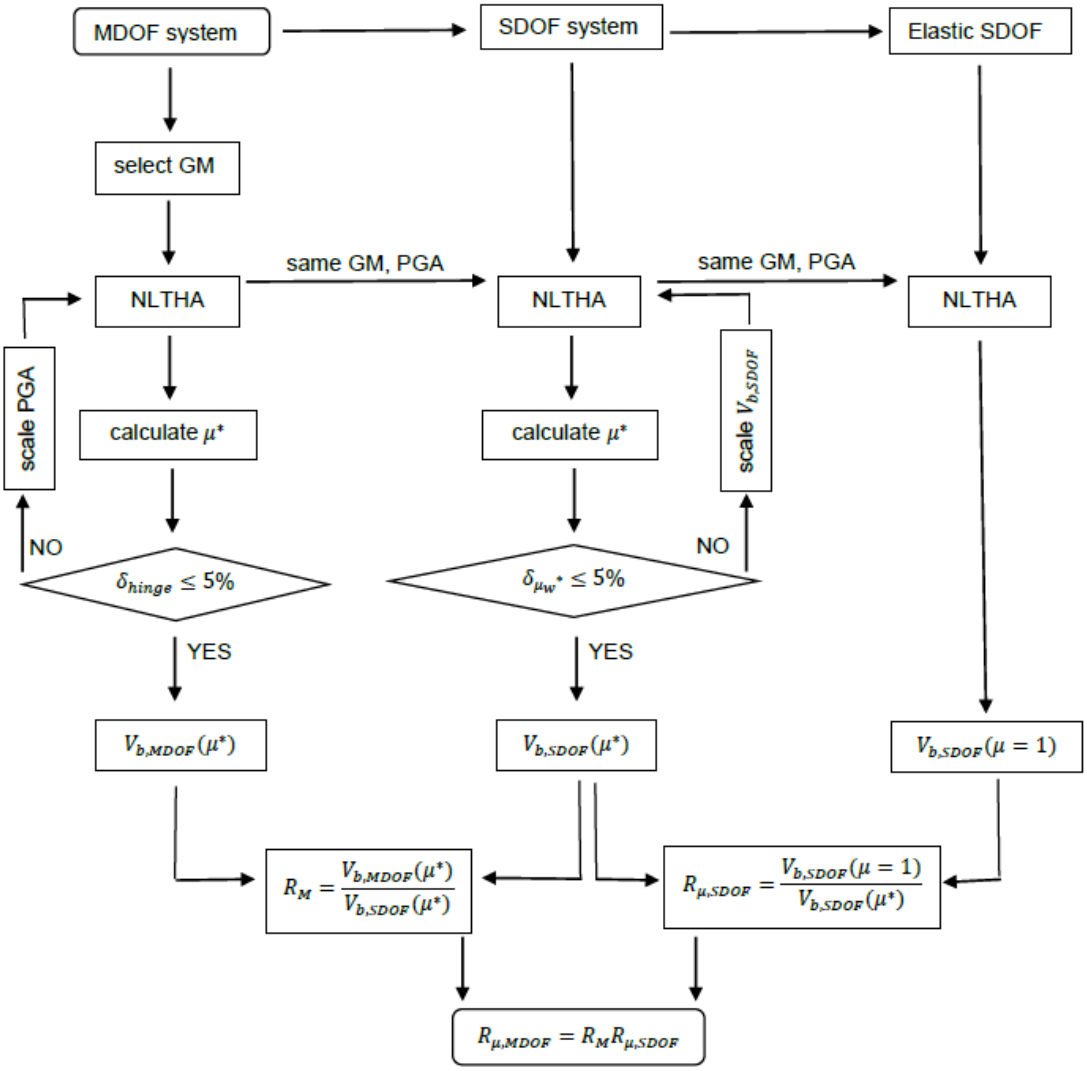

Figure 28: Flowchart for the calculation of ductility reduction factor of wall and frame structures.

4.2.4. Ductility reduction factor computation for frame system

Similarly to wall systems, the procedure to calculate the reduction factor for frame systems is defined by the following steps and graphically shown in the flowchart of Figure 28.

The procedure to calculate the reduction factor for frame systems is defined by the following steps.

1. The properties of the equivalent SDOF system are defined in Section 4.1.2.
   The base shear of the MDOF system, $V_{b,MDOF,f}(\mu = \mu_f \equiv \mu_f{}^*)$, is computed by scaling the intensity of the ground motion until the maximum displacement, $d_{u,f,i} = d_{u,f,i,max}$, in one of the n_s hinges, is attained within a 5% tolerance. For this reason, the scaling factor is obtained using an iterative procedure. The target ductility for the MDOF system, $\mu_f{}^*$, is defined as the maximum interstorey drift ductility. The

interstorey drift ductility at each iteration is calculated as the maximum ratio of the ultimate displacement, $d_{u,f,i}$, and the yield displacement, $d_{y,f,i}$, among the n_s storeys divided by the storey height, h_s.

$$\mu_f{}^* = max\left(\frac{\frac{d_{u,f,i} - d_{u,f,i-1}}{h_s}}{\frac{d_{y,f,i} - d_{y,f,i-1}}{h_s}}\right) = max\left(\frac{d_{u,f,i} - d_{u,f,i-1}}{d_{y,f,i} - d_{y,f,i-1}}\right) \tag{141}$$

The yield displacement for the *i-th* storey, $d_{y,f,i}$, is the analytical yield displacement given by:

$$d_{y,f,i} = \frac{\frac{M_{y,i}}{h_s/2}}{\frac{12E_{c,f}I_{f,y}}{h_s{}^3}} = \frac{M_{y,i}h_s{}^2}{6E_{c,f}I_{f,y}} \tag{142}$$

2. The base shear of the SDOF system at the maximum target ductility capacity, $V_{b,SDOF,f}(\mu = \mu_f{}^*)$, is computed by iteration on the yield moment of the hinges of the SDOF system, when subjected to the same ground motion and same scale factor of step 2, until the maximum storey displacement ductility, μ , of the SDOF structure is equal to the target ductility $\mu_f{}^*$ within a 5% tolerance error. The yield displacement is identified as the top displacement which corresponding to the yield shear in the hinge.
3. The base shear of the elastic SDOF system, $V_{b,SDOF,f}(\mu = 1)$, is computed for the elastic SDOF system when subjected to the same ground motion and same scale factor of step 2.
4. The ductility reduction factor for the SDOF frame system, $R_{\mu,SDOF,f}$, the ductility reduction factor for the MDOF frame system, $R_{\mu,MDOF,f}$, and the modification factor for frame system, $R_{M,f}$, are straightforward calculated making use of Equations (18), (21) and (22), respectively.

4.2.5. Ductility reduction factor computation for dual system

The procedure to calculate the reduction factor for dual systems is defined by the following steps.

1. The properties of the two equivalent SDOF systems are defined in Section 4.1.3.
2. The base shear of the MDOF system at the maximum target ductility capacity, $V_{b,MDOF,d}(\mu = \mu_w \equiv \mu_w{}^*) \equiv V_{b,MDOF,d}(\mu = \mu_f \equiv \mu_f{}^*)$, is computed by scaling the intensity of the ground motion until the maximum rotation, $\theta_{u,w,i} = \theta_{u,w,i,max}$, in one of the n_s hinges in of the wall, or until the maximum displacement, $d_{u,f,i} = d_{u,f,i,max}$, in one of the n_s hinges of the frame, is attained within a 5% tolerance. For

this reason, the scaling factor is obtained using an iterative procedure. The target ductilities for the MDOF system, $\mu_w{}^*$ and $\mu_f{}^*$, are defined at Point 2 in Sections 4.1.1 and 4.1.2, respectively.

3. The base shear of the elastic wall-equivalent SDOF system, $V_{b,SDOF,w,d}(\mu = 1)$, is computed for the elastic wall-equivalent SDOF system when subjected to the same ground motion and same scale factor of step 2.
4. The base shear of the elastic frame-equivalent SDOF system, $V_{b,SDOF,f,d}(\mu = 1)$, is computed for the elastic frame-equivalent SDOF system when subjected to the same ground motion and same scale factor of step 2.
5. The ductility reduction factor for the wall-equivalent MDOF system, $R_{\mu,MDOF,w,d}$, is straightforward calculated making use of Equation (21).
6. The ductility reduction factor for the frame-equivalent MDOF system, $R_{\mu,MDOF,f,d}$, is straightforward calculated making use of Equations (21).

Following the proposed approach, the two ductility reduction factors are obtained, for wall-equivalent and frame-equivalent systems respectively. This is due to the implemented concept of ductility, that is expressed as "global" ductility for wall systems and as "local" ductility for frame systems. Thus, the ductility reduction factor for dual system structures, $R_{\mu,MDOF,d}$, must be defined.

In the present work, $R_{\mu,MDOF,d}$ is determined as the weighted average of $R_{\mu,MDOF,w,d}$ and $R_{\mu,MDOF,f,d}$ assuming as a weight parameter the energy dissipated by the different structural systems, as expressed in the following Equation (143).

$$R_{\mu,MDOF,d} = \frac{R_{\mu,MDOF,w,d} u_w v_w + R_{\mu,MDOF,f,d} u_f v_f}{u_w v_w + u_f v_f} \tag{143}$$

where: $R_{\mu,MDOF,w,d}$, u_w and v_w are respectively the MDOF ductility reduction factor, the use rate and the base shear ratio for the wall-equivalent system; $R_{\mu,MDOF,f,d}$, u_f and v_f are respectively the MDOF ductility reduction factor, the use rate and the base shear ratio for the frame-equivalent system.

The use rates are defined as the ratio between the displacement demand and the displacement capacity of wall and frame systems, named u_w and u_f, respectively. The u_w is defined in Equation (144) as the ratio of the ultimate displacement demand, $d_{d,w}$, and the ultimate displacement capacity, $d_{c,w}$, of the wall system evaluated at the equivalent height $h_w{}^*$. Because the use rate u_w is a measure of the exploitation of the wall system, it can be equivalently expressed as the ratio of the rotational demand $\theta_{d,w}$ and rotational capacity $\theta_{c,w}$ of the wall base hinge.

$$u_w = \frac{d_{d,w}(h_w{}^*)}{d_{c,w}(h_w{}^*)} = \frac{\theta_{d,w} h_w{}^*}{\theta_{c,w} h_w{}^*} = \frac{\theta_{d,w}}{\theta_{c,w}} \tag{144}$$

The u_f is defined in Equation (145) as the maximum ratio of the ultimate interstorey drift demand and the ultimate interstorey drift capacity of the frame system, where $d_{d,f,i}$ is the

ultimate displacement demand; $d_{c,f,i}$ is the ultimate displacement capacity; i indicates the number of storeys where the shear-displacement hinges are located.

$$u_f = max\left(\frac{\frac{d_{d,f,i} - d_{d,f,i-1}}{h_s}}{\frac{d_{c,f,i} - d_{c,f,i-1}}{h_s}}\right) = max\left(\frac{d_{d,f,i} - d_{d,f,i-1}}{d_{c,f,i} - d_{c,f,i-1}}\right) \quad (145)$$

The base shear ratios are define in Equations (146) and (147) as the ratio between the base shear of the wall or frame systems and the total base shear of the dual system; they are named v_w and v_f respectively.

$$v_w = \frac{V_{b,MDOF,w,d}}{V_{b,MDOF,d}} = \frac{V_{b,MDOF,w,d}}{V_{b,MDOF,w,d} + V_{b,MDOF,f,d}} = 1 - v_f \quad (146)$$

$$v_f = \frac{V_{b,MDOF,f,d}}{V_{b,MDOF,d}} = \frac{V_{b,MDOF,f,d}}{V_{b,MDOF,w,d} + V_{b,MDOF,f,d}} = 1 - v_w \quad (147)$$

The total base shear of the dual system, $V_{b,MDOF,d}$, is the sum of the base shear of wall system, $V_{b,MDOF,w,d}$, and frame system, $V_{b,MDOF,f,d}$, which composed the frame-wall structure:

$$V_{b,MDOF,d} = V_{b,MDOF,w,d} + V_{b,MDOF,f,d} \quad (148)$$

Results are discussed in detail in Section 5.

5. Results

Results of wall, frame and dual systems are reported in Section 5.1, 5.2 and 5.3, respectively. Description of results will refer to low, medium and high number for storey, n_s, and it is noted that low, medium and high refer to the range of storeys in the present work (from 3 to 12). Therefore low-rise and mid-rise structures are investigated, but high-rise buildings are not studied in the present work.

5.1. Results for wall systems

In this Section a detailed comparison of numerical results of Section 4 and analytical results of Section 3 are reported.

Results of wall systems W1, W2 and W3 are illustrated in Figure 29-Figure 31 and also reported as numerical values in Table 12-Table 14, respectively. Numerical values are indicated with "OS" label in figures.

Each Figure is composed of four plots.

In Plot (a), the numerical ductility reduction factor for SDOF systems, $R_{\mu,SDOF,w,OS}$, and MDOF systems, $R_{\mu,MDOF,w,OS}$, are compared to the analytical ductility reduction factor for SDOF systems, $R_{\mu,SDOF,w}$, and MDOF systems, $R_{\mu,MDOF,w}$, respectively, as a function of the number of storeys, n_s.

In Plot (b), the statistical dispersion of $R_{\mu,MDOF,w,OS}$ is shown. All analyses (100%) and 68% coverage of population are plotted as a function of the number of storeys, n_s.

In Plot (c), the comparison between the numerical modification factor, $R_{M,w,OS}$, and the analytical modification factor, $R_{M,w}$, is illustrated as a function of the number of storeys, n_s.

In Plot (d), the comparison between the numerical target ductility, ${\mu_{w,OS}}^*$, and the analytical target ductility, ${\mu_w}^*$, is shown as a function of the number of storeys, n_s. Let's recall that the target ductility, ${\mu_w}^*$, is the maximum displacement ductility at the effective height, ${h_w}^*$, which can be exploited by the system.

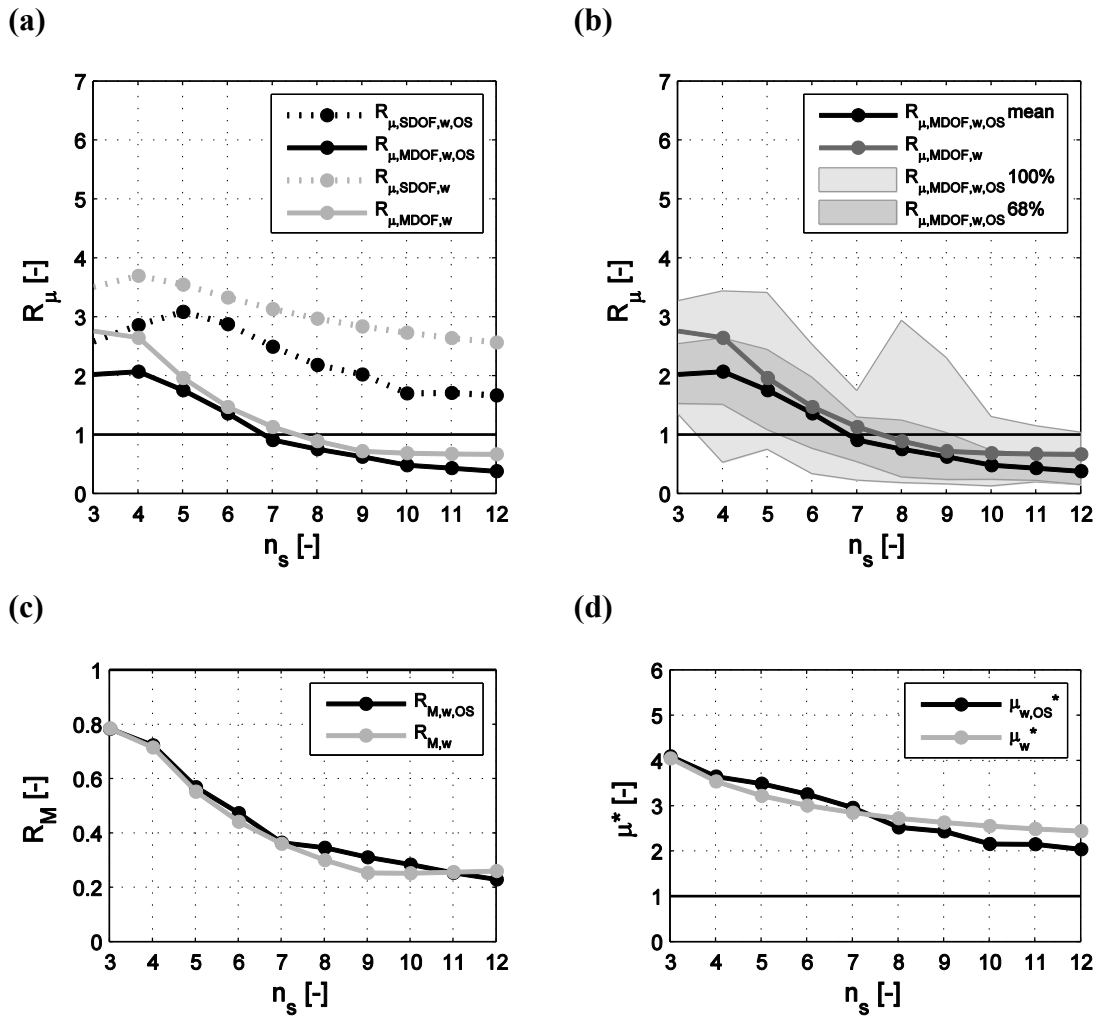

Figure 29: Results for W1 wall system, (a, b): $R_{\mu,SDOF,w}$, $R_{\mu,MDOF,w}$, (c): $R_{M,w}$, (d): ${\mu_w}^*$

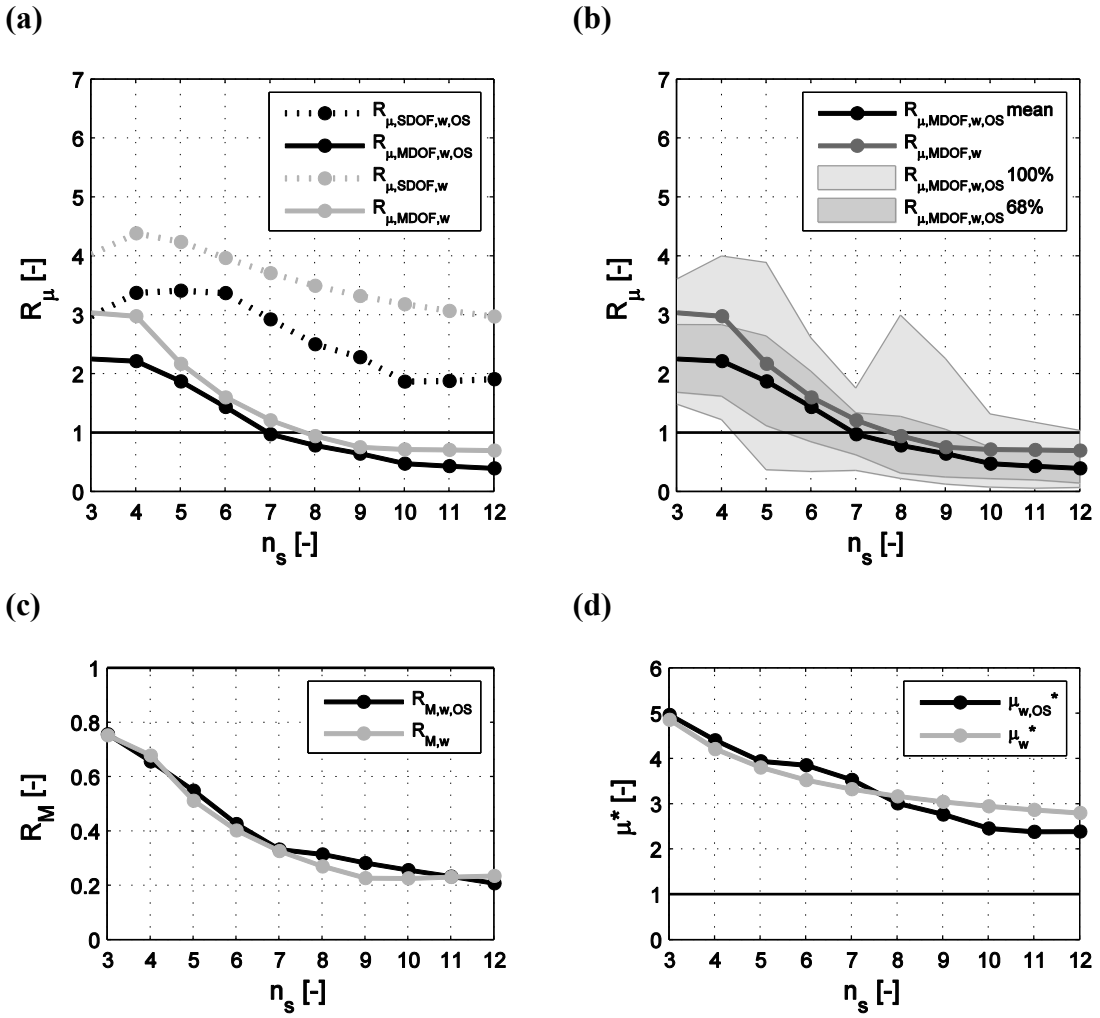

Figure 30: Results of W2 wall system, (a, b): $R_{\mu,SDOF,w}$, $R_{\mu,MDOF,w}$, (c): $R_{M,w}$, (d): $\mu_w{}^*$

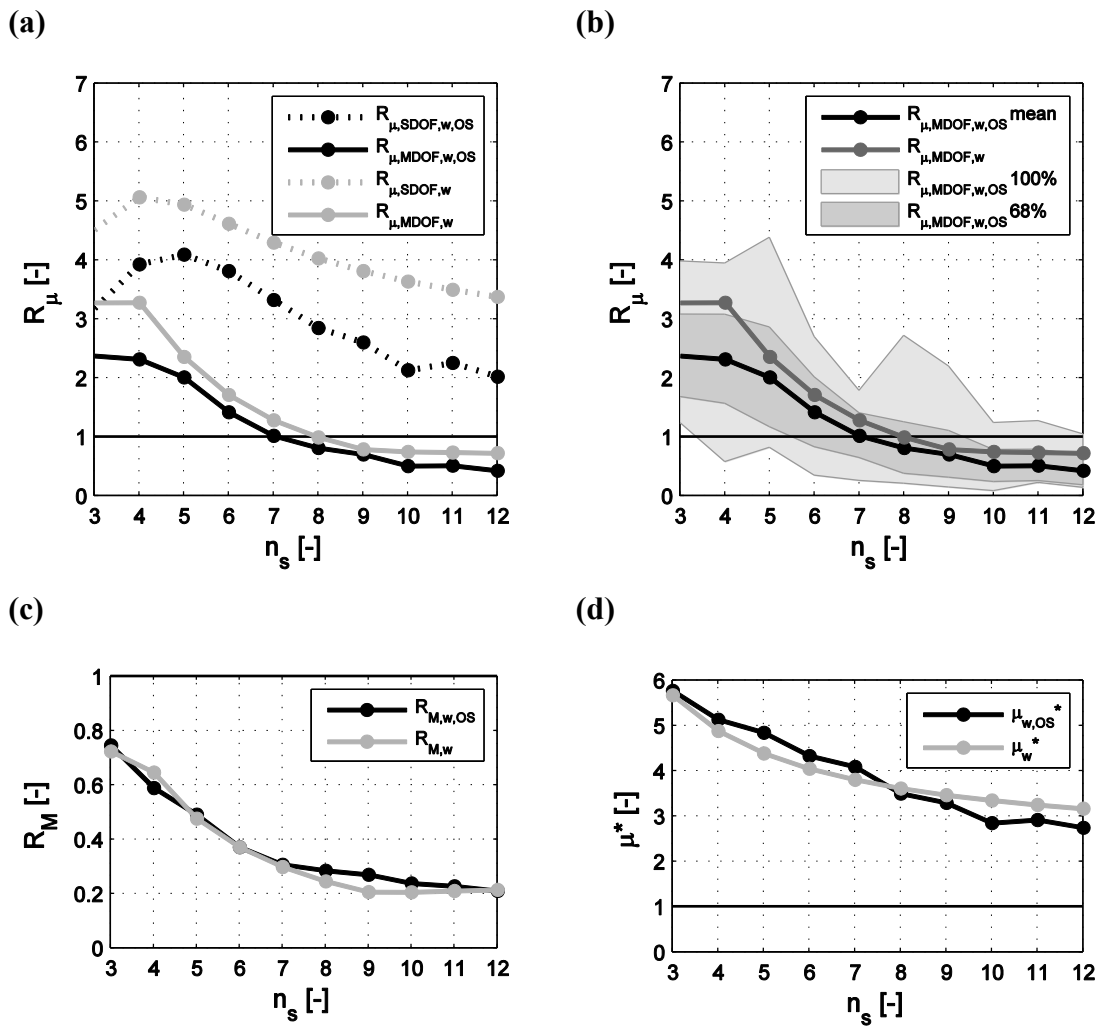

Figure 31: Results of W3 wall system, (a, b): $R_{\mu,SDOF,w}$, $R_{\mu,MDOF,w}$, (c): $R_{M,w}$, (d): ${\mu_w}^*$

Table 12: Results of W1 wall system.

	OpenSees				Proposed analytical method			
n_s	$R_{\mu,SDOF,w}$	$R_{\mu,MDOF,w}$	$R_{M,w}$	${\mu_w}^*$	$R_{\mu,SDOF,w}$	$R_{\mu,MDOF,w}$	$R_{M,w}$	${\mu_w}^*$
3	2.59	2.03	0.78	4.10	3.52	2.77	0.79	4.06
4	2.86	2.08	0.72	3.66	3.70	2.65	0.72	3.55
5	3.09	1.76	0.57	3.50	3.55	1.97	0.55	3.23
6	2.88	1.37	0.47	3.27	3.33	1.48	0.44	3.02
7	2.50	0.92	0.37	2.96	3.14	1.14	0.36	2.86
8	2.19	0.76	0.35	2.54	2.98	0.90	0.30	2.74
9	2.03	0.63	0.31	2.45	2.85	0.73	0.26	2.64
10	1.71	0.49	0.29	2.16	2.74	0.69	0.25	2.57
11	1.72	0.44	0.26	2.16	2.65	0.68	0.26	2.50
12	1.67	0.39	0.23	2.05	2.57	0.67	0.26	2.45

Table 13: Results of W2 wall system.

n_s	OpenSees				Proposed analytical method			
	$R_{\mu,SDOF,w}$	$R_{\mu,MDOF,w}$	$R_{M,w}$	${\mu_w}^*$	$R_{\mu,SDOF,w}$	$R_{\mu,MDOF,w}$	$R_{M,w}$	${\mu_w}^*$
3	2.98	2.26	0.76	4.97	4.03	3.04	0.75	4.87
4	3.38	2.22	0.66	4.41	4.39	2.98	0.68	4.22
5	3.42	1.88	0.55	3.95	4.24	2.18	0.51	3.81
6	3.37	1.44	0.43	3.86	3.97	1.60	0.40	3.53
7	2.93	0.98	0.33	3.54	3.71	1.22	0.33	3.33
8	2.51	0.79	0.32	3.02	3.50	0.95	0.27	3.18
9	2.29	0.65	0.28	2.78	3.33	0.76	0.23	3.06
10	1.87	0.48	0.26	2.47	3.19	0.72	0.23	2.96
11	1.88	0.44	0.23	2.39	3.07	0.71	0.23	2.88
12	1.92	0.40	0.21	2.40	2.98	0.70	0.24	2.81

Table 14: Results ofW3 wall system.

n_s	OpenSees				Proposed analytical method			
	$R_{\mu,SDOF,w}$	$R_{\mu,MDOF,w}$	$R_{M,w}$	${\mu_w}^*$	$R_{\mu,SDOF,w}$	$R_{\mu,MDOF,w}$	$R_{M,w}$	${\mu_w}^*$
3	3.19	2.38	0.75	5.77	4.52	3.28	0.72	5.68
4	3.93	2.32	0.59	5.13	5.07	3.28	0.65	4.89
5	4.09	2.01	0.49	4.85	4.94	2.36	0.48	4.39
6	3.82	1.42	0.37	4.33	4.62	1.72	0.37	4.05
7	3.33	1.02	0.31	4.09	4.30	1.29	0.30	3.81
8	2.85	0.81	0.29	3.51	4.03	0.99	0.25	3.62
9	2.60	0.71	0.27	3.30	3.82	0.79	0.21	3.47
10	2.13	0.51	0.24	2.85	3.64	0.75	0.21	3.35
11	2.26	0.52	0.23	2.92	3.50	0.74	0.21	3.25
12	2.03	0.43	0.21	2.75	3.38	0.73	0.22	3.17

The following considerations concerning result mean values can be drawn:

(i) It is evident that ductility reduction factors, $R_{\mu,SDOF,w}$ and $R_{\mu,MDOF,w}$, modification factor, $R_{M,w}$, and target ductility, ${\mu_w}^*$, decreases with the number of storeys (Figure 29-Figure 31), that can be explained as the loss of capability of the system to exploit the base sectional inelasticity and the importance of higher mode effects with the number of storeys.

(ii) The ductility reduction factor for the equivalent SDOF systems, $R_{\mu,SDOF,w}$, and the ductility reduction factor for the MDOF systems, $R_{\mu,MDOF,w}$, are overestimated by the proposed analytical model with errors of 40% and 33% on average, respectively (Figure 29a-Figure 31a). $R_{\mu,SDOF,w}$ and $R_{\mu,MDOF,w}$ decrease with the number of storeys and they show a concave up trend, except to lower number of storeys. It is noted that for high number of storeys $R_{\mu,MDOF,w}$ is a value less than 1, which means that the system is not able to exploit the base sectional inelasticity and the structure should be designed elastically. Numerical models give values of $R_{\mu,MDOF,w}$ ranged from 2.0 to 0.4; from 2.3 to 0.4 and from 2.4 and 0.4 for W1, W2 and W3, respectively.

(iii) The modification factor, $R_{M,w}$, is well predicted by the proposed analytical model and it is underestimated with an error of 5% on average (Figure 29c-Figure 31c). $R_{M,w}$ decreases with the number of storeys, which means that the higher mode effects progressively increase the base shear in MDOF systems. Numerical models give values ranged from 0.8 to 0.2 for all group of walls, then $R_{M,w}$ is lightly affected by the sectional ductility capacity of the wall but it is mainly controlled by n_s.

(iv) The target ductility, $\mu_w{}^*$, is well predicted by the proposed analytical model and it is overestimated with an error of 4% on average, (Figure 29d-Figure 31d). $\mu_w{}^*$ decreases with the number of storeys that can be explained as the loss of capability of the system to exploit the base section ductility with the increasing of the number of storeys due to higher mode effects. Numerical models give values ranged from 4.1 to 2.5, from 4.9 to 2.8 and from 5.7 and 3.2 for W1, W2 and W3, respectively. The increasing of $\mu_w{}^*$ from W1 to W3 groups is obvious because the sectional ductility of the walls are 9.3, 11.7 and 14.0 for W1, W2 and W3, respectively (Table 8 of Section 4.2.1). Furthermore, $\mu_w{}^*$ decreases with the number of storeys, that is the system is less efficient to exploit the sectional ductility and to convert it in available capacity ductility, $\mu_w{}^*$, with the increasing of n_s.

(v) The dispersion of data is considerable when all analyses are considered, but a lower scatter is evidenced when 68% coverage of population is assumed (Figure 29b-Figure 31b).

It is evident from Figure 29a,c-Figure 31a,c that $R_{\mu,MDOF,w}$ and $R_{M,w}$ are not significantly different among the groups of walls.

It is to be noticed that some convergence problems occurred during the numerical analysis due to convergence failures in the numerical procedure to calculate the ductility reduction factors, in particular when the convergence errors exceeded the 5% tolerance on the search for the ground motion scale factor (MDOF system) or the target ductility (equivalent SDOF system), within 20 iterations. The percentage of successful analyses, which is the ratio of successful analyses number and the total analyses number, is equal to 92%. Analyses fail randomly varying the number of storeys and ground motions; so they do not show systematic bias due to certain patterns.

The comparison of fundamental periods given by the numerical model, $T_{1,w,OS}$, and analytical model, $T_{1,w}$, given by Equation (75), is illustrated in Figure 32 and listed in Table 15. The analytical fundamental periods underestimate the numerical ones of 14% on average. The numerical period is different from the analytical one because the analytical formula is exact for uniformly distributed mass along the height of the structure, instead considered numerical models are lumped mass systems.

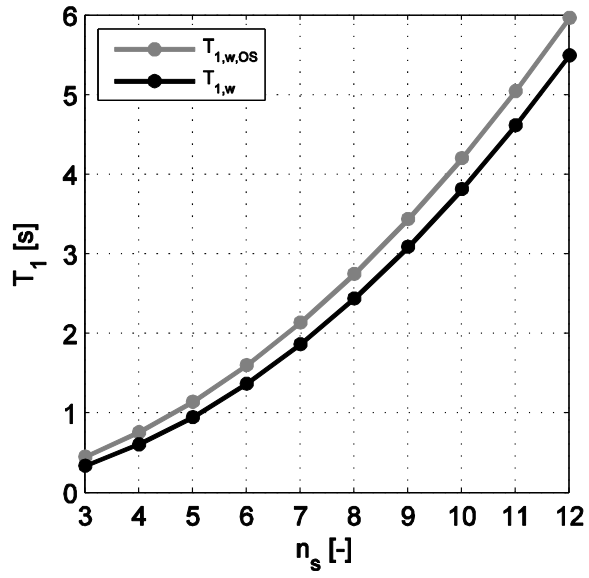

Figure 32: Fundamental periods of wall systems.

Table 15: Fundamental period [s] of wall systems.

n_s	OpenSees	Analytical prediction	Relative error
3	0.4599	0.3441	-25%
4	0.7660	0.6117	-20%
5	1.1488	0.9557	-17%
6	1.6082	1.3762	-14%
7	2.1443	1.8732	-13%
8	2.7572	2.4467	-11%
9	3.4467	3.0965	-10%
10	4.2131	3.8229	-9%
11	5.0562	4.6257	-9%
12	5.9762	5.5050	-8%

5.2. Results for frame systems

In this Section a detailed comparison of numerical results of Section 4 and analytical results of Section 3 are reported.

Results of frame systems F1, F2 and F3 are illustrated in Figure 33-Figure 35, respectively and also reported as numerical values in Table 16-Table 18, respectively.

Each Figure is composed of four plots.

In Plot (a), the numerical ductility reduction factor for SDOF systems, $R_{\mu,SDOF,f,OS}$, and MDOF systems, $R_{\mu,MDOF,f,OS}$, are compared to the analytical ductility reduction factor for SDOF systems, $R_{\mu,SDOF,f}$, and MDOF systems, $R_{\mu,MDOF,f}$, respectively, as a function of the number of storeys, n_s.

In Plot (b), the statistical dispersion of $R_{\mu,MDOF,f,OS}$ is shown. All analyses (100%) and 68% coverage of population are plotted as a function of the number of storeys, n_s.

In Plot (c), the comparison between the numerical modification factor, $R_{M,f,OS}$, and the analytical modification factor, $R_{M,f}$, is illustrated as a function of the number of storeys, n_s.

In Plot (d), the comparison between the numerical target ductility, ${\mu_{f,OS}}^*$, and the analytical target ductility, ${\mu_f}^*$, is shown as a function of the number of storeys, n_s. Let's recall that the target ductility, ${\mu_f}^*$, is the maximum interstorey drift ductility which can be exploited by the system.

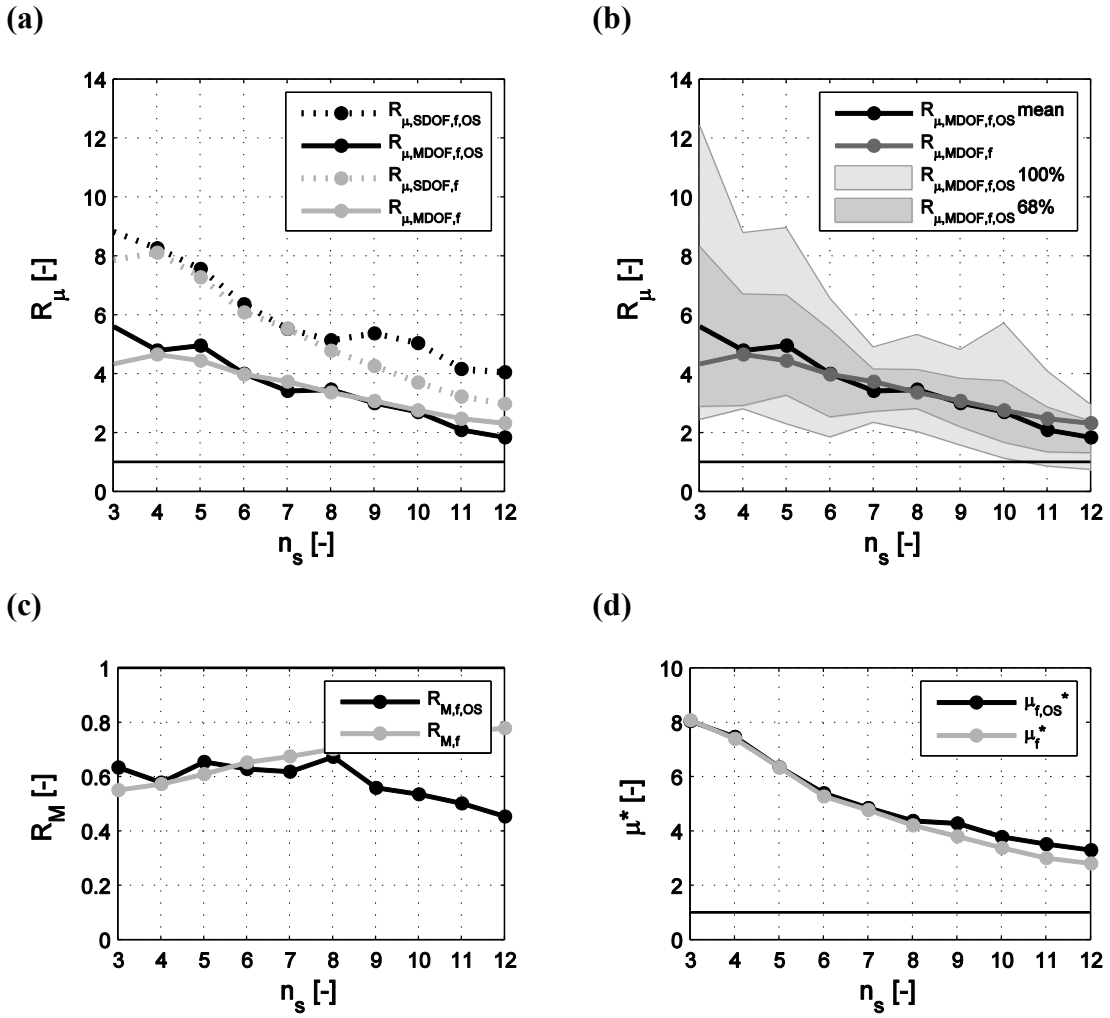

Figure 33: Results of F1 frame system, (a, b): $R_{\mu,SDOF,f}$, $R_{\mu,MDOF,f}$, (c): $R_{M,f}$, (d): ${\mu_f}^*$

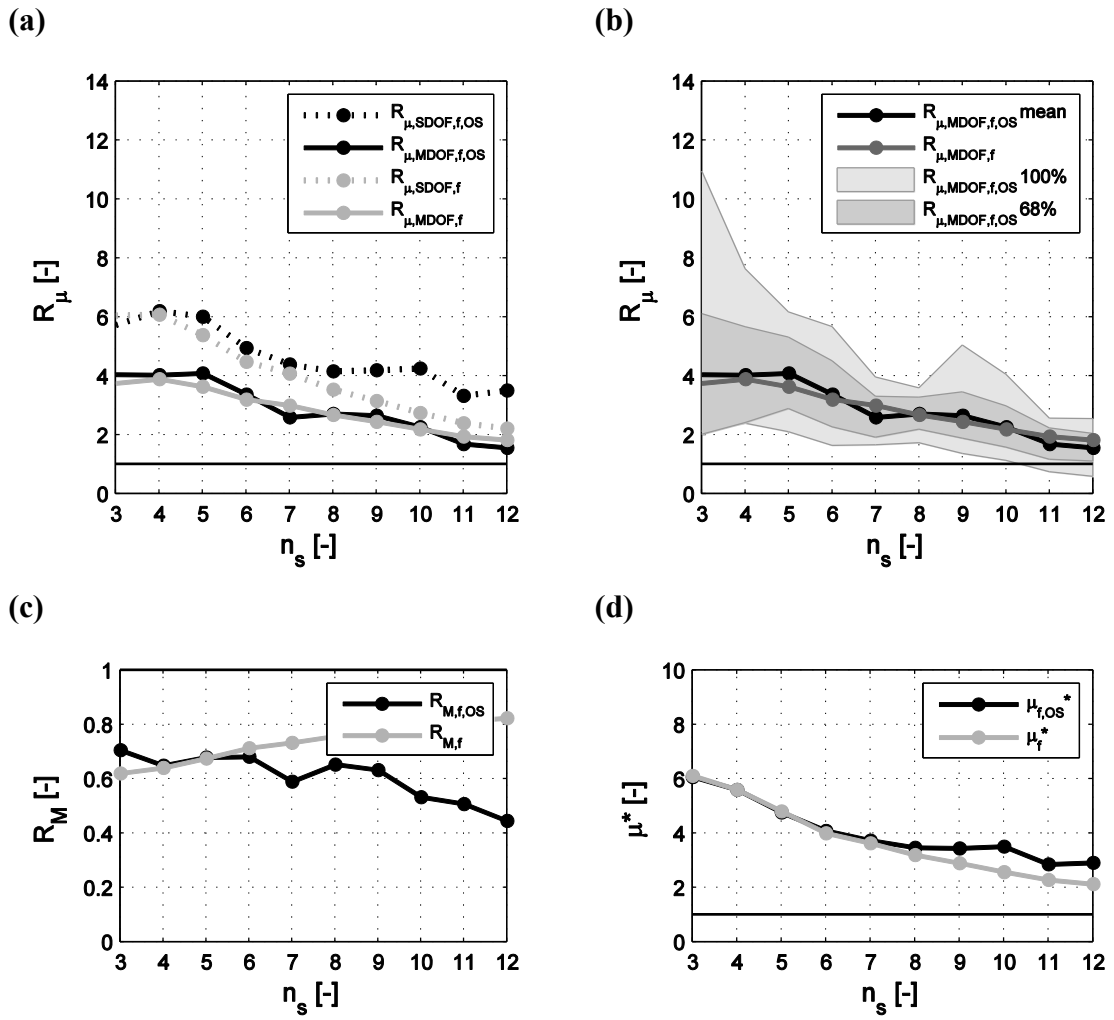

Figure 34: Results of F2 frame system, (a, b): $R_{\mu,SDOF,f}$, $R_{\mu,MDOF,f}$, (c): $R_{M,f}$, (d): ${\mu_f}^*$

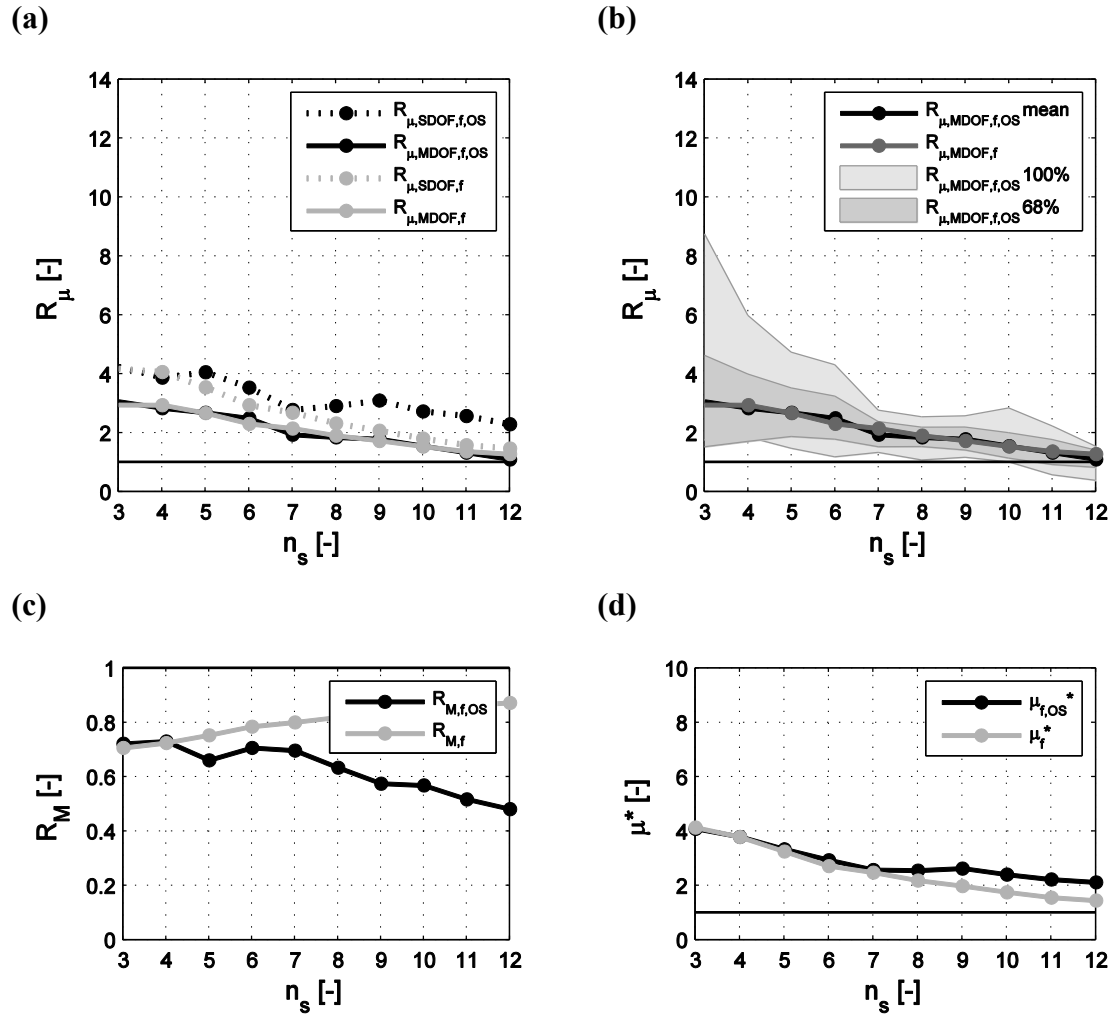

Figure 35: Results of F3 frame system, (a, b): $R_{\mu,SDOF,f}$, $R_{\mu,MDOF,f}$, (c): $R_{M,f}$, (d): ${\mu_f}^*$

Table 16: Results of F1 frame system.

	OpenSees				Proposed analytical method			
n_s	$R_{\mu,SDOF,f}$	$R_{\mu,MDOF,f}$	$R_{M,f}$	${\mu_f}^*$	$R_{\mu,SDOF,f}$	$R_{\mu,MDOF,f}$	$R_{M,f}$	${\mu_f}^*$
3	8.82	5.61	0.64	8.08	7.88	4.35	0.55	8.10
4	8.28	4.80	0.58	7.49	8.12	4.67	0.57	7.41
5	7.58	4.97	0.66	6.37	7.29	4.46	0.61	6.36
6	6.37	4.01	0.63	5.36	6.09	3.99	0.65	5.28
7	5.54	3.43	0.62	4.92	5.54	3.75	0.68	4.79
8	5.15	3.48	0.67	4.42	4.80	3.37	0.70	4.22
9	5.39	3.02	0.56	4.32	4.27	3.09	0.72	3.82
10	5.05	2.71	0.54	3.79	3.72	2.78	0.75	3.39
11	4.18	2.10	0.50	3.48	3.24	2.49	0.77	3.01
12	4.07	1.85	0.45	3.33	2.99	2.34	0.78	2.82

Table 17: Results of F2 frame system.

n_s	OpenSees				Proposed analytical method			
	$R_{\mu,SDOF,f}$	$R_{\mu,MDOF,f}$	$R_{M,f}$	$\mu_f{}^*$	$R_{\mu,SDOF,f}$	$R_{\mu,MDOF,f}$	$R_{M,f}$	$\mu_f{}^*$
3	5.74	4.05	0.71	6.08	6.05	3.76	0.62	6.12
4	6.20	4.03	0.65	5.60	6.09	3.90	0.64	5.60
5	6.02	4.09	0.68	4.77	5.39	3.64	0.68	4.81
6	4.95	3.38	0.68	4.10	4.49	3.21	0.71	4.00
7	4.40	2.60	0.59	3.73	4.09	3.00	0.73	3.64
8	4.16	2.72	0.65	3.47	3.54	2.68	0.76	3.21
9	4.20	2.66	0.63	3.45	3.16	2.45	0.78	2.90
10	4.26	2.27	0.53	3.51	2.75	2.19	0.80	2.58
11	3.33	1.69	0.51	2.86	2.40	1.95	0.81	2.29
12	3.51	1.57	0.45	2.92	2.22	1.83	0.82	2.14

Table 18: Results of F3 frame system.

n_s	OpenSees				Proposed analytical method			
	$R_{\mu,SDOF,f}$	$R_{\mu,MDOF,f}$	$R_{M,f}$	$\mu_f{}^*$	$R_{\mu,SDOF,f}$	$R_{\mu,MDOF,f}$	$R_{M,f}$	$\mu_f{}^*$
3	4.25	3.07	0.72	4.10	4.18	2.96	0.71	4.14
4	3.88	2.84	0.73	3.83	4.07	2.95	0.73	3.79
5	4.06	2.69	0.66	3.34	3.55	2.68	0.75	3.26
6	3.54	2.50	0.71	2.93	2.94	2.31	0.79	2.72
7	2.79	1.94	0.70	2.58	2.69	2.15	0.80	2.49
8	2.92	1.85	0.63	2.56	2.33	1.91	0.82	2.19
9	3.11	1.79	0.58	2.61	2.08	1.73	0.83	1.99
10	2.73	1.56	0.57	2.41	1.82	1.55	0.85	1.76
11	2.58	1.33	0.52	2.24	1.59	1.38	0.87	1.56
12	2.30	1.11	0.48	2.12	1.47	1.29	0.87	1.45

The following considerations concerning result mean values can be drawn:

(i) It is evident that ductility reduction factors, $R_{\mu,SDOF,f}$ and $R_{\mu,MDOF,f}$, and target ductility, $\mu_f{}^*$, decreases with the number of storeys (Figure 33a,b,d-Figure 35a,b,d), that can be explained as the loss of capability of the system to exploit the sectional inelasticity.

(ii) The ductility reduction factor for the equivalent SDOF systems, $R_{\mu,SDOF,f}$, is underestimated by the proposed analytical model with an error of 16% on average. Instead, the ductility reduction factor for the MDOF systems, $R_{\mu,MDOF,f}$, is well predicted by the proposed analytical model and overestimated with an error of 2% on average (Figure 33a-Figure 35a). $R_{\mu,SDOF,f}$ and $R_{\mu,MDOF,f}$ decrease with the number of storeys, and they show a linear trend. Numerical models give values of $R_{\mu,MDOF,f}$ ranged from 5.6 to 1.9, from 4.1 to 1.6 and from 3.1 and 1.1 for F1, F2 and F3, respectively.

(iii) The modification factor, $R_{M,f}$, is basically constant and lightly affected by both the sectional ductility capacity of the base column and the number of storeys. $R_{M,f}$ is

overestimated by the proposed model with an error of 25% on average. (Figure 33c-Figure 35c). Numerical models give values ranged from 0.7 to 0.4 for all group of frames.

(iv) The target ductility, $\mu_f{}^*$, is underestimated by the proposed model with an error of 10% on average (Figure 33d-Figure 35d). $\mu_f{}^*$ decreases with n_s that can be explained as the loss of capability of the system to exploit the section ductility with the increasing of the number of storeys due to higher mode effects. Numerical models give values ranged from 8.1 to 3.3, from 6.1 to 2.9 and from 4.1 and 2.1 for F1, F2 and F3, respectively. The decreasing of $\mu_f{}^*$ from F1 to F3 groups is obvious because the sectional ductility of the base column decreases for F1, F2 and F3, respectively (Table 9 of Section 4.2.1). Furthermore, $\mu_f{}^*$ decreases with the number of storeys, that is the system is less efficient to exploit the sectional ductility and to convert it in available capacity ductility, $\mu_f{}^*$, with the increasing of n_s.

(v) The dispersion of data is considerable when all analyses are considered, but a lower scatter is evidenced when 68% coverage of population is assumed (Figure 33b-Figure 35b).

It is evident from Figure 33a-Figure 35a that $R_{\mu,MDOF,f}$ is not significantly different among the groups of frames, differently from wall systems; instead from Figure 33c-Figure 35c it is noted that $R_{M,f}$ is not significantly different among the groups of frames, as for wall systems. Furthermore, $R_{\mu,MDOF,f}$ is significantly higher than $R_{\mu,MDOF,w}$, especially at high the number of storeys, and $R_{\mu,MDOF,w}$ decreases rapidly than $R_{\mu,MDOF,f}$.

It is to be noticed that some convergence problems occurred during the numerical analysis due to convergence failures in the numerical procedure to calculate the ductility reduction factors, in particular when the convergence errors exceeded the 5% tolerance on the search for the ground motion scale factor (MDOF system) or the target ductility (equivalent SDOF system), within 20 iterations. The percentage of successful analyses, which is the ratio of successful analyses number and the total analyses number, is equal to 76%. Analyses fail randomly varying the number of storeys and ground motions; so they do not show systematic bias due to certain patterns.

The comparison of fundamental periods given by the numerical model, $T_{1,f,OS}$, and analytical model, $T_{1,w}$, given by Equation (99), is illustrated in Figure 36 and listed in Table 19. The analytical fundamental periods overestimate the numerical values of 11% on average. The numerical period is different from the analytical one because the analytical formula is exact for uniformly distributed mass along the height of the structure, instead considered numerical models are lumped mass systems.

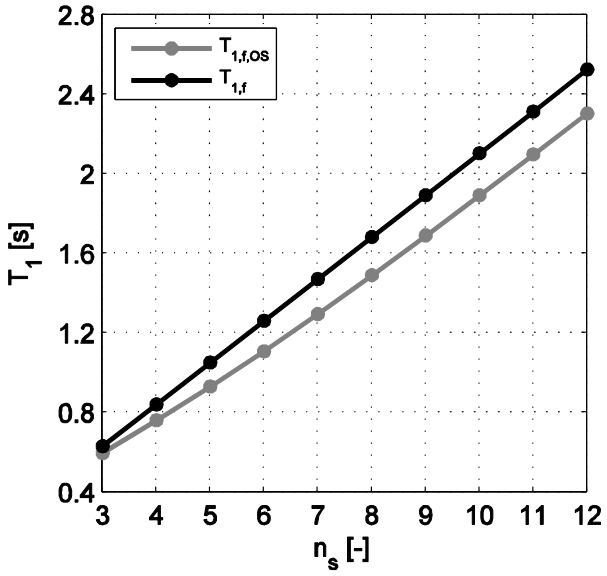

Figure 36: Fundamental periods of frame systems.

Table 19: Fundamental period [s] of frame systems.

n_s	OpenSees	Analytical prediction	Relative error
3	0.5974	0.6313	+6%
4	0.7628	0.8418	+10%
5	0.9322	1.0522	+13%
6	1.1082	1.2627	+14%
7	1.2958	1.4731	+14%
8	1.4914	1.6836	+13%
9	1.6916	1.8940	+12%
10	1.8942	2.1045	+11%
11	2.0988	2.3149	+10%
12	2.3042	2.5254	+10%

5.3. Results for dual systems

In this Section a detailed comparison of numerical results of Section 4 and analytical results of Section 3 are reported.

Results of dual systems are illustrated in Figure 38-Figure 52 and listed in Table 21-Table 35. For the sake of brevity, the subscript "MDOF" is omitted from labels in figures, because they always refer to MDOF systems. Numerical values are indicated with "OS" label in figures.

Each Figure is composed of six plots.

In Plot (a), the numerical ductility reduction factor for dual system structures, $R_{\mu,MDOF,d,OS}$, and the relative ductility reduction factor for the wall-equivalent system, $R_{\mu,MDOF,w,d,OS}$, and the ductility reduction factor for the frame-equivalent system, $R_{\mu,MDOF,f,d,OS}$, are shown as a function of the number of storeys, n_s.

In Plot (b), the comparison between the numerical ductility reduction factor for dual system structures, $R_{\mu,MDOF,d,OS}$, and the analytical ductility reduction factor for the wall and frame systems considered as single systems, $R_{\mu,MDOF,w}$ and $R_{\mu,MDOF,f}$, respectively, is illustrated. The dispersion of $R_{\mu,MDOF,d,OS}$ is also shown. All analyses (100%) and 68% coverage of population are plotted as a function of the number of storeys, n_s.

In Plot (c) and Plot (d), the wall use rate, u_w, the frame use rate, u_f, and the wall base shear ratio, v_w, the frame base shear ratio, v_f, are drawn, respectively, as a function of the number of storeys, n_s.

In Plot (e), the target ductility of the wall, ${\mu_{w,d}}^*$, and the target ductility of the frame system, ${\mu_{f,d}}^*$, in the dual systems are compared with the target ductility of the wall, ${\mu_w}^*$, and the target ductility of the frame system, ${\mu_f}^*$, when they are considered single systems, i.e., target ductilities given by the proposed analytical model for single systems. Target ductilities are plotted as a function of the number of storeys, n_s.

In Plot (f), the comparison between the numerical ductility reduction factor for dual system structures, $R_{\mu,MDOF,d}$, and the analytical expressions, $R_{\mu,MDOF,d,1}$ and $R_{\mu,MDOF,d,2}$, given by Expression (149) and Expression (150), is shown as a function of the number of storeys, n_s.

The first expression, $R_{\mu,MDOF,d,1}$, is a polynomial regression of results. This expression has been determined as the best fit of results and it is given by:

$$R_{\mu,MDOF,d,1} = a_1 \frac{{R_{\mu,MDOF,w}}^{c_1}}{{\mu_w}^{*b_1}} + a_2 \frac{{R_{\mu,MDOF,f}}^{c2}}{{\mu_f}^{*b_2}} = 0.76{\mu_w}^{*0.36} {R_{\mu,MDOF,w}}^{0.38} + 0.99 \frac{{R_{\mu,MDOF,f}}^{8.63}}{{\mu_f}^{*6.89}} \quad (149)$$

The second expression, $R_{\mu,MDOF,d,2}$, is a simpler expression than Equation (121):

$$R_{\mu,MDOF,d,2} = a_1 R_{\mu,MDOF,w} + a_2 \frac{R_{\mu,MDOF,f}}{\sqrt{\mu_f}^*} = 0.08 R_{\mu,MDOF,w} + 1.64 \frac{R_{\mu,MDOF,f}}{\sqrt{\mu_f}^*} \quad (150)$$

It is to be noticed that some convergence problems occurred during the numerical analysis due to convergence failures in the numerical procedure to calculate the ductility reduction factors, in particular when the convergence errors exceeded the 5% tolerance on the search for the ground motion scale factor (MDOF system) or the target ductility (equivalent SDOF systems), within 20 iterations. The percentage of successful analyses, which is the ratio of successful analyses number and the total analyses number, is equal to 73%. Analyses fail randomly varying the number of storeys and ground motions; so they do not show systematic bias due to certain patterns.

Analyses prove that an estimation of the elastic fundamental period of a frame-wall structure, $T_{1,d}$, can be taken as a linear combination of the elastic fundamental period of the wall system, $T_{1,w}$, and the frame system, $T_{1,f}$, which the dual system is composed of.

$$T_{1,d} = 0.1 T_{1,w} + 0.7 T_{1,f} \quad (151)$$

The comparison of fundamental periods given by the numerical model, $T_{1,d,OS}$, and by Equation (151), $T_{1,d}$, are illustrated in Figure 37 and listed in Table 20. The analytical fundamental periods underestimate the numerical values of 3% on average. It is noted that in Figure 37 five numerical sets of periods which refer to C2, C5, C10, C15 and C20 OpenSees models are compared to the proposed analytical period of dual systems.

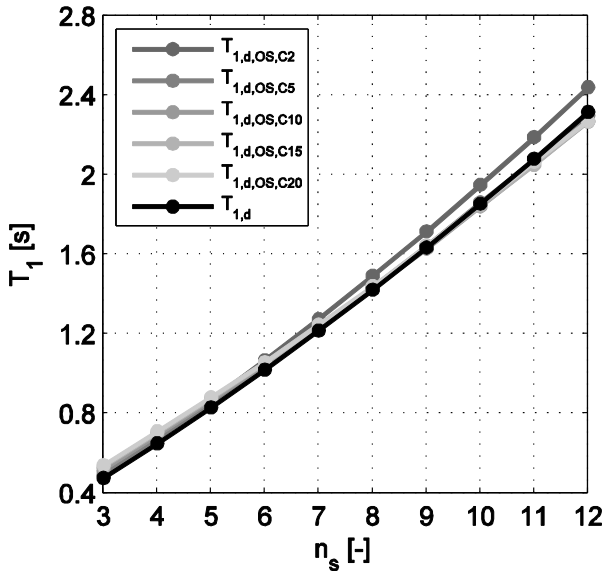

Figure 37: Fundamental periods of dual systems.

Table 20: Fundamental period [s] of dual systems.

n_s	OpenSees					Analytical prediction
	C1	C5	C10	C15	C20	
3	0.4829	0.5029	0.5217	0.5334	0.5415	0.4763
4	0.6741	0.6783	0.6923	0.7028	0.7106	0.6504
5	0.8685	0.8572	0.8670	0.8754	0.8822	0.8321
6	1.0687	1.0419	1.0463	1.0540	1.0585	1.0215
7	1.2752	1.2344	1.2327	1.2390	1.2466	1.2185
8	1.4936	1.4364	1.4305	1.4330	1.4412	1.4232
9	1.7177	1.6448	1.6306	1.6357	1.6445	1.6355
10	1.9508	1.8625	1.8429	1.8465	1.8562	1.8554
11	2.1909	2.0763	2.0552	2.0508	2.0656	2.0830
12	2.4422	2.2996	2.2688	2.2704	2.2717	2.3182

5.3.1. W1F1 group

In this section, results of group W1F1 are discussed in detail; results are illustrated in Figure 38-Figure 42 and also reported as numerical values in Table 21-Table 25.

The following considerations concerning result mean values can be drawn:

(i) The numerical ductility reduction factor for dual system structures, $R_{\mu,MDOF,d,OS}$, is a value intermediate between the ductility reduction factor for the wall-equivalent system, $R_{\mu,MDOF,w,d,OS}$, and the ductility reduction factor for the frame-equivalent system, $R_{\mu,MDOF,f,d,OS}$, (Figure 38a-Figure 42a).

(ii) $R_{\mu,MDOF,w,d,OS}$ is always lower than $R_{\mu,MDOF,f,d,OS}$ (Figure 38a-Figure 42a) as well as the analytical ductility reduction factor for wall system, $R_{\mu,MDOF,w}$, is always lower than analytical ductility reduction factor for frame system, $R_{\mu,MDOF,f}$, (Figure 38b-Figure 42b).

(iii) The wall use rate, $u_{w,OS}$, is equal to 1 for all cases, it means that the wall is always the system to fail. The frame use rate, $u_{f,OS}$, is between 0.3 for number of storeys and almost 1 for high number of storeys (Figure 38c-Figure 42c).

(iv) The wall base shear ratio, $v_{w,OS}$, remains nearly constant with the number of storeys but it decreases with the increasing of the number of columns, from C2 to C20. Wall base shear ratios have values ranged from 0.2 to 0.8, approximately (Figure 38d-Figure 42d). Vice versa, the frame base shear ratio, $v_{f,OS}$, increases with the increasing of the number of columns, from C2 to C20. Base shear ratios have values ranged from 0.2 to 0.8, approximately and wall base shear ratio, $v_{w,OS}$, is higher than frame base shear ratio, $v_{f,OS}$, for W1F1C2 and W1F1C5.

(v) The target ductility of the wall, $\mu_{w,d,OS}{}^{*}$, in the dual system is always lower than the target ductility of the wall, $\mu_{w}{}^{*}$, when it is considered single system. Instead, the target ductility of the frame, $\mu_{f,d,OS}{}^{*}$, in the dual system is generally lower than the target ductility of the frame, $\mu_{f}{}^{*}$, when it is considered single system, except to high number of storeys and in particular the W1F1C2 structures (Figure 38e-Figure 42e).

(vi) Both analytical expressions, $R_{\mu,MDOF,d1}$ and $R_{\mu,MDOF,d2}$, show a good match with the numerical ductility reduction factor for dual system structures, $R_{\mu,MDOF,d,OS}$ (Figure 38f-Figure 42f).

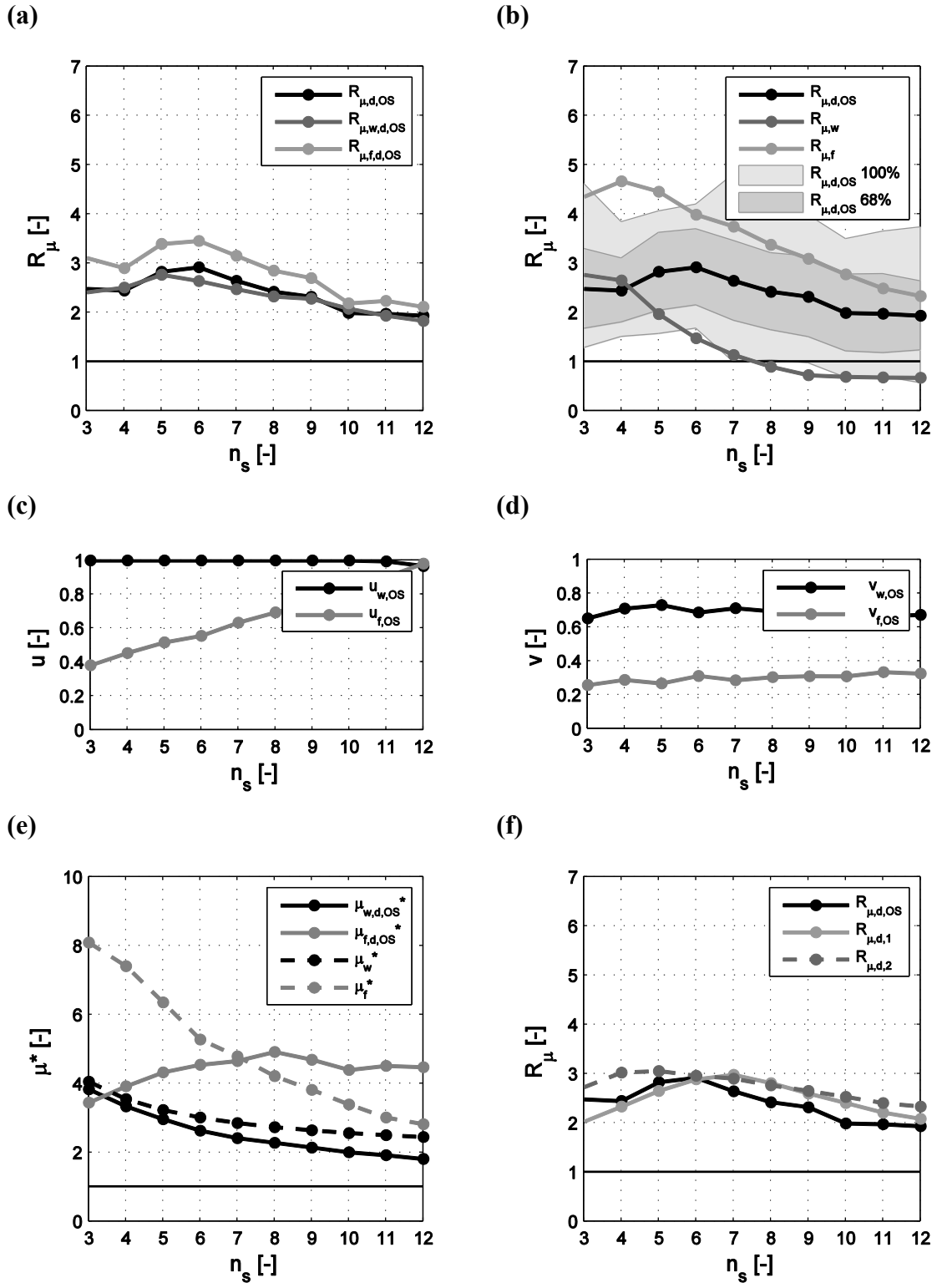

Figure 38: Results of W1F1C2 dual system, (a, b): $R_{\mu,MDOF,d}$, (c): use rates, (d): base shear ratios, (e): target ductilities, (f): analytical expressions.

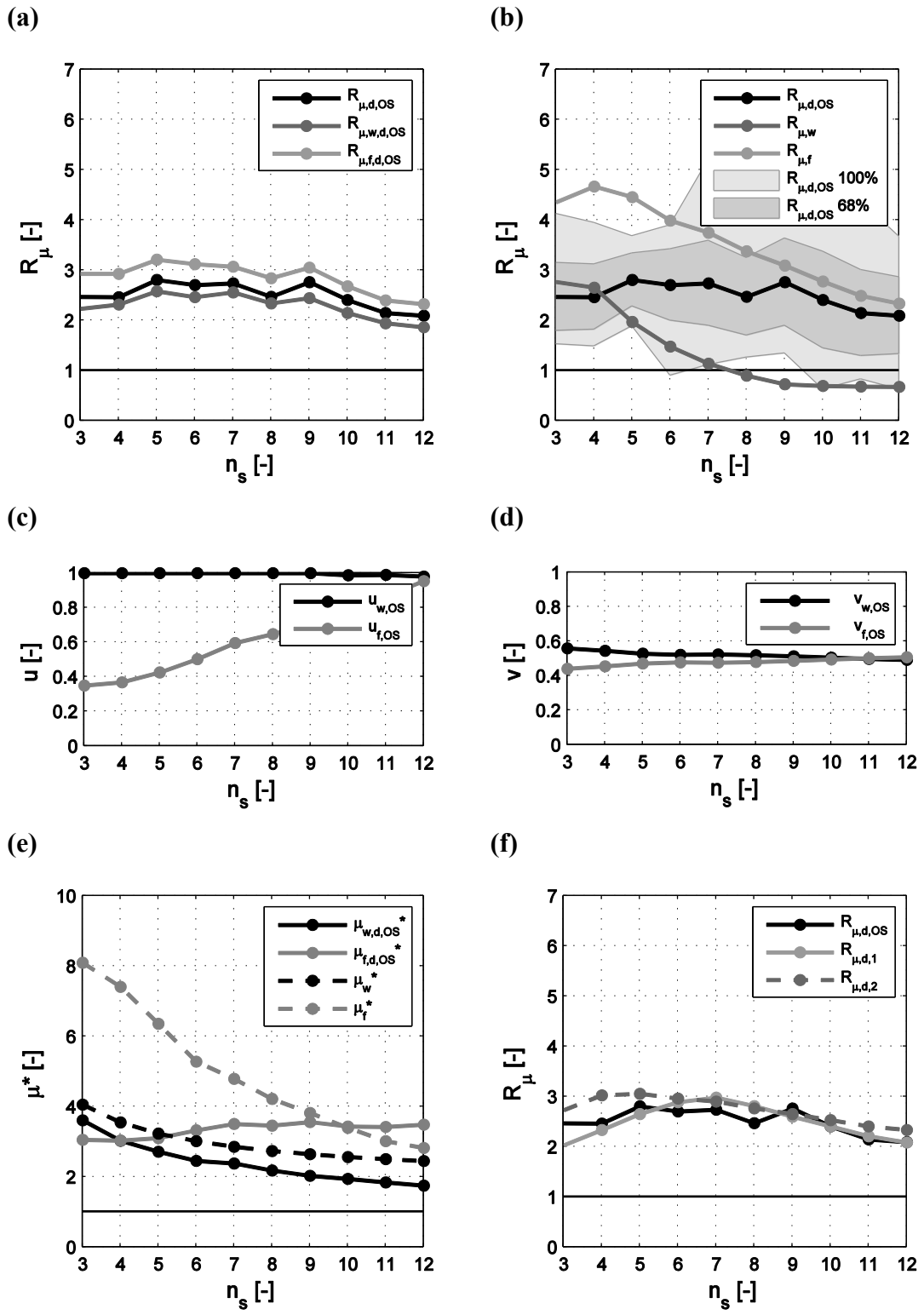

Figure 39: Results of W1F1C5 dual system, (a, b): $R_{\mu,MDOF,d}$, (c): use rates, (d): base shear ratios, (e): target ductilities, (f): analytical expressions.

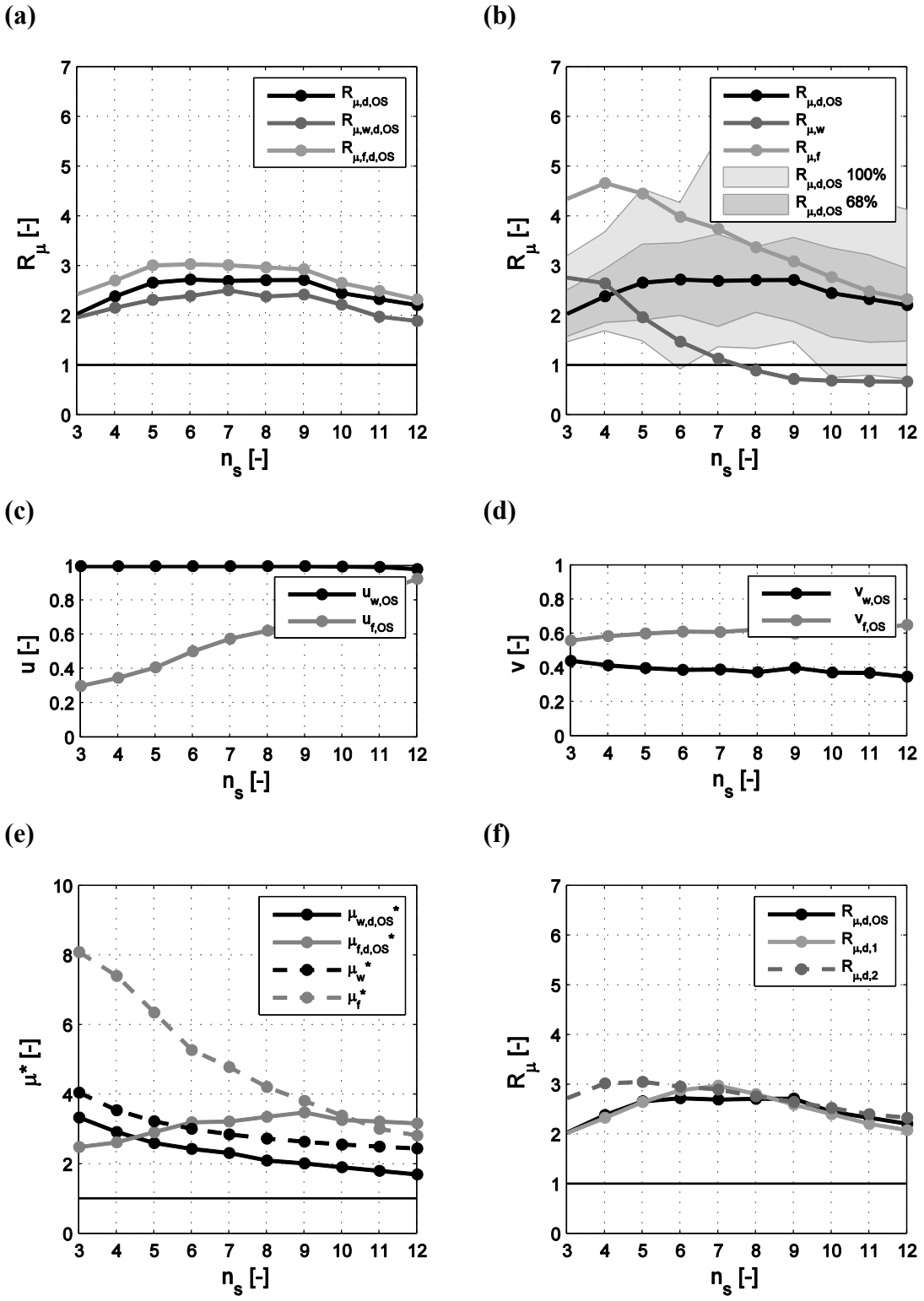

Figure 40: Results of W1F1C10 dual system, (a, b): $R_{\mu,MDOF,d}$, (c): use rates, (d): base shear ratios, (e): target ductilities, (f): analytical expressions.

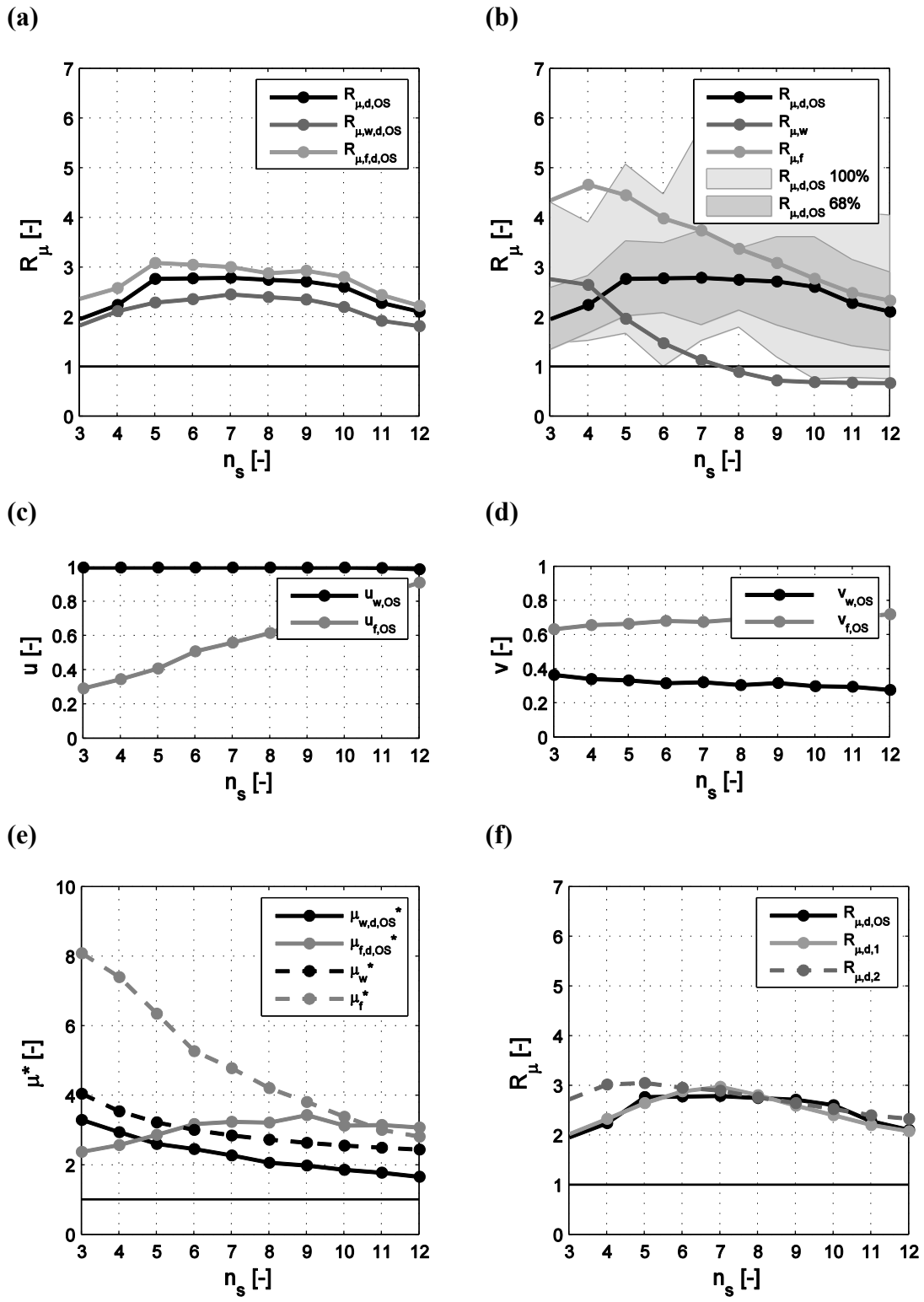

Figure 41: Results of W1F1C15 dual system, (a, b): $R_{\mu,MDOF,d}$, (c): use rates, (d): base shear ratios, (e): target ductilities, (f): analytical expressions.

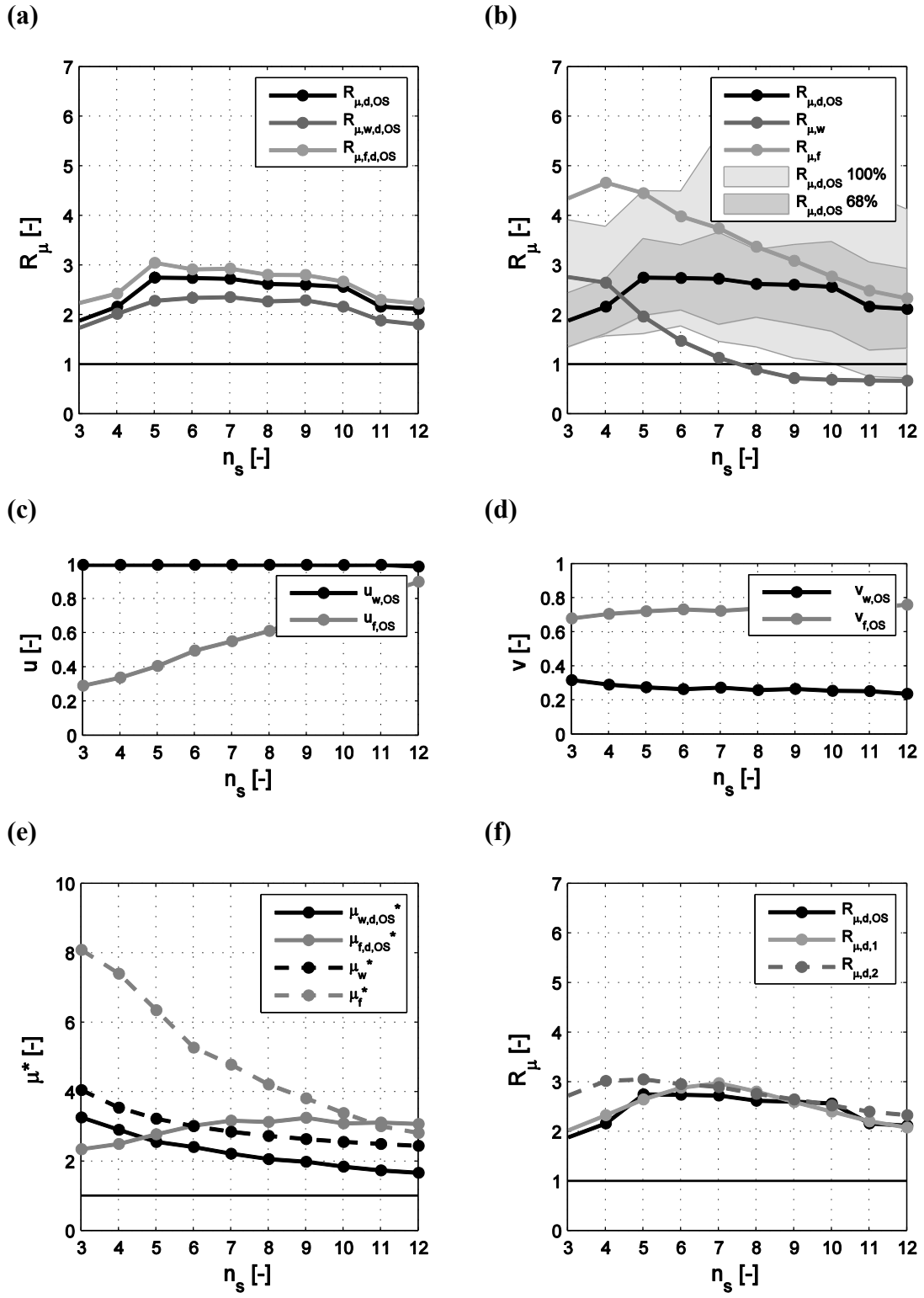

Figure 42: Results of W1F1C20 dual system, (a, b): $R_{\mu,MDOF,d}$, (c): use rates, (d): base shear ratios, (e): target ductilities, (f): analytical expressions.

Table 21: Results of W1F1C2 dual system.

n_s	$R_{\mu,w,d}$	$R_{\mu,f,d}$	$R_{\mu,d}$	u_w	u_f	v_w	v_f	$\mu_{w,d}{}^*$	$\mu_{f,d}{}^*$	$R_{\mu,d,1}$	$R_{\mu,d,2}$
3	2.41	3.11	2.48	1.0	0.4	0.7	0.3	3.84	3.45	1.92	2.61
4	2.51	2.90	2.45	1.0	0.5	0.7	0.3	3.34	3.92	2.35	2.89
5	2.77	3.39	2.83	1.0	0.5	0.7	0.3	2.97	4.33	2.70	2.93
6	2.64	3.46	2.92	1.0	0.6	0.7	0.3	2.64	4.55	2.91	2.84
7	2.47	3.15	2.64	1.0	0.6	0.7	0.3	2.42	4.65	2.97	2.78
8	2.33	2.85	2.42	1.0	0.7	0.7	0.3	2.29	4.92	2.79	2.66
9	2.28	2.70	2.32	1.0	0.8	0.7	0.3	2.14	4.69	2.58	2.55
10	2.08	2.19	1.99	1.0	0.8	0.7	0.3	2.01	4.39	2.39	2.43
11	1.93	2.24	1.98	1.0	0.9	0.7	0.3	1.92	4.51	2.19	2.31
12	1.83	2.12	1.93	1.0	1.0	0.7	0.3	1.81	4.48	2.06	2.25

Table 22: Results of W1F1C5 dual system.

n_s	$R_{\mu,w,d}$	$R_{\mu,f,d}$	$R_{\mu,d}$	u_w	u_f	v_w	v_f	$\mu_{w,d}{}^*$	$\mu_{f,d}{}^*$	$R_{\mu,d,1}$	$R_{\mu,d,2}$
3	2.23	2.93	2.47	1.0	0.4	0.6	0.4	3.61	3.06	1.92	2.61
4	2.32	2.93	2.46	1.0	0.4	0.5	0.5	3.03	3.03	2.35	2.89
5	2.58	3.21	2.81	1.0	0.4	0.5	0.5	2.71	3.10	2.70	2.93
6	2.46	3.12	2.71	1.0	0.5	0.5	0.5	2.46	3.32	2.91	2.84
7	2.56	3.07	2.74	1.0	0.6	0.5	0.5	2.38	3.50	2.97	2.78
8	2.34	2.84	2.47	1.0	0.6	0.5	0.5	2.18	3.46	2.79	2.66
9	2.44	3.05	2.76	1.0	0.7	0.5	0.5	2.03	3.56	2.58	2.55
10	2.15	2.68	2.41	1.0	0.8	0.5	0.5	1.95	3.43	2.39	2.43
11	1.94	2.40	2.15	1.0	0.9	0.5	0.5	1.84	3.42	2.19	2.31
12	1.86	2.32	2.09	1.0	1.0	0.5	0.5	1.75	3.48	2.06	2.25

Table 23: Results of W1F1C10 dual system.

n_s	$R_{\mu,w,d}$	$R_{\mu,f,d}$	$R_{\mu,d}$	u_w	u_f	v_w	v_f	$\mu_{w,d}{}^*$	$\mu_{f,d}{}^*$	$R_{\mu,d,1}$	$R_{\mu,d,2}$
3	1.97	2.44	2.04	1.0	0.3	0.4	0.6	3.34	2.49	1.92	2.61
4	2.16	2.71	2.39	1.0	0.3	0.4	0.6	2.93	2.63	2.35	2.89
5	2.32	3.01	2.67	1.0	0.4	0.4	0.6	2.60	2.92	2.70	2.93
6	2.40	3.03	2.73	1.0	0.5	0.4	0.6	2.44	3.20	2.91	2.84
7	2.51	3.02	2.70	1.0	0.6	0.4	0.6	2.32	3.23	2.97	2.78
8	2.39	2.97	2.72	1.0	0.6	0.4	0.6	2.10	3.36	2.79	2.66
9	2.42	2.93	2.72	1.0	0.7	0.4	0.6	2.02	3.49	2.58	2.55
10	2.22	2.66	2.46	1.0	0.8	0.4	0.6	1.91	3.27	2.39	2.43
11	1.98	2.50	2.33	1.0	0.9	0.4	0.6	1.81	3.22	2.19	2.31
12	1.89	2.33	2.21	1.0	0.9	0.3	0.7	1.71	3.17	2.06	2.25

Table 24: Results of W1F1C15 dual system.

n_s	$R_{\mu,w,d}$	$R_{\mu,f,d}$	$R_{\mu,d}$	u_w	u_f	v_w	v_f	${\mu_{w,d}}^*$	${\mu_{f,d}}^*$	$R_{\mu,d,1}$	$R_{\mu,d,2}$
3	1.84	2.37	1.96	1.0	0.3	0.4	0.6	3.30	2.39	1.92	2.61
4	2.12	2.59	2.25	1.0	0.3	0.3	0.7	2.95	2.58	2.35	2.89
5	2.30	3.09	2.77	1.0	0.4	0.3	0.7	2.61	2.88	2.70	2.93
6	2.37	3.06	2.78	1.0	0.5	0.3	0.7	2.47	3.18	2.91	2.84
7	2.46	3.01	2.79	1.0	0.6	0.3	0.7	2.28	3.25	2.97	2.78
8	2.41	2.88	2.75	1.0	0.6	0.3	0.7	2.08	3.23	2.79	2.66
9	2.36	2.93	2.72	1.0	0.7	0.3	0.7	2.00	3.44	2.58	2.55
10	2.20	2.81	2.61	1.0	0.8	0.3	0.7	1.87	3.14	2.39	2.43
11	1.93	2.45	2.29	1.0	0.8	0.3	0.7	1.79	3.16	2.19	2.31
12	1.82	2.23	2.11	1.0	0.9	0.3	0.7	1.67	3.09	2.06	2.25

Table 25: Results of W1F1C20 dual system.

n_s	$R_{\mu,w,d}$	$R_{\mu,f,d}$	$R_{\mu,d}$	u_w	u_f	v_w	v_f	${\mu_{w,d}}^*$	${\mu_{f,d}}^*$	$R_{\mu,d,1}$	$R_{\mu,d,2}$
3	1.74	2.24	1.89	1.0	0.3	0.3	0.7	3.27	2.35	1.92	2.61
4	2.02	2.43	2.17	1.0	0.3	0.3	0.7	2.92	2.50	2.35	2.89
5	2.28	3.05	2.75	1.0	0.4	0.3	0.7	2.56	2.78	2.70	2.93
6	2.35	2.92	2.75	1.0	0.5	0.3	0.7	2.42	3.03	2.91	2.84
7	2.36	2.93	2.73	1.0	0.6	0.3	0.7	2.22	3.18	2.97	2.78
8	2.28	2.81	2.63	1.0	0.6	0.3	0.7	2.07	3.14	2.79	2.66
9	2.30	2.81	2.61	1.0	0.7	0.3	0.7	1.99	3.26	2.58	2.55
10	2.17	2.67	2.57	1.0	0.8	0.3	0.7	1.85	3.10	2.39	2.43
11	1.89	2.30	2.17	1.0	0.8	0.3	0.7	1.74	3.12	2.19	2.31
12	1.81	2.23	2.12	1.0	0.9	0.2	0.8	1.67	3.08	2.06	2.25

5.3.2. W2F2 group

In this section, results of group W2F2 are discussed in detail; results are illustrated in Figure 43-Figure 47 and also reported in Table 26-Table 30.

The following considerations concerning result mean values can be drawn:

(i) The numerical ductility reduction factor for dual system structures, $R_{\mu,MDOF,d,OS}$, is a value intermediate between the ductility reduction factor for the wall-equivalent system, $R_{\mu,MDOF,w,d,OS}$, and the ductility reduction factor for the frame-equivalent system, $R_{\mu,MDOF,f,d,OS}$.

(ii) $R_{\mu,MDOF,w,d,OS}$ is always lower than $R_{\mu,MDOF,f,d,OS}$ (Figure 43a-Figure 47a) as well as the analytical ductility reduction factor for wall system, $R_{\mu,MDOF,w}$, is always lower than analytical ductility reduction factor for frame system, $R_{\mu,MDOF,f}$, (Figure 43b-Figure 47b).

(iii) The wall use rate, $u_{w,OS}$, is equal to 1 for number of storeys lower than 7 and the frame use rate, $u_{f,OS}$, is equal to 1 for number of storeys higher than 7. It means that it is the wall to fail for low number of storeys systems and the frame is the system to fail for high number of storeys systems (Figure 43c-Figure 47c).

(iv) The wall base shear ratio, $v_{w,OS}$, remains nearly constant with the number of storeys but it decreases with the increasing of the number of columns, from C2 to C20. Wall base shear ratios have values ranged from 0.2 to 0.8, approximately (Figure 38d-Figure 42d). Vice versa, the frame base shear ratio, $v_{f,OS}$, increases with the increasing of the number of columns, from C2 to C20. Base shear ratios have values ranged from 0.2 to 0.8, approximately and wall base shear ratio, $v_{w,OS}$, is higher than frame base shear ratio, $v_{f,OS}$, for W2F2C2 and W2F2C5.

(v) The target ductility of the wall, ${\mu_{w,d,OS}}^*$, in the dual system is always lower than the target ductility of the wall, ${\mu_w}^*$, when it is considered single system. Instead, the target ductility of the frame, ${\mu_{f,d,OS}}^*$, in the dual system is generally lower than the target ductility of the frame, ${\mu_f}^*$, when it is considered single system, only for systems with low number of storeys (Figure 43e-Figure 47e).

(vi) Both analytical expressions, $R_{\mu,MDOF,d1}$ and $R_{\mu,MDOF,d2}$, show a good match with the numerical ductility reduction factor for dual system structures, $R_{\mu,MDOF,d,OS}$; in particular $R_{\mu,MDOF,d1}$ is capable to better fit the numerical curve shape at medium number of storeys (Figure 43f-Figure 47f).

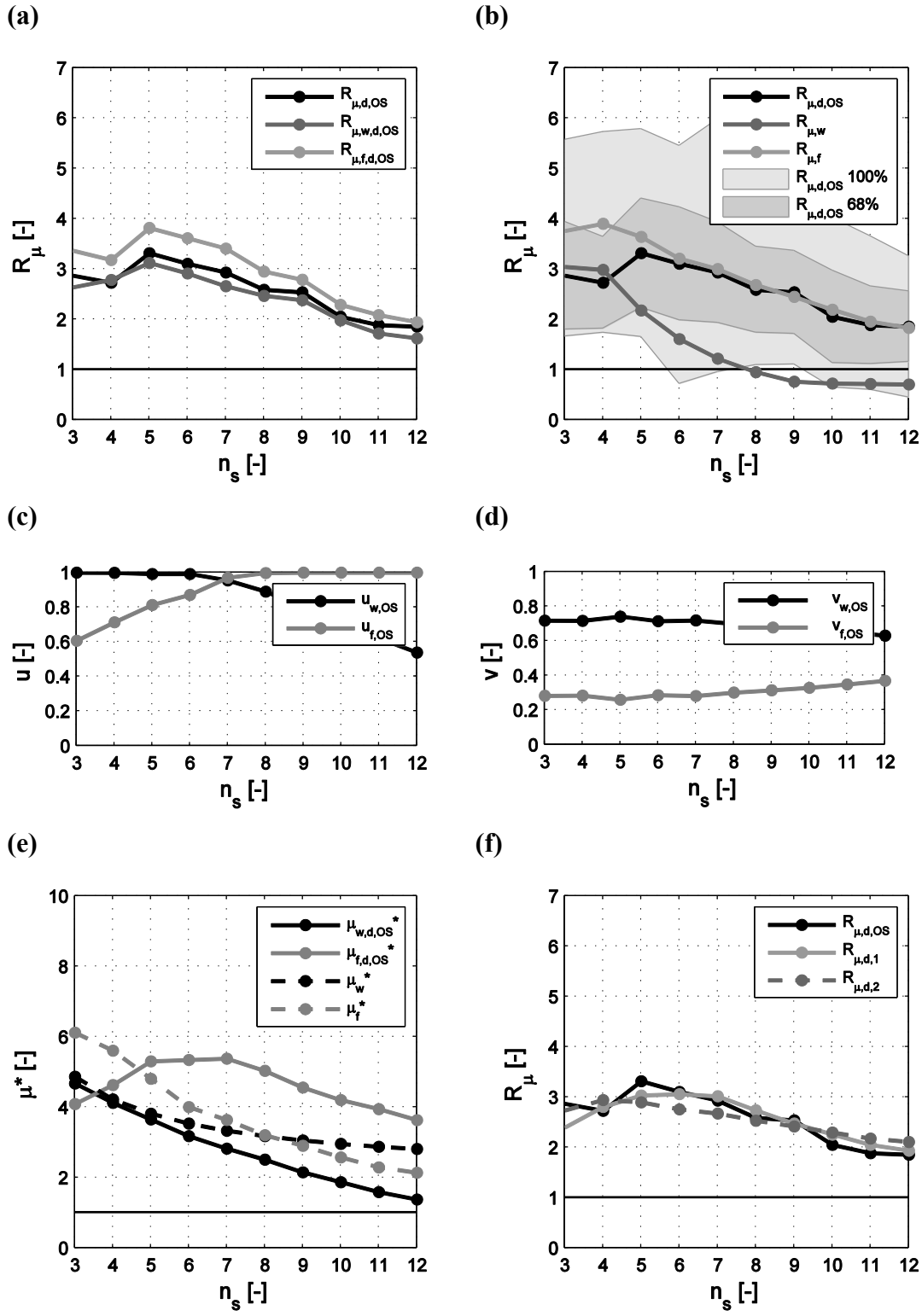

Figure 43: Results of W2F2C2 dual system, (a, b): $R_{\mu,MDOF,d}$, (c): use rates, (d): base shear ratios, (e): target ductilities, (f): analytical expressions.

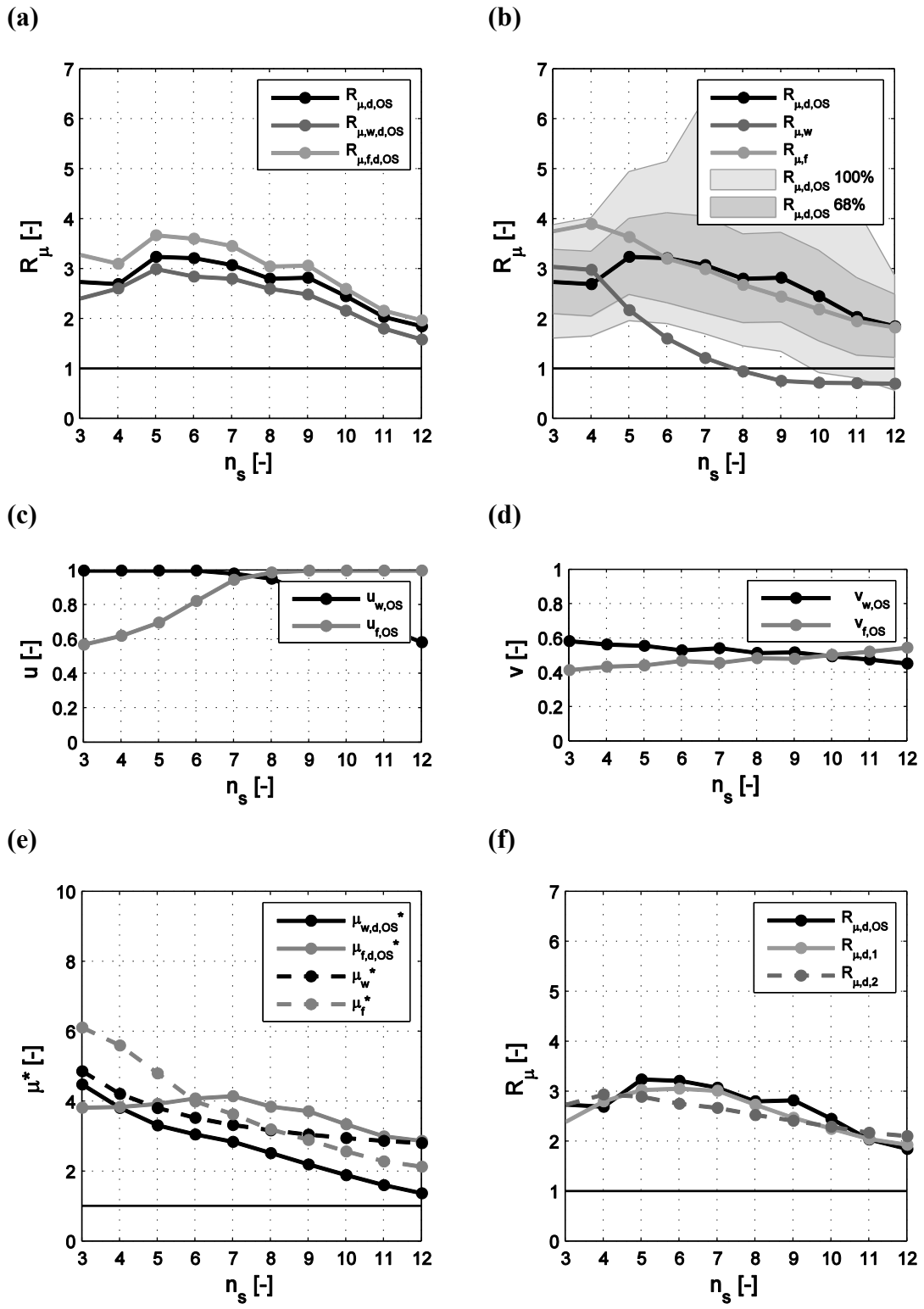

Figure 44: Results of W2F2C5 dual system, (a, b): $R_{\mu,MDOF,d}$, (c): use rates, (d): base shear ratios, (e): target ductilities, (f): analytical expressions.

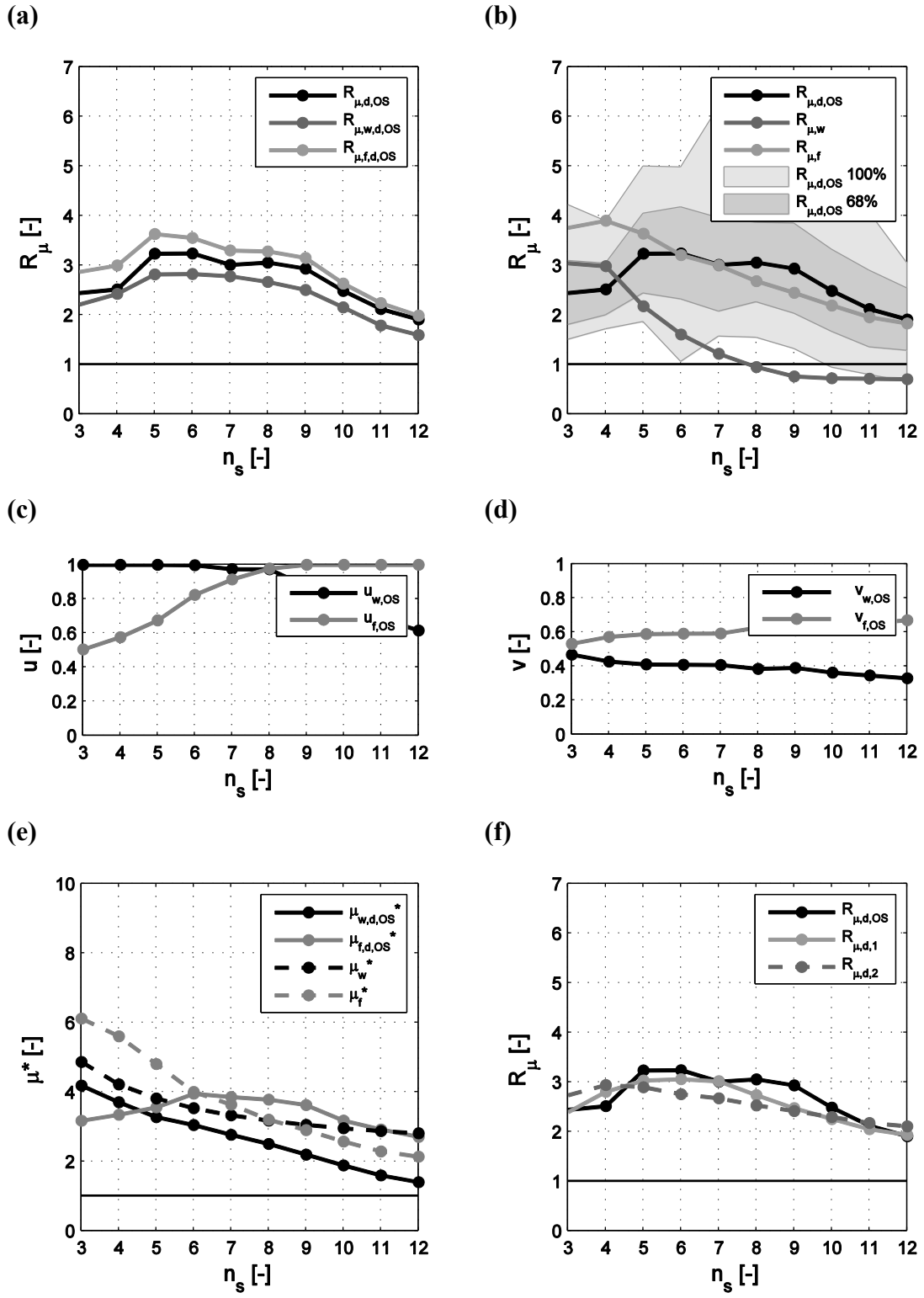

Figure 45: Results of W2F2C10 dual system, (a, b): $R_{\mu,MDOF,d}$, (c): use rates, (d): base shear ratios, (e): target ductilities, (f): analytical expressions.

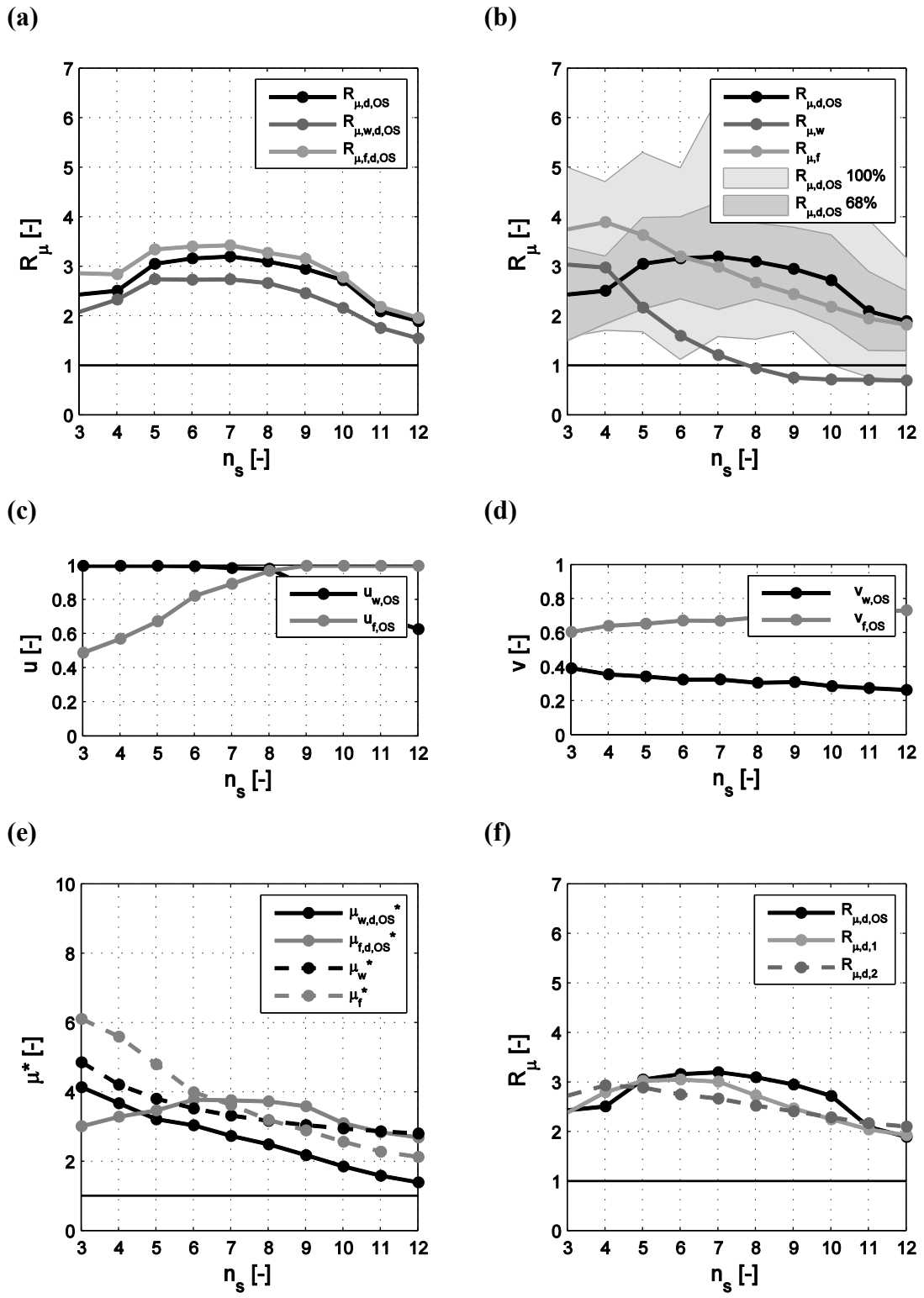

Figure 46: Results of W2F2C15 dual system, (a, b): $R_{\mu,MDOF,d}$, (c): use rates, (d): base shear ratios, (e): target ductilities, (f): analytical expressions.

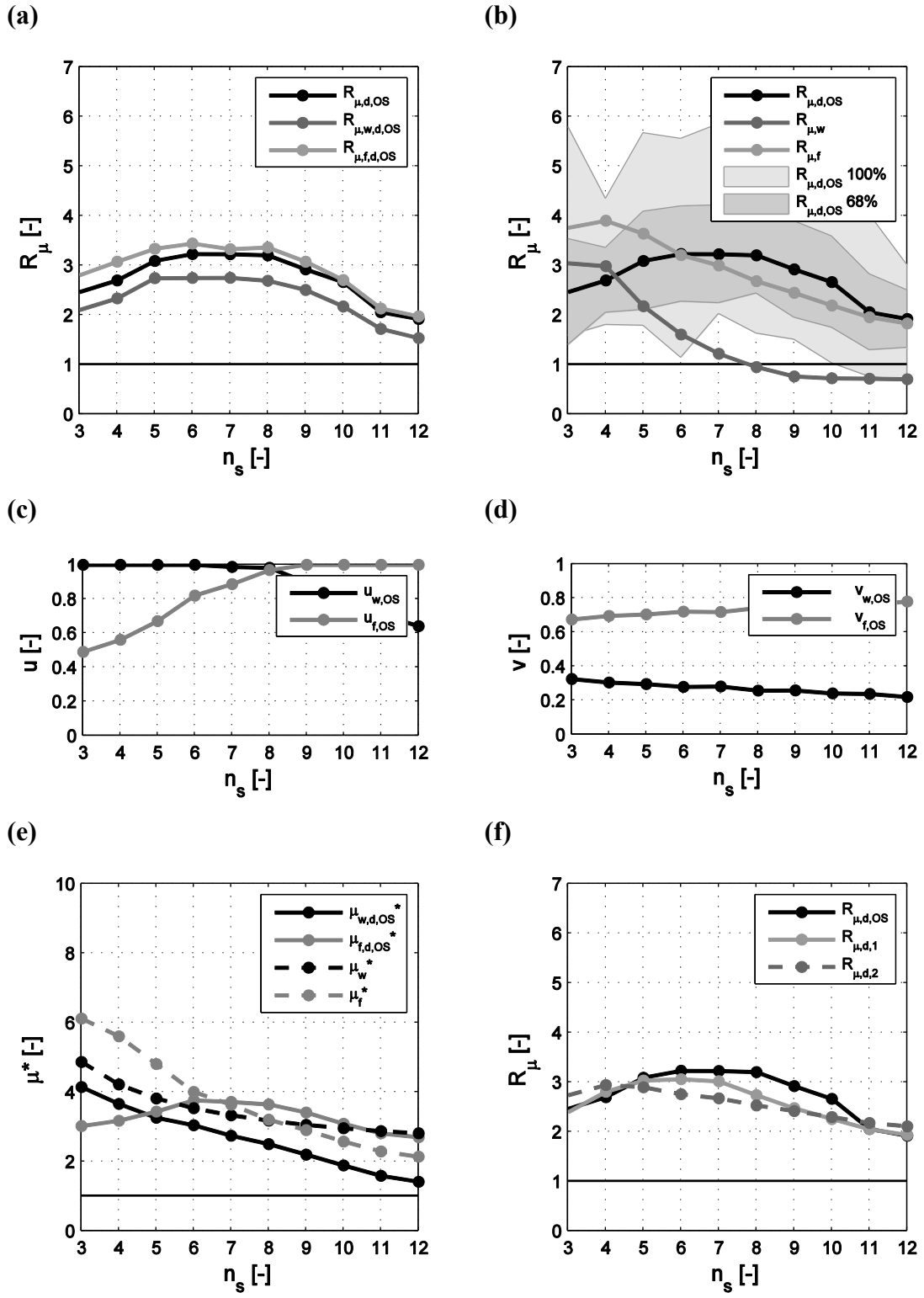

Figure 47: Results of W2F2C20 dual system, (a, b): $R_{\mu,MDOF,d}$, (c): use rates, (d): base shear ratios, (e): target ductilities, (f): analytical expressions.

Table 26: Results of W2F2C2 dual system.

n_s	$R_{\mu,w,d}$	$R_{\mu,f,d}$	$R_{\mu,d}$	u_w	u_f	v_w	v_f	$\mu_{w,d}^*$	$\mu_{f,d}^*$	$R_{\mu,d,1}$	$R_{\mu,d,2}$
3	2.64	3.37	2.87	1.0	0.6	0.7	0.3	4.67	4.09	2.36	2.61
4	2.78	3.18	2.73	1.0	0.7	0.7	0.3	4.12	4.63	2.86	2.81
5	3.12	3.82	3.32	1.0	0.8	0.7	0.3	3.65	5.30	3.06	2.78
6	2.91	3.61	3.11	1.0	0.9	0.7	0.3	3.18	5.34	3.04	2.64
7	2.66	3.41	2.93	1.0	1.0	0.7	0.3	2.82	5.38	2.97	2.57
8	2.47	2.95	2.59	0.9	1.0	0.7	0.3	2.51	5.03	2.69	2.43
9	2.38	2.79	2.54	0.8	1.0	0.7	0.3	2.15	4.56	2.43	2.32
10	1.98	2.29	2.05	0.7	1.0	0.7	0.3	1.87	4.20	2.20	2.21
11	1.72	2.09	1.88	0.6	1.0	0.7	0.3	1.59	3.94	2.00	2.09
12	1.62	1.94	1.86	0.5	1.0	0.6	0.4	1.38	3.63	1.88	2.03

Table 27: Results of W2F2C5 dual system.

n_s	$R_{\mu,w,d}$	$R_{\mu,f,d}$	$R_{\mu,d}$	u_w	u_f	v_w	v_f	$\mu_{w,d}^*$	$\mu_{f,d}^*$	$R_{\mu,d,1}$	$R_{\mu,d,2}$
3	2.41	3.28	2.74	1.0	0.6	0.6	0.4	4.49	3.82	2.36	2.61
4	2.61	3.10	2.70	1.0	0.6	0.6	0.4	3.82	3.84	2.86	2.81
5	3.00	3.68	3.24	1.0	0.7	0.6	0.4	3.32	3.93	3.06	2.78
6	2.85	3.61	3.22	1.0	0.8	0.5	0.5	3.06	4.09	3.04	2.64
7	2.81	3.46	3.08	1.0	0.9	0.5	0.5	2.85	4.15	2.97	2.57
8	2.60	3.05	2.80	1.0	1.0	0.5	0.5	2.53	3.85	2.69	2.43
9	2.49	3.07	2.83	0.9	1.0	0.5	0.5	2.20	3.72	2.43	2.32
10	2.16	2.60	2.46	0.7	1.0	0.5	0.5	1.89	3.35	2.20	2.21
11	1.80	2.17	2.04	0.7	1.0	0.5	0.5	1.61	3.01	2.00	2.09
12	1.59	1.97	1.85	0.6	1.0	0.5	0.5	1.38	2.87	1.88	2.03

Table 28: Results of W2F2C10 dual system.

n_s	$R_{\mu,w,d}$	$R_{\mu,f,d}$	$R_{\mu,d}$	u_w	u_f	v_w	v_f	$\mu_{w,d}^*$	$\mu_{f,d}^*$	$R_{\mu,d,1}$	$R_{\mu,d,2}$
3	2.21	2.87	2.44	1.0	0.5	0.5	0.5	4.19	3.17	2.36	2.61
4	2.43	3.00	2.51	1.0	0.6	0.4	0.6	3.71	3.35	2.86	2.81
5	2.82	3.63	3.24	1.0	0.7	0.4	0.6	3.28	3.56	3.06	2.78
6	2.82	3.55	3.24	1.0	0.8	0.4	0.6	3.05	3.95	3.04	2.64
7	2.78	3.30	3.01	1.0	0.9	0.4	0.6	2.77	3.86	2.97	2.57
8	2.66	3.28	3.06	1.0	1.0	0.4	0.6	2.51	3.78	2.69	2.43
9	2.51	3.15	2.93	0.9	1.0	0.4	0.6	2.20	3.62	2.43	2.32
10	2.15	2.63	2.49	0.8	1.0	0.4	0.6	1.88	3.18	2.20	2.21
11	1.79	2.24	2.12	0.7	1.0	0.3	0.7	1.60	2.92	2.00	2.09
12	1.60	1.99	1.91	0.6	1.0	0.3	0.7	1.41	2.71	1.88	2.03

Table 29: Results of W2F2C15 dual system.

n_s	$R_{\mu,w,d}$	$R_{\mu,f,d}$	$R_{\mu,d}$	u_w	u_f	v_w	v_f	$\mu_{w,d}^*$	$\mu_{f,d}^*$	$R_{\mu,d,1}$	$R_{\mu,d,2}$
3	2.09	2.87	2.44	1.0	0.5	0.4	0.6	4.15	3.02	2.36	2.61
4	2.34	2.85	2.52	1.0	0.6	0.4	0.6	3.68	3.29	2.86	2.81
5	2.75	3.35	3.06	1.0	0.7	0.3	0.7	3.22	3.48	3.06	2.78
6	2.74	3.41	3.17	1.0	0.8	0.3	0.7	3.05	3.79	3.04	2.64
7	2.75	3.43	3.21	1.0	0.9	0.3	0.7	2.74	3.77	2.97	2.57
8	2.67	3.28	3.10	1.0	1.0	0.3	0.7	2.50	3.74	2.69	2.43
9	2.47	3.16	2.96	0.9	1.0	0.3	0.7	2.19	3.60	2.43	2.32
10	2.17	2.79	2.73	0.8	1.0	0.3	0.7	1.86	3.11	2.20	2.21
11	1.77	2.19	2.10	0.7	1.0	0.3	0.7	1.60	2.85	2.00	2.09
12	1.55	1.97	1.90	0.6	1.0	0.3	0.7	1.41	2.70	1.88	2.03

Table 30: Results of W2F2C20 dual system.

n_s	$R_{\mu,w,d}$	$R_{\mu,f,d}$	$R_{\mu,d}$	u_w	u_f	v_w	v_f	$\mu_{w,d}^*$	$\mu_{f,d}^*$	$R_{\mu,d,1}$	$R_{\mu,d,2}$
3	2.10	2.80	2.46	1.0	0.5	0.3	0.7	4.14	3.02	2.36	2.61
4	2.33	3.08	2.70	1.0	0.6	0.3	0.7	3.66	3.18	2.86	2.81
5	2.74	3.33	3.09	1.0	0.7	0.3	0.7	3.26	3.44	3.06	2.78
6	2.74	3.44	3.23	1.0	0.8	0.3	0.7	3.04	3.76	3.04	2.64
7	2.75	3.33	3.22	1.0	0.9	0.3	0.7	2.74	3.72	2.97	2.57
8	2.69	3.36	3.20	1.0	1.0	0.3	0.7	2.50	3.64	2.69	2.43
9	2.50	3.07	2.92	0.9	1.0	0.3	0.7	2.20	3.41	2.43	2.32
10	2.17	2.70	2.66	0.8	1.0	0.2	0.8	1.89	3.09	2.20	2.21
11	1.72	2.13	2.05	0.7	1.0	0.2	0.8	1.59	2.81	2.00	2.09
12	1.53	1.97	1.92	0.6	1.0	0.2	0.8	1.41	2.70	1.88	2.03

5.3.3. W3F3 group

In this section, results of group W3F3 are discussed in detail; results are illustrated in Figure 48-Figure 52 and also reported in Table 31-Table 35.

The following considerations concerning result mean values can be drawn:

(i) The numerical ductility reduction factor for dual system structures, $R_{\mu,MDOF,d,OS}$, is a value intermediate between the ductility reduction factor for the wall-equivalent system, $R_{\mu,MDOF,w,d,OS}$, and the ductility reduction factor for the frame-equivalent system, $R_{\mu,MDOF,f,d,OS}$ (Figure 48a-Figure 52a).

(ii) $R_{\mu,MDOF,w,d,OS}$ is always lower than $R_{\mu,MDOF,f,d,OS}$ (Figure 48a-Figure 52a) as well as the analytical ductility reduction factor for wall system, $R_{\mu,MDOF,w}$, is always lower than analytical ductility reduction factor for frame system, $R_{\mu,MDOF,f}$, except to low number of storeys (Figure 48b-Figure 52b).

(iii) The frame use rate, $u_{f,OS}$, is equal to 1 for all cases (except to $n_s = 3$ where it is very close to 1); this means that the frame is always the first system to fail. The wall use rate, $u_{w,OS}$, is between 0.2 for high number of storeys and almost 1 for low number of storeys (Figure 48c-Figure 52c).

(iv) The wall base shear ratio, $v_{w,OS}$, remains nearly constant with the number of storeys but it decreases with the increasing of the number of columns, from C2 to C20. Base shear ratios have values ranged from 0.2 to 0.8, approximately (Figure 48d-Figure 52d). Vice versa, the frame base shear ratio, $v_{f,OS}$, increases with the increasing of the number of columns, from C2 to C20. Base shear ratios have values ranged from 0.2 to 0.8, approximately and wall base shear ratio, $v_{w,OS}$, is higher than frame base shear ratio, $v_{f,OS}$, for W3F3C2 and W3F3C5 at low number of storey only.

(v) The target ductility of the wall, $\mu_{w,d,OS}{}^*$, in the dual system is lower than the target ductility of the wall, $\mu_w{}^*$, when it is considered single system, except to very low number of storeys systems. Instead, the target ductility of the frame, $\mu_{f,d,OS}{}^*$, in the dual system is generally higher than the target ductility of the frame, $\mu_f{}^*$, when it is considered single system, except to $n_s = 3$ in for W3F3C10, W3F3C15 and W3F3C20 (Figure 48e-Figure 52e).

(vi) Analytical expression $R_{\mu,MDOF,d1}$ shows a good match with the numerical ductility reduction factor for dual system structures, $R_{\mu,MDOF,d,OS}$; instead $R_{\mu,MDOF,d2}$ shows a worst agreement with the numerical curve shape, especially at low number of storeys (Figure 48f-Figure 52f).

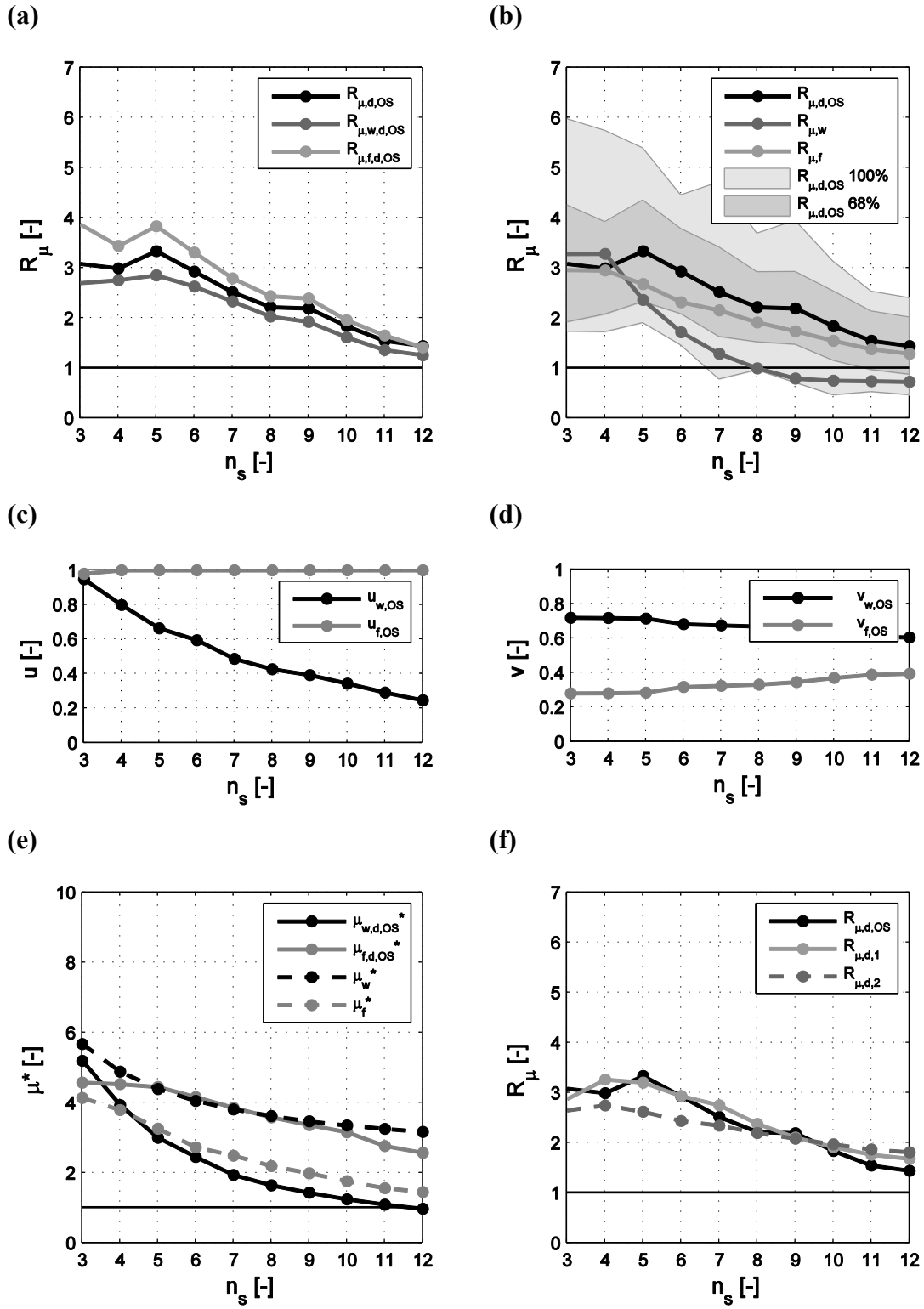

Figure 48: Results of W3F3C2 dual system, (a, b): $R_{\mu,MDOF,d}$, (c): use rates, (d): base shear ratios, (e): target ductilities, (f): analytical expressions.

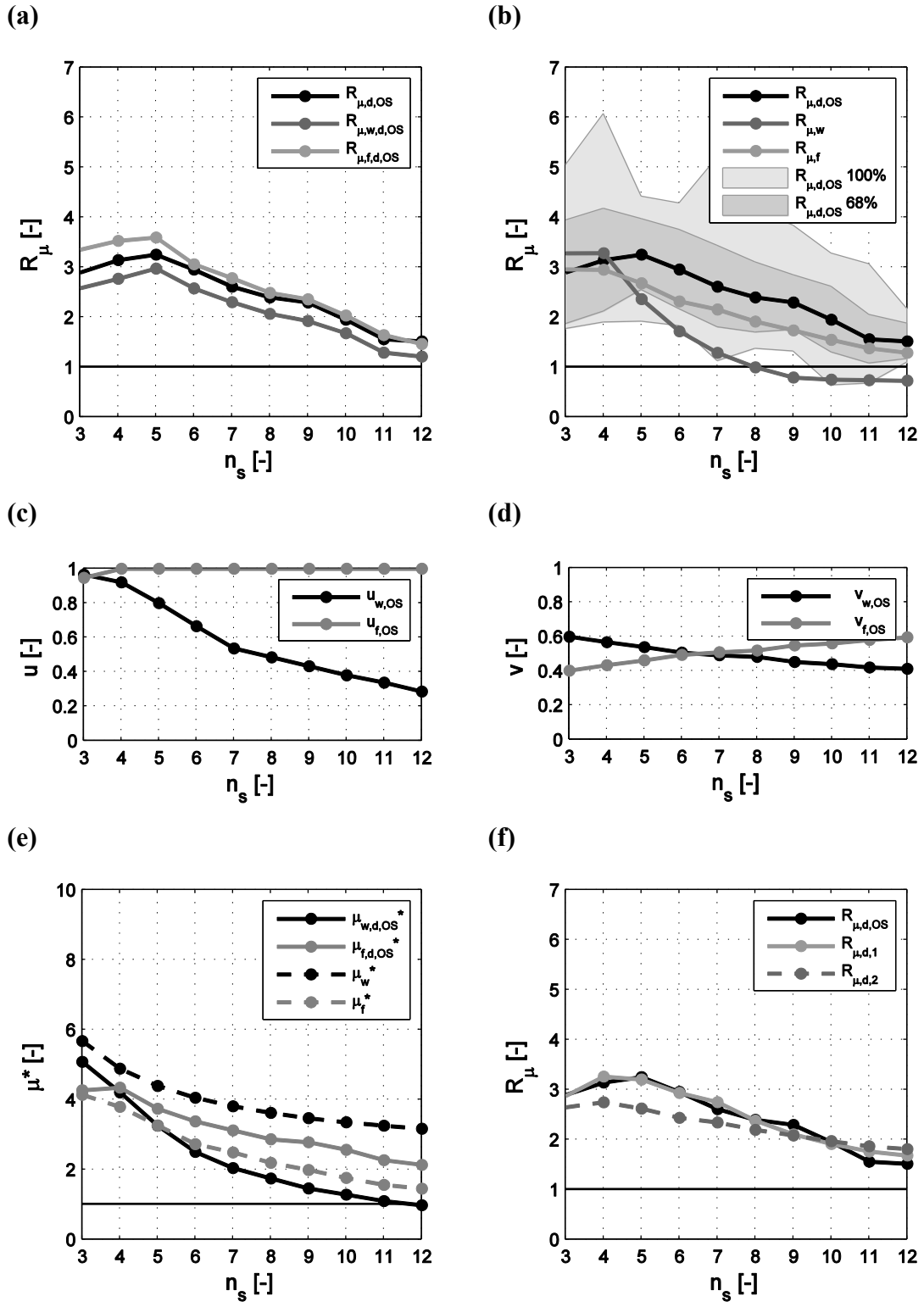

Figure 49: Results of W3F3C5 dual system, (a, b): $R_{\mu,MDOF,d}$, (c): use rates, (d): base shear ratios, (e): target ductilities, (f): analytical expressions.

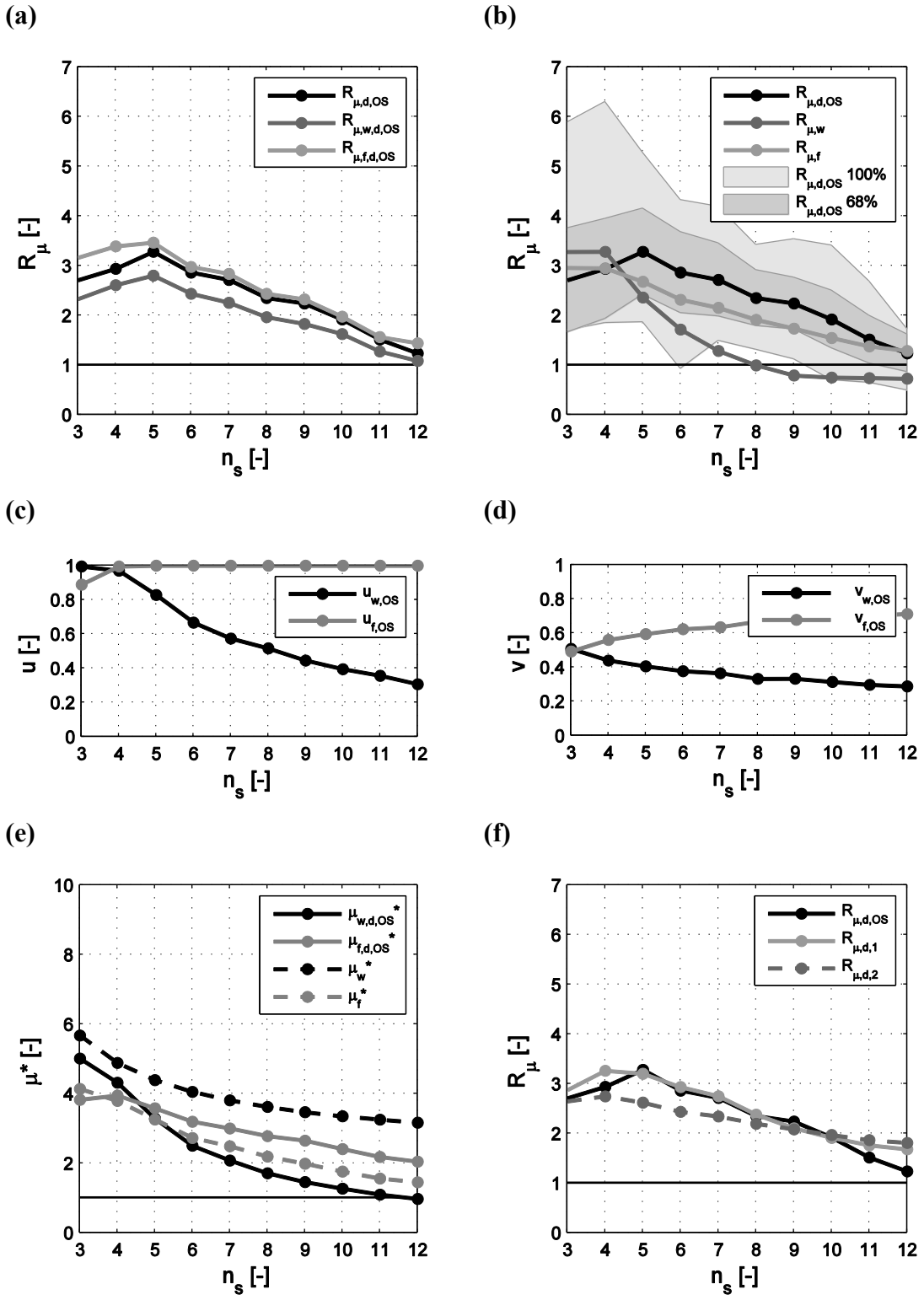

Figure 50: Results of W3F3C10 dual system, (a, b): $R_{\mu,MDOF,d}$, (c): use rates, (d): base shear ratios, (e): target ductilities, (f): analytical expressions.

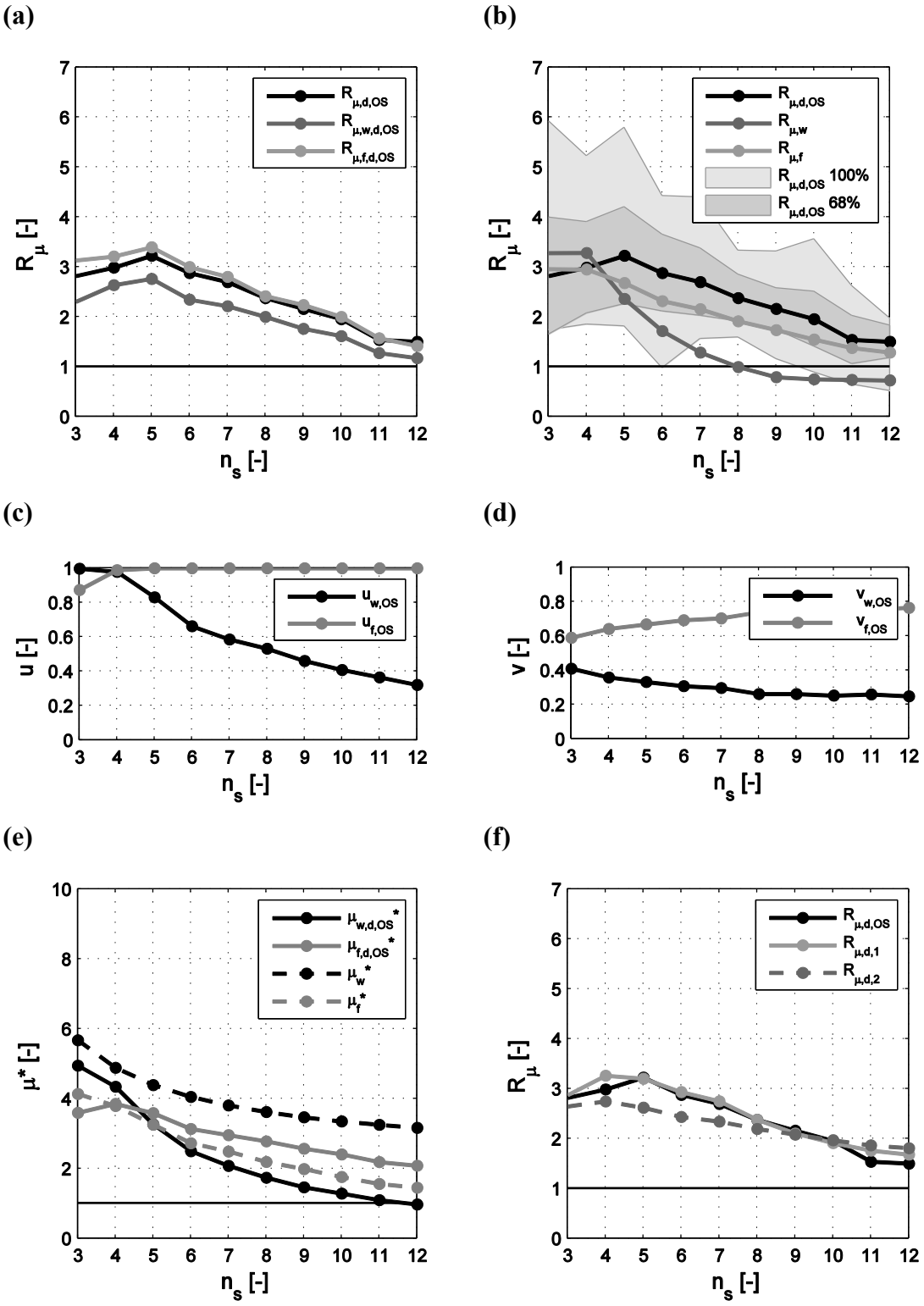

Figure 51: Results of W3F3C15 dual system, (a, b): $R_{\mu,MDOF,d}$, (c): use rates, (d): base shear ratios, (e): target ductilities, (f): analytical expressions.

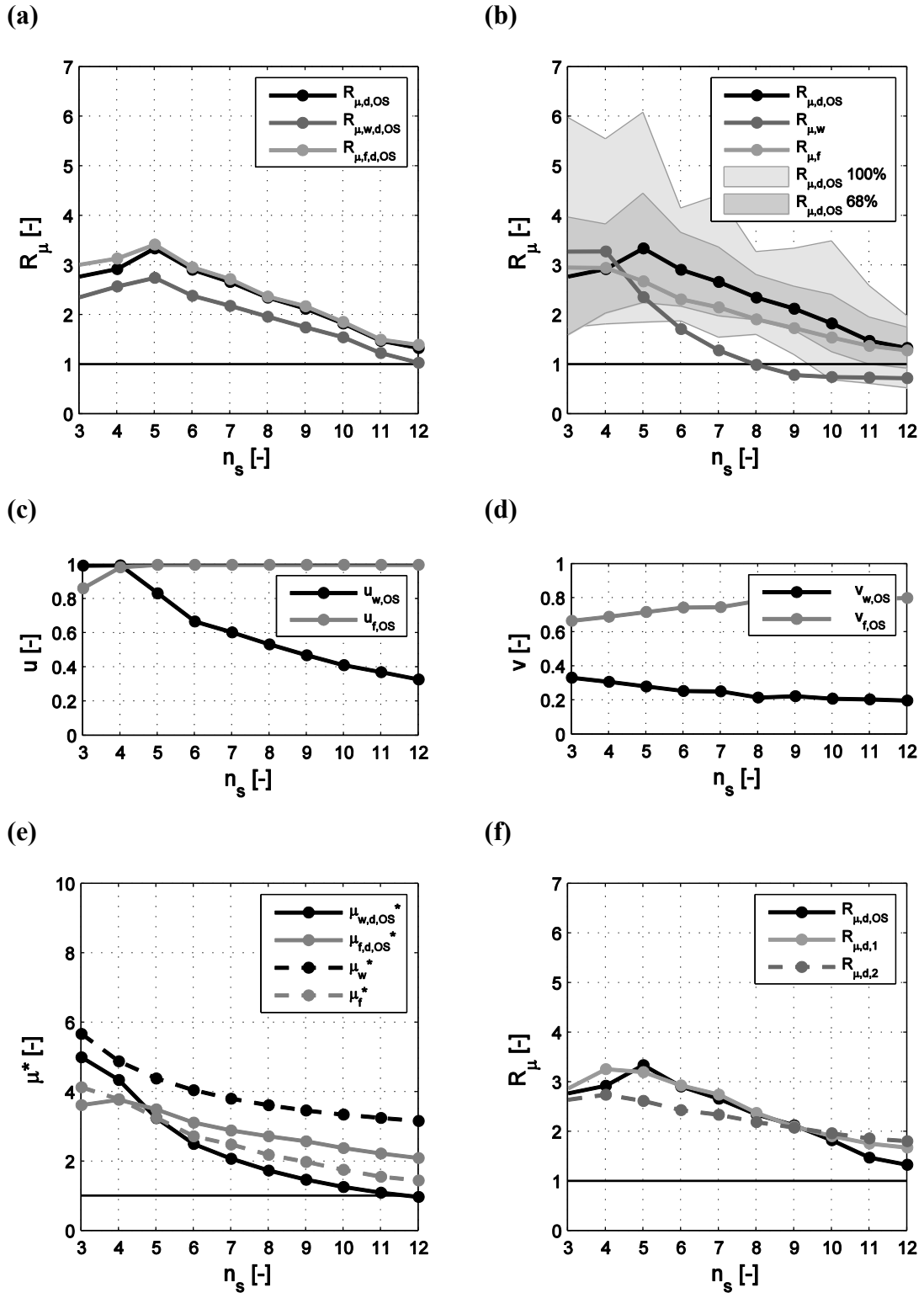

Figure 52: Results of W3F3C20 dual system, (a, b): $R_{\mu,MDOF,d}$, (c): use rates, (d): base shear ratios, (e): target ductilities, (f): analytical expressions.

Table 31: Results of W3F3C2 dual system.

n_s	$R_{\mu,w,d}$	$R_{\mu,f,d}$	$R_{\mu,d}$	u_w	u_f	v_w	v_f	$\mu_{w,d}^*$	$\mu_{f,d}^*$	$R_{\mu,d,1}$	$R_{\mu,d,2}$
3	2.70	3.87	3.08	0.9	1.0	0.7	0.3	5.19	4.57	2.92	2.53
4	2.75	3.44	2.99	0.8	1.0	0.7	0.3	3.93	4.53	3.32	2.62
5	2.85	3.83	3.33	0.7	1.0	0.7	0.3	3.00	4.45	3.19	2.51
6	2.63	3.31	2.93	0.6	1.0	0.7	0.3	2.45	4.16	2.88	2.34
7	2.33	2.79	2.52	0.5	1.0	0.7	0.3	1.94	3.85	2.67	2.25
8	2.03	2.44	2.22	0.4	1.0	0.7	0.3	1.64	3.58	2.30	2.11
9	1.92	2.39	2.19	0.4	1.0	0.7	0.3	1.43	3.36	2.03	2.00
10	1.61	1.96	1.84	0.3	1.0	0.6	0.4	1.24	3.16	1.83	1.89
11	1.36	1.65	1.55	0.3	1.0	0.6	0.4	1.09	2.76	1.67	1.79
12	1.25	1.41	1.44	0.2	1.0	0.6	0.4	0.98	2.57	1.58	1.74

Table 32: Results of W3F3C5 dual system.

n_s	$R_{\mu,w,d}$	$R_{\mu,f,d}$	$R_{\mu,d}$	u_w	u_f	v_w	v_f	$\mu_{w,d}^*$	$\mu_{f,d}^*$	$R_{\mu,d,1}$	$R_{\mu,d,2}$
3	2.58	3.35	2.90	1.0	0.9	0.6	0.4	5.08	4.27	2.92	2.53
4	2.77	3.53	3.14	0.9	1.0	0.6	0.4	4.21	4.35	3.32	2.62
5	2.97	3.59	3.25	0.8	1.0	0.5	0.5	3.26	3.74	3.19	2.51
6	2.58	3.06	2.95	0.7	1.0	0.5	0.5	2.50	3.38	2.88	2.34
7	2.30	2.78	2.61	0.5	1.0	0.5	0.5	2.04	3.12	2.67	2.25
8	2.07	2.49	2.40	0.5	1.0	0.5	0.5	1.75	2.87	2.30	2.11
9	1.92	2.36	2.29	0.4	1.0	0.5	0.5	1.46	2.78	2.03	2.00
10	1.68	2.03	1.95	0.4	1.0	0.4	0.6	1.28	2.56	1.83	1.89
11	1.29	1.64	1.56	0.3	1.0	0.4	0.6	1.10	2.27	1.67	1.79
12	1.21	1.46	1.51	0.3	1.0	0.4	0.6	0.98	2.13	1.58	1.74

Table 33: Results of W3F3C10 dual system.

n_s	$R_{\mu,w,d}$	$R_{\mu,f,d}$	$R_{\mu,d}$	u_w	u_f	v_w	v_f	$\mu_{w,d}^*$	$\mu_{f,d}^*$	$R_{\mu,d,1}$	$R_{\mu,d,2}$
3	2.33	3.16	2.71	1.0	0.9	0.5	0.5	5.01	3.83	2.92	2.53
4	2.61	3.39	2.94	1.0	1.0	0.4	0.6	4.32	3.95	3.32	2.62
5	2.80	3.47	3.28	0.8	1.0	0.4	0.6	3.28	3.58	3.19	2.51
6	2.44	2.98	2.86	0.7	1.0	0.4	0.6	2.50	3.19	2.88	2.34
7	2.26	2.83	2.71	0.6	1.0	0.4	0.6	2.08	3.00	2.67	2.25
8	1.97	2.44	2.35	0.5	1.0	0.3	0.7	1.71	2.78	2.30	2.11
9	1.83	2.32	2.24	0.4	1.0	0.3	0.7	1.46	2.65	2.03	2.00
10	1.63	1.98	1.92	0.4	1.0	0.3	0.7	1.27	2.41	1.83	1.89
11	1.27	1.56	1.51	0.4	1.0	0.3	0.7	1.10	2.18	1.67	1.79
12	1.09	1.44	1.24	0.3	1.0	0.3	0.7	0.97	2.05	1.58	1.74

Table 34: Results of W3F3C15 dual system.

n_s	$R_{\mu,w,d}$	$R_{\mu,f,d}$	$R_{\mu,d}$	u_w	u_f	v_w	v_f	$\mu_{w,d}^*$	$\mu_{f,d}^*$	$R_{\mu,d,1}$	$R_{\mu,d,2}$
3	2.30	3.13	2.82	1.0	0.9	0.4	0.6	4.94	3.60	2.92	2.53
4	2.63	3.21	2.99	1.0	1.0	0.4	0.6	4.34	3.85	3.32	2.62
5	2.76	3.39	3.23	0.8	1.0	0.3	0.7	3.27	3.59	3.19	2.51
6	2.35	3.00	2.88	0.7	1.0	0.3	0.7	2.50	3.13	2.88	2.34
7	2.21	2.80	2.70	0.6	1.0	0.3	0.7	2.08	2.96	2.67	2.25
8	2.00	2.41	2.38	0.5	1.0	0.3	0.7	1.74	2.78	2.30	2.11
9	1.76	2.24	2.16	0.5	1.0	0.3	0.7	1.46	2.57	2.03	2.00
10	1.61	2.00	1.96	0.4	1.0	0.3	0.7	1.29	2.41	1.83	1.89
11	1.27	1.57	1.54	0.4	1.0	0.3	0.8	1.10	2.19	1.67	1.79
12	1.17	1.42	1.50	0.3	1.0	0.2	0.8	0.97	2.08	1.58	1.74

Table 35: Results of W3F3C20 dual system.

n_s	$R_{\mu,w,d}$	$R_{\mu,f,d}$	$R_{\mu,d}$	u_w	u_f	v_w	v_f	$\mu_{w,d}^*$	$\mu_{f,d}^*$	$R_{\mu,d,1}$	$R_{\mu,d,2}$
3	2.36	3.01	2.78	1.0	0.9	0.3	0.7	5.00	3.63	2.92	2.53
4	2.57	3.14	2.93	1.0	1.0	0.3	0.7	4.35	3.77	3.32	2.62
5	2.75	3.42	3.34	0.8	1.0	0.3	0.7	3.25	3.50	3.19	2.51
6	2.39	2.96	2.91	0.7	1.0	0.3	0.7	2.51	3.12	2.88	2.34
7	2.18	2.72	2.67	0.6	1.0	0.3	0.7	2.08	2.89	2.67	2.25
8	1.97	2.37	2.35	0.5	1.0	0.2	0.8	1.74	2.72	2.30	2.11
9	1.75	2.18	2.13	0.5	1.0	0.2	0.8	1.48	2.58	2.03	2.00
10	1.55	1.86	1.83	0.4	1.0	0.2	0.8	1.27	2.39	1.83	1.89
11	1.23	1.50	1.48	0.4	1.0	0.2	0.8	1.10	2.23	1.67	1.79
12	1.04	1.40	1.33	0.3	1.0	0.2	0.8	0.98	2.10	1.58	1.74

5.3.4. General remarks on dual systems

In this Section, general remarks on results of dual systems are discussed.

In Figure 53(a,b,c) the numerical ductility reduction factors, $R_{\mu,MDOF,d,OS}$, corresponding to different number of columns , n_c, are shown for different groups of dual systems: W1F1, W2F2 and W3F3 respectively, as a function of the number of storeys, n_s. Instead, the numerical ductility reduction factors for all of the considered dual systems are shown together in Figure 53(d).

In Figure 54(a,b,c) the numerical use ratio for single systems, $u_{w,OS}$ and $u_{f,OS}$, for different groups of dual systems W1F1, W2F2 and W3F3 are shown , respectively, as a function of the number of storeys, n_s.

In Figure 55(a,b,c) the numerical target ductilities for wall and frame in the dual system, $\mu_{w,d,OS}{}^{*}$ and $\mu_{f,d,OS}{}^{*}$, are compared with the analytical target ductilities for wall and frame when they are considered single systems, $\mu_w{}^{*}$ and $\mu_f{}^{*}$, for different groups of dual systems W1F1, W2F2 and W3F3, respectively, as a function of the number of storeys, n_s.

In Figure 56(a,b,c) the analytical ductility reduction factor for single systems, $R_{\mu,MDOF,w}$ and $R_{\mu,MDOF,f}$, are compared to the numerical ductility reduction factors, $R_{\mu,MDOF,d,OS}$, of different groups of dual systems: W1F1, W2F2 and W3F3, respectively, as a function of the number of storeys, n_s.

In Figure 57(a,b,c) the numerical normalised base shear for dual systems, $v_{b,MDOF,d,OS}$, of different groups of dual systems, W1F1, W2F2 and W3F3, is shown, respectively, as a function of the number of storeys, n_s. $v_{b,MDOF,d,OS}$ is given by:

$$v_{b,MDOF,d,OS} = \frac{V_{b,MDOF,d,OS}}{V_{b,MDOF,tot,OS}} = \frac{V_{b,MDOF,d,OS}}{V_{b,MDOF,w,OS} + n_c V_{b,MDOF,f,OS}} \tag{152}$$

where: $V_{b,MDOF,w,OS}$ and $V_{b,MDOF,f,OS}$ are the numerical base shears of wall and frame as single systems; $V_{b,MDOF,d,OS}$ is the numerical base shear of dual systems; n_c, the number of columns.

In Figure 58(a,b,c) the analytical ductility reduction factor for dual system, $R_{\mu,MDOF,d1}$, is compared to the numerical ductility reduction factors $R_{\mu,MDOF,d,OS}$ of different groups of dual systems: W1F1, W2F2 and W3F3, respectively, as a function of the number of storeys, n_s.

For the sake of brevity, the subscript “MDOF” is omitted from labels in figures, because they always refer to MDOF systems. Numerical values are indicated with “OS” label in figures.

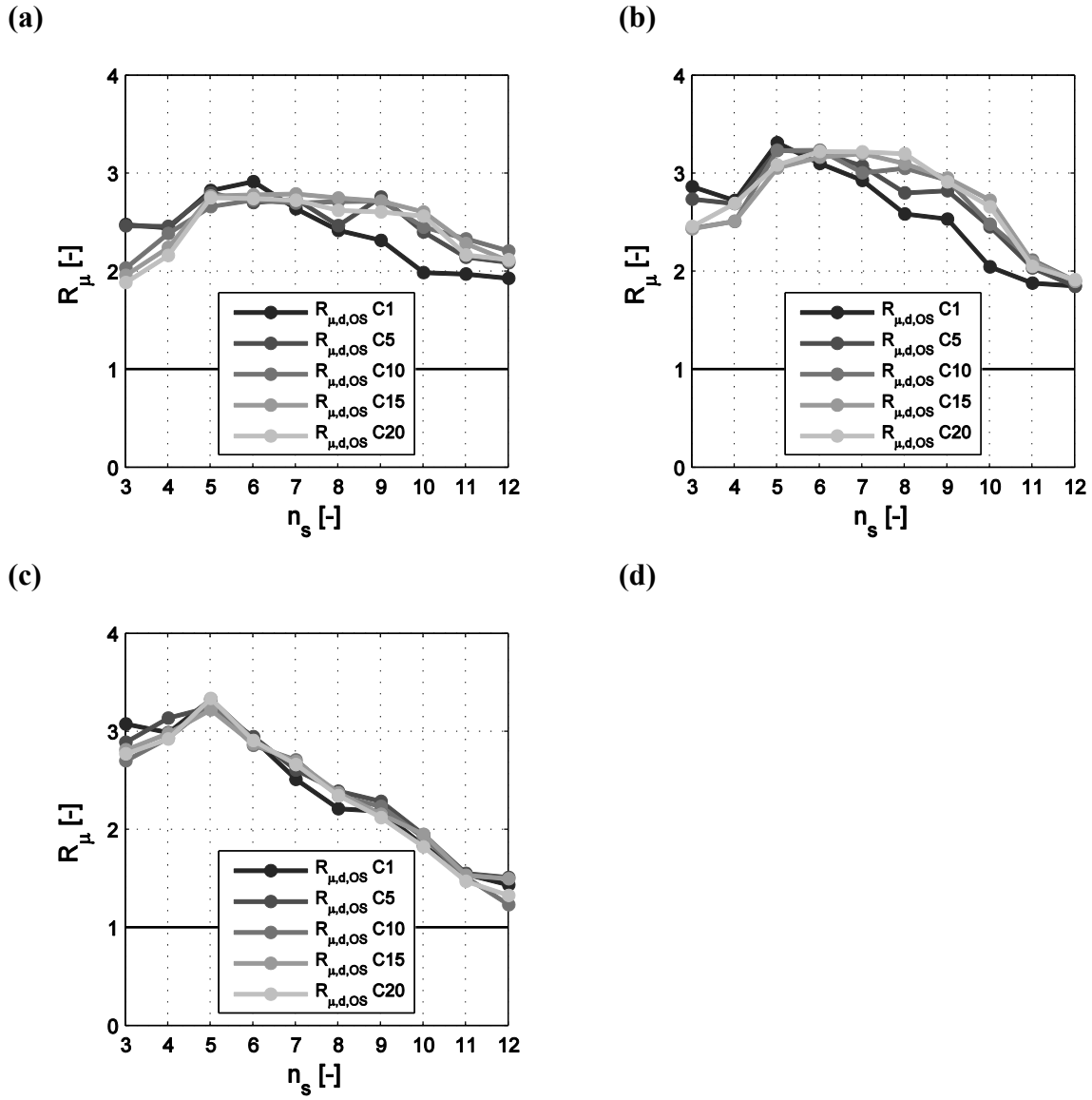

Figure 53: Numerical ductility reduction factor of dual systems, (a): W1F1 group, (b): W2F2 group, (c): W3F3 group, (d): all groups.

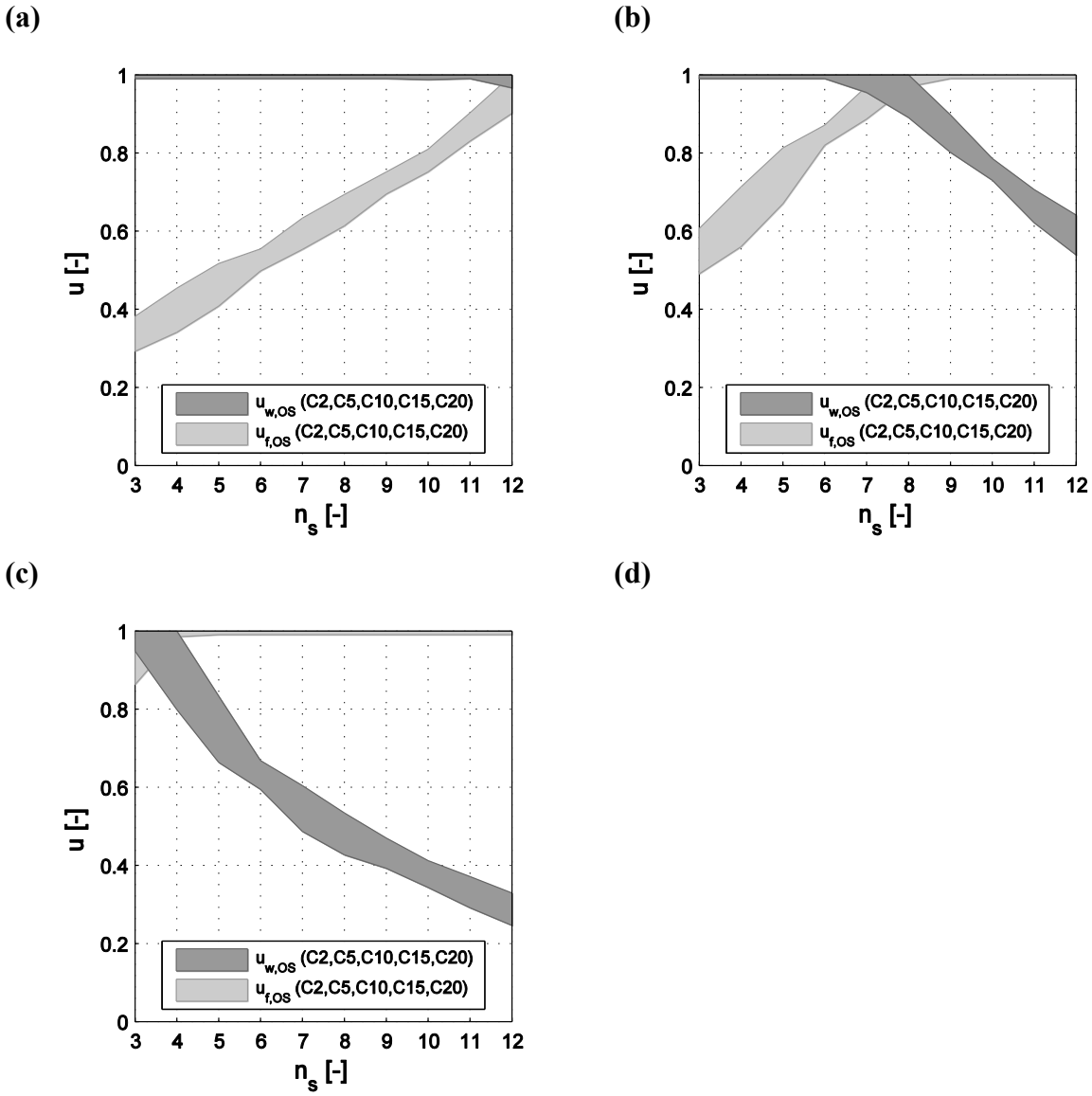

Figure 54: Use ratios of dual systems, (a): W1F1 group, (b): W2F2 group, (c): W3F3 group.

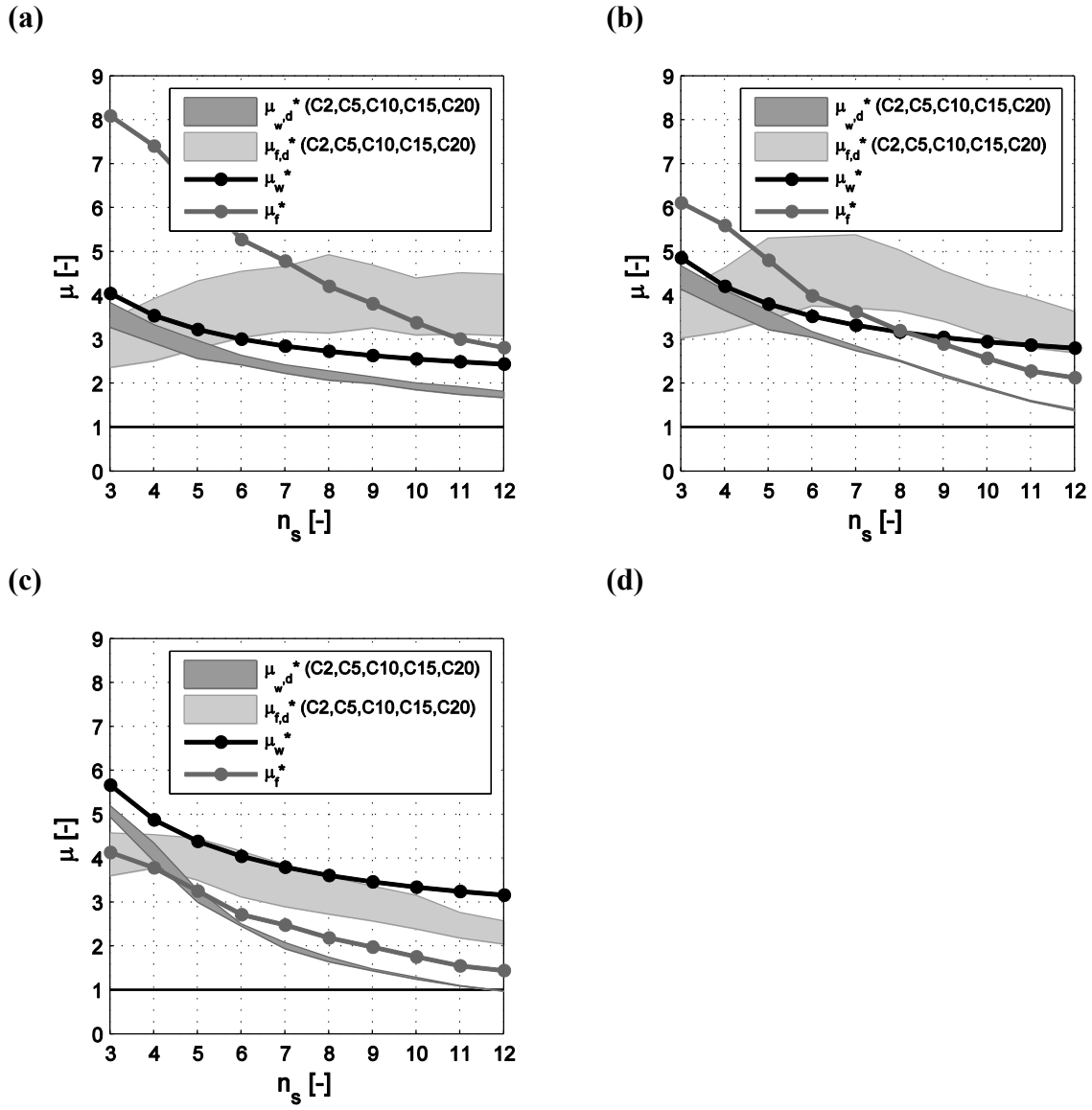

Figure 55: Target ductilities ratios of dual and single systems, (a): W1F1 group, (b): W2F2 group, (c): W3F3 group.

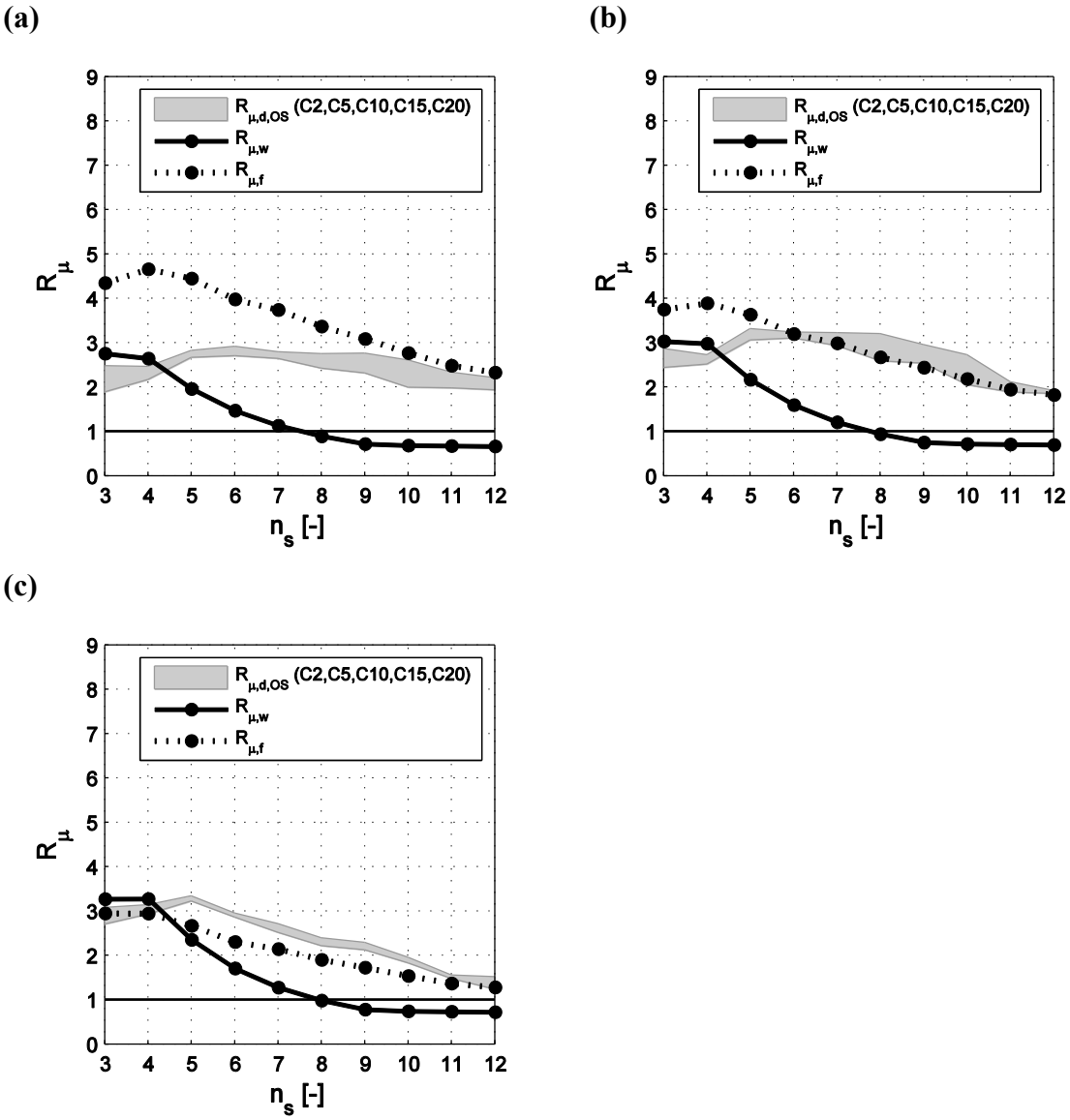

Figure 56: Comparison of numerical results of dual systems and analytical expressions for single systems, (a): W1F1 group, (b): W2F2 group, (c): W3F3 group.

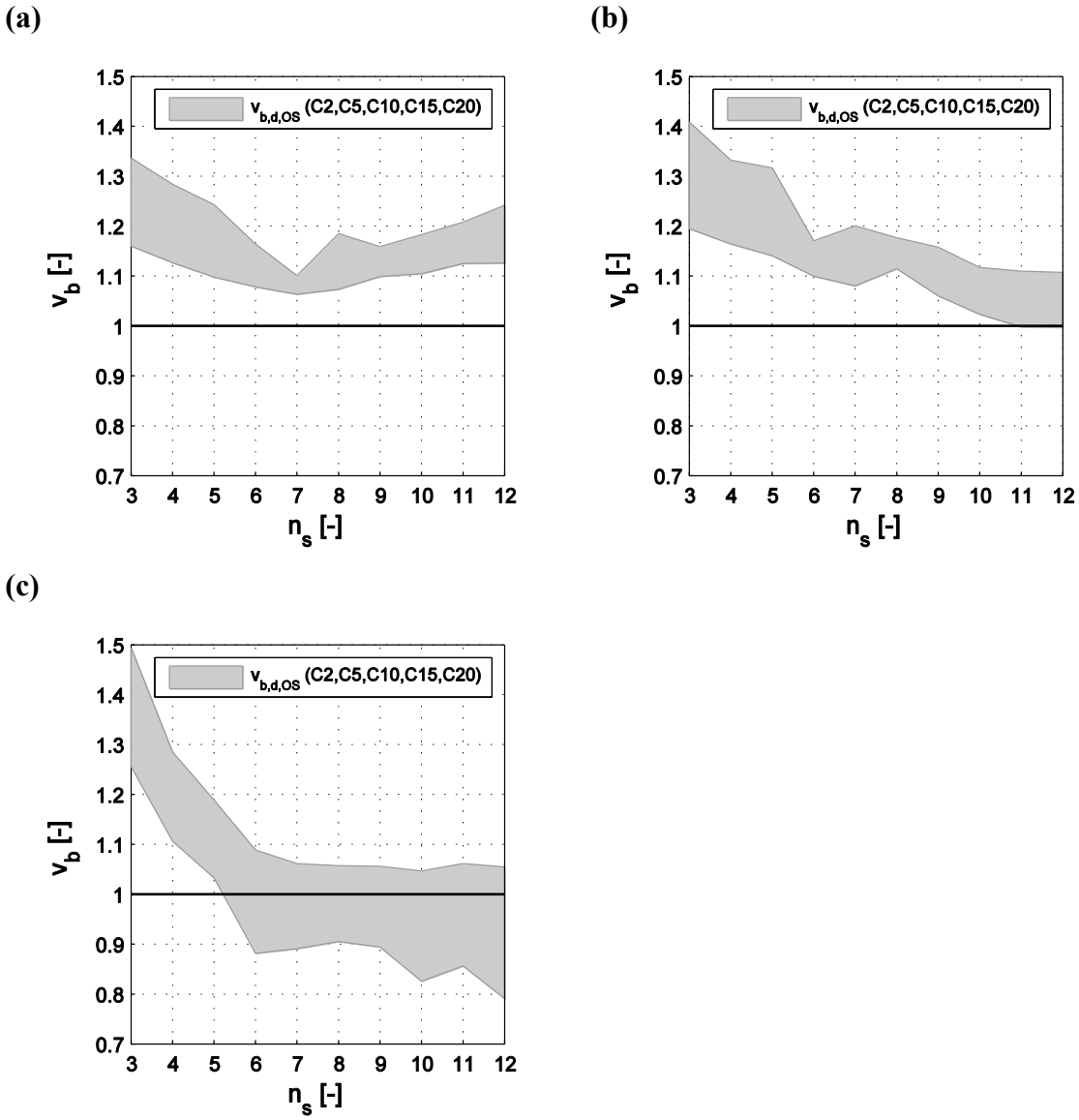

Figure 57: Comparison of numerical base shears of dual systems and single systems, (a): W1F1 group, (b): W2F2 group, (c): W3F3 group.

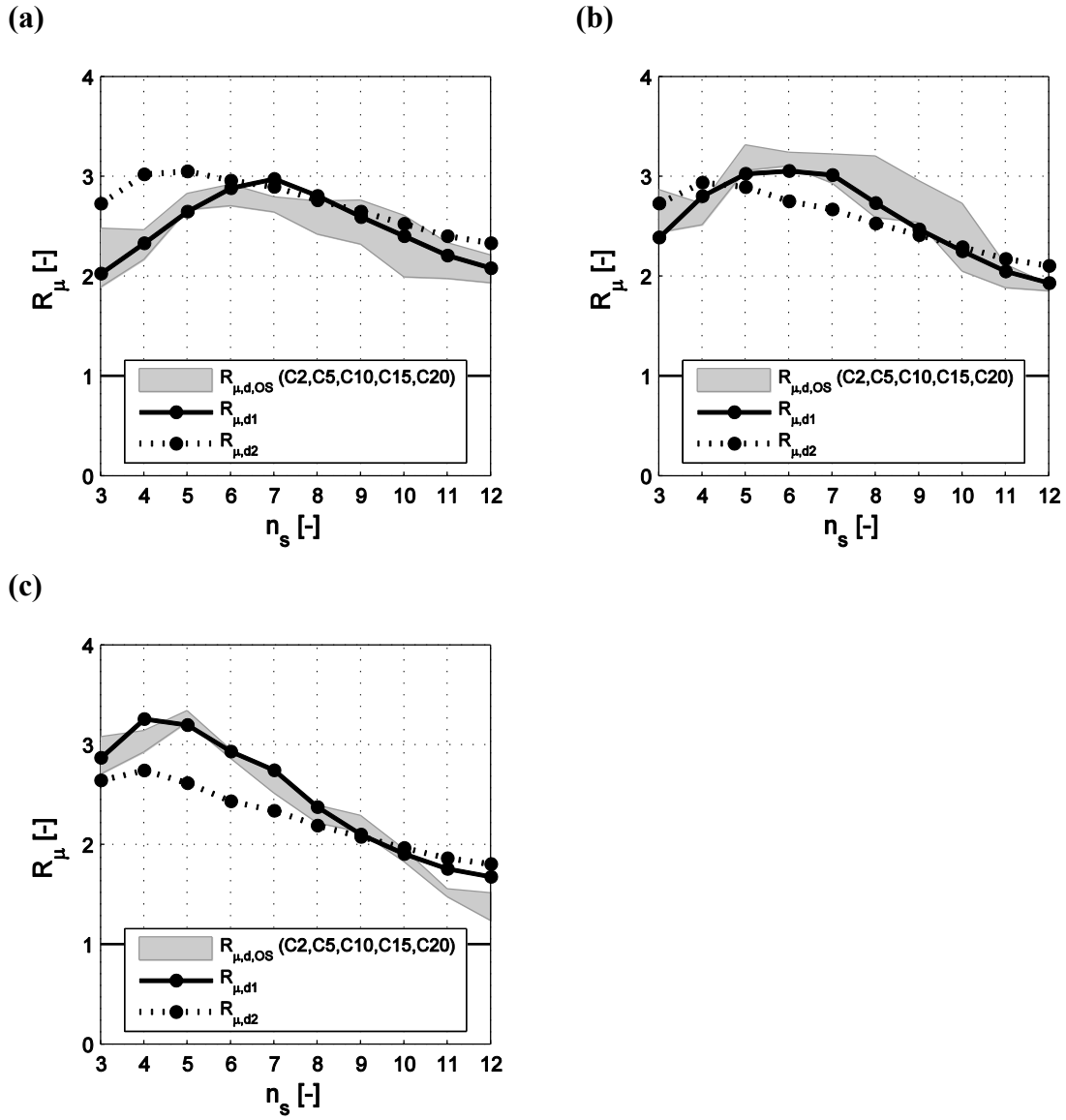

Figure 58: Comparison of numerical results and analytical expressions of dual systems, (a): W1F1 group, (b): W2F2 group, (c): W3F3 group.

The following considerations concerning result mean values can be drawn:

(i) The number of columns, n_c, lightly affects the ductility reduction factor and only in W2F2 group $R_{\mu,MDOF,d,OS}$ significantly increases as n_c increases for medium number of storeys. The number of columns can be interpreted as the importance of frame system respect to the wall system; in other words, frame base shear ratio, v_f, increases with n_c (Figure 53a,b,c).

(ii) The numerical ductility reduction factor $R_{\mu,MDOF,d,OS}$ is higher at high number of storeys for W1F1 group, which is the group where the frame is more ductile and failure is reached in the wall, i.e., the wall use ratio, $u_{w,OS}$, is equal to 1, but also the frame shows a use rate, $u_{f,OS}$, close to 1 (Figure 53d and Figure 54a). Instead, the numerical ductility reduction factor $R_{\mu,MDOF,d,OS}$ is higher at low number of storeys

for W3F3 group, which is the group where the wall is more ductile and failure is reached in the frame, i.e., the frame use ratio, $u_{f,OS}$, is equal to 1, but also the wall shows a use rate, $u_{w,OS}$, close to 1 (Figure 53d and Figure 54c). Lastly, $R_{\mu,MDOF,d,OS}$ is higher at medium number of storeys for W2F2 group, which is the group where the wall and frame reach an equilibrated failure and both systems are properly exploited, i.e., $u_{w,OS}$ and $u_{f,OS}$ are equal to 1 or very close to 1 (Figure 53d and Figure 54b).

(iii) The remarks described in Paragraph (ii) can be also explained by observing the target ductilities in Figure 55, in particular the ductility of frame in the dual system is relevant. The highest numerical ductility reduction factor, $R_{\mu,MDOF,d,OS}$, at high number of storeys for W1F1 group can be also explained by observing the target ductility of frame in the dual system, ${\mu_{f,d,OS}}^*$, which increases with the number of storeys, differently than the ductility of the frame when it is considered a single system, which decreases (Figure 55a). Instead, the highest numerical ductility reduction factor, $R_{\mu,MDOF,d,OS}$, at medium number of storeys for W2F2 mainly depends on the numerical target ductility of frame in the dual system, ${\mu_{f,d,OS}}^*$, which reaches the highest values for number of storeys ranged from 5 to 8 (Figure 55b). Lastly, the highest numerical ductility reduction factor, $R_{\mu,MDOF,d,OS}$, at low number of storeys for W3F3 are related to the numerical target ductility of both walls and frame in the dual system, ${\mu_{w,d,OS}}^*$ and ${\mu_{f,d,OS}}^*$, which decrease with the number of storeys and they reach the highest values for low number of storeys (Figure 55c).

(iv) The ductility reduction factor, $R_{\mu,MDOF,d}$, takes as much advantage of synergy between single systems as the number of storeys increases (Figure 56). It is evident that $R_{\mu,MDOF,d}$ increases or at least decreases less than the ductility reduction factor of single systems, $R_{\mu,MDOF,w}$ and $R_{\mu,MDOF,f}$. Therefore, this trend suggests that the performance of dual systems is better for a medium number of storeys than a low number of storeys; in other words, low-rise buildings are not able to activate the synergy between walls and frame effectively. This behaviour can be also explained by the mutual support between systems: walls hold the frame at lower storeys, where frame is more deformable and wall stiffer, and the frame holds walls at higher storeys, where walls are more deformable and frame stiffer, due to their different opposite concavity of the first mode displacement shape.

(v) Dual structures exploit more effectively the frame for a high number of storeys, then it is convenient to design the dual system with a ductile frame which can provide a higher ductility reduction factor (W1F1 group, Figure 56a). Instead, dual structures exploit more effectively the walls for a low number of storeys, then it is suitable to design the dual system with ductile walls, which can provide a higher ductility reduction factor (W3F3 group, Figure 56c). Lastly, dual structures exploit effectively both walls and frame for a medium number of storeys, then it is convenient to design the dual system with a balanced ductility between walls and frame, which can provide a higher ductility reduction factor thanks to their high mutual synergy (W2F2 group, Figure 56b).

(vi) The numerical normalised base shears for dual systems, $v_{b,MDOF,d,OS}$, are generally higher than the normalised sum of base shears for wall and frame when considered single systems, except to high number of storey of W3F3 group and for high number

of storeys of W2F2 group (Figure 57). Let's recall that the group W3F3 couples a more ductile wall with a less ductile frame. Therefore, the frame seems to be the most important system when dual structures are designed, except to low-rise structures. In other words, the frame is the system that provides the reserve of ductility when the dual structure attains ultimate capacity during strong earthquakes. Moreover, this behaviour is associated to a low wall use rate, $u_{w,OS}$, in these cases (Figure 54) and it suggests that the best performance in terms of supported base shear is obtained when the wall is the first system to fail ($u_{w,OS} = 1$).

(vii) The first proposed analytical expression for the ductility reduction factor for dual system – $R_{\mu,MDOF,d1}$, Equation (149) – approximates accurately numerical results in all cases and residual sum squares RSS_1 among all 15 considered cases is equal to 5.99. Instead, the second expression – $R_{\mu,MDOF,d2}$, Equation (150) – shows a worst agreement with the numerical values with a mean residual sum squares RSS_2 equal to 18.68 (Figure 58). RSS is the sum of the squares of residuals which are the deviations predicted from numerical values of data, given by following Equations (153) and (154).

$$RSS_1 = \sum_{i=1}^{n} \left(R_{\mu,MDOF,d,OS,i} - R_{\mu,MDOF,d1,i}\right)^2 \tag{153}$$

$$RSS_2 = \sum_{i=1}^{n} \left(R_{\mu,MDOF,d,OS,i} - R_{\mu,MDOF,d2,i}\right)^2 \tag{154}$$

where $R_{\mu,MDOF,d,OS,i}$ is the *i-th* value of the numerical ductility reduction factor for dual system; $R_{\mu,MDOF,d1,i}$ and $R_{\mu,MDOF,d2,i}$ is the analytical ductility reduction factor for dual system predicted by Equation (149) and Equation (150) respectively; n is the total number of analyses equal to 150 (n = 3 groups · 5 numbers of columns (n_c) · 10 number of storeys (n_s) = 150 analyses). Despite its more complex shape, $R_{\mu,MDOF,d1}$ expression given by Equation (149), is definitely more reliable and it is to be preferred when estimating the ductility reduction factor for dual systems R.

6. Design examples

Two design examples are developed to show the application of the proposed analytical design method for dual system step-by-step in Section 6.1 and 6.2, respectively.

Two RC frame-wall structures are designed following the method and compared with the same structures designed following UNI EN 1998-1 (2013) for medium ductility class (DCM). To perform numerical analyses the commercial FEM code Midas/Gen (2016) developed by MIDAS Information Technology Co., Ltd., is used.

The performance of structures is assessed by means of N2 method that is a simplified method applicable to plane structures whose behaviour shows a dominant first mode (Fajfar, 2000). In this Section the N2 method is used as a tool to compare the performance of designed structures only. Further nonlinear time history analyses are necessary to better evaluate the performance of the structures designed following the proposed method and the Eurocode 8.

Both examples are designed by considering the elastic acceleration spectrum shown in Figure 59, where S_{ae} is the elastic acceleration divided by $g = 9.806\, m/s^2$ and T is the vibration period in seconds. This spectrum is representative of the Italian seismic zone classified of high seismic risk.

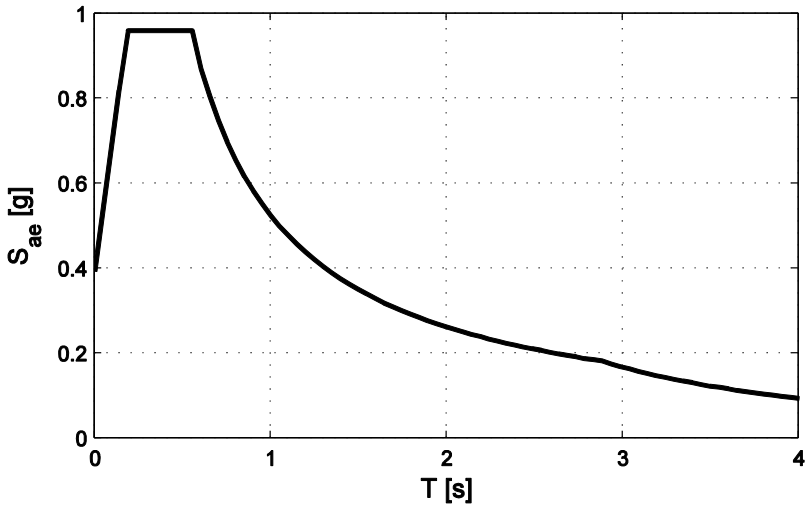

Figure 59: Elastic acceleration spectrum.

6.1. Example 1

The structure considered in Example 1 is the RC frame-wall structure composed of two RC walls ($n_w = 2$) linked to a 7-bay frame, corresponding to a number of columns $n_c = 8$; the number of storeys is $n_s = 5$ and the storey height is $h_s = 3.00\ m$. A portrayal of the structure is reported in Figure 60.

Material properties are the following: mean concrete compressive strength $f_c = 38.0\ MPa$; mean steel yield strength $f_{y,s} = 550.0\ MPa$; mean steel tensile strength $f_{u,s} = 632.5\ MPa$; steel Young modulus $E_s = 200\ GPa$; maximum diameter of walls and frame rebar $d_{bl} = d_{bl,w} = d_{bl,f} = 20\ mm$. Structural RC member weight is assumed equal to 25.0 kN/m^3.

Storey gravity loads in seismic combination, q_E, is equal to 7.8 kN/m^2 on a influence area of 25.0 m^2, which means a bay length, l_b, of 5.0 m and a storey span, i_b, of 5.0 m; these floor and weight loads are applied to both walls and frames.

Geometrical and mechanical properties of walls and columns are listed in Table 8 and Table 37, where strength properties of sections are given for axial force due to gravity load in the seismic combination. Beam section dimensions are $b_b = 0.50\ m$ and $h_b = 0.40\ m$.

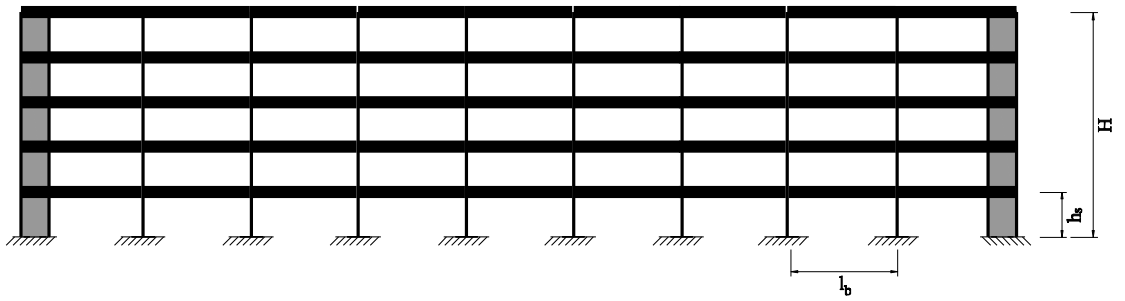

Figure 60: Portrayal of structure of Example 1.

Table 36: Geometrical and mechanical properties of walls.

Properties	**Walls**
Section width, b_w $[m]$	0.30
Section length, l_w $[m]$	1.50
Yield moment, $M_{y,w}$ $[KNm]$	1321
Ultimate moment, $M_{u,w}$ $[KNm]$	1660
Yield curvature, $\varphi_{y,w}$ $[m^{-1}]$	0.00209
Ultimate curvature, $\varphi_{u,w}$ $[m^{-1}]$	0.01130
Curvature ductility, $\mu_{\varphi,w}$ $[-]$	5.4067
Storey mass, $m_{s,w}$ $[kg]$	23330

Table 37: Geometrical and mechanical properties of base columns.

Properties	**Columns**
Section width, $b_c\ [m]$	0.45
Section length, $h_c\ [m]$	0.45
Yield moment, $M_{y,f}\ [KNm]$	471
Ultimate moment, $M_{u,f}\ [KNm]$	508
Yield curvature, $\varphi_{y,f}\ [m^{-1}]$	0.0109
Ultimate curvature, $\varphi_{u,f}\ [m^{-1}]$	0.0191
Curvature ductility, $\mu_{\varphi,f}\ [-]$	1.7523
Storey mass, $m_{s,f}\ [kg]$	23980

6.1.1. Design of Example 1 applying the proposed analytical method

The proposed analytical method for wall structures presented in Section 3.2 is shown step-by-step in this Section.

The building total height, H, is then equal to:

$$H = H_w = H_f = n_s h_s = 5 \cdot 3.00 = 15.00\ m \tag{155}$$

The fundamental period of the wall system, $T_{1,w}$, is given by:

$$T_{1,w} = \frac{2\pi}{3.516}\sqrt{\frac{m_{l,w}}{EI_{w,y}}}H^2 = \frac{2\pi}{3.516}\sqrt{\frac{7.7767}{6.3206 \cdot 10^5}}15.00^2 = 1.4104\ s \tag{156}$$

where $m_{l,w}$ and $EI_{w,y}$ are the mass per unit height and the yield flexural stiffness of the wall, respectively, given as:

$$m_{l,w} = \frac{m_{s,w}}{h_s} = \frac{23330}{3.00} = 7776.7\frac{kg}{m} \tag{157}$$

$$EI_{w,y} = \frac{M_{y,w}}{\varphi_{y,w}} = \frac{1321}{0.00209} = 6.3206 \cdot 10^5\ \frac{kNm}{m} \tag{158}$$

where: $M_{y,w}$ and $\varphi_{y,w}$ are the yield moment and the yield curvature of the base section of the wall, respectively. The plastic hinge length, $L_{p,w}$, is expressed as:

$$\begin{aligned} L_{p,w} &= \max\{kL_{s,w} + 0.2l_w + L_{sp,w};\ 2L_{sp,w}\} \\ &= \max\{0.03 \cdot 11.00 + 0.2 \cdot 1.50 + 0.2420;\ 2 \cdot 0.2420\} \\ &= \max\{0.8720;\ 0.4840\} = 0.8720\ m \end{aligned} \tag{159}$$

where:

$$L_{s,w} = h_G = \frac{\sum_{i=1}^{n_s} F_i h_i}{\sum_{i=1}^{n_s} F_i} \overset{serie}{\Longrightarrow} \frac{2n_s + 1}{3n_s} H = \frac{2 \cdot 5 + 1}{3 \cdot 5} 15.00 = 11.00\ m \tag{160}$$

$$L_{sp,w} = 0.022 f_y d_{bl,w} = 0.022 \cdot 550.0 \cdot 0.020 = 0.2420\ m \tag{161}$$

$$k = 0.2\left(\frac{f_u}{f_y} - 1\right) = 0.2\left(\frac{632.5}{550.0} - 1\right) = 0.03 \tag{162}$$

where: $L_{s,w}$ and $L_{sp,w}$ are the shear span length and the strain penetration length; f_y and f_u are the mean steel yield strength and the mean steel tensile strength; $d_{bl,w}$ is the maximum diameter of rebars in the base section of the wall; l_w is the section height, respectively.

The displacement shape for wall structures is estimated through the following expression:

$$\begin{aligned} \phi_{i,w} &= \frac{3}{2}\frac{{h_i}^2}{H^2}\left(1 - \frac{h_i}{3H}\right) \\ &= \begin{cases} \frac{3}{2}\frac{3.00^2}{15.00^2}\left(1 - \frac{3.00}{3 \cdot 15.00}\right) = 0.056; i = 1;\ h_i = 3.00\ m \\ \frac{3}{2}\frac{6.00^2}{15.00^2}\left(1 - \frac{6.00}{3 \cdot 15.00}\right) = 0.208; i = 2;\ h_i = 6.00\ m \\ \frac{3}{2}\frac{9.00^2}{15.00^2}\left(1 - \frac{9.00}{3 \cdot 15.00}\right) = 0.432; i = 3;\ h_i = 9.00\ m \\ \frac{3}{2}\frac{12.00^2}{15.00^2}\left(1 - \frac{12.00}{3 \cdot 15.00}\right) = 0.704; i = 4;\ h_i = 12.00\ m \\ \frac{3}{2}\frac{15.00^2}{15.00^2}\left(1 - \frac{15.00}{3 \cdot 15.00}\right) = 1.000; i = 5;\ h_i = 15.00\ m \end{cases} \end{aligned} \tag{163}$$

where $\phi_{i,w}$ is the first mode deflected shape ordinate for the *i-th* storey of the wall structure.

The mass, ${m_w}^*$, the height, ${h_w}^*$, and the stiffness, ${k_w}^*$, of the equivalent SDOF system are given by:

$$\begin{aligned} {m_w}^* &= \sum_{i=1}^{n_s} m_{i,w} = \sum_{i=1}^{n_s} m_{s,w} = n_s m_{s,w} = 5 \cdot 23330 \\ &= 116650\ kg \end{aligned} \tag{164}$$

$$\begin{aligned} {h_w}^* &= \frac{\sum_{i=1}^{n_s} m_{i,w}\phi_{i,w}h_i}{\sum_{i=1}^{n_s} m_{i,w}\phi_{i,w}} = \frac{\sum_{i=1}^{n_s} m_{s,w}\phi_{i,w}h_i}{\sum_{i=1}^{n_s} m_{s,w}\phi_{i,w}} = \frac{\sum_{i=1}^{n_s} \phi_{i,w}h_i}{\sum_{i=1}^{n_s} \phi_{i,w}} \\ &= \frac{0.056 \cdot 3.00 + 0.208 \cdot 6.00 + 0.432 \cdot 9.00 + 0.704 \cdot 12.00 + 1.000 \cdot 1}{0.056 + 0.208 + 0.432 + 0.704 + 1.000} \\ &= 11.98\ m \end{aligned} \tag{165}$$

$$k_w{}^* = \frac{4\pi^2 m_w{}^*}{T_{1,w}{}^2} = \frac{4\pi^2 116650}{1.4104^2} = 2315.2\ \frac{kN}{m} \tag{166}$$

The yield base shear, $V_{y,w}{}^*$, the failure base shear, $V_{u,w}{}^*$, the yield displacement, $d_{y,w}{}^*$, of the equivalent SDOF system are respectively:

$$V_{y,w}{}^* = \frac{M_{y,w}}{h_w{}^*} = \frac{1321}{11.98} = 110.27\ kN \tag{167}$$

$$V_{u,w}{}^* = \frac{M_{u,w}}{h_w{}^*} = \frac{1660}{11.98} = 138.56\ kN \tag{168}$$

$$d_{y,w}{}^* = \frac{V_{y,w}{}^*}{k_w{}^*} = \frac{110.27}{2315.2} = 0.0476\ m \tag{169}$$

where: $M_{y,w}$ and $M_{u,w}$ are the yield and the ultimate moment of the base section of the wall, respectively. The equivalent yield curvature, $\varphi_{y,w}{}^*$, for the equivalent SDOF system is given by:

$$\varphi_{y,w}{}^* = \frac{3M_{y,w}}{k_w{}^* h_w{}^{*3}} = \frac{3 \cdot 1321}{2315.2 \cdot 11.98^3} = 9.9557 \cdot 10^{-4} \tag{170}$$

In order to obtain the same sectional ductility, $\mu_{\varphi,w}$, of the wall section and the plastic hinge of the equivalent SDOF system, the ultimate curvature of the equivalent SDOF system, $\varphi_{u,w}{}^*$, is written as:

$$\begin{aligned}\varphi_{u,w}{}^* = \mu_{\varphi,w}\varphi_{y,w}{}^* = \frac{\varphi_{u,w}}{\varphi_{y,w}}\varphi_{y,w}{}^* = \frac{0.01130}{0.00209}9.9557 \cdot 10^{-4} \\ = 5.3827 \cdot 10^{-3}\end{aligned} \tag{171}$$

where: $\varphi_{y,w}$ and $\varphi_{u,w}$ are the yield and ultimate curvature of the base section of the wall respectively. The plastic displacement, $d_{p,w}{}^*$, ultimate displacement, $d_{u.w}{}^*$, and displacement ductility, $\mu_w{}^*$, for the equivalent SDOF system are then given by, respectively:

$$\begin{aligned}d_{p,w}{}^* &= \left(\varphi_{u,w}{}^* - \varphi_{y,w}{}^*\right) L_{p,w} h_w{}^* \\ &= (5.3827 \cdot 10^{-3} - 9.9557 \cdot 10^{-4}) \cdot 0.872 \cdot 11.98 \\ &= 0.0458\ m\end{aligned} \tag{172}$$

$$\begin{aligned}d_{u.w}{}^* = d_{y,w}{}^* \frac{V_{u,w}{}^*}{V_{y,w}{}^*} = d_{y,w}{}^* \frac{M_{u,w}}{M_{y,w}} + d_{p,w}{}^* = 0.0476\frac{1660}{1321} + 0.0458 \\ = 0.1057\ m\end{aligned} \tag{173}$$

$$\mu_w{}^* = \frac{d_{u,w}{}^*}{d_{y,w}{}^*} = \frac{0.1057}{0.0476} = 2.2189 \tag{174}$$

Once the structural ductility, $\mu_w{}^*$, is known, the force reduction factor for the equivalent SDOF system, $R_{\mu,SDOF,w}$, can be estimated the expression of Nassar and Krawinkler (1991) presented in Section 2.3:

$$R_{\mu,SDOF,w} = (c_w(\mu_w{}^* - 1) + 1)^{\frac{1}{c_w}} = (0.7740 \cdot (2.2189 - 1) + 1)^{\frac{1}{0.7740}} = 2.3596 \tag{175}$$

$$c_w = \frac{T_{1,w}{}^{a_w}}{1 + T_{1,w}{}^{a_w}} + \frac{b_w}{T_{1,w}} = \frac{1.4104^{0.80}}{1 + 1.4104^{0.80}} + \frac{0.29}{1.4104} = 0.7740 \tag{176}$$

where parameters, a_w and b_w, are calculated with Equations (33) and (34):

$$a_w = 0.80 \tag{177}$$

$$b_w = 0.29 \tag{178}$$

The post-yield stiffness for equivalent SDOF wall system, α_w, is defined as:

$$\alpha_w = \frac{F_{u,w}{}^* - F_{y,w}{}^*}{d_{u,w}{}^* - d_{y,w}{}^*} \frac{d_{y,w}{}^*}{F_{y,w}{}^*} = \frac{138.56 - 110.27}{0.1057 - 0.0476} \frac{0.0476}{110.27} = 0.2105 \tag{179}$$

Finally, the ductility reduction factor for MDOF system of wall structures, $R_{\mu,MDOF,w}$, is given by the following expression:

$$R_{\mu,MDOF,w} = R_{M,w} R_{\mu,SDOF,w} = 0.5111 \cdot 2.3596 = 1.2059 \tag{180}$$

where the modification factor $R_{M,w}$ is introduced to take into account higher mode effects for wall structures:

$$\omega_{v,Ti} = 1 + \frac{\mu_w{}^*}{\phi^0} c_{2,Tw} = 1 + \frac{2.2189}{1} 0.4311 = 1.9567 \tag{181}$$

$$c_{2,Tw} = 0.067 + 0.4\left(T_{1,w} - 0.5\right) = 0.067 + 0.4(1.4104 - 0.5) = 0.4311 \quad \begin{cases} \leq 1.150 \\ \geq 0.067 \end{cases} \tag{182}$$

where ϕ^0 is the overstrength factor relating the maximum feasible flexural strength to design strength; in this work ϕ^0 is equal to 1 because mean values of material properties are assumed instead of design ones. The modification factor for wall structures, $R_{M,w}$, is equal to:

$$R_{M,w} = \frac{V_{b,SDOF,w}}{V_{b,MDOF,w}} = \frac{1}{\phi^0 \omega_{v,Ti}} = \frac{1}{1 \cdot 1.9567} = 0.5111 \quad (183)$$

As for the wall system, the proposed analytical method for frame structures presented in Section 3.3 is shown step-by-step in this Section.

The fundamental period of the frame system, $T_{1,f}$, is given by:

$$T_{1,f} = 4\sqrt{\frac{m_{l,f}}{kGA_{f,y}}}H = 4\sqrt{\frac{7.9933}{\frac{5}{6} \cdot 57615}}15 = 0.7742\ s \quad (184)$$

where: k is the shape factor to account for nonuniform distribution of shear stresses, equal to $5/6$ for rectangular sections and $m_{l,f}$; $GA_{f,y}$ and $EI_{f,y}$ are the mass per unit height, the base column yield shear stiffness and the base column yield flexural stiffness of the shear cantilever, respectively, that are given by the following expressions:

$$m_{l,f} = \frac{m_{s,f}}{h_s} = \frac{23980}{3.00} = 7993.3\frac{kg}{m} \quad (185)$$

$$GA_{f,y} = \frac{12EI_{f,y}}{{h_s}^2} = \frac{12EI_{f,y}}{{h_s}^2} = \frac{12 \cdot 43211}{3.00^2} = 57615\frac{kN}{m^2} \quad (186)$$

$$EI_{f,y} = \frac{M_{y,f}}{\varphi_{y,f}} = \frac{471}{0.0109} = 43211\frac{kNm}{m} \quad (187)$$

where: $M_{y,f}$ and $\varphi_{y,f}$ are the yield moment and the yield curvature of the base column of the frame, respectively. The plastic hinge length, $L_{p,f}$, is defined as:

$$L_{p,f} = 0.08h_s + L_{sp,f} = 0.08 \cdot 3.00 + 0.2420 = 0.4820\ m \quad (188)$$

$$L_{sp,f} = 0.022f_y d_{bl,f} = 0.022 \cdot 550.0 \cdot 0.020 = 0.2420\ m \quad (189)$$

where: $L_{sp,f}$ is the strain penetration length; h_s is the storey height; $d_{bl,f}$ is the maximum diameter of rebars in the base columns of the frame.

The displacement shape for frame structures is estimated through the following expression:

$$\phi_{i,f} = \frac{4}{3}\frac{h_i}{H}\left(1-\frac{h_i}{4H}\right) = \begin{cases} \frac{4}{3}\frac{3.00}{15.00}\left(1-\frac{3.00}{4\cdot 15.00}\right) = 0.253; i=1;\ h_i = 3.00\ m \\ \frac{4}{3}\frac{6.00}{15.00}\left(1-\frac{6.00}{4\cdot 15.00}\right) = 0.480; i=2;\ h_i = 6.00\ m \\ \frac{4}{3}\frac{9.00}{15.00}\left(1-\frac{9.00}{4\cdot 15.00}\right) = 0.680; i=3;\ h_i = 9.00\ m \\ \frac{4}{3}\frac{12.00}{15.00}\left(1-\frac{12.00}{4\cdot 15.00}\right) = 0.853; i=4;\ h_i = 12.00\ m \\ \frac{4}{3}\frac{15.00}{15.00}\left(1-\frac{15.00}{4\cdot 15.00}\right) = 1.000; i=5;\ h_i = 15.00\ m \end{cases} \quad (190)$$

where $\phi_{i,f}$ is the first mode deflected shape ordinate for the *i-th* storey for the frame structure.

The mass, $m_f{}^*$, the height, $h_f{}^*$, and the stiffness, $k_w{}^*$, of the equivalent SDOF system are given by, respectively:

$$m_f{}^* = \sum_{i=1}^{n_s} m_{i,f} = \sum_{i=1}^{n_s} m_{s,f} = n_s m_{s,f} = 5\cdot 23980 = 119900\ kg \quad (191)$$

$$h_f{}^* = \frac{\sum_{i=1}^{n_s} m_{i,f}\phi_{i,f}h_i}{\sum_{i=1}^{n_s} m_{i,f}\phi_{i,f}} = \frac{\sum_{i=1}^{n_s} m_{s,f}\phi_{i,f}h_i}{\sum_{i=1}^{n_s} m_{s,f}\phi_{i,f}} = \frac{\sum_{i=1}^{n_s} \phi_{i,f}h_i}{\sum_{i=1}^{n_s} \phi_{i,f}} = \frac{0.253\cdot 3.00 + 0.480\cdot 6.00 + 0.680\cdot 9.00 + 0.853\cdot 12.00 + 1.000\cdot 1}{0.253+0.480+0.680+0.853+1.000} = 10.71\ m \quad (192)$$

$$k_f{}^* = \frac{4\pi^2 m_f{}^*}{T_{1,f}{}^2} = \frac{4\pi^2 119900}{0.7742^2} = 7897.7\ \frac{kN}{m} \quad (193)$$

The yield base shear, $V_{y,f}{}^*$, the failure base shear, $V_{u,f}{}^*$, the yield displacement, $d_{y,f}{}^*$, of the equivalent SDOF system are respectively:

$$V_{y,f}{}^* = \frac{M_{y,f}}{h_s/2} = \frac{471}{3.00/2} = 314.00\ kN \quad (194)$$

$$V_{u,f}{}^* = \frac{M_{u,f}}{h_s/2} = \frac{508}{3.00/2} = 338.67\ kN \quad (195)$$

$$d_{y,f}{}^* = \frac{F_{y,f}{}^*}{k_f{}^*} = \frac{314.00}{7897.7} = 0.0398\ m \quad (196)$$

where: $M_{y,f}$ and $M_{u,f}$ are the yield and ultimate moment of the base column of the frame, respectively.

The yield displacement, ${d_{y1,f}}^*$, and the plastic displacement, ${d_{p1,f}}^*$, for the first-storey equivalent SDOF system are given by:

$$ {d_{y1,f}}^* = \frac{{V_{y,f}}^*}{12EI_f/{h_s}^3} = \frac{314.00}{12 \cdot 43211/3.00^3} = 0.0164\ m \tag{197} $$

$$ {d_{p1,f}}^* = (\varphi_{u,f} - \varphi_{y,f}) L_{p,f} h_s = (0.0191 - 0.0109) \cdot 0.4820 \cdot 3.00 = 0.0119\ m \tag{198} $$

where: $\varphi_{u,f}$ and $\varphi_{u,f}$ are the yield and ultimate curvature of the base column of the frame, respectively.

In order to obtain the same plastic displacement for the equivalent SDOF system, ${d_{p,f}}^*$, the plastic displacement for the first-storey equivalent SDOF, ${d_{p1,f}}^*$, is written as:

$$ {d_{p,f}}^* = \frac{{d_{p1,f}}^*}{{d_{y1,f}}^*} {d_{y,f}}^* = \frac{0.0119}{0.0164} 0.0398 = 0.0288\ m \tag{199} $$

The ultimate displacement, ${d_{u.f}}^*$, and displacement ductility, ${\mu_f}^*$, for the equivalent SDOF system are then given by, respectively:

$$ {d_{u.f}}^* = {d_{y,f}}^* \frac{{V_{u,f}}^*}{{V_{y,f}}^*} + {d_{p,f}}^* = {d_{y,f}}^* \frac{M_{u,f}}{M_{y,f}} + {d_{p,f}}^* = 0.0398 \frac{508}{471} + 0.0288 = 0.0717\ m \tag{200} $$

$$ {\mu_f}^* = \frac{{d_{u,f}}^*}{{d_{y,f}}^*} = \frac{0.0717}{0.0398} = 1.8038 \tag{201} $$

Once the structural ductility, ${\mu_f}^*$, is known, the force reduction factor for the equivalent SDOF system can be estimated using the expression of Nassar and Krawinkler (1991). The ductility reduction factor for the equivalent SDOF system for frame structures, $R_{\mu,SDOF,f}$, is given by:

$$ R_{\mu,SDOF,f} = \left(c_f \left({\mu_f}^* - 1\right) + 1\right)^{\frac{1}{c_f}} = (0.8261(1.8038 - 1) + 1)^{\frac{1}{0.8261}} = 1.8523 \tag{202} $$

$$ c_f = \frac{{T_{1,f}}^{a_f}}{1 + {T_{1,f}}^{a_f}} + \frac{b_f}{T_{1,f}} = \frac{0.7742^{0.8059}}{1 + 0.7742^{0.8059}} + \frac{0.2923}{0.7742} = 0.8261 \tag{203} $$

where parameters, a_f and b_f, are calculated with Equations (31) and (32).

$$a_f = 1.0625 - 2.625\alpha_f = 1.0625 - 2.625 \cdot 0.0977 = 0.8059 \quad (204)$$

$$b_f = 0.39 - \alpha_f = 0.39 - 0.0977 = 0.2923 \quad (205)$$

The post-yield stiffness for equivalent SDOF frame system, α_f, is defined as:

$$\alpha_f = \frac{V_{u,f}{}^* - V_{y,f}{}^*}{d_{u,f}{}^* - d_{y,f}{}^*} \frac{d_{y,f}{}^*}{F_{y,f}{}^*} = \frac{338.67 - 314.00}{0.0717 - 0.0398} \frac{0.0398}{314.00} = 0.0977 \quad (206)$$

Finally, the ductility reduction factor for MDOF system of wall structures, $R_{\mu,MDOF,f}$, is given by the following expression:

$$R_{\mu,MDOF,f} = R_{M,f} R_{\mu,SDOF,f} = 0.8472 \cdot 1.8523 = 1.5692 \quad (207)$$

where the modification factor, $R_{M,f}$, is introduced to take into account higher mode effects for frame structures:

$$\omega_{v,\mu} = \phi^0 + 0.1\mu_f{}^* = 1 + 0.1 \cdot 1.8038 = 1.1804 \quad (208)$$

where ϕ^0 is the overstrength factor relating the maximum feasible flexural strength to design strength; in this work ϕ^0 is equal to 1 because mean values of material properties are assumed instead of design ones. The modification factor for wall structures, $R_{M,f}$, is defined equal to:

$$R_{M,f} = \frac{V_{b,SDOF,f}}{V_{b,MDOF,f}} = \frac{1}{\omega_{v,\mu}} = \frac{1}{1.1804} = 0.8472 \quad (209)$$

Finally, the proposed analytical expressions for dual structures presented in Section 3.4 are shown in this section.

The expression of the ductility reduction factor of the dual system, $R_{\mu,MDOF,d,1}$, is equal to.

$$\begin{aligned} R_{\mu,MDOF,d,1} &= 0.76{\mu_w}^{*0.36} {R_{\mu,MDOF,w}}^{0.38} + 0.99 \frac{{R_{\mu,MDOF,f}}^{8.63}}{{\mu_f}^{*6.89}} \\ &= 0.76 \cdot 2.2189^{0.36} 1.2059^{0.38} + 0.99 \frac{1.5692^{8.63}}{1.8038^{6.89}} \\ &= 1.9176 \end{aligned} \quad (210)$$

The fundamental period of the dual system, $T_{1,d}$, is given by:

$$T_{1,d} = 0.1T_{1,w} + 0.7T_{1,f} = 0.1 \cdot 1.4104 + 0.7 \cdot 0.7742 = 0.6830\ s \quad (211)$$

The structure of Example 1 is finally designed following UNI EN 1998-1 (2013) requirements and detailing. A modal response spectrum analysis is performed using a reduction factor, R, given by:

$$R = R_\mu R_S = R_{\mu,MDOF,d,1} R_S = 1.92 \cdot 2.34 = 4.49 \quad (212)$$

where $R_{\mu,MDOF,d,1}$ is the ductility reduction factor for dual systems calculated by Equation (121) and R_S is the overstrength factor, expressed by:

$$R_S = \alpha_u / \alpha_1 = 2.34 \quad (213)$$

The ratio α_u/α_1 represents the overall structural overstrength: α_1 is the value by which the horizontal seismic design action is multiplied in order to reach the first flexural resistance in any member of the structure, while all other design actions remain constant; α_u is the value by which the horizontal seismic design action is multiplied, in order to form plastic hinges in a number of sections sufficient for the development of the overall structural instability, while all other design actions remain constant.

The overstrength factor R_S is not studied in the present work so, in order to assess the proposed procedure, the exact value of R_S is assumed through an explicit calculation by nonlinear static analysis (pushover). The design has been iterative because R_S was tentatively selected at each iteration and it was checked with pushover analysis after the design process until convergence was reached.

6.1.2. Performance of Example 1 designed applying the proposed method

Once the structure is designed following UNI EN 1998-1 (2013) requirements but with the proposed reduction factor, a nonlinear static analysis is executed to assess the performance of the structure through the N2-method (Fajfar, 2000) and to validate the proposed method. The N2 method is reported in Section 2.7. Reinforcement detailing of walls, base columns and beams are reported in Table 38, Table 39 and Table 40, respectively. Concrete cover is 50 mm for walls and 60 mm for beams and columns, respectively.

Table 38: Reinforcement of walls.

End vertical reinforcement			**Vertical reinforcement**		**Horizontal reinforcement**	
n	$Ø\ [mm]$	$s\ [mm]$	$Ø\ [mm]$	$s\ [mm]$	$Ø\ [mm]$	$s\ [mm]$
8	20	100	12	300	10	90

Table 39: Reinforcement of base columns.

Longitudinal reinforcement			**Stirrups**		
n total	$\emptyset\ [mm]$	n top/bottom	n	$\emptyset\ [mm]$	$s\ [mm]$
20	20	8	3	10	60

Table 40: Reinforcement of beams.

Top reinforcement		**Bottom reinforcement**		**Stirrups**		
n	$\emptyset\ [mm]$	n	$\emptyset\ [mm]$	n	$\emptyset\ [mm]$	$s\ [mm]$
7	20	4	20	2	10	80

Nonlinear static analysis are performed using Midas Gen (2014) software and a concentrated plasticity model is considered. Midas Gen software allows checking hinge the capacity of hinges designed to Eurocode 8 (Fardis, 2009; Biskinis and Fardis, 2010a,b).

The MDOF curve, the SDOF curve and the bilinearised SDOF curve of the Example 1 designed to the proposed method are shown in Figure 10.

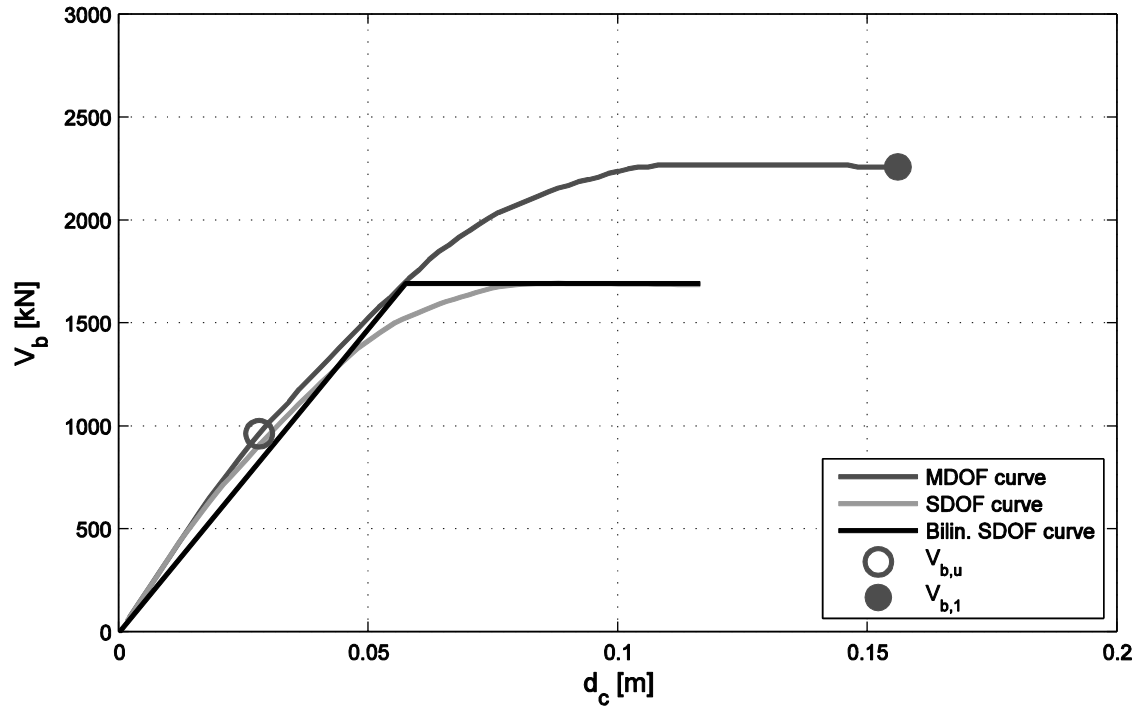

Figure 61: Bilinearization of SDOF curve of Example 1 designed applying the proposed method.

Furthermore the values of the ultimate base shear, $V_{b,u}$, and the base shear at first flexural resistance, $V_{b,1}$, are plotted in Figure 10. It is noted that the ratio α_u/α_1 is equal to the ratio $V_{b,u}/V_{b,1}$:

$$R_s = \frac{\alpha_u}{\alpha_1} = \frac{V_{b,u}}{V_{b,1}} = \frac{2263}{965} = 2.34 \tag{214}$$

The performance evaluation is graphically illustrated in Figure 11.

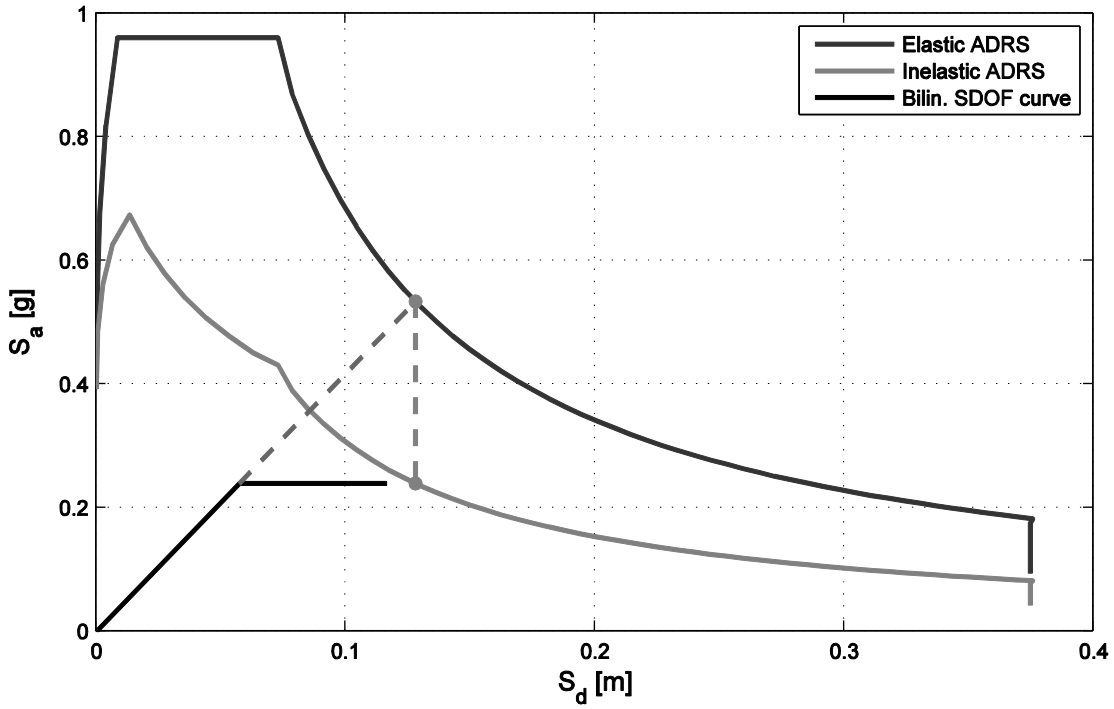

Figure 62: Structural performance of Example 1 designed applying the proposed method.

The performance assessment of the structure is given by the ratio γ_d:

$$\gamma_d = \frac{d_c^*}{d_d^*} = \frac{0.116}{0.128} = 0.91 \tag{215}$$

The ratio γ_d slightly smaller than 1 means that the structure is lightly inadequate and it has a 9% deficiency in displacement capacity. It is noted that the proposed method is based on mean values given by numerical analyses so cases of slightly inadequate design can be also expected. Moreover, further statistical analyses are recommended to improve the reliability of the proposed method.

The displacement ductility, μ, and the ductility reduction factor, R_μ, provided by the N2 method are both equal to 2.23 (equal displacement region for $T^* > T_c$), therefore the proposed ductility reduction factor $R_{\mu,MDOF,d,1} = 1.92$ is close the R_μ provided by the N2 method and with an error of 14%.

6.1.3. Design of Example 1 applying UNI EN 1998-1 (2013)

To compare the proposed design method to UNI EN 1998-1 (2013) standard design method, the same structure of Example 1 is designed using the force reduction factor provided by the Eurocode 8:

$$R = q = q_0 k_w = 3.0 \frac{\alpha_u}{\alpha_1} k_w = 3.0 \cdot 1.2 \cdot 1 = 3.6 \geq 1.5 \tag{216}$$

where $q_0 = 3.0$ for dual systems; $\alpha_u/\alpha_1 = 1.2$ for regular wall-equivalent dual system; k_w is the factor reflecting the prevailing failure mode in structural systems with walls, as reported in Section 2.6.

It is noted that the considered structure is classifiable as wall-equivalent dual structures because 77% of the total base shear given by the modal analysis is carried by the walls, so the k_w factor is expressed as:

$$k_w = \frac{1 + \alpha_0}{3} = \frac{1 + 10}{3} = 3.67 \leq 1 \quad \Rightarrow \quad k_w = 1 \tag{217}$$

Where α_0 is the prevailing aspect ratio of the walls of the structural system, given by:

$$\alpha_0 = \frac{h_w}{l_w} = \frac{H}{l_w} = \frac{15.00}{1.50} = 10 \tag{218}$$

Since the R value provided by Eurocode 8 is 20% lower than that provided by the proposed analytical method, the structure requires higher resistance to support seismic actions. Consequently, section dimensions of walls and columns are increased: l_w, b_c and h_c are assigned equal to 2.10 m, 0.50 m and 0.50 m, respectively. Reinforcement detailing of walls, base columns and beams are reported in Table 41, Table 42 and Table 43, respectively. Concrete cover is 50 mm for walls and 60 mm for beams and columns, respectively.

Table 41: Reinforcement of walls.

End vertical reinforcement			**Vertical reinforcement**		**Horizontal reinforcement**	
n	Ø $[mm]$	s $[mm]$	Ø $[mm]$	s $[mm]$	Ø $[mm]$	s $[mm]$
8	24	100	12	300	10	90

Table 42: Reinforcement of base columns.

Longitudinal reinforcement			**Stirrups**		
n total	Ø $[mm]$	n top/bottom	n	Ø $[mm]$	s $[mm]$
20	20	6	2	10	50

Table 43: Reinforcement of beams.

Top reinforcement		Bottom reinforcement		Stirrups		
n	$Ø\ [mm]$	n	$Ø\ [mm]$	n	$Ø\ [mm]$	$s\ [mm]$
8	20	4	20	2	10	80

6.1.4. Performances of Example 1 designed applying UNI EN 1998-1 (2013)

The performance assessment of Example 1 designed using Eurocode 8 is performed using the N2 method as well .The MDOF curve, the SDOF curve and the bilinearised SDOF curve of the Example 1 designed to Eurocode 8 are shown in Figure 63.

The overstrength factor $\alpha_u/\alpha_1 = 1.2$ is very different from the actual structural overstrength $R_s = 2857/1120 = 2.34$ obtained by the pushover analysis

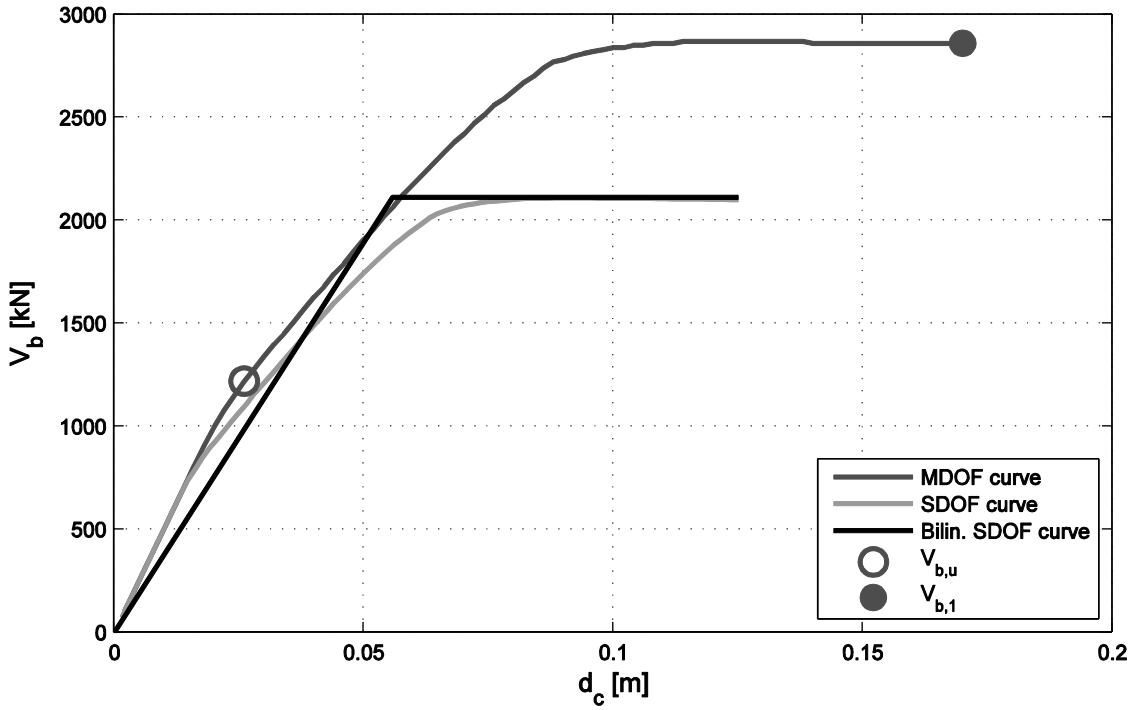

Figure 63: Bilinearization of SDOF curve of Example 1 designed applying Eurocode 8.

The performance evaluation is graphically illustrated in Figure 64.

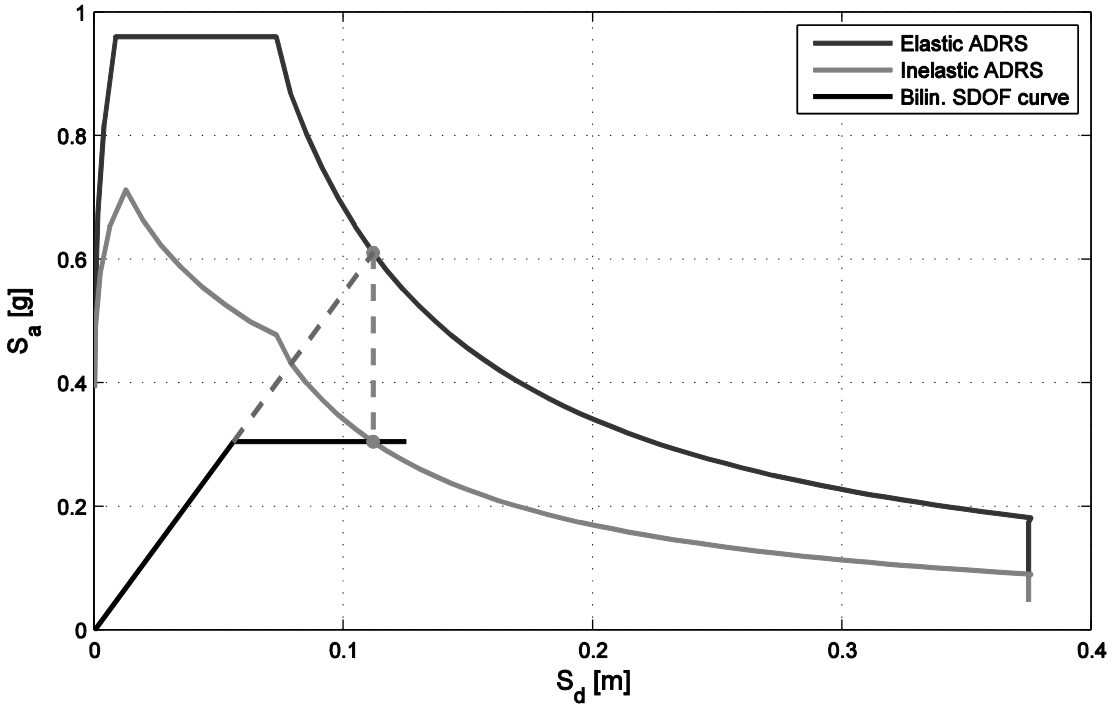

Figure 64: Structural performance of Example 1 designed applying Eurocode 8.

The performance assessment is given by $\gamma_d = 0.125/0.112 = 1.12$. The displacement ductility, μ, and the ductility reduction factor, R_μ, provided by the N2 method are both equal to 2.01 (equal displacement region for $T^* > T_c$).

Furthermore, the structure is classified as wall-equivalent dual structures because 77% of the total base shear given by the modal analysis is carried by the walls, but the nonlinear static analysis shows that only 46% of the total base shear at failure is carried by walls. Therefore the classification of dual systems is ambiguous, since it is based on the shear distribution at the elastic stage, which is totally different from the shear distribution at the plastic stage.

In conclusion, Example 1 shows that the design performed using the ductility reduction factor provided by the proposed method is more accurate than the design performed using the ductility reduction factor provided by UNI EN 1998-1 (2013), which does not provide a clear definition of meaning about the terms which compose the reduction factor. In fact, q_0 and α_u/α_1 do not correspond to the ductility reduction factor and overstrength, respectively. Moreover, Eurocode 8 application yields a stiffer and more resistant structure, with a 13% higher mean volume size of RC elements than the proposed method. The proposed method yields a lightly underdesigned structure, instead the UNI EN 1998-1 (2013) yields a lightly overdesigned structure and Example 1 shows that Eurocode 8 is more precautionary. Probably this event happens because the analytical method is based on mean numerical results and further statistical analyses are recommended to improve the reliability of the proposed method.

6.2. Example 2

The structure considered in Example 2 is the RC frame-wall structure similar to Example 1 but with a number of storeys $n_c = 10$. A portrayal of the structure is reported in Figure 65.

Material properties and applied loads are the same of Example 1.

Geometrical and mechanical properties for walls and columns are listed in Table 44 and Table 45, resistance properties of sections are given for the applied seismic axial load. Beam section dimensions are $b_b = 0.50\ m$ and $h_b = 0.50\ m$.

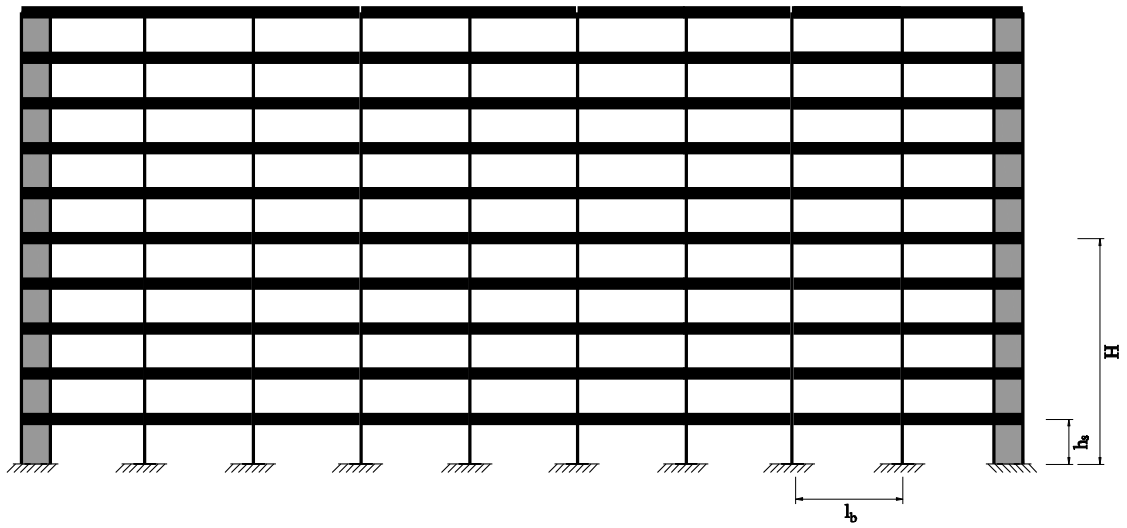

Figure 65: Portrayal of structure of Example 2.

Table 44: Geometrical and mechanical properties of walls.

Properties	**Walls**
Section width, $b_w\ [m]$	0.30
Section length, $l_w\ [m]$	2.10
Yield moment, $M_{y,w}\ [KNm]$	2937
Ultimate moment, $M_{u,w}\ [KNm]$	3670
Yield curvature, $\varphi_{y,w}\ [m^{-1}]$	0.00149
Ultimate curvature, $\varphi_{u,w}\ [m^{-1}]$	0.00793
Curvature ductility, $\mu_{\varphi,w}\ [-]$	5.3221
Storey mass, $m_{s,w}\ [ton]$	24.70

Table 45: Geometrical and mechanical properties of base columns.

Properties	Columns
Section width, b_c $[m]$	0.55
Section length, h_c $[m]$	0.55
Yield moment, $M_{y,f}$ $[KNm]$	963
Ultimate moment, $M_{u,f}$ $[KNm]$	996
Yield curvature, $\varphi_{y,f}$ $[m^{-1}]$	0.00982
Ultimate curvature, $\varphi_{u,f}$ $[m^{-1}]$	0.01237
Curvature ductility, $\mu_{\varphi,f}$ $[-]$	1.2597
Storey mass, $m_{s,f}$ $[ton]$	25.39

6.2.1. Design of Example 2 applying the proposed analytical method

The proposed analytical method is applied as in Section 6.1.1. For the sake of brevity, only results are reported.

Concerning the wall system, the obtained parameters are: $R_{\mu,SDOF,w} = 2.0543$; $R_{\mu,MDOF,w} = 0.6275$; $R_{M,w} = 0.3054$; $\mu_w = 1.9773$; $T_{1,w} = 3.2870\ s$.

Then, concerning the frame system, the obtained parameters are: $R_{\mu,SDOF,f} = 1.2929$; $R_{\mu,MDOF,f} = 1.1457$; $R_{M,f} = 0.8862$; $\mu_f = 1.2846$; $T_{1,\mathrm{f}} = 1.0576\ s$.

Finally, concerning the dual system, the obtained parameters are: $R_{\mu,MDOF,d,1} = 1.3839$; $T_{1,d} = 1.0690\ s$.

As for Example 1, the structure of Example 2 is designed applying UNI EN 1998-1 (2013) requirements and detailing. A modal response spectrum analysis is performed using a reduction factor, R, given by:

$$R = R_\mu R_s = R_{\mu,MDOF,d,1} R_s = 1.38 \cdot 2.25 = 3.11 \tag{219}$$

where $R_{\mu,MDOF,d,1}$ is the ductility reduction factor for dual systems calculated by Equation (121) and R_s is the overstrength factor given by Equation (213).

6.2.2. Performance of Example 2 designed applying the proposed method

Once the structure is designed following UNI EN 1998-1 (2013) requirements but with the proposed reduction factor, a nonlinear static analysis is executed to assess the performance of the structure through the N2-method (Fajfar, 2000) and to validate the proposed method. Reinforcement detailing of walls, base columns and beams are reported in Table 46, Table 47 and Table 48, respectively. Concrete cover is 50 mm for walls and 60 mm for beams and columns, respectively.

Table 46: Reinforcement of walls.

End vertical reinforcement			**Vertical reinforcement**		**Horizontal reinforcement**	
n	Ø $[mm]$	s $[mm]$	Ø $[mm]$	s $[mm]$	Ø $[mm]$	s $[mm]$
8	30	100	12	300	10	90

Table 47: Reinforcement of base columns.

Longitudinal reinforcement			**Stirrups**		
n total	Ø $[mm]$	n top=n bottom	n	Ø $[mm]$	s $[mm]$
26	24	8	3	10	50

Table 48: Reinforcement of beams.

Top reinforcement		**Bottom reinforcement**		**Stirrups**		
n	Ø $[mm]$	n	Ø $[mm]$	n	Ø $[mm]$	s $[mm]$
9	20	6	20	2	10	80

The MDOF curve, the SDOF curve and the bilinearised SDOF curve of the Example 2 designed to the proposed method are shown in Figure 66.

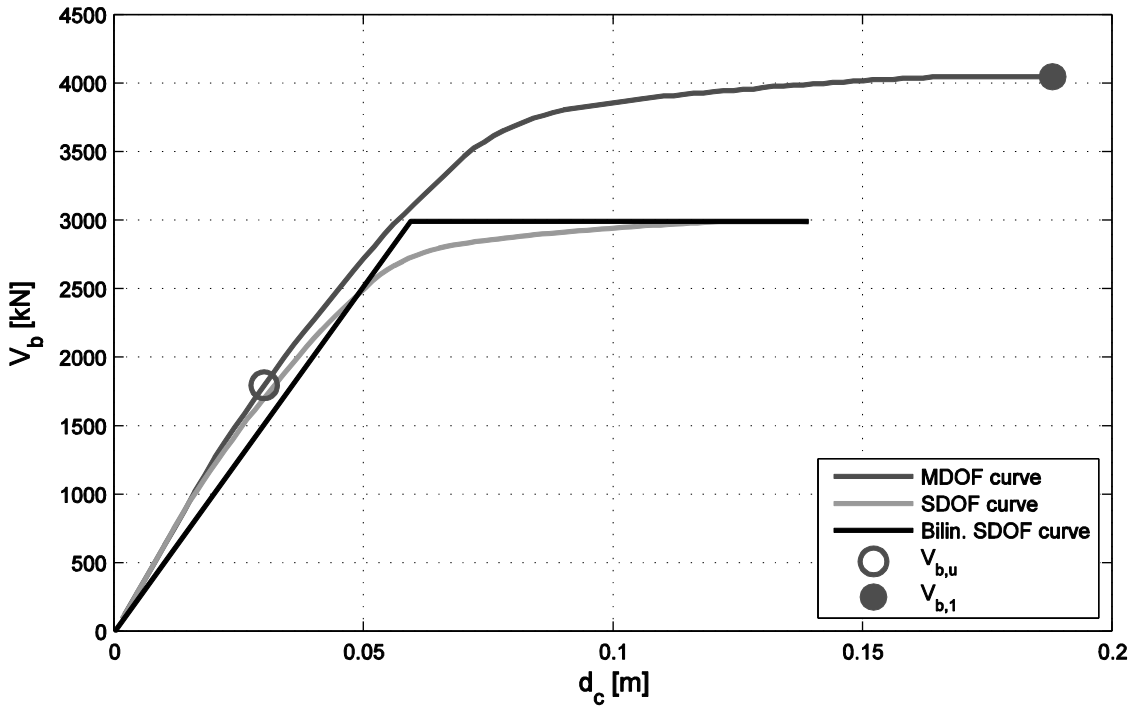

Figure 66: Bilinearization of SDOF curve of Example 2 designed applying the proposed method.

Furthermore the values of the ultimate base shear, $V_{b,u}$, and the base shear at first flexural resistance, $V_{b,1}$, are plotted. It is noted that the ratio α_u/α_1 is equal to the ratio $V_{b,u}/V_{b,1}$:

$$R_s = \frac{\alpha_u}{\alpha_1} = \frac{V_{b,u}}{V_{b,1}} = \frac{4047}{1800} = 2.25 \tag{220}$$

The performance evaluation is graphically illustrated in Figure 67.

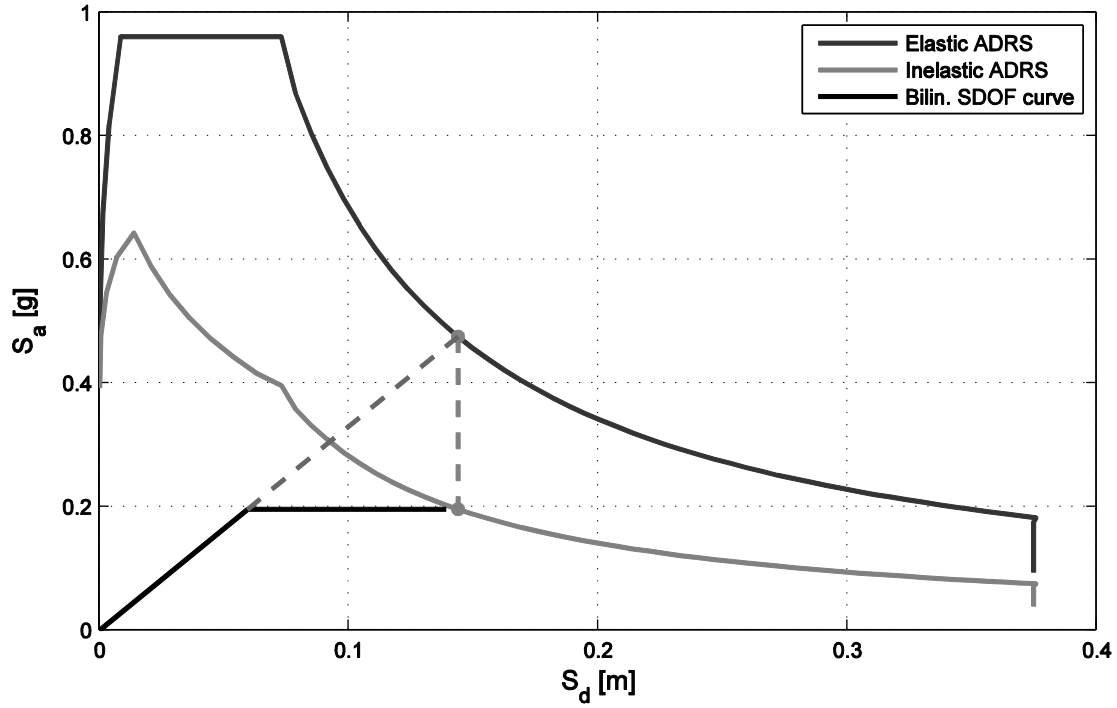

Figure 67: Structural performance of Example 2 designed applying the proposed method.

The performance assessment of the structure is given by the ratio γ_d:

$$\gamma_d = \frac{d_c^*}{d_d^*} = \frac{0.139}{0.144} = 0.97 \tag{221}$$

The displacement ductility, μ, and the ductility reduction factor, R_μ, provided by the N2 method are both equal to 2.43 (equal displacement region for $T^* > T_c$).

6.2.3. Design of Example 2 applying UNI EN 1998-1 (2013)

To compare the proposed method to UNI EN 1998-1 (2013) standard, the same structure of Example 2 is designed using the force reduction factor, R, provided by the Eurocode 8, which is equal to 3.6 as for Example 1.

Because of R provided by Eurocode 8 is 16% higher than one provided by the proposed analytical method, the structure requires lower resistance to support seismic actions. Consequently, section dimensions of beams and columns cab be decreased: h_b, b_c and h_c are assigned equal to 0.45 m, 0.50 m and 0.50 m, respectively. Reinforcement detailing of

walls, base columns and beams are reported in Table 49, Table 50 and Table 51, respectively. Concrete cover is 50 mm for walls and 60 mm for beams and columns, respectively.

Table 49: Reinforcement of walls.

End vertical reinforcement			**Vertical reinforcement**		**Horizontal reinforcement**	
n	Ø $[mm]$	s $[mm]$	Ø $[mm]$	s $[mm]$	Ø $[mm]$	s $[mm]$
8	30	100	12	300	10	90

Table 50: Reinforcement of base columns.

Longitudinal reinforcement			**Stirrups**		
n total	Ø $[mm]$	n top=n bottom	n	Ø $[mm]$	s $[mm]$
28	20	11	4	10	80

Table 51: Reinforcement of beams.

Top reinforcement		**Bottom reinforcement**		**Stirrups**		
n	Ø $[mm]$	n	Ø $[mm]$	n	Ø $[mm]$	s $[mm]$
9	20	5	20	2	10	80

6.2.4. Performance of Example 2 designed applying UNI EN 1998-1 (2013)

The MDOF curve, the SDOF curve and the bilinearised SDOF curve of the Example 2 designed to Eurocode 8 are shown in Figure 68.

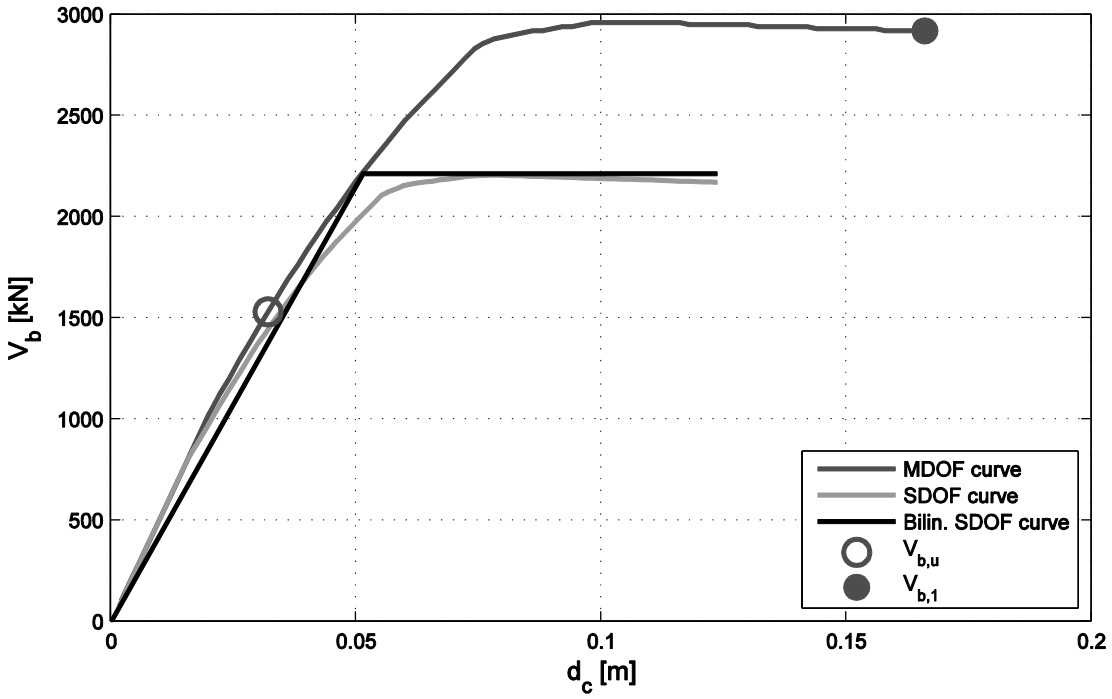

Figure 68: Bilinearization of SDOF curve of Example 2 designed applying Eurocode 8.

The performance evaluation is graphically illustrated in Figure 69.

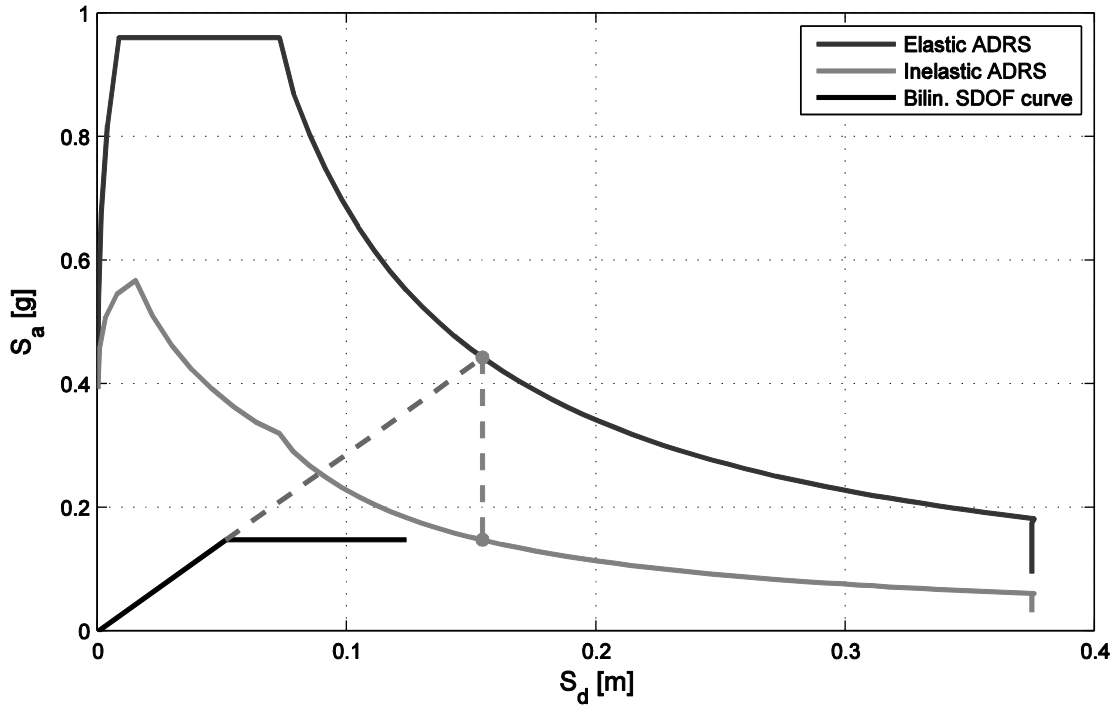

Figure 69: Structural performance of Example 2 designed applying Eurocode 8.

The performance assessment is given by $\gamma_d = 0.124/0.154 = 0.80$. The displacement ductility, μ, and the ductility reduction factor, R_μ, provided by the N2 method are both equal

to 3.00 (equal displacement region for $T^* > T_c$). The overstrength factor $\alpha_u/\alpha_1 = 1.2$ is very different from the actual structural overstrength $R_s = 2917/1528 = 1.91$ obtained by the pushover analysis.

Furthermore, the structure is classified as wall-equivalent dual structures because 76% of the total base shear given by the modal analysis is carried by the walls; in this case the nonlinear static analysis confirms the classification because 64% of the total base shear at failure is carried by walls.

In conclusion, Example 2 shows that the design performed using the ductility reduction factor provided by the proposed method is more accurate than the design performed using the ductility reduction factor provided by UNI EN 1998-1 (2013). Moreover, Eurocode 8 yields a less stiff and less resistant structure, with a 11% lower mean volume size of RC elements than the proposed method. The proposed method yields a well-designed structure, instead the UNI EN 1998-1 (2013) yields a significantly underdesigned structure.

6.3. Conclusions on Example 1 and Example 2

Results of the Example 1 and Example 2 are summarised in Table 52 and Table 53, respectively; the reduction factor, R, the ductility reduction factor, R_μ, the overstrength factor, R_s, the performance ratio, γ_d, and the total concrete volume of the resisting structures, V_c, are listed with relative difference in per cent, respectively.

Table 52: Results of Example 1.

	Design			**N2 method**		
	Proposed method	**Eurocode 8**	**Difference [%]**	**Proposed method**	**Eurocode 8**	**Difference [%]**
$\boldsymbol{R}$	4.49	3.60	-25%	2.23	2.00	-12%
$\boldsymbol{R_\mu}$	1.92	3.00	+36%	2.23	2.00	-12%
$\boldsymbol{R_s}$	2.34	1.20	-95%	1.00	1.00	0%
$\boldsymbol{\gamma_d}$	-	-	-	0.91	1.12	+19%
$\boldsymbol{V_c\ [m^3]}$	414	470	+12%	-	-	-

Table 53: Results of Example 2.

	Design			**N2 method**		
	Proposed method	**Eurocode 8**	**Difference [%]**	**Proposed method**	**Eurocode 8**	**Difference [%]**
$\boldsymbol{R}$	3.11	3.60	+14%	2.43	3.00	+19%
$\boldsymbol{R_\mu}$	1.38	3.00	+54%	2.43	3.00	+19%
$\boldsymbol{R_s}$	2.25	1.20	-88%	1.00	1.00	0%
$\boldsymbol{\gamma_d}$	-	-	-	0.97	0.80	-21%
$\boldsymbol{V_c\ [m^3]}$	557	497	-11%	-	-	-

The following conclusion can be drawn:

(i) Example 1 shows that Eurocode 8 provides a 25% smaller reduction factor R than the proposed method, which yields stiffer and more resistant structure, with a 13% higher mean volume size of RC elements than the proposed method. Instead, Example 2 shows that Eurocode 8 provides a 14% larger reduction factor R than the proposed method, which yields a less stiff and less resistant structure, with a 11% lower mean volume size of RC elements than the proposed method. This effect is due to the force reduction factor which is pre-defined and constant for a certain type of structural system. As a result of this, for the same design input, structures of the same type but different geometry are subjected to different ductility demands and show therefore a different performance during an earthquake.

(ii) Structures of Example 1 and 2 designed applying the proposed method show a performance ratio γ_d equal to 0.91 and 0.97, respectively, therefore, a uniform performance is provided during an earthquake. Ratios γ_d slightly smaller than 1 mean that the structure have a light deficiency in displacement capacity, probably because the proposed method is based on mean values given by numerical analyses and cases of inadequate design can be also expected. Moreover, the proposed method is applied making use of mean material properties; the application of design material properties and a proper overstrength factor relating the maximum feasible flexural strength to design strength factor, ϕ^0, can adjust structural performance. Otherwise, a safety factor can be introduced to correct the ductility reduction factor performing a statistical analyses to calibrate the analytical model to be safe in all cases.

(iii) Structures of Example 1 and 2 designed applying Eurocode 8 show a performance ratio γ_d equal to 1.12 and 0.80, respectively, therefore the code application yields not uniform performance under seismic actions.

(iv) The proposed method is more accurate than the design performed using the ductility reduction factor provided by UNI EN 1998-1 (2013), which does not provide a clear definition of meaning about the terms which compose the reduction factor. In fact, q_0 and α_u/α_1 do not correspond to the ductility reduction factor and overstrength, respectively; Eurocode 8 provides q_0 overestimated of 36% and 54% and α_u/α_1 underestimated of 95% and 88% for Example 1 and 2, respectively.

(v) It is noted that the ductility reduction factor, R_μ, provided by N2 method has a different meaning respect to the actual R_μ of the system, because the N2 method is developed to assess the nonlinear global displacement capacity of the structure. Furthermore, the split of the reduction factor, R, in the ductility term, R_μ, and overstrength term, R_s, does not occur in the N2 formulation, which transforms the structure in a bilinear equivalent SDOF system without hardening (elastic-perfectly plastic force-displacement curve); in other words $R_s = 1$ and $R = R_\mu$. This evidence is proved by observing that R_μ given by N2 method is a value between R and R_μ given by the proposed method.

(vi) The N2 method confirms that a smaller value of R provided by Eurocode 8 in Example 1 (-25% compared to the analytical model) brings a smaller value of R_μ given by N2 method (-12% compared to the analytical model). Vice versa in Example 2, a larger value of R provided by Eurocode 8 (+14% compared to the analytical model) brings a larger value of R_μ given by N2 method (+19% compared to the analytical model).

(vii) In conclusion, the force reduction factor provided by Eurocode 8 and other international codes should be improved to obtain structures designed to uniform performance under seismic actions, in particular R_μ is more accurate if calculated as a function of input data available when starting the design process, such as geometry and general material properties. The proposed analytical method is based on this assumptions and further studies can allow refining the method and to extend it to other types of dual system.

7. Conclusions and outlook

This Section reports the conclusions of the present work and the future research outlook in Section 7.1 and 7.2, respectively.

7.1. Conclusions

Nowadays, the Force-Based Design (FBD) method is the current standard method to design structures to seismic loads. This approach has proven to be robust and easy to apply by design engineers and – in combination with capacity design principles – it provides a good protection against premature structural failures. This FBD method requires static analyses, which are easy to apply and fast to perform. Inelasticity behavior is based on the force reduction factor or behavior factor, which allows converting nonlinear behavior in a reduction of static forces to be applied in static analyses.

The force reduction factor mainly depends on the ductility of the structure and on the structural overstrength. The current generation of seismic design codes suffers from some shortcomings. One of these relates to the fact that the base shear is computed using a pre-defined force reduction factor, which is constant for a certain type of structural system. As a result of this, for the same design input, structures of the same type but different geometry are subjected to different ductility demands and show therefore a different performance during an earthquake.

Basically, the seismic demand is provided by the inelastic acceleration spectra obtained from the response of single-degree-of-freedom (SDOF) systems when a certain structural ductility is put into account. A lot of research have been done in the past about the ductility reduction factor for SDOF systems and several expressions have been proposed. These studies concluded that two parameters mainly governing the ductility reduction factor are the displacement ductility and the fundamental period of the system (Newmark and Hall, 1973; Miranda and Bertero, 1994)

Instead, few literature is available about the ductility reduction factor for MDOF systems (Chopra, 1995). It is evidenced that MDOF system has larger base shear than the corresponding SDOF due to higher mode effects. Numerical procedures to evaluate the ductility force reduction factor for MDOF systems, in particular shear-type building, were developed by Santa-Ana and Miranda (2000), Santa-Ana (2004), Wang *et al*. (2013); aim of

these works was to investigate the correlation between SDOF and MDOF force reduction factor by introducing the modification factor, R_M.

In the present work, an analytical method to estimate the ductility force reduction factor was proposed for wall and frame when considered single systems and then for dual systems, in particular frame-wall structures. Key points of the study are summarised in the following:

(i) The MDOF wall system and the MDOF frame system were modelled as a flexural beam and a shear beam, respectively; MDOF dual system was modelled with coupling a flexural beam and a shear beam.
(ii) Concerning wall and frame systems, the proposed analytical models described the deflected shape at yield and ultimate displacement of the structure and only input data that are available when starting the design process, such as geometry and general material properties, are required. The so computed displacement ductility was taken as proxy of the force reduction factor. Such analytical models allowed linking global to local ductility demands and therefore to compute an estimate of the force ductility reduction factors. These properties were used to define an equivalent SDOF system (Chopra, 2006) in order to calculate the ductility reduction factor. The modification factor was estimated by analytical expressions (Priestley *et al*., 2007), which take into account higher mode effects on the base shear. Once the modification factor was known, the ductility reduction factor for MDOF system was obtained from the ductility reduction factor for SDOF system.
(iii) Combining the ductility reduction factor for wall and frame systems was possible to estimate the ductility reduction factor for dual system by introducing an empirical expression based on regression of numerical results.
(iv) Three levels of sectional ductility were investigated for both wall and frame structures and three combinations of the precedent sectional ductilities were investigated for frame-wall structures. Structures with a number of storeys ranged from 3 to 12 were considered in the present work. Therefore, low-rise and mid-rise structures were investigated, but high-rise buildings were not studied in the present work.
(v) To validate the applicability of the proposed method, a database of 34 natural ground motions was selected and a total of 1020 nonlinear time history analyses (NLTHA) were computed for wall and frame systems and 5100 NLTHA analyses for dual systems, respectively. An iterative procedure was implemented.

Results of wall, frame and dual systems showed a good agreement between ductility reduction factor provided by analytical model and numerical analyses. Main conclusion are reported in the following:

(i) Concerning wall systems, it was evident that ductility reduction factors for SDOF and MDOF systems, modification factor and target ductility decrease with the number of storeys, the loss of capability of the system to exploit the base sectional ductility capacity and the importance of higher mode effects with the number of storeys was highlighted. Finally, the proposed Expression (94) approximated accurately numerical results of ductility reduction factor for wall systems.
(ii) Concerning frame systems, it was evident that ductility reduction factors for SDOF and MDOF systems and target ductility decrease with the number of storeys, as for wall systems; differently, the modification factor is basically constant and lightly affected by

both the sectional ductility capacity of the base column and the number of storeys. Finally, the proposed Expression (117) approximated accurately numerical results of ductility reduction factor for frame systems.

(iii) Concerning dual systems, it was evident that the ductility reduction factor for dual system takes as much advantage of synergy between single systems as the number of storeys increases, therefore, low-rise buildings are not able to activate the synergy between walls and frame effectively. This behaviour was explained by the mutual support between systems: walls hold the frame at lower storeys, where frame is more deformable and wall stiffer, and the frame holds walls at higher storeys, where walls are more deformable and frame stiffer, due to their different opposite concavity of the first mode displacement shape. Therefore, the frame seems to be the most important system when dual structure is designed, except to low-rise structures. In other words, the frame is the system that provides the reserve of ductility when the dual structure attains ultimate capacity during strong earthquakes. Moreover, this observed behaviour was associated to a low use rate of the wall, and it suggested that the best performance in terms of supported base shear was obtained when the wall is the first system to fail. Finally the proposed empirical Expression (149) approximated accurately numerical results of ductility reduction factor for dual systems.

The examples performed concluded that the force reduction factor provided by Eurocode 8 should be improved to design structures with uniform performance under seismic actions. In particular, the force reduction factor would be more accurate if calculated as a function of input data available when starting the design process such as geometry and general material properties. The proposed analytical method was based on this assumptions and further studies can allow refining the proposed method and to extend it to other types of dual system. It was noted that the proposed method was based on mean values given by numerical analyses so cases of slightly inadequate design could be also expected. Moreover, further statistical analyses are recommended to improve the reliability of the proposed method.

The presented work aims to contribute to the development of revised force-based design guidelines for the next generation of seismic design codes.

7.2. Outlook

On the basis of this study, several topics on which further research is needed can be defined, in particular the following areas of interest:

(i) Additional analyses could be carried out in order to obtain more reliable expressions to estimate the ductility force reduction factor for dual system. Expression (149) is empirical and based on results of 5100 analyses, but an extension of range of number of storeys and sectional ductilities is recommended.

(ii) Additional design examples could be computed to assess the reliability of the proposed method and provide a statistical comparison with the current building codes. Moreover, nonlinear time history analyses are computationally costly but more reliable than the simplified N2 method. This aspect will be object of the author's next studies.

(iii) Application of the methodology proposed by FEMA P695 (2009) to reliably quantify the building system performance.

(iv) A mechanical model for dual systems could be developed in order to obtain a similar tool to estimate the ductility reduction factor as introduced for wall and frame systems. Empirical Expression (149) is to be considered a pioneering and simple approach to provide ductility force reduction factor for dual systems.

(v) As developed for ductility reduction factor, an analytical method to assess the overstrength factor for single and dual systems is suggested to complete the method and evaluate the force reduction factor in both its main terms, which are the ductility and the overstrength.

(vi) The extension of proposed method to existing buildings, which are often inadequate with respect to the seismic performance required by modern codes, could be useful to assess seismic vulnerability of structures. The majority of them were designed without any earthquake resistance criterion and without adequate detailing, because they were built when codes required design for gravity loads only. Seismic upgrading is necessary to obtain safer structures, especially for public buildings that are strategic for social purposes. Therefore, a design method which is applicable to existing structures could lead to suitable retrofit solutions (Zerbin and Aprile, 2015).

(vii) The extension of the procedure to systems of different material, such as steel and masonry structures, could be useful to update the current generation of building codes in order to obtain a more uniform design in term of performance.

8. References

Arie, G. (2003), "*Quaderni del Manuale di Progettazione Edilizia - Le Strutture*", Hoepli, Milano, IT-25, Italy.

ASCE SEI 7-10 (2010), *Minimum design loads for buildings and other structures*, American Society of Civil Engineers (ASCE), Reston, VA, US.

ATC-19 (1995), *Structural response modification factors*, Applied Technology Council (ATC), Redwood City, CA, US.

Aydemir, M.E. and Aydemir, C. (2016), "Overstrength factors for SDOF and MDOF systems with soil structure interaction", *Earthq. Struct*. **10**(6), 1273-1289.

Bathe, K.J. (1996), "*Finite Element Procedures*", Pearson Prentice-Hall, Upper Saddle River, NJ, US.

BCJ (2013), *Building Standard Law*, Building Center of Japan (BCJ), Tokyo, JP-13, Japan.

Biot, M.A. (1932), "*Transient Oscillations in Elastic Systems*", Ph.D. Thesis No. 259, Aeronautics Department, Calif. Inst. of Tech., Pasadena, CA, US.

Biskinis, D. and Fardis, M.N. (2010a), "Deformations at flexural yielding of members with continuous or lap-spliced bars", *Struct. Concrete*, **11**(3), 127-138.

Biskinis, D. and Fardis, M.N. (2010b), "Flexure-controlled ultimate deformations of members with continuous or lap-spliced bars", *Struct. Concrete*., **11**(2), 93-108.

Borzi, B. and Elnashai, A.S. (2000), "Refined force reduction factors for seismic design", *Eng. Struct.,* **22**, 1244-1260.

Chopra, A.K. (1995), "*Dynamics of Structures: Theory and Applications to Earthquake Engineering*", First Edition, Pearson Prentice-Hall, Upper Saddle River, NJ, US.

Chopra, A.K. (2006), "*Dynamics of Structures: Theory and Applications to Earthquake Engineering*", Third Edition, Pearson Prentice-Hall, Upper Saddle River, NJ, US.

DM 14/1/2008 (2008), *Norme tecniche per le costruzioni*, Ministry of Infrastructure and Transport, Rome, IT-62, Italy.

Elghadamsi, F.E. and Mohraz, B. (1987), "Inelastic earthquake spectra", *Earthq. Eng. Struct. D.*, **15**, 91-104.

Elnashai, A.S. and Mwafy, A.M., (2002), "Overstrength and force reduction factors of multistorey reinforced-concrete buildings", *Struct. Design. Tall. Build*., **11**, 329-351.

Fajfar, P. (2000), "A nonlinear analysis method for performance based seismic design", *Earthq. Spectra.,* **16**(3), 573-592.

Fardis, M.N. (2009), "*Seismic Design, Assessment and Retrofitting of Concrete Buildings based on EN-Eurocode 8*", Springer Netherlands, Dordrecht, ZH, Netherlands.

FEMA P695 (2009), *Quantification of Building Seismic Performance Factors*, Applied Technology Council (ATC), Redwood City, CA, US.

Gerami, M., Siahpolo, N. and Vahdani, R. (2015), "Effects of higher modes and MDOF on strength reduction factor of elastoplastic structures under far and near-fault ground motions", *Ain Shams Engineering Journal*, in press.

Goodsir, W.J. (1985), "The design of coupled frame-wall structures for seismic actions", Ph.D. Thesis, University of Canterbury, Christchurch, CAN, New Zealand.

Goel, R.K. and Chopra, A.K. (1998), "Period formulas for concrete shear wall buildings", *J. Struct. Eng.*, **124**(4), 426-433.

Hidalgo, P.A. and Arias, A. (1990), "New chilean code for earthquake-resistant design of buildings", *Proc. 4th U.S. Nat. Conf. Earthquake Engrg.*, Palm Springs, CA, US, Vol. 2, 927-936.

Housner, G.W. (1959), "Behaviour of structures during earthquakes", *J. Eng. Mech. Div. ASCE*, **4**, 109-129.

International Conference of Building Officials, ICBO (1958), *Uniform building code (UBC)*, 2nd ed., Vol. 1, Los Angeles, CA, US.

Karavasilis, T. L., Bazeos, N. and Beskos, D. E. (2007), "Bahavior factor for performance-based seismic design of plane steel moment resisting frames", *J. earthq. Eng.,* **11**, 531-559.

Karavasilis, T.L., Bazeos, N. and Beskos, D.E. (2008a), "Drift and ductility estimates in regular steel MRF subjected to ordinary ground motions: A design-oriented approach", *Earthq. Spectra.,* **24**(2), 431-451.

Karavasilis, T.L., Bazeos, N.and Beskos, D.E. (2008b), "Seismic response of plane steel MRF with setbacks: Estimation of inelastic deformation demands", *J. Constr. Steel. Res.,* **64**(6), 644-654.

Karavasilis, T.L., Bazeos, N. and Beskos, D.E. (2008c), "Estimation of seismic inelastic deformation demands in plane steel MRF with vertical mass irregularities", *Eng. Struct.,* **30**(11), 3265-3275.

Lai, S.P. and Biggs, J.M. (1980), "Inelastic response spectra for a seismic building design", *ASCE J. Struct. Div.*, **106**(ST6), 1995-1310.

MacLeod, I.A. (1971), "Simplified equations for deflection of multistory frames", *Build. Sci*., **6**(1), 25-31.

MacLeod, I.A. (1972), "Simplified analysis for shear wall-frame interaction", *Build. Sci*., **7**(2), 121-125.

MATLAB (2013), Version R2013a, The MathWorks, Inc., MA, USA, https://it.mathworks.com/.

Mazzoni, S., McKenna, F., Scott, M.H., Fenves, G.L. (2007), "*OpenSees command language manual*", Open System for Earthquake Engineering Simulation (PEER), University of California, Berkeley, CA, US, http://opensees.berkeley.edu.

Midas/Gen (2016), Integrated design system for buildings and general structures, Version 2.1, MIDAS Information Technology Co., Ltd., Seongnam, KR-41 Korea, https://www.midasuser.com/.

Miranda, E. (1993), "Site-dependent strength reduction factors", *J. Struct. Eng.*, **119**(12), 3503-3519.

Miranda, E. and Akkar, S.D. (2006). "Generalized interstory drift spectrum", *J. Struct. Eng.*, **132**(6), 840-852.

Miranda, E. and Bertero, V.V. (1994). "Evaluation of strength reduction factors for earthquake-resistant design", *Earthq. Spectra.*, **10**(2), 357-379.

Miranda, E. and Taghavi, S. (2005). "Approximate floor acceleration demands in multistory buildings. I: Formulation", *J. Struct. Eng.*, **131**(2), 203-211.

Moghaddam, H. and Mohammadi, R.K. (2001), "Ductility reduction factor of MDOF shear-building structures", *J. Earthq. Eng*., **5**(3), 425-440.

Mwafy, A.M. and Elnashai, A.S. (2002), "Calibration of force reduction factors of RC buildings", *J. earthq. Eng.,* **6**(2), 239-273.

Nassar, A. and Krawinkler, K. (1991), "*Seismic Demands for SDOF and MDOF*", Report No.95, Dept. of Civil Engineering, Stanford University, Stanford, CA, US.

Newmark, N.M. and Hall, W.J. (1973), "*Seismic design criteria for nuclear reactor facilities*", Report No. 46, Building Practices for Disaster Mitigation, National Bureau of Standards (NBS), Department of Commerce, Gaithersburg, MD, US, 209-236.

NRCC (2015), *National Building Code of Canada*, National Research Council of Canada, Ottawa, ON, Canada.

NZS 1170.5 (2004), *Structural design actions - Part 5: Earthquake actions*, Standards New Zealand, Wellington, WGN, New Zealand.

OpenSees (2015), Open System for Earthquake Engineering Simulation, Version 2.4.5, Pacific Earthquake Engineering Research Center (PEER), CA, US, http://opensees.berkeley.edu/.

Ordaz, M. and Perez-Rocha, L.E. (1998), "Estimation of strength-reduction factors for elastoplastic systems: A new approach", *Earthq. Eng. Struct. Dyn*. **27**(9), 889-901.

Paparo, A., and Beyer, K. (2015), "Development of a Displacement-Based Design Approach for Mixed RC-URM Wall Structures", *Earthq. Struct.,* **33**(4), 421-444.

Paulay, T. (2002), "A displacement-focused seismic design of mixed building systems", *Earthq. Spectra*, 18(4), 689-718.

PEER (2005), Pacific Earthquake Engineering Research Centre, Strong Motion Database, University of California, Berkeley, CA, US, http://peer.berkeley.edu/.

Priestley, M.J.N. (2003), "*Myths and fallacies in earthquake engineering, Revisited. The 9th Mallet Milne Lecture*", IUSS Press, Pavia, IT-25, Italy.

Priestley, M.J.N., Calvi, G.M. and Kowalsky, M. (2007), "*Displacement-based seismic design of structures*", IUSS Press, Pavia, IT-25, Italy.

Priestley, M.J.N. and Kowalsky, M. (2000), "Direct displacement-based seismic design of concrete buildings", *Bulletin, NZSEE,* **9**(4), 789-830.

Pozzati, P. and Ceccoli, C. (1977), *Teoria e tecnica delle strutture*, vol. 2, part.II, UTET, Torino, IT-21, Italy.

Riddel, R., Hidalgo, P. and Cruz, E. (1989), "Response modification factors for earthquake resistant design of short period structures", *Earthq. Spectra.*, **5**(3), 571-590.

Riddel, R. and Newmark, N.M. (1979), "Statistical analysis of response of nonlinear systems subjected to earthquakes", *Structural Research Series No. 468*, Dept. Of Civ. Engrg., University of Illinois, Urbana, IL, US.

Rosman, R. (1974) "Stability and dynamics of shear-wall frame structures", *Building Science*, **9**, 55-63.

Santa-Ana, P.R. and Miranda, E. (2000), "Strength reduction factors for multi-degree-of-freedom systems", *12th WCEE*, Auckland, AUK, New Zealand, no. 1446.

Santa-Ana, P.R. (2004), "Estimation of strength reduction factors for elastoplastic structures: modification factor", *13th WCEE*, Vancouver, BC, Canada, no. 126.

SEAOC Blue Book (1959), *Seismic Design Recommendations*, Structural Engineers Association of California (SEAOC), Sacramento, CA, US.

Sullivan, T.J., Calvi, G.M., Priestley, M.J.N. and Kowalsky, M.J. (2003), "The limitations and performances of different displacement based design methods", *Eng. Struct.*, **7**(1), 201-241.

Sullivan, T.J., Priestley, M.J.N. and Calvi, G.M. (2005), "Development of an innovative seismic design procedure for frame-wall structures", *J. Earthqu. Eng.*, **9**(2), 279-307.

Sullivan, T.J., Priestley, M.J.N. and Calvi, G.M. (2006), "Seismic design of frame-wall structures", *Research Report ROSE-2006/02*, IUSS press, Pavia, IT-25, Italy.

Taghavi, S. and Miranda, E. (2005). "Approximate floor acceleration demands in multistory buildings. II: Applications", *J. Struct. Eng.*, **131**(2), 212-220.

Tzimas. A.S., Karavasilis, T.L., Bazeos N. and Beskos, D.E. (2013), "A hybrid force/displacement seismic design method for steel building frames", *Eng. Struct.*, **56**, 1452-1463.

UNI EN 1992-1-1 (2004), *Eurocode 2: Design of Concrete Structures. Part 1-1: General rules and rules for buildings*, European Committee for Standardization, Brussels, BRU, Belgium.

UNI EN 1998-1 (2013), *Eurocode 8: Design of Structures for Earthquake Resistance. Part 1: General Rules, Seismic Actions and Rules for Buildings*, European Committee for Standardization, Brussels, BRU, Belgium.

Veletsos, A.S. and Vann, W.P. (1971), "Response of ground-excited elasto-plastic systems", *J. Struct. Div. ASCE*., **97**(4), 1257-1281.

Veletsos, A.S. and Newmark, N.M. (1960), "Effect of inelastic behaviour on response of simple system to earthquake motion", *Proc. 2nd World Conference on Earthquake Engineering,* Tokyo, JP-13, Japan, 855-912.

Vamvatsikos, D. and Cornell, C.A. (2006), "Direct estimation of the seismic demand and capacity of oscillators with multi-linear static pushovers through IDA", *Earthq. Eng. Struct. D*., **35**(9), 1097-1117.

Vidic, T., Fajfar, P. and Fischinger, M. (1994), "Consistent inelastic design spectra: strength and displacement", *Earthq. Eng. Struct. D.,* **23**(5), 507-521.

Wang, H.Y., Cai, J. And Bu, G.B. (2013), "Influence of high mode effects on ductility reduction factors for MDOF shear-type structures", *International Journal of Advancements in Computing Technology (IJACT)*, **5**(9), 1150-1157.

Wang, H., Cai, J. And Zhou, J. (2014), "Comparison of ductility reduction factors for MDOF flexure-type and shear-type systems", *International Journal of Vibroengineering*, **16**(1), 231-239.

Watanabe, G. and Kawashima, K. (2002). "An evaluation of the force reduction factor in the force based seismic design", *NIST special publication SP*, National Institute of Standards and Technology (NIST), Department of Commerce, Gaithersburg, MD, US, 201-218.

Zerbin, M. and Aprile, A. (2015), "Sustainable retrofit design of RC frames evaluated for different seismic demand", *Earthq. Struct*., **9**(6), 1337-1353.